Univerza
v Ljubljani

Fakulteta
za gradbeništvo
in geodezijo

Jamova 2
1000 Ljubljana, Slovenija
telefon (01) 47 68 500
faks (01) 42 50 681
fgg@fgg.uni-lj.si

D O K T O R S K A D I S E R T A C I J A

št. 171

Kandidat:

SIMON SCHNABL

Naslov naloge:

MEHANSKA IN POŽARNA ANALIZA KOMPOZITNIH NOSILCEV

Temo doktorske disertacije je odobril Senat Univerze v Ljubljani
na 29. seji dne 28. junija 2005 in imenoval
mentorja: izr.prof.dr. Goran Turk, in somentorja: izr.prof.dr. Igor Planinc

Ljubljana, 08. junij 2007

Univerza
v Ljubljani
Fakulteta
za gradbeništvo
in geodezijo

Jamova 2
1000 Ljubljana, Slovenija
telefon (01) 47 68 500
faks (01) 42 50 681
fgg@fgg.uni-lj.si

Komisijo za oceno ustreznosti teme doktorske disertacije v sestavi

izr.prof.dr. Goran Turk
izr.prof.dr. Igor Planinc
izr.prof.dr. Stanislav Srpčič
prof.dr. Franc Kosel (UL, Fakulteta za strojništvo)

je imenoval Senat Fakultete za gradbeništvo in geodezijo na 18. seji dne 30. marca 2005

Komisijo za oceno doktorske disertacije v sestavi

izr.prof.dr. Goran Turk
izr.prof.dr. Igor Planinc
izr.prof.dr. Stanislav Srpčič
prof.dr. Franc Kosel (UL, Fakulteta za strojništvo)

je imenoval Senat Fakultete za gradbeništvo in geodezijo na 7. redni seji dne 25. aprila 2007

Komisijo za zagovor doktorske disertacije v sestavi

prof.dr. Bojan Majes, dekan, predsednik
izr.prof.dr. Goran Turk
izr.prof.dr. Igor Planinc
izr.prof.dr. Stanislav Srpčič
prof.dr. Franc Kosel (UL, Fakulteta za strojništvo)

je imenoval Senat Fakultete za gradbeništvo in geodezijo na 8. redni seji dne 30. maja 2007

Univerza
v Ljubljani

Fakulteta
za gradbeništvo
in geodezijo

Jamova 2
1000 Ljubljana, Slovenija
telefon (01) 47 68 500
faks (01) 42 50 681
fgg@fgg.uni-lj.si

Podpisani **Simon Schnabl, univ.dipl.inž.grad.** izjavljam, da sem avtor doktorske naloge z naslovom:
" MEHANSKA IN POŽARNA ANALIZA KOMPOZITNIH NOSILCEV ".

Ljubljana, 08. junij 2007

BIBLIOGRAFSKO-DOKUMENTACIJSKA STRAN IN IZVLEČEK

UDK **614.84:624.072(043.3)**
Avtor: **Simon Schnabl**
Mentor: **izr.prof.dr. Goran Turk**
Somentor: **izr.prof.dr. Igor Planinc**
Naslov: **Mehanska in požarna analiza kompozitnih nosilcev**
Obseg in oprema: **190 str., 11 pregl., 55 sl., 337 en.**
Ključne besede: **kompozitni nosilci, požar, Reissnerjeve enačbe, Timoshenkov nosilec, zdrs, oglenenje**

Izvleček

V disertaciji je predstavljen računski postopek in programska oprema za določitev napetostnega in deformacijskega stanja nelinearnih slojevitih kompozitnih nosilcev z upoštevanjem delne povezanosti slojev, strižne deformacije prečnih prerezov in oglenenja lesa pri sočasnem delovanju zunanje statične mehanske obtežbe in obtežbe požara. Glede na zahtevnost problema je disertacija vsebinsko razdeljena na dva zaključena dela. V prvem delu analiziramo temperaturno-vlažnostno stanje slojevitih lesenih kompozitnih nosilcev pri požaru z upoštevanjem oglenenja lesa. Pri tem za opis temperaturno-vlažnostnega stanja kompozitnih nosilcev uporabimo nelinearni parcialni diferencialni enačbi Luikova. Na ta način upoštevamo temperaturno in vlažnostno odvisne materialne in termične lastnosti lesa. Enačbe začetnega robnega problema povezanega prehoda toplote in vlage v slojevitih lesenih kompozitnih nosilcih, ki izpostavljeni požaru oglenijo, diskretiziramo in rešimo z uporabo numerične metode končnih razlik. Rezultate enodimenzionalnega širjenja oglenenja primerjamo z rezultati empiričnih modelov in eksperimentalnimi rezultati, ki jih najdemo v tehnični literaturi. Predstavljeni matematični model oglenenja v nadaljevanju uporabimo za parametrično študijo vpliva različnih parametrov na hitrost oglenenja. Na koncu prikažemo oglenenje dvodimenzionalnih homogenih in slojevitih prečnih prerezov kompozitnih nosilcev. V drugem delu disertacije predstavimo osnovne enačbe, ki opisujejo mehansko stanje slojevitih kompozitnih nosilcev z upoštevanjem zdrsa med sloji in strižne deformacije prečnega prereza. Posebno pozornost namenimo analitičnemu reševanju osnovnih enačb. Predstavljena algoritma za analitično reševanje Bernoullijevih in Timoshenkovih nosilcev prikažemo z računskimi primeri. Izvedemo tudi parametrično študijo vpliva strižne deformacije prečnega prereza na mehansko obnašanje omenjenih nosilcev. V nadaljevanju s pomočjo modificiranega principa virtualnega dela izpeljemo družino deformacijskih končnih elementov za nelinearno analizo kompozitnih nosilcev z upoštevanjem zdrsa med sloji ter strižne deformacije prečnega prereza. Z analizo različnega števila končnih elementov, stopnje interpolacije neznanih funkcij in izbire kolokacijskih točk pokažemo, da so razviti končni elementi točni, učinkoviti in odporni na kakršnokoli vrsto blokiranja. Družino deformacijskih končnih elementov kasneje priredimo za analizo mehanskega odziva slojevitih lesenih kompozitnih nosilcev pri sočasnem delovanju zunanje statične mehanske obtežbe in obtežbe požara. Pri določitvi napetostnega in deformacijskega stanja v poljubnem materialnem vlaknu prečnega prereza, poleg mehanske deformacije, upoštevamo tudi prispevke temperaturne deformacije lesa. Uporabnost predlaganega matematičnega modela za račun odziva slojevitih kompozitnih nosilcev na hkratno delovanje zunanje statične obtežbe in obtežbe požara prikažemo z računskimi primeri.

BIBLIOGRAPHIC-DOCUMENTALISTIC INFORMATION

UDC **614.84:624.072(043.3)**
Author: **Simon Schnabl**
Supervisor: **izr.prof.dr. Goran Turk**
Co-supervisor: **izr.prof.dr. Igor Planinc**
Title: **Analysis of composite beams exposed to fire**
Notes: **190 p., 11 tab., 55 fig., 337 eq.**
Key words: **composites, fire, Reissner's beam theory, shear, interlayer slip, charring**

Summary

This thesis presents a numerical model and a computer program for stress-strain analysis of non-linear multi-layered composite beams with interlayer slip, shear deformation and charring of timber when simultaneously exposed to static loading and fire. The text is divided into two major parts. In the first part we analyse the temperature and moisture content distribution in timber composite beams when exposed to fire. The simultaneous heat and moisture transfer in porous media like wood is governed by the two second order non-linear partial differential equations provided by Luikov. In this way, the anisotropy and temperature and moisture content dependent permeability and material properties of timber and char are assumed. A non-linear system of governing equations which describes the initial boundary value problem of heat and moisture transfer in timber is discretized and solved by the use of numerical procedure such as finite difference method. The calculated one-dimensional charring rate and depth are compared to the results of empirical models and experimental results published in the technical literature. In addition, the present numerical model is also used to analyse a two-dimensional behaviour of timber solid and composite beams when exposed to fire from three sides. In the second part we introduce first the governing equations which describe the mechanical behaviour of multi-layered composite beams with interlayer slip and shear deformation. A special attention is devoted to the analytical treatment of geometrically and materially linear multi-layered composite beams with a significant interlayer slip. The solution algorithms for Bernoulli and Timoshenko composite beams are represent by the numerical examples. A parametric study is performed also to investigate the influence of shear deformation on the mechanical behaviour of the above mentioned structures. Further, a modified principle of virtual work is used to derive the new strain-based family of finite elements for a non-linear analysis of multi-layered composite beams with interlayer slip and shear. The calculations with different number of finite elements, degree of interpolation functions and different selection of collocation points confirm, that the derived strain-based family of finite elements is completely locking-free. The same strain-based finite elements are employed in the mechanical response analysis of the multi-layered composite beams when simultaneously exposed to static loading and fire. The geometric strain increment is assumed to be the sum of increments of elastic and temperature strains. The applicability of the present numerical model for the stress-strain analysis of the non-linear multi-layered composite beams subjected to mechanical and fire loads is clearly illustrated by the numerical examples.

Zahvale

Iskreno se zahvaljujem mentorju izr.prof.dr. Goranu Turku in somentorju izr.prof.dr. Igorju Planincu za spodbudo in nesebično pomoč pri vsakdanjem delu.

Iskrena hvala staršem in Katji, za razumevanje, potrpežljivost in podporo.

Iskrena hvala sodelavcem s Katedre za mehaniko za prijetno delovno vzdušje.

Iskrena hvala prijateljem, ki so mi ves čas stali ob strani.

Iskrena hvala Ministrstvu za šolstvo, znanost in šport Republike Slovenije za dodeljeno štipendijo.

Iskrena hvala vsem, ki ste me na najrazličnejše načine spremljali na moji življenjski poti.

Vsebina

Kazalo slik

List of Figures

Kazalo preglednic

List of Tables

1 UVOD

Predstavitev problema

Slojeviti kompozitni nosilci sodijo med inovativnejše konstrukcijske elemente. V gradbeništvu se pogosto uporabljajo v mostogradnji, pri ojačitvah in sanacijah že obstoječih objektov oziroma njihovih delov, pri medetažnih konstrukcijah in podobno. Značilni primeri takih konstrukcij so armiranobetonske, sovprežne, lamelirane, sendvič konstrukcije ter mnogo drugih. Poleg gradbeništva, njihova uporaba strmo narašča tudi v drugih panogah, kot so letalska, vesoljska, ladijska industrija, itd. Mehansko obnašanje omenjenih konstrukcij je v veliki meri odvisno od načina povezanosti slojev oziroma od uporabljenih veznih sredstev. Absolutno togega stika tudi v primeru uporabe izredno togih veznih sredstev praktično ni mogoče zagotoviti. Posledica je medsebojni zdrs. Ker pa ima zdrs običajno pomemben vpliv na mehansko obnašanje slojevitih kompozitnih konstrukcij, ga moramo pri analizi takih konstrukcij upoštevati.

Poleg upoštevanja delne povezanosti slojev kompozitnih nosilcev moramo pri zagotavljanju splošne varnosti omenjenih konstrukcij upoštevati oziroma zagotavljati tudi ustrezno požarno odpornost. Slojeviti kompozitni nosilci iz lesa so v pogledu požarne varnosti v primerjavi z nekaterimi drugimi vrstami gradbenih konstrukcij razmeroma varni. To je v največji meri pogojeno z relativno slabo toplotno prevodnostjo lesa in oglja. Naraščanje temperature povzroča zmanjšanje trdnosti lesa. Les je vnetljiv in gorljiv material. Izpostavljen požaru oziroma visokim temperaturam je podvržen toplotni degradaciji oziroma tako imenovani pirolizi. Piroliza je izjemno kompleksen pojav. Predstavlja vzajemno delovanje raznih kemijskih procesov s procesom prehoda toplote in vlage. Posledica toplotnega razkroja lesa je nastanek oglja, najrazličnejših plinov, smol in kislin (ogljikov dioksid, ogljikov monoksid, metan, formaldehid, mravljična in acetilenska kislina, katran, itd.). Posledično se spremenijo lastnosti lesa, npr. specifična gostota, toplotna prehodnost, itd. Les pri visokih temperaturah poka, se krči in postane črn. Pravimo, da ogleni. Pri temperaturah med 270 in $300\,^{\circ}\mathrm{C}$ se vname. Temperaturo pri kateri se les vname imenujemo vnetišče lesa.

Požar je zelo buren kemični proces. Zelo velika količina sproščene energije je vzrok drastičnemu povečanju temperature okoliškega zraka in konstrukcije. Količina sproščene energije je odvisna od mnogih parametrov. Zlasti pomembni so vrsta in količina gorljivega materiala, količina prisotnega kisika, termične lastnosti konstrukcije, velikost in razporeditev odprtin, itd. Veliko število težko določljivih parametrov požara je razlog za težko in dokaj nezanesljivo oceno temperature požarnega prostora, ki predstavlja izhodiščni podatek pri požarni analizi konstrukcij. V ta namen so bile na osnovi številnih teoretičnih in eksperimentalnih raziskav v požarnih laboratorijih izdelane različne standardne požarne krivulje, s katerimi lahko ocenimo časovni razvoj temperature požarnega prostora. Poznavanje lesa pri visokih temperaturah je s stališča dimenzioniranja požarne odpornosti lesenih elementov in konstrukcij izredno pomembno. Požarno odpornost lahko določimo z eksperimenti ali ocenimo z uporabo računskih postopkov. Eksperimenti so v veliki večini primerov izredno zahtevni in dragi. Poleg tega

moramo običajno na osnovi majhnega števila relativno majhnih, omejenih preiskušancev sklepati na požarno odpornost gradbenih konstrukcij. To je tudi razlog, da številni raziskovalci veliko pozornost namenjajo razvoju učinkovitih računskih postopkov za analizo mehanskega odziva požaru izpostavljenih konstrukcij. Matematično modeliranje običajno poenostavimo tako, da ga razdelimo v tri fizikalno smiselne ločene faze. V prvi fazi določimo časovno razporeditev temperature in vlage po požarnem prostoru. V drugi fazi izračunamo časovno razporeditev temperature in vlage po obravnavanih konstrukcijskih elementih, ki je posledica temperaturnega in vlažnostnega spreminjanja požarnega prostora. V tretji fazi opazujemo časovni mehanski odziv obravnavane konstrukcije na sočasen vpliv zunanje statične mehanske obtežbe in spremembe temperature. Pri določitvi temperaturnega in vlažnostnega polja kompozitnega nosilca, ki je izpostavljen požaru, je potrebno upoštevati, da se toplota in vlaga med požarom in nosilcem prenašata na različne načine (konvekcija, kondukcija, radiacija). Poleg tega moramo upoštevati izhlapevanje, izparevanje in kondenziranje vode ter oglenenje lesa. Uspešnost analize odziva slojevitih kompozitnih lesenih nosilcev na sočasen vpliv zunanje statične mehanske obtežbe in obtežbe požara je v veliki meri odvisna od ustrezne izbire temperaturno in vlažnostno odvisnih mehanskih, materialnih, reoloških in termičnih lastnosti lesa in veznih sredstev.

Vsebina dela

Jedro disertacije predstavlja izpeljava matematičnega modela za določitev napetostnega in deformacijskega stanja nelinearnih slojevitih kompozitnih nosilcev z upoštevanjem delne povezanosti slojev, strižne deformacije prečnega prereza in oglenenja lesa pri sočasnem delovanju statične mehanske obtežbe in obtežbe požara. V ta namen smo izdelali računalniški program v programskem okolju *Matlab*.

V prvem delu naloge analiziramo temperaturno-vlažnostno stanje slojevitih lesenih kompozitnih nosilcev pri požaru z upoštevanjem oglenenja lesa. Pri tem za opis temperaturno-vlažnostnega stanja kompozitnih nosilcev uporabimo nelinearni parcialni enačbi Luikova (1966). Na ta način upoštevamo temperaturno in vlažnostno odvisne materialne in termične lastnosti lesa. Ker analitičnih rešitev v splošnem ne poznamo, enačbe začetnega robnega problema povezanega prehoda toplote in vlage v slojevitih lesenih kompozitnih nosilcih, ki izpostavljeni požaru oglenijo, diskretiziramo in rešimo z uporabo numerične metode končnih razlik. Dobljene rezultate hitrosti enodimenzionalnega oglenenja homogenih nosilcev primerjamo z rezultati empiričnih modelov enodimenzionalnega oglenenja homogenih nosilcev, ki jih najdemo v tehnični literaturi. Poleg tega rezultate enodimenzionalnega oglenenja primerjamo z eksperimentalnimi rezultati švedskega raziskovalca Fredlunda (1988, 1993). Predstavljeni matematični model oglenenja v nadaljevanju uporabimo za parametrično študijo vpliva različnih parametrov na hitrost oglenenja. Na koncu prikažemo oglenenje dvodimenzionalnih homogenih in slojevitih prečnih prerezov kompozitnih nosilcev. Rezultat analize je časovna razporeditev temperature, vlage in oglja po prečnem prerezu dvoslojnega kompozitnega nosilca v različnih časih po začetku požara. Omenjeno razporeditev potrebujemo v drugem delu naloge, kjer analiziramo mehanski odziv slojevitega kompozitnega nosilca na sočasno zunanjo statično mehansko obtežbo in obtežbo požara.

V drugem delu disertacije predstavimo osnovne enačbe, ki opisujejo obnašanje kompozitnih nosilcev z upoštevanjem zdrsa med sloji in strižne deformacije prečnega prereza. Posebno pozornost namenimo analitičnemu reševanju osnovnih enačb slojevitih Bernoullijevih in Timoshenkovih kompozitnih nosilcev. V ta namen predstavimo algoritma za analitično reševanje. Razvita algoritma v nadaljevanju uporabimo pri reševanju konkretnih primerov kompozitnih nosilcev. V prvem primeru analitično rešitev razširimo s prostoležečih troslojnih kompozitnih nosilcev na kontinuirne troslojne kompozitne nosilce. V drugem primeru analitično rešitev Timoshenkovih kompozitnih nosilcev prikažemo na primeru dvoslojnega prostoležečega kompozitnega nosilca. Na osnovi analitične rešitve Timoshenkovih kompozitnih nosilcev izvedemo detajlno parametrično analizo vpliva strižne deformacije prečnega prereza na mehan-

sko obnašanje omenjenih konstrukcij. V nadaljevanju z modificiranim principom virtualnega dela (Planinc, 1998) izpeljemo družino deformacijskih končnih elementov za nelinearno analizo kompozitnih nosilcev z upoštevanjem zdrsa med sloji ter strižne deformacije prečnega prereza. Z analizo različnega števila končnih elementov, stopnje interpolacije neznanih funkcij in izbire kolokacijskih točk pokažemo, da so tako razviti končni elementi točni, učinkoviti in odporni na kakršnokoli vrsto blokiranja. To je tudi razlog, da družino razvitih deformacijskih končnih elementov kasneje priredimo za analizo mehanskega odziva slojevitih kompozitnih lesenih nosilcev pri sočasnem delovanju mehanske statične obtežbe in obtežbe požara. Pri določitvi napetostnega in deformacijskega stanja v poljubnem materialnem vlaknu prečnega prereza, v analizi poleg mehanske deformacije upoštevamo tudi prispevke temperaturne deformacije lesa. Z uporabo razporeditve temperature, vlage in oglja po prerezu, ki jo določimo v prvem delu disertacije, z računskim primerom prikažemo uporabnost predlaganega matematičnega modela za račun odziva slojevitih kompozitnih nosilcev zaradi zunanje statične obtežbe in požara.

Disertacija ima poleg uvoda še tri poglavja. V drugem poglavju analiziramo temperaturno in vlažnostno stanje lesenih homogenih in slojevitih kompozitnih nosilcev, ki izpostavljeni požaru oglenijo. V tretjem poglavju poleg analitičnega reševanja osnovnih enačb kompozitnih nosilcev obravnavamo tudi mehanski odziv omenjenih konstrukcij na sočasno delovanje zunanje statične mehanske obtežbe in obtežbe požara. V četrtem poglavju podamo zaključke.

2 TEMPERATURNO-VLAŽNOSTNA ANALIZA NOSILCEV Z UPOŠTEVANJEM OGLENENJA

2.1 Pregled literature

Začetki modeliranja povezanega prenosa toplote in vlage segajo v štirideseta leta prejšnjega stoletja, ko je beloruski znanstvenik Luikov z uporabo metod neuravnotežene termodinamike razvil model povezanega prenosa toplote in vlage v kapilarno poroznih materialih. Model, ki ga sestavlja sistem nelinearnih parcialnih diferencialnih enačb je prvič objavil mnogo kasneje (Luikov, 1966). Neodvisno od njega, so zelo podobne modele povezanega prehoda toplote in vlage v poroznih materialih izpeljali tudi De-Vries (1968), Harmathy (1969) in kasneje še Whitaker (1977). Poleg izpeljave in validacije modela je Luikov (1966) za različne materiale eksperimentalno določil vrednosti materialnih parametrov modela. V preglednem članku je Luikov (1975) podal tudi natančen pregled njegovega dela in ostalih ruskih avtorjev do leta 1973.

Ko je bil problem formuliran, ga je bilo potrebno rešiti. Številni raziskovalci so poskušali poiskati analitične rešitve Luikovega modela, ki so možne le za izjemno preprosto geometrijo ter robne pogoje. Z namenom, da bi bil sistem enačb matematično bolje obvladljiv, so Luikov (1966, 1980) ter Luikov in Mikhailov (1966) predlagali, da se pri računu povezanega prenosa toplote in vlage upošteva konstantne koeficiente prevodnosti znotraj posameznega časovnega koraka. Na ta način je rešitev nelinearnega sistema enačb sestavljena iz rešitev linearnih sistemov s konstantnimi koeficienti. Ostali raziskovalci so raziskovali analitične rešitve ob upoštevanju konstantnih koeficientov prevodnosti. Lobo s sodelavci (1987) je opozoril na obstoj kompleksnih lastnih vrednosti pri reševanju linearnega sistema enačb. Velika večina rešitev do tedaj je zanemarila obstoj kompleksnih lastnih vrednosti, zato je njihova veljavnost vprašljiva. Liu in Cheng (1991) sta potrdila le eno kompleksno vrednost. Zaradi omejitve te metode, sta Ribeiro in Cotta (1995) predlagala alternativno približno rešitev Luikovih enačb, ki ne zahteva izračuna kompleksnih lastnih vrednosti. Kasneje so bile s to tehniko, ki je kombinacija bisekcije in Newton-Raphsonove metode, najdene tako realne kot kompleksne lastne vrednosti. Poleg tega so analitične rešitve predstavili še Pandey s sodelavci (1999a, 1999b), Chang in Weng (2000), Qin in Belarbi (2005), itd.

V veliki večini primerov pa analitične rešitve ni mogoče dobiti. V teh primerih je potrebna uporaba numeričnih metod za določitev približnih rešitev. Thomas s sodelavci (1980) je z metodo končnih razlik obravnaval nelinearne Luikove enačbe. Podobno je Irudayaray s sodelavci (1990) analiziral sušenje lesa z uporabo metode končnih elementov. Podal je podroben opis uporabljenih numeričnih metod za rešitev nelinearnih Luikovih enačb. Metodo končnih razlik je za rešitev Luikovih enačb uporabil tudi Gams (2003). Rezultate je primerjal z analitično rešitvijo enodimenzionalnega prehoda toplote in vlage skozi homogeni leseni prerez, ki sta jo predstavila Chang in Weng (2000) ter rezultati oziroma meritvami

temperature in vlage dvodimenzionalnega homogenega in lameliranega prereza, ki je bil izpostavljen spremenljivim vplivom okolja. V obeh primerih je dobil dobro ujemanje rezultatov.

Povezan prehod toplote in vlage v različnih materialih so študirali številni avtorji. Lien in Wittmann (1995) sta obravnavala povezan prehod toplote in vlage v betonskih elementih, ki so izpostavljeni visokim temperaturam. Nijdam s sodelavci (2000) je obravnaval sušenje lesa iglavcev. Zanimivo delo je objavil Can (1998), ki je analiziral sušenje tiskarskega črnila. Večina modelov v literaturi je eno ali dvodimenzionalnih. Trodimenzionalni nestacionarni model prevajanja toplote in vlage v primeru sušenja lesa pri visokih temperaturah z upoštevanjem Luikovih enačb obravnavata Younsi s sodelavci (2006a, 2006b) ter Kocaefe s sodelavci (2006). Podobno sušenje lesa pri visokih temperaturah z uporabo enačb, ki jih predstavi Whitaker (1977) obravnavajo Younsi s sodelavci (2006c, 2006). S parametrično študijo vpliva različnih parametrov na razporeditev temperature in vsebnosti vlage po nosilcu ter primerjavo z eksperimentalnimi rezultati pokažejo, da so Luikove enačbe primerne za opis povezanega prehoda toplote in vlage v primeru sušenja lesa pri visokih temperaturah.

Za natančno temperaturno-vlažnostno analizo lesenih nosilcev pri požaru moramo poleg povezanega prehoda toplote in vlage v lesenem nosilcu poznati tudi hitrost oglenenja oziroma stopnjo zoglenitve lesa. Po drugi svetovni vojni je bilo razvitih mnogo modelov oglenenja lesa, in sicer od zelo preprostih analitičnih enačb do zelo kompleksnih numeričnih rešitev. Modeli se razlikujejo po težavnosti oziroma zahtevnosti fizikalnih in kemijskih pojavov in privzetih predpostavk vključenih v model. Nekateri modeli obravnavajo povezan prehod toplote in vlage, medtem ko drugi povsem zanemarijo prehod vlage in hlapov in obravnavajo samo enačbo za prehod toplote skozi snov (prevajanje). V nadaljevanju omenimo le nekatere modele. Na osnovi velikega števila eksperimentov lesenih nosilcev pri požaru so Lawson *et al.* (1952), Schaffer (1965), Lie (1977), Mikkola (1990), White in Nordheim (1992), White (1994), Janssens in White (1994) in drugi, prišli do podobnih empiričnih modelov oglenenja. Večina predlaga konstantno hitrost oglenenja. Tako Lie (1977) predlaga konstantno hitrost oglenenja ne glede na vrsto lesa in vsebnosti vlage. Nelinearni model enodimenzionalnega oglenenja je prvi razvil Lawson *et al.* (1952). Obravnaval je oglenenje smrekovih nosilcev različnih debelin in 12 % vsebnosti vlage, ki so bili izpostavljeni razmeram standardnega požara. Nelinearni model sta podala tudi White in Nordheim (1992). Njun empirični model je osnovan na rezultatih eksperimenta enainštiridesetih nosilcev iz osem različnih vrst lesa. Natančen pregled literature empiričnih modelov podajajo Lau s sodelavci (1999) ter White in Tran (2004).

Pomembna omejitev velike večine modelov je, da so omejeni na enodimenzionalne probleme in standardne požarne obremenitve, ki so običajno podane s standardnimi požarnimi krivuljami podanimi v Evrokodu 1 (2004), v avstralskem standardu AS 1720.4 (1990) in drugod. Z namenom boljšega opisa oglenenja je Fredlund (1988, 1993) razvil model oglenenja lesa, ki upošteva prehod toplote in mase v lesu, oksidacijo oglja, itd. Izdelal je računalniški program WOOD1, ki temelji na metodi končnih elementov. Opozoril je, da je kritična točka pri opisu oglenenja lesa določitev materialnih karakteristik lesa in oglja pri visokih temperaturah. Karakteristike, ki jih je uporabil v računih je določil eksperimentalno. Rezultate je primerjal z meritvami, ki jih je dobil na osnovi eksperimentov oglenenja smrekovih nosilcev v skladu s standardom ISO 834 (1999). Primerjava je pokazala izredno dobro ujemanje rezultatov. Model oglenenja, ki ga je predstavil Fredlund (1988, 1993), ne upošteva krčenja oglja. Na to je opozoril Janssens (2004). V svoj model je vključil tudi vpliv kontrakcije oglja. Izdelal je računalniški program CROW za analizo enodimenzionalnega oglenenja lesa, ki temelji na metodi končnih razlik. Podoben model kot Fredlund (1988, 1993) smo izdelali tudi v okviru doktorskega dela (Schnabl in Turk, (2006a, 2006b, 2006c)). V modelu upoštevamo nelinearne parcialne diferencialne enačbe Luikova, ki opisujejo povezan prehod toplote in vlage v poroznem materialu, kot je les. Na ta način smo upoštevali

temperaturno in vlažnostno odvisne termomehanske lastnosti lesa in oglja. S parametrično analizo sta obravnavala vpliv različnih parametrov lesa na hitrost oglenenja le tega.

Zanimiva članka s tega področja v zadnjem obdobju sta delo avtorjev, kot so Yang s sodelavci (2003) ter Theuns *et al.* (2005).

2.2 Osnovne enačbe prevajanja toplote in vlage

Osnovne enačbe povezanega prevajanja toplote in vlage v kapilarno poroznih snoveh je podal Luikov (1966). Enačbe so kasneje za opis temperaturno-vlažnostnega stanja uporabili številni avtorji, kot na primer Thomas *et al.* (1980), Irudayaraj *et al.* (1990), Gams (2003), Younsi *et al.* (2006a, 2006b), Kocaefe *et al.* (2006), itd. V večini primerov so avtorji uporabili enačbe za opis sušenja lesa. Gams (2003) je enačbe Luikova uporabil za opis temperaturno-vlažnostnega stanja homogenega in lameliranega lesenega nosilca, ki je bil izpostavljen spremenljivim vplivom okolja. Younsi s sodelavci (2006a, 2006b, 2006c) je z omenjenimi enačbami analiziral sušenje lesa pri zelo visokih temperaturah. V vseh primerih je primerjava rezultatov z eksperimentalno dobljenimi rezultati pokazala, da je bila uporaba Luikovih enačb povezanega prehoda toplote in vlage v teh primerih zelo smiselna. To je bil tudi eden od razlogov, da smo se v okviru naloge odločili, da uporabimo Luikove enačbe za opis temperaturno-vlažnostnega stanja kompozitnih lesenih nosilcev, ki zaradi izpostavljenosti požarni obtežbi oglenijo.

Povezan prehod toplote in vlage v kapilarno poroznih snoveh opisujeta dve nelinearni parcialni diferencialni enačbi. Izpeljani sta z uporabo zakona o ohranitvi energije in mase infinitezimalno majhnega dela snovi. Z upoštevanjem naslednjih predpostavk:

- homogen in ortogonalno anizotropen material,
- gravitacijske sile zanemarimo ker so veliko manjše od sil, ki nastopajo v kapilarah,
- materialni in prevodnosti parametri lesa in oglja so odvisni od temperature in vlage,
- krčenje in nabrekanje ter ostale mehanske spremembe lesa in oglja zanemarimo,
- maso plinov oziroma hlapov zanemarimo, masni tok je sestavljen le iz toka kapljevine,
- hitrost pretoka kapljevine skozi snov zanemarimo,
- izparevanje/kondenziranje vode deluje kot energijski izvor/ponor,
- kompozitni nosilec se nahaja v okolju s konstantnim zračnim tlakom,

se enačbe, ki opisujejo povezan problem prehoda toplote in vlage skozi kapilarno porozno snov glasijo

$$\frac{\partial(\rho c_p T)}{\partial t} - (\varepsilon\, h_{LV} + \gamma)\frac{\partial(\rho c_m w)}{\partial t} = \operatorname{div}(\boldsymbol{k}\,\operatorname{grad} T) \tag{2.1}$$

in

$$\frac{\partial(\rho\, c_m w)}{\partial t} = \operatorname{div}\big(\boldsymbol{D_m}\operatorname{grad} w + \boldsymbol{D_T}\operatorname{grad} T\big), \tag{2.2}$$

oziroma v komponentni obliki v primeru dvodimenzionalnega prehoda kot

$$\frac{\partial(\rho c_p T)}{\partial t} - (\varepsilon\, h_{LV} + \gamma)\frac{\partial(\rho c_m w)}{\partial t} = \frac{\partial}{\partial y}\Big(k_y \frac{\partial T}{\partial y}\Big) + \frac{\partial}{\partial z}\Big(k_z \frac{\partial T}{\partial y}\Big) \tag{2.3}$$

ter

$$\frac{\partial(\rho\, c_m w)}{\partial t} = \frac{\partial}{\partial y}\Big(D_{my}\,\frac{\partial w}{\partial y}\Big) + \frac{\partial}{\partial z}\Big(D_{mz}\,\frac{\partial w}{\partial z}\Big) + \frac{\partial}{\partial y}\Big(D_{my}\,\delta_y\,\frac{\partial T}{\partial y}\Big) + \frac{\partial}{\partial z}\Big(D_{mz}\,\delta_z\,\frac{\partial T}{\partial z}\Big). \tag{2.4}$$

V enačbah (2.1–2.2) predstavlja $\boldsymbol{k}$ simetrični tenzor toplotne prevodnosti, ki ima v primeru ortogonalne anizotropije diagonalno obliko. k_y, k_z v (2.3) tako pomenita koeficienta toplotne prevodnosti (W/mK) v dveh pravokotnih smereh y in z pravokotnega prečnega prereza nosilca. Podobno $\boldsymbol{D_m}$ predstavlja diagonalni tenzor prevodnosti vlage, kjer člena D_{my} in D_{mz} v (2.4) predstavljata prevodnostna koeficienta vlage ($\mathrm{kg/m\,s\,^\circ M}$). ρ je specifična gostota snovi ($\mathrm{kg/m^3}$), c_p je specifična toplota snovi ($\mathrm{J/kgK}$), T je temperatura snovi ($^\circ\mathrm{C}$), c_m specifična vlaga snovi ($\mathrm{kg/kg\,^\circ M}$), ε je delež vlage v plinastem stanju, h_{LV} je izparilna toplota snovi (J/kg), γ je toplota sorbcije in desorbcije (J/kg), w je potencial vlage ($^\circ\mathrm{M}$), t je čas (s) in $\boldsymbol{D_T}$ diagonalni termogradientni tenzor, ki ga v primeru otrotropnega materiala izračunamo kot $\boldsymbol{D_T}$=$\boldsymbol{D_m\delta}$. δ_y ter δ_z v (2.4) tako predstavljata termogradientna koeficienta ($^\circ\mathrm{M/K}$) snovi v dveh pravokotnih smereh y in z.

Enačbi (2.1) oziroma (2.3) predstavljata enačbo prehoda toplote skozi snov. Toplota se ne pretaka samo zaradi gradientov temperature. Poleg konstitucijskih enačb toplote, ki so izražene preko Fourierjevega zakona kondukcije toplote, upošteva enačba prehoda toplote tudi vpliv latentne toplote izparevanja in vpliv spremembe potenciala vlage na potek temperature. Vpliv slednjega imenujemo Dufourjev efekt in predstavlja drugi člen na levi strani enačb (2.1) in (2.3). Običajno je ta vpliv v primeru sušenja lesa zanemarljiv, a ga vseeno upoštevamo v enačbah. Podobno, enačbi (2.2) oziroma (2.4) predstavljata pretok mase skozi snov. Poleg konstitucijskih enačb za vlago (Fickov zakon), upoštevata tudi pretok mase (vlage), ki je posledica gradienta temperature (Soretov efekt).

Enačbi (2.1) in (2.3) oziroma (2.2) ter (2.4) predstavljata enačbi za potenciala temperature in vlage. Na ta način dobimo rezultate izražene s potencialoma ($^\circ\mathrm{C}, ^\circ\mathrm{M}$). Vlažost običajno izražamo z vlažnostjo lesa V, ki je definirana kot delež vode glede na maso suhega lesa (kg/kg). Vlažnost lesa V je s potencialom vlage w povezana preko linearne zveze (Luikov, 1966)

$$V = c_m\, w. \tag{2.5}$$

Če želimo rešiti sistem dveh parcialnih diferencialnih enačb (2.1–2.2) oziroma (2.3–2.4), moramo poznati ustrezne robne in začetne pogoje. Začetni pogoji predpisujejo temperaturo in potencial vlage po prečnem prerezu ob začetnem času $t = 0$

$$T(y, z, 0) = T_0(y, z), \tag{2.6}$$

in

$$w(y, z, 0) = w_0(y, z). \tag{2.7}$$

Robni pogoji so lahko različnih tipov in sicer:

- predpisana temperatura in potencial vlage na robu,
- predpisana toplotni in vlažnostni tok na površini,
- toplotni in vlažnostni tok sta linearno odvisna od razlike med temperaturo in vlago na robu in v okolici (naravna ali prisiljena konvekcija),
- toplotni in vlažnostni tok sta nelinearno odvisna od razlike med temperaturo in vlago na robu in v okolici.

V disertaciji bomo upoštevali kombinacijo zadnjih dveh robnih pogojev. Robni pogoj toplotnega prehoda dodatno upošteva vpliv latentne toplote izparevanja, vlažnostni robni pogoj pa vpliv temperaturnega gradienta. Robni pogoji na izpostavljenih zunanjih površinah izenačujejo toplotni pretok s prevajanjem

in vlažnostni pretok po elementu s pretokom, ki je posledica radiacije in konvekcije toplote oziroma konvekcijo vlage med nosilcem in okolico. Robni pogoji se za poljubne poševne robove glasijo

$$-\boldsymbol{n}^T \boldsymbol{k} \mathrm{grad}\, T = h_c\,(T - T_A) + \varepsilon_R\,\sigma\,(T^4 - T_A^4) + (1-\varepsilon)\,h_{LV}\,h_m\,(w - w_A), \tag{2.8}$$

$$-\boldsymbol{n}^T \boldsymbol{D_m} \mathrm{grad}\, w - \boldsymbol{n}^T \boldsymbol{D_T} \mathrm{grad}\, T = h_m\,(w - w_A). \tag{2.9}$$

oziroma v komponentni obliki

$$-k_y \frac{\partial T}{\partial y}\, e_{ny} - k_z \frac{\partial T}{\partial z}\, e_{nz} = h_c\,(T - T_A) + \varepsilon_R \sigma (T^4 - T_A^4) + (1-\varepsilon)\,h_{LV}\,h_m\,(w - w_A) \tag{2.10}$$

in

$$D_{My} \frac{\partial w}{\partial y}\, e_{ny} + D_{Mz} \frac{\partial w}{\partial z}\, e_{nz} + D_{My}\,\delta_y \frac{\partial T}{\partial y}\, e_{ny} + D_{Mz}\,\delta_z \frac{\partial T}{\partial z}\, e_{nz} = -h_m\,(w - w_A). \tag{2.11}$$

V enačbah (2.8–2.9) predstavlja $\boldsymbol{n}$ zunanjo normalo na mejno ploskev. e_{ny} in e_{nz} v enačbah (2.10–2.11) sta tako komponenti zunanje normale $\boldsymbol{n}$, h_c in h_m predstavljata toplotni prestopni koeficient ($\mathrm{W/m^2\,K}$) in vlažnostni prestopni koeficient ($\mathrm{kg/s\,m^2\,{}^\circ M}$). T_A in w_A sta temperatura in potencial vlažnostni okolice (ambienta). Drugi člen na desni strani enačb (2.8) in (2.10) predstavlja vpliv radiacije, kjer je ε_R efektivna površinska emisivnost zunanje strani nosilca in je σ Stephan–Boltzmannova konstanta radiacije, ($\sigma = 5.671 \times 10^{-8}\ W/\mathrm{m^2}K^4$). Temperaturni robni pogoj dodatno upošteva vpliv latentne toplote izparevanja, vlažnostni robni pogoj pa vpliv temperaturnega gradienta.

Kompozitni nosilci so pogosto sestavljeni iz elementov (slojev), ki imajo različne fizikalne lastnosti. Poleg robnih pogojev na površini moramo zato na stiku dveh teles definirati dodatne pogoje. Prvi pogoj je, da sta temperatura in potencial vlage na stiku enaka za oba sloja. Drugi pa, da sta toplotni in vlažnostni tok skozi mejno površino stika enaka za oba sloja. Za delce, ki ležijo na stiku, se dodatni pogoji stika glasijo

$$T_j^i = T_j^{i+1}, \qquad w_j^i = w_j^{i+1}, \tag{2.12}$$

$$-\boldsymbol{n}_j^{iT} \boldsymbol{k}_j^i \mathrm{grad}\, T_j^i = -\boldsymbol{n}_j^{i+1,T} \boldsymbol{k}_j^{i+1} \mathrm{grad}\, T_j^{i+1}, \qquad (i = j = 1, \ldots, N_{\mathrm{sl}}) \tag{2.13}$$

$$-\boldsymbol{n}_j^{iT} \boldsymbol{D_m}_j^i \mathrm{grad}\, w_j^i = -\boldsymbol{n}_j^{i+1,T} \boldsymbol{D_m}_j^{i+1} \mathrm{grad}\, w_j^{i+1}, \tag{2.14}$$

kjer smo z zgornjim indeksom i označili sloj, s spodnjim indeksom j pa stik med slojema i in $i+1$. T_j^i tako predstavlja temperaturo sloja i v j-tem stiku. $\boldsymbol{n}_j^{i+1}$ je vektor zunanje normale sloja $i+1$ na stično površino stika j.

Enačbe (2.1–2.2), (2.8–2.9) in (2.12–2.14) tvorijo začetni-robni problem povezanega prehoda toplote in vlage v lesenem kompozitnem nosilcu, ki je izpostavljen požaru. V kompaktni obliki jih zapišemo v oknu 2.1.

Okno 2.1: Začetni-robni problem povezanega prehoda toplote in vlage v lesenem nosilcu, ki je izpostavljen požaru

Problem povezanega prehoda toplote in vlage kompozitnega nosilca opisuje:

OSNOVNI SISTEM ENAČB:

- $(i = j = 1, \ldots, N_{\mathrm{sl}};\ j \neq N_{\mathrm{sl}})$

$$\frac{\partial(\rho c_p T)}{\partial t} - (\varepsilon\, h_{LV} + \gamma)\frac{\partial(\rho c_m w)}{\partial t} = \operatorname{div}(\boldsymbol{k}\operatorname{grad} T) \tag{2.15}$$

$$\frac{\partial(\rho\, c_m w)}{\partial t} = \operatorname{div}\big(\boldsymbol{D_m}\operatorname{grad} w + \boldsymbol{D_T}\operatorname{grad} T\big), \tag{2.16}$$

pripadajoči naravni (Neumannovi) in bistveni (Dirichletovi) robni pogoji na površini

$$-\boldsymbol{n}^T\boldsymbol{k}\operatorname{grad} T = h_c\,(T - T_A) + \varepsilon_R\,\sigma\,(T^4 - T_A^4) + (1-\varepsilon)\,h_{LV}\,h_m\,(w - w_A), \tag{2.17}$$

$$-\boldsymbol{n}^T\boldsymbol{D_m}\operatorname{grad} w - \boldsymbol{n}^T\boldsymbol{D_T}\operatorname{grad} T = h_m\,(w - w_A). \tag{2.18}$$

ter na stiku dveh slojev

- $(i = j = 1, \ldots, N_{\mathrm{sl}} - 1)$ $\qquad T_j^i = T_j^{i+1}, \qquad w_j^i = w_j^{i+1},$ (2.19)

$$-\boldsymbol{n}_j^{iT}\boldsymbol{k}_j^i\operatorname{grad} T_j^i = -\boldsymbol{n}_j^{i+1,T}\boldsymbol{k}_j^{i+1}\operatorname{grad} T_j^{i+1}, \qquad (i = j = 1, \ldots, N_{\mathrm{sl}}) \tag{2.20}$$

$$-\boldsymbol{n}_j^{iT}\boldsymbol{D_m}{}_j^i\operatorname{grad} w_j^i = -\boldsymbol{n}_j^{i+1,T}\boldsymbol{D_m}{}_j^{i+1}\operatorname{grad} w_j^{i+1}, \tag{2.21}$$

Neznanki osnovnega sistema sta: T^i, w^i

2.3 Diskretizacija. Metoda končnih diferenc

V naravi so problemi povezanega prehoda toplote in vlage praviloma vedno nelinearni in nestacionarni. Kadar so kompozitni leseni nosilci izpostavljeni velikim spremembah temperature, kot je to v primeru požara, je nelinearno in nestacionarno obnašanje še bolj izrazito. Materialne lastnosti lesa so odvisne od temperature in vsebnosti vlage. Analitične rešitve sistema enačb povezanega prehoda toplote in vlage v kapilarno poroznih materialih (2.1–2.2) so tako možne samo v najpreprostejših primerih. V vseh ostalih primerih je reševanje možno le z uporabo numeričnih metod za reševanje nelinearnih parcialnih diferencialnih enačb. Najboj poznane in tudi najpogosteje uporabljene so metoda končnih diferenc, metoda končnih elementov, metoda robnih elementov, itd.

Osrednja točka poglavja je diskretizacija začetnega robnega problema oziroma aproksimacija neznanih funkcij in izbira numerične metode, s katero začetni-robni problem povezanega prehoda toplote in vlage (2.15–2.21) preslikamo v algebrajskega. V ta namen smo v nalogi izbrali metodo končnih diferenc. Osnovna ideja te metode je, da namesto odvodov oziroma neznanih funkcij uporabimo končne razlike točkovnih vrednosti iskanih funkcij. Rešitev problema tako niso vrednosti iskanih zveznih funkcij definiranih po celotnem območju veljavnosti, temveč množica točkovnih vrednosti neznanih funkcij v vnaprej izbranih točkah diferenčne mreže. Uporaba metode končnih diferenc je preprosta in uporabna predvsem za račun problemov, definiranih na pravokotnih območjih različnih dimenzij. S postopnim zgoščevanjem diferenčne mreže metoda v večini primerov konvergira k pravilni rešitvi. Dobra lastnost metode je, da lahko ocenimo njeno natančnost. Metoda je tako zelo uporabna za kontrolo natančnosti nekaterih drugih numeričnih metod, pri katerih napake metode ne moremo oceniti. Taka metoda je na primer metoda končnih elementov. Lastnosti in uporabo diferenčne metode v reševanju problemov prehoda toplote in vlage je v svojih knjigah natančno opisal Özisik (1985, 1994).

Začetni-robni problem (2.15–2.21) lahko torej z diskretizacijo približno rešimo le v vnaprej izbranih točkah diferenčne mreže. Na ta način smo izgubili informacijo o poteku iskanih funkcij med diskretnimi točkami. Vrednosti neznanih funkcij v diskretnih točkah prevedemo na celotno območje z vmesno interpolacijo z uporabo. Zavedati se moramo, da so rešitve v diskretnih točkah le približne in da so v splošnem približne tudi oblikovne funkcije. Izbira oblikovnih funkcij je torej za natančnost rešitve zelo pomembna. Izbira oblikovnih funkcij je v našem primeru relativno preprosta. Glede na to, da v (2.15–2.21) nastopajo drugi odvodi po kraju in prvi odvodi po času, izberemo kvadratičen potek temperature in potenciala vlage po kraju in linearen potek teh količin po času. Izpeljava oblikovnih funkcij je analogna izpeljavi, ki jo je v svoji diplomski nalogi naredil Gams (2003), zato se v nalogi izpeljavi izognemo. Z znanimi oblikovnimi funkcijami lahko temperaturo in potencial vlage v poljubni točki zapišemo v odvisnosti od njunih vrednosti v diskretnih točkah mreže. V primeru dvodimenzionalnega problema se temperatura in potencial vlage glasita

$$T(y,z,t) = \sum_{l=i-1}^{i+1} \sum_{m=j-1}^{j+1} \sum_{n=k}^{k+1} T_{l,m,n} N_{l,m} M_k, \tag{2.22}$$

$$w(y,z,t) = \sum_{l=i-1}^{i+1} \sum_{m=j-1}^{j+1} \sum_{n=k}^{k+1} w_{l,m,n} N_{l,m} M_k, \tag{2.23}$$

kjer so $T_{l,m,n}$ in $w_{l,m,n}$ točkovne vrednosti temperature in potenciala vlaga v točkah diferenčne mreže, $N_{l,m}$ so krajevne in M_k so časovne oblikovne funkcije. Indeks i v tem primeru označuje koordinato y, indeks j koordinato z ter indeks k časovno koordinato, (glej sliko 2.1).

Iz enačb (2.15–2.21) je razvidno, da v teh enačbah nastopajo prvi in drugi odvodi nekaterih funkcij. Z upoštevanjem odvodov oblikovnih funkcij in brezdimenzijskih koordinat (glej Gams (2003)), lahko aproksimirane izraze, ki jih potrebujemo v (2.15–2.21) v razviti obliki zapišemo na naslednji način

$$T = (1-t_b)T_{i,j,k} + t_b T_{i,j,k+1}, \tag{2.24}$$

$$\frac{\partial T}{\partial y} = \frac{(1-t_b)}{2\Delta y}(T_{i+1,j,k} - T_{i-1,j,k}) + \frac{t_b}{2\Delta y}(T_{i+1,j,k+1} - T_{i-1,j,k+1}), \tag{2.25}$$

$$\frac{\partial T}{\partial z} = \frac{(1-t_b)}{2\Delta z}(T_{i+1,j,k} - T_{i-1,j,k}) + \frac{t_b}{2\Delta z}(T_{i+1,j,k+1} - T_{i-1,j,k+1}), \tag{2.26}$$

$$\frac{\partial^2 T}{\partial y^2} = \frac{(1-t_b)}{\Delta y^2}(T_{i+1,j,k} - 2T_{i,j,k} + T_{i-1,j,k}) + \frac{t_b}{\Delta y^2}(T_{i-1,j,k+1} - 2T_{i,j,k+1} + T_{i-1,j,k+1}), \tag{2.27}$$

$$\frac{\partial^2 T}{\partial z^2} = \frac{(1-t_b)}{\Delta z^2}(T_{i,j+1,k} - 2T_{i,j,k} + T_{i,j-1,k}) + \frac{t_b}{\Delta z^2}(T_{i,j+1,k+1} - 2T_{i,j,k+1} + T_{i,j-1,k+1}), \tag{2.28}$$

$$w = (1-t_b)w_{i,j,k} + t_b w_{i,j,k+1}, \tag{2.29}$$

$$\frac{\partial w}{\partial y} = \frac{(1-t_b)}{2\Delta y}(w_{i+1,j,k} - w_{i-1,j,k}) + \frac{t_b}{2\Delta y}(w_{i+1,j,k+1} - w_{i-1,j,k+1}), \tag{2.30}$$

$$\frac{\partial w}{\partial z} = \frac{(1-t_b)}{2\Delta z}(w_{i+1,j,k} - w_{i-1,j,k}) + \frac{t_b}{2\Delta z}(w_{i+1,j,k+1} - w_{i-1,j,k+1}), \tag{2.31}$$

$$\frac{\partial^2 w}{\partial y^2} = \frac{(1-t_b)}{\Delta y^2}(w_{i+1,j,k} - 2w_{i,j,k} + w_{i-1,j,k}) + \frac{t_b}{\Delta y^2}(w_{i-1,j,k+1} - 2w_{i,j,k+1} + w_{i-1,j,k+1}), \quad (2.32)$$

$$\frac{\partial^2 w}{\partial z^2} = \frac{(1-t_b)}{\Delta z^2}(w_{i,j+1,k} - 2w_{i,j,k} + w_{i,j-1,k}) + \frac{t_b}{\Delta z^2}(w_{i,j+1,k+1} - 2w_{i,j,k+1} + w_{i,j-1,k+1}), \quad (2.33)$$

$$\rho = (1-t_b)\rho_{i,j,k} + t_b\rho_{i,j,k+1}, \quad (2.34)$$

$$\frac{\partial k_y}{\partial y} = \frac{(1-t_b)}{2\Delta y}\Big((k_y)_{i+1,j,k} - (k_y)_{i-1,j,k}\Big) + \frac{t_b}{2\Delta y}\Big((k_y)_{i+1,j,k+1} - (k_y)_{i-1,j,k+1}\Big), \quad (2.35)$$

itd. Z vstavitvijo izrazov (2.24–2.35) v (2.15–2.21) dobimo enačbe za notranje točke diferenčne mreže prereza (slika 2.2). Izrazi so zelo dolgi, zato jih podamo na priloženi zgoščenki.

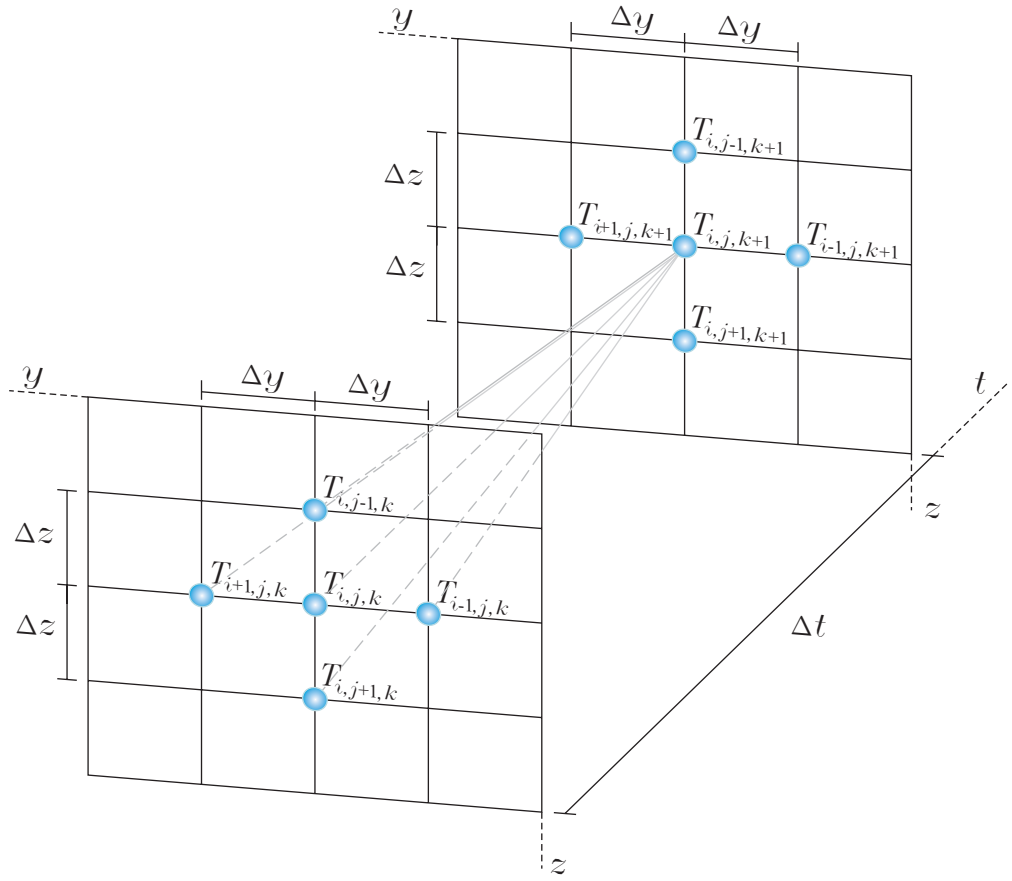

Slika 2.1: Oznake temperatur v točkah diferenčne mreže pri dveh različnih časih.
Figure 2.1: Finite difference points at two different times

Enačbe za robne in vogalne točke ter točke na stiku med sloji lahko izpeljemo z uporabo nesimetričnih ali simetričnih formul (Turk (1987), Gams (2003)). Računanje je praviloma boljše, če pri zapisu enačb uporabimo središčne interpolacije. V tem primeru moramo vpeljati pomožna vozlišča z namišljenimi vrednostmi temperature in potenciala vlage. Na ta način moramo določiti dodatne neznanke, za kar potrebujemo dodatne enačbe. Dobimo jih, če enačbe za notranje točke zapišemo še v robnih točkah (glej sliko 2.2). Izpeljava robnih enačb in enačb na stiku je podrobno predstavljena na zgoščenki.

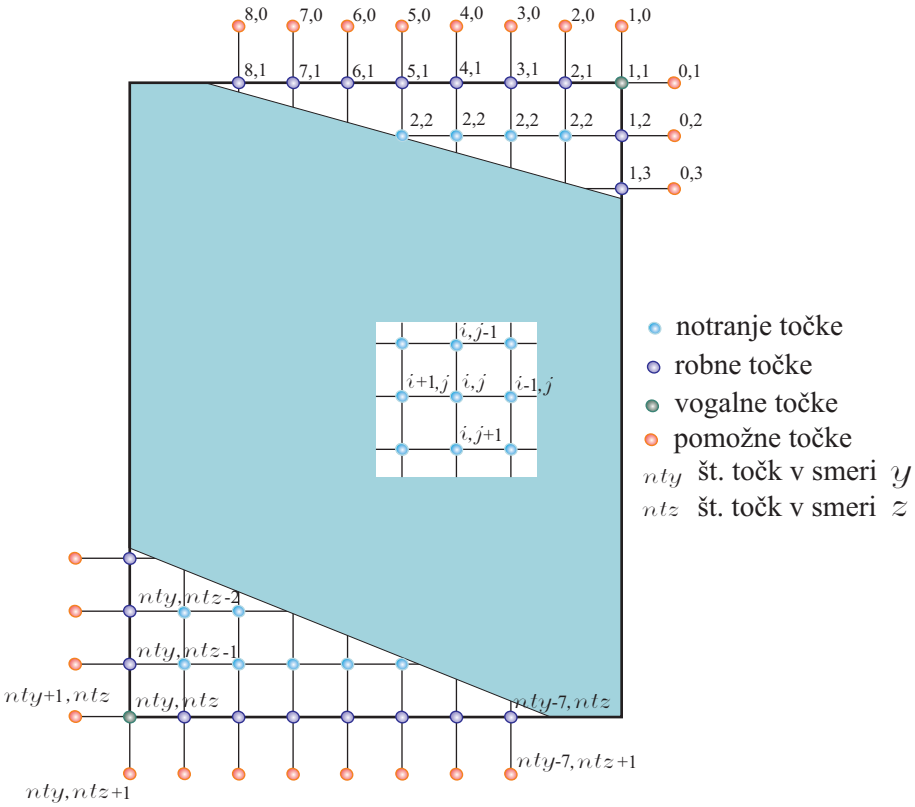

Slika 2.2: Oznake vozlišč izbrane diferenčne mreže glede na lego v prerezu.
Figure 2.2: Finite difference points and their position in the cross-section

V izrazih (2.24–2.35) smo pustili brezdimenzijski čas $0 \leq t_b \leq 1$, kot prosti parameter. Diferenčni metodi, ki brezdimenzijski čas upošteva kot prosti parameter rečemo kombinirana diferenčna metoda. Če hočemo rešiti diskretizirani sistem enačb prehoda toplote in vlage, moramo izbrati vrednost t_b. Glede na izbiro parametra t_b se diferenčna metoda nadalje deli na *čisto eksplicitno* ali *Eulerjevo metodo* ($t_b = 0$), *Cranc-Nicolsonovo metodo* ($t_b = 0.5$), *Galerkinovo metodo* ($t_b = 0.67$) ter *čisto implicitno metodo* ($t_b = 1$).

Z izbiro parametra t_b določimo pri katerem času zadoščamo diferencialnim enačbam, ki jih rešujemo. $t_b = 0$ predstavlja začetek časovnega koraka, $t_b = 1$ pa njegov konec. Različne izbire dajejo v splošnem različno točne rezultate. Pri $0 \leq t_b < 0.5$ je diferenčna metoda pogojno stabilna. Pogoje pogojne stabilnosti podrobno obravnava Özisik (1985, 1994). Stabilnost je v teh primerih odvisna predvsem od izbire velikosti časovnega koraka. Pri $t_b = 0$ dobimo diagonalno matriko, pri $t_b > 0$ pa pasovno matriko. Implicitne metode ($t_b > 0.5$) konverirajo za poljuben časovni korak.

Materialne lastnosti lesa so v veliki meri odvisne od nivoja temperature in vsebnosti vlage. Z vstavitvijo izrazov (2.24–2.35) v enačbe (2.15–2.21) začetnega-robnega problema dobimo diskretiziran sistem enačb prehoda in vlage zapisan v obliki sistema nelinearnih algebrajskih enačb za neznane vrednosti temperature in potenciala vlage v izbranih točkah diferenčne mreže. Za rešitev sistema nelinearnih algebrajskih enačb moramo uporabiti eno izmed iterativnih metod za reševanje sistemov nelinearnih enačb (npr. Navadna oz. Jacobijeva iteracija, Newtonova metoda, kvazi-Newtonove metode, variacijske metode, itd.). Ne glede na izbiro metode je togostna matrika običajno odvisna od temperature in potenciala vlage. Poleg tega je togostna matrika pogosto tudi razpršena in pasovna. Upoštevanje algoritmov za reševanje razpršenih in pasovnih matrik lahko v takem primeru zelo izboljša natančnost rešitev in hitrost

konvergence.

2.4 Piroliza lesa in modeli oglenenja

Les je vnetljiv in gorljiv material. Izpostavljen požaru oziroma visokim temperaturam je podvržen toplotni degradaciji oziroma tako imenovani pirolizi. Piroliza lesa je izjemno kompleksen proces. Predstavlja vzajemno delovanje raznih kemijskih procesov s procesom prehoda toplote in vlage. V nadaljevanju opišemo njene osnove faze. V temperaturnem območju lesa do $100\,^{\circ}\mathrm{C}$ poteka izhlapevanje in izparevanje proste vode ter drugih hlapnih komponent. Izparevanje kemijsko vezane vode je energijsko bolj potraten proces kot izparevanje proste vode v porah. Poteka nad $100\,^{\circ}\mathrm{C}$ pa vse do $220\,^{\circ}\mathrm{C}$, (Younsi, 2006). Pretežen del vodne pare potuje v smeri požaru izpostavljene zunanje površine, manjši del pa v nasprotni smeri. Del vodne pare, ki potuje v smeri zmanjševanja temperature, ponovno kondenzira v območju s temperaturo pod $100\,^{\circ}\mathrm{C}$. Pri temperaturah lesa med $110\,\mathrm{in}\,200^{\circ}\mathrm{C}$ poteka razkroj najmanj stabilnih vlaken lesa. Bolj stabilna vlakna začnejo razpadati v območju med $200\,\mathrm{in}\,270^{\circ}\mathrm{C}$. Posledica razkroja je nastanek najrazličnejših plinov, smol in kislin (ogljikov dioksid, ogljikov monoksid, metan, formaldehid, mravljična in acetilenska kislina, katran, itd.). Tok omenjenih snovi v lesu je podobno kot v primeru vodne pare pretežno v smeri povečevanja temperature. Les pri teh temperaturah poka, se krči in postane črn. Pravimo, da ogleni. Pri temperaturah nekje med $270\,\mathrm{in}\,300^{\circ}\mathrm{C}$ se vname. Temperaturo, pri kateri se les vname, imenujemo vnetišče lesa. Volumen z gorenjem nastalega oglja je manjši kot volumen lesa na začetku. Sloj nastalega oglja zaradi svojih materialnih lastnosti predstavlja nekakšen izolacijski sloj. Pri nadaljnjem povečevanju temperature oglje dodatno razpoka. Razpokanost oglja vpliva na povečan prehod toplote in vlage ter drugih snovi med okoljem (ognjem) ter materialom, ki je podvržen toplotni degradaciji. Pod določenimi pogoji lahko kisik na površini reagira z ogljem, kar povzroči dodatno oksidacijo oglja, ki ima za posledico gorenje in žarenje oglja, (glej sliko 2.3).

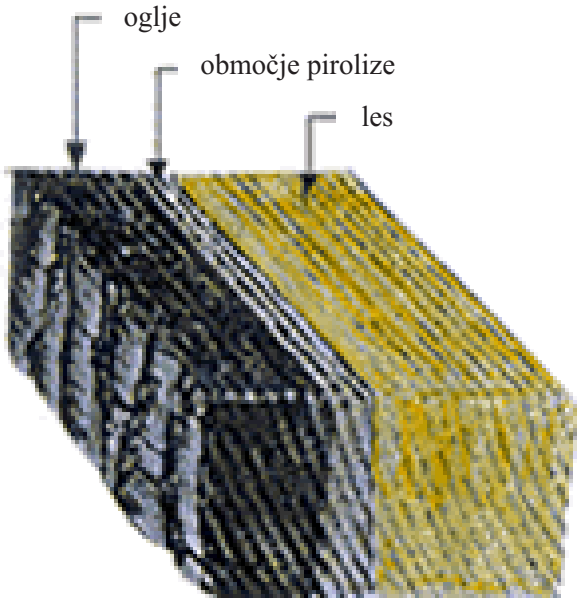

Slika 2.3: Toplotna degradacija lesa.
Figure 2.3: Thermal degradation of wood

Poznavanje lesa pri visokih temperaturah je s stališča dimenzioniranja požarne odpornosti lesenih elementov in konstrukcij izredno pomembno. Požarno odpornost lahko določimo z eksperimenti ali z

uporabo računskih postopkov. Eksperimenti so v večini primerov izredno zahtevni in dragi. Raziskovalci so in še vedno veliko pozornost namenjajo razvoju učinkovitih računskih postopkov za račun požarne odpornosti lesenih konstrukcij. Pomembnost in zahtevnost določitve požarne odpornosti lesa je tudi vzrok velikemu številu člankov na temo toplotne degradacije in oglenenja lesa kot poroznega materiala. Razvitih je bilo mnogo različnih modelov, od zelo preprostih, ki uporabljajo preproste empirične enačbe, pa vse do zelo kompleksnih matematičnih modelov, ki upoštevajo enačbe termodinamike. Velika večina modelov predstavlja enodimenzionalno oglenenje. V literaturi obstaja tudi nekaj modelov dvodimenzionalnega oglenenja, ki so običajno omejeni z velikostjo prečnih prerezov. Modeli se med seboj razlikujejo glede na obseg in zahtevnost v modelu upoštevanih fizikalnih in kemijskih procesov ter osnovnih predpostavk. Nekateri upoštevajo povezan prehod toplote in mase, medtem ko drugi prehod vode in plinov v snovi povsem zanemarijo.

2.4.1 Empirični modeli oglenenja

Številni raziskovalci so na osnovi mnogih rezultatov eksperimentov lesenih nosilcev pri požaru izdelali empirične formule za določitev tako debeline oglja kot tudi hitrosti oglenenja lesenih elementov pri požaru in sicer v odvisnosti od različnih parametrov, kot so vsebnost vlage, gostota lesa, vrsta lesa, tip požarne obtežbe, temperatura vnetišča lesa, itd. Oglenenje lesa opišejo s hitrostjo zmanjševanja mase lesa (g/s) ali s hitrostjo širjenja oglja (mm/s) v notranjost prečnega prereza, izpostavljenega požaru.

V nadaljevanju opišemo poenostavljene modele in empirične formule za določitev hitrosti in debeline oglenenja lesenih elementov v primeru različnih vrst požarne obtežbe in konstantnih lastnosti materiala. V veliki večini primerov je splošna oblika modela naslednja

$$\frac{\partial x}{\partial t} \approx a\, t^n, \tag{2.36}$$

kjer $\dfrac{\partial x}{\partial t}$ pomeni hitrost oglenenja, x je debelina oglja, t je čas izpostavljenosti požarni obtežbi, a in n pa sta regresijski konstanti, ki ju določimo s kalibracijo z eksperimentalnimi rezultati. Eksponent n določa, ali hitrost oglenenja s časom narašča ($n > 0$), pada ($n < 0$) ali je konstantna ($n = 0$). Modeli poleg vpliva časovne izpostavljenosti požarni obtežbi upoštevajo tudi prehodnostne lastnosti materiala, gostoto, vsebnost vlage, itd. Glede na vrsto požarne obtežbe delimo poenostavljene metode na modele, ki določajo hitrost oglenenja v primeru:
(a) standardnega požara (požarna krivulja ASTM E119 (1976) ali ISO 834 (1999)),
(b) nestandardnega požara,
(c) konstantne temperature.

2.4.1.1 Standardni požari

Standardna požarna obtežba je podana s krivuljo časovnega spreminjanja temperature požarnega prostora. Poenostavljeni modeli oglenenja so bili razviti za zelo podobni požarni krivulji (ASTM E119 (1976) ali ISO 834 (1999)). V obeh primerih temperatura požarnega prostora ves čas narašča. Temperatura v primeru požarne krivulje ASTM E119 (1976), ki se uporablja pretežno v Severni Ameriki, se s časom spreminja po naslednji formuli

$$T_g = T_0 + 750\left(1 - e^{-0.49\sqrt{t}}\right) + 22\sqrt{t}, \tag{2.37}$$

medtem, ko se temperatura požarnega prostora po krivulji ISO 834 (1999) spreminja v skladu z enačbo

$$T_g = T_0 + 345\log_{10}(8t + 1), \tag{2.38}$$

kjer T_g pomeni povprečno temperaturo požarnega prostora v °C, T_0 je temperatura okoliškega zraka ob nastopu požarne obtežbe v °C in t je čas izpostavljenosti požaru izražen v minutah.

2.4.1.1.1 AS 1720.4 (1990)

AS 1720.4 je avstralski standard po katerem je hitrost oglenenja podana z enačbo

$$\dot{c} = 0.4 + \left(\frac{280}{\rho}\right)^2, \tag{2.39}$$

kjer je $\dot{c}$ hitrost oglenenja (mm/min), ρ je specifična gostota lesa (kg/m^3) z vsebnostjo vlage 12%. Efektivna globina oglja d_c (mm) je tako določena z linearno funkcijo

$$d_c = \dot{c}\, t + 7.5. \tag{2.40}$$

2.4.1.1.2 Evrokod 5 (2004)

V Evrokodu 5 (2004) je globina oglja d_{char} (mm) v primeru enodimenzionalnega oglenenja lesa, ki požarno ni zaščiten, podana s preprostim izrazom

$$d_{char} = \beta_0 t, \tag{2.41}$$

kjer je β_0 hitrost enodimenzionalnega oglenenja (mm/min) za različne vrste in gostote lesa. Običajno je med $0.5 \leq \beta_0 \leq 0.7$. Evrokod 5 podaja tudi hitrost oglenenja požarno zaščitenih elementov. Predlaga metodo računanja efektivnega prečnega prereza. Pri tej metodi izračunamo efektivni prečni prerez z upoštevanjem zmanjšanja originalnega prečnega prereza zaradi oglenenja. Debelino oglja izračunamo na osnovi izraza

$$d_{ef} = d_{char,n} + k_0\, d_0, \tag{2.42}$$

kjer je $d_0 = 7$ mm. $d_{char,n}$ izračunamo z izrazom (2.41), v katerem namesto koeficienta β_0 upoštevamo koeficient β_n, ki upošteva povečano hitrost oglenenja zaradi vpliva zaokrožitve prečnega prereza ($0.5 \leq \beta_n \leq 0.8$). Koeficient k_0 je v veliki večini primerov enak 1.

2.4.1.1.3 White in Nordheim (1992)

Raziskovalca White in Nordheim (1992), sta empirični model oglenenja določila z regresijsko analizo rezultatov štiridesetih eksperimentov lesenih nosilcev iz osmih različnih vrst lesa, ki so bili izpostavljeni požarni obtežbi določeni z ASTM E 119 (1976). Globino oglja določa izraz

$$t = m\, x_c^{1.23}, \tag{2.43}$$

kjer je m (min/mm) recipročna vrednost hitrosti oglenenja, x_c (mm) je debelina oglja ter t čas izpostavljenosti požaru. Recipročna vrednost hitrosti oglenenja je podana v odvisnosti od specifične gostote v peči sušenega lesa ρ (kg/m^3), njegove vlažnosti u ($\%$) ter faktorja skrčitve f_c kot

$$m = -0.147 + 0.000564\rho + 0.0121u + 0.532 f_c. \tag{2.44}$$

Faktor skrčitve f_c je definiran, kot razmerje debeline oglja na koncu požara in debeline lesa, ki v požaru ogleni. Z uporabo podobne regresijske metode kot zgoraj, sta avtorja v odvisnosti od vrste lesa določila izraz za f_c, ki ima naslednjo obliko

$$f_c = 0.732 - 0.00423d + 0.203c - 0.00164cd - 0.270\rho c. \tag{2.45}$$

V izrazu (2.45) pomeni c klasifikacijski faktor, ki določa tip lesa (1 za les iglavcev, -1 za les listavcev). d (mm) je debelina globinske zaščite lesa z različnimi premazi ($d = 3$ za malo in $d = 36$ za dobro zaščitene vrste lesa).

2.4.1.1.4 Schaffer (1965)

Podobno kot White in Nordheim (1992) je tudi Shaffer (1965) podal izraze recipročne hitrosti oglenenja različnih vrst lesa (B, min/inch) v odvisnosti od vlažnosti lesa M (%) in njegove gostote $\rho(\mathrm{lb/inch^3})$.

$$B = 2\Big((28.726 + 0.578M)\rho + 4.187\Big), \qquad \text{jelka} \tag{2.46}$$

$$B = 2\Big((5.832 + 0.012M)\rho + 12.862\Big), \qquad \text{bor} \tag{2.47}$$

$$B = 2\Big((20.036 + 0.403M)\rho + 7.519\Big). \qquad \text{hrast} \tag{2.48}$$

Vrednosti hitrosti oglenenja c v merskih enotah SI dobimo s preprosto pretvorbo

$$c = 25.4/B \ (\mathrm{mm/min}). \tag{2.49}$$

2.4.1.1.5 Lawson *et al.* (1952)

Lawson s sodelavci (1952) je analiziral oglenenje elementov iz lesa jelke debeline med 38 in 50 mm ter 12% vsebnosti vlage pri požarni obtežbi ASTM E 119 (1976). Hitrost oglenenja je podal z izrazom

$$\frac{\partial x}{\partial t} = 1.04 t^{-0.2}, \tag{2.50}$$

kjer x (mm) pomeni debelino oglja in t čas trajanja izpostavljenosti požaru.

2.4.1.2 Nestandarni požari in požari s konstantno temperaturo

Spreminjanje temperature s časom je v primeru realnih požarov seveda drugačno kot spreminjanje temperature, ki je določeno s standardnimi požarnimi krivuljami. Nekateri avtorji so tako analizirali oglenenje lesa pri nestandardnih požarnih obremenitvah. Modelov na tem področju je zelo malo in v večini primerov veljajo le za točno določeno požarno obremenitev.

2.4.1.2.1 Leceister (1983)

Na podlagi številnih eksperimentov je Leceister (1983) podal oceno za končno debelino oglja z izrazom

$$h_{\text{eff}} = 360\frac{t_{FS}}{\rho} + 1.5\sqrt{t_{FS}} \qquad \text{in pogojem} \qquad 1.5\sqrt{t_{FS}} < 10. \tag{2.51}$$

V izrazu (2.51) je s h_{eff} (mm) označil končno debelino oglja, s t_{FS} čas trajanja požarne obtežbe nad $300\,^{\circ}\mathrm{C}$ in z ρ (kg/m^3) gostoto suhega lesa.

2.4.1.2.2 Mikkola (1990)

Mikkola (1990) je modificiral izraz (2.51), ki ga je podal Leceister (1983), tako da je dodal vpliv specifične gostote in vlažnosti materiala ter koncentracije kisika ambientnega zraka na hitrost oglenenja oziroma končno debelino oglja. Končna debelina oglja izračunana z (2.51) je tako:
(a) obratno sorazmerna z gostoto materiala

$$\frac{1}{\rho(\mathrm{kg/m^2}) + 120}, \tag{2.52}$$

(b) obratno sorazmerna z vlažnostjo

$$\frac{1}{1+2.5w(\%)}. \tag{2.53}$$

Zmanjšanje koncentracije kisika ambientnega zraka z 21% na $8-10\%$ lahko zmanjša hitrost oglenenja za približno 20%. V primeru polno razvitega požara, kjer je koncentracija kisika v zraku lahko zanemarljiva, je možno zmanjšanje hitrosti oglenenja od 35 do 50%.

2.4.1.2.3 Lau *et al.* (1999)

Lau s sodelavci (1999) je analiziral oglenenje petinpetdesetih vzorcev iz borovega lesa v primeru obtežbe s konstantno temperaturo $500\,^{\circ}\mathrm{C}$ in konstantne sile velikosti tretjine natezne nosilnosti. Hitrost oglenenja se je spreminjala od 0.397 mm/min pri $t = 0$, pa do 0.524 mm/min pri $t = 1000$ s. Povprečna hitrost oglenenja je bila približno 0.451 mm/min. Z metodo linearne regresije so določili približno velikost efektivnega prečnega prereza z naslednjim izrazom

$$A(t) = -1.628t + 3080, \tag{2.54}$$

kjer je A (mm^2) efektivni prečni prerez in t (s) čas. Z enačbo (2.54) so določili koeficient hitrosti oglenenja β (mm/min) in sicer kot

$$\beta(t) = -\frac{\alpha}{8}\left[\frac{\alpha t}{4} + \frac{1}{16}(a_0 + b_0)^2\right]^{1/2}, \tag{2.55}$$

kjer je t čas, a_0 in b_0 sta dimenziji prečnega prereza v milimetrih in $\alpha = \dfrac{\partial A(t)}{\partial t} = -1.628$.

2.4.1.2.4 Schaffer (1965)

Schaffer (1965) je preiskoval hitrost oglenenja v primeru desk debeline približno 10 cm in vlažnostjo med 6 in 18%, ki so bile podvržene konstantni temperaturi $500, 816$ in $927\,^{\circ}\mathrm{C}$ le z ene strani. V primeru jelke, izraz, iz katerega izračunamo hitrost oglenenja lesa, izgleda takole:

$$t = -k\ln\left(1 - \frac{x}{3}\right)e^{\frac{JE}{RT}}, \tag{2.56}$$

kjer je

$$k = (28.576 + 0.576\omega)\rho + 4.548 \tag{2.57}$$

in je $J = 4.184$ J/cal Joulova konstanta, $R = 8.14$ J/g mol/K je plinska konstanta, $E = 3108$ cal/gmol je reakcijska energija, x (inch) je debelina oglja, ω (%) je vsebnost vlage, T (K) je temperatura lesa in t (s) je čas.

2.4.2 Numerični modeli oglenenja

Območje veljavnosti razvitih empiričnih modelov oglenenja lesa je pogosto omejeno na enodimenzionalne primere s preprosto geometrijo in konstantnimi materialnimi karakteristikami ter standardnimi požarnimi obtežbami. Potreba po splošnejšem opisu oglenenja lesa je pripeljala do razvoja matematičnih modelov oglenenja. Ti se med seboj razlikujejo glede na stopnjo opisa fizikalnih in kemijskih procesov, ki potekajo v lesu med požarom. Večina modelov upošteva samo prehod toplote brez upoštevanja vlage, medtem ko drugi poleg prehoda toplote in mase (vlaga, plini, smole, itd.) upoštevajo tudi vpliv drugih parametrov, kot so koncentracija kisika v zraku in krčenje oglja. Razlikujejo se tudi glede upoštevanja različnih faz v procesu oglenenja lesa in določitvi pogojev, ki določajo prehod med njimi. Kljub velikemu zanimanju po splošnejšem opisu oglenenja lesa, obstaja v literaturi zelo malo matematičnih modelov na to temo. V nadaljevanju zelo na kratko opišemo nekaj modelov.

2.4.2.1 Takeda (2003)

Takeda (2003) je razvil dvodimenzionalni model za račun oglenenja mavčnih in lesenih desk. Razviti model temelji na osnovni enačbi dvodimenzionalnega prevajanja toplote skozi snov

$$c_p\rho\frac{\partial T}{\partial t} = \frac{\partial}{\partial x}\Big(k\frac{\partial T}{\partial x}\Big) + \frac{\partial}{\partial y}\Big(k\frac{\partial T}{\partial y}\Big), \tag{2.58}$$

kjer je za toplotno odvisne materialne parametre (c_p, ρ, k) upošteval eksperimentalne rezultate, ki jih je dobil v literaturi. V robnih pogojih je upošteval prevajanje toplote s konvekcijo in radiacijo. Pomembna omejitev modela je, da ne upošteva vpliva vsebnosti vlage na razporeditev temperature po snovi in s tem tudi na proces oglenenja. Kljub temu poroča, da se rezultati dobro ujemajo z rezultati eksperimentov, ki jih je opravil.

2.4.2.2 Janssens (2004)

Zelo podoben model, kot ga je predstavil Takeda (2003), je izpeljal tudi Janssens (2004). Enačbi prevajanja toplote skozi snov je dodal člen s katerim je zajel vpliv izparevanja in kondenziranja vode v lesu med požarom. Omenjena vpliva je upošteval kot ponor oziroma izvor toplotne energije. Razviti model oglenenja upošteva enačbo enodimenzionalnega prevajanja toplote skozi snov

$$c_p\rho\frac{\partial T}{\partial t} = \frac{\partial}{\partial x}\Big(k\frac{\partial T}{\partial x}\Big) - (\Delta h_v + \Delta h_w)\rho_0\frac{\partial u}{\partial t}, \tag{2.59}$$

kjer je ρ_0 gostota suhega lesa (kg/m^3), u je vsebnost vlage v lesu (kg), Δh_v je latentna toplota izparevanja (J/kg) in Δh_w je toplota kondenzacije (J/kg). Model oglenenja upošteva materialne lastnosti lesa ($T \leq 200\,^\circ$C), delno zoglenelega lesa ($200\,^\circ\text{C} < T < 800\,^\circ$C) in oglja ($T \geq 800\,^\circ$C). Poleg tega upošteva tudi vpliv krčenja oglja.

2.4.2.3 Fredlund (1988)

Fredlund (1988, 1993) je razvil izredno izpopolnjen model oglenenja. Pri tem je upošteval tako pretok energije, kot tudi pretok mase. Upošteval je pretok energije zaradi prevajanja toplote (kondukcija) skozi snov kot tudi zaradi konvekcijskega toka produktov pirolize in vodne pare skozi pore obravnavanega lesa. Pri tem je upošteval, da je v vsaki točki obravnavanega telesa izpolnjeno termodinamično ravnovesje. Originalno vlažen les je razdelil na štiri različne faze: les, oglje, vodno paro, vodo. Količina energije na enoto volumna je tako enaka vsoti energij posameznih komponent. Toplotne lastnosti materiala v določeni točki je izračunal kot povprečno vrednost toplotnih lastnosti posameznih materialnih komponent. Osnovna enačba o ohranitvi energije ima tako v dveh dimenzijah obliko

$$\rho c\frac{\partial T}{\partial t} = \frac{\partial}{\partial x}\Big(\lambda_x\frac{\partial T}{\partial x}\Big) + \frac{\partial}{\partial y}\Big(\lambda_y\frac{\partial T}{\partial y}\Big) - \kappa_x\frac{\partial T}{\partial x} - \kappa_y\frac{\partial T}{\partial y} + Q_1^* + Q_2^*, \tag{2.60}$$

kjer pomeni T temperaturo, c specifično toploto, λ je koeficient toplotne prehodnosti, κ je konvekcijski koeficient (W/m^2), Q_1^* in Q_2^* pa sta ponora/izvora energije zaradi pirolize lesa ter izhlapevanja oziroma kondenziranja vode oziroma vodne pare.

Prehod vlage skozi snov lahko poteka na dva načina: s pretokom pare pare in tokom tekočine. Gonilne sile, ki povzročajo prehod vlage skozi snov so gradienti vlage, pritiska in temperature po snovi. Razlike v vsebnosti vlage so posledica toka vlage, ki je opisan s Fickovim zakonom, kot posledica gradientov pritiska pa z Darcyjevim zakonom. Model masnega pretoka, ki ga uporabi Fredlund (1988, 1993) temelji

na spremembi pritiskov v lesu. Poleg tega dodatno upošteva, da je masni tok vlage v obliki tekočine zaradi majhnih hitrosti zanemarljiv. Osnovna diferencialna enačba masnega pretoka je tako

$$\omega \frac{\partial P}{\partial t} = \frac{\partial}{\partial x}\left(\phi_x \frac{\partial P}{\partial x}\right) + \frac{\partial}{\partial y}\left(\phi_y \frac{\partial P}{\partial y}\right) + \psi P + G^*, \tag{2.61}$$

kjer je P pritisk (Pa), ω je masna kapaciteta (mol/J), ϕ je koeficient masnega pretoka (mol s/kg), ψ je koeficient toplotnega raztezka (mol/Js). Robni pogoji v primeru enačbe (2.60) predstavljajo izmenjavo energije telesa z okolico in so podani kot predpisan toplotni tok ali predpisana temperatura na robu. V prvem primeru tako upoštevajo vpliv konvekcije in radiacije energije na robu. Robni pogoji v primeru enačbe 2.61 pa so predpisani masni tokovi na robovih elementa. Primerjava modela z eksperimentalnimi rezultati pokaže zelo dobro ujemanje.

Na koncu omenimo še, da je Fredlund (1988, 1993) analiziral tudi hitrost oglenenja oziroma povečevanje debeline oglja. V ta namen je definiral pogoj nastanka oglja. Določil je, da oglje v določeni točki nastane, ko gostota materiala v tej točki pade pod 300 kg/m^3. Tudi v tem primeru je dobil zelo dobro ujemanje z eksperimentalno dobljenimi rezultati debeline oglja.

2.4.2.4 Schnabl in Turk (2006)

V disertaciji predstavimo model, ki smo ga razvili v okviru doktorskega dela in predstavili v Schnabl in Turk (2006a, 2006b, 2006c). Matematični model oglenenja ni tako splošen kot model Fredlunda (1988, 1993). V procesu pirolize upoštevamo le dve materialni fazi: les in oglje. Poleg tega zanemarimo vpliv tlaka na povezan prehod toplote in vlage v porozni snovi ter vpliv konvekcijskega dela toka tekočine (vlage in drugih produktov pirolize) k energijskemu oziroma toplotnemu toku skozi snov. Osnovni enačbi, ki opisujeta matematični model sta enačbi Luikova (2.3–2.4):

$$\frac{\partial(\rho c_p T)}{\partial t} - (\varepsilon\, h_{LV} + \gamma)\frac{\partial(\rho c_m w)}{\partial t} = \frac{\partial}{\partial y}\left(k_y \frac{\partial T}{\partial y}\right) + \frac{\partial}{\partial z}\left(k_z \frac{\partial T}{\partial y}\right) \tag{2.62}$$

ter

$$\frac{\partial(\rho\, c_m w)}{\partial t} = \frac{\partial}{\partial y}\left(D_{my}\, \frac{\partial w}{\partial y}\right) + \frac{\partial}{\partial z}\left(D_{mz}\, \frac{\partial w}{\partial z}\right) + \frac{\partial}{\partial y}\left(D_{my}\, \delta_y\, \frac{\partial T}{\partial y}\right) + \frac{\partial}{\partial z}\left(D_{mz}\, \delta_z\, \frac{\partial T}{\partial z}\right). \tag{2.63}$$

Poleg enačb (2.3–2.4), osnovne enačbe modela sestavljajo tudi začetni in robni pogoji ter pogoji na meji med dvema materialoma, glej enačbe v oknu 2.1, (2.17–2.21). Pomen oznak smo že razložili v poglavju Osnovne enačbe prevajanja toplote in vlage. Pri določitvi temperaturno-vlažnostnega stanja in oglenenja lesa v primeru požara, model upošteva povezan prehod toplote in vlage skozi snov. Pri tem omogoča upoštevanje poljubne požarne obtežbe in materialnih karakteristik materiala, ki so lahko odvisne od smeri materialnih vlaken, od temperature, nivoja vlage, gostote materiala, vrste lesa, itd. Tudi temperatura vnetišča lesa, to je temperatura, ko les začne goreti in nastane oglje, je poljubna. V večini primerov vzamemo, da je temperatura vnetišča lesa od 270 do $300\,^\circ$C.

2.5 Materialne lastnosti lesa pri visokih temperaturah

Matematični modeli oglenenja predstavljajo v primerjavi z eksperimenti zelo poceni in uporabno sredstvo za opis obnašanja lesa v primeru visokih temperatur, kot je požar. Za primerno oceno obnašanja lesenih elementov med požarom moramo zanesljivo določiti materialne lastnosti pri visokih temperaturah. Materialne lastnosti lesa so poleg temperature odvisne tudi od vsebnosti vlage, gostote materiala,

smeri materialnih vlaken, vrste lesa, načina obdelave lesa, itd. V literaturi obstaja veliko eksperimentalnih podatkov in empiričnih formul za določitev lastnosti materiala v odvisnosti od najrazličnejših parametrov. Raztros rezultatov je zelo velik. V nadaljevanju grafično predstavimo odvisnosti parametrov, kot so koeficient toplotne prehodnosti k, specifične toplote materiala c in gostote materiala ρ, v odvisnosti od temperature. Slika 2.4 prikazuje temperaturno odvisnost koeficienta toplotne prevodnosti k, kot so jo določili različni avtorji.

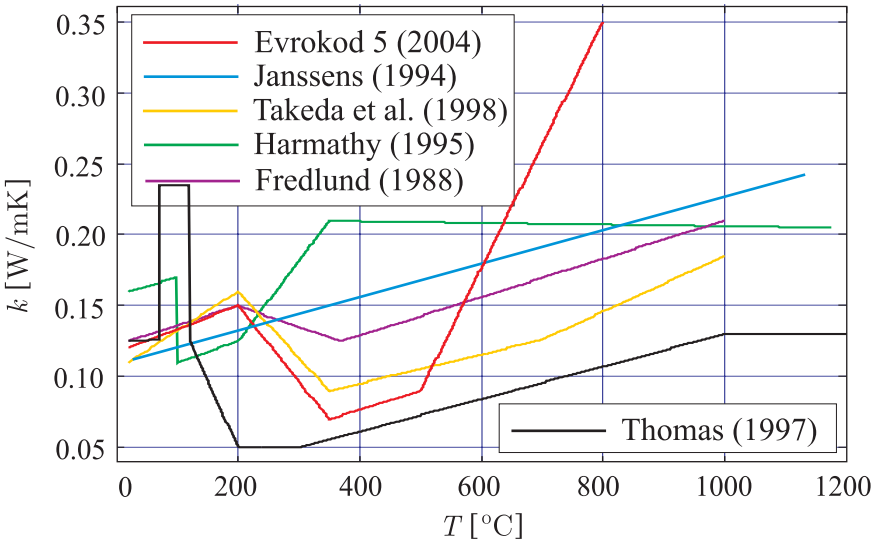

Slika 2.4: Koeficient toplotne prevodnosti lesa k v odvisnosti od temperature T.
Figure 2.4: Thermal conductivity k of wood as a function of temperature T

S slike 2.4 je razvidno, da toplotna prevodnost v območju temperatur od 100 do $200\,^{\circ}\mathrm{C}$ narašča, potem v območju od 100 do $350\,^{\circ}\mathrm{C}$ linearno pada in nato pri temperaturi nad $350\,^{\circ}\mathrm{C}$ ponovno narašča. Kljub temu, da je trend razporeda toplotne prevodnosti v odvisnosti od temperature za različne avtorje podoben, se vrednosti zelo razlikujejo. Ker je raztros rezultatov velik, je izredno težko določiti krivuljo srednje vrednosti toplotne prevodnosti. Raztros je posledica analize različnih vrst lesa z različnimi gostotami in vsebnostmi vlažnosti. Raztros je tudi posledica uporabe različnih metod za določitev toplotne prevodnosti. Takeda *et al.* (1998) je za določitev k uporabil različne vrednosti iz literature. Thomas (1997) je vrednosti k določil s kombinacijo dveh različnih izrazov za določitev k, ki jih je našel v literaturi. Harmathy (1995) in Fredlund (1988) sta k določila eksperimentalno, medtem ko je Janssens (1994) odvisnost izračunal na osnovi gostote suhega lesa in vsebnosti vlage.

Specifična toplota lesa c_p v odvisnosti od temperature T je podana na sliki 2.5. Skok specifične toplote v območju $90 < T < 110\,^{\circ}\mathrm{C}$ je posledica izparevanja vode v lesu. Podobno kot v primeru toplotne prevodnosti je tudi tukaj raztros rezultatov dokaj velik. Vzrok raztrosa rezultatov je podoben kot pri analizi toplotne prevodnosti.

Zmanjševanje gostote materiala ρ z višanjem temperature T prikazuje slika 2.6. V splošnem je gostota lesa med 300 in 700 kg/m^3. Evrokod (2004), Janssens (1994) in Takeda *et al.* (1998) predlagajo podobne vrednosti razmerja gostote lesa pri temperaturi T proti gostoti lesa pri $T = 20\,^{\circ}\mathrm{C}$. Zmanjševanje gostote lesa pri temperaturah do $200\,^{\circ}\mathrm{C}$ je v glavni meri posledica izhlapevanja in izparevanja vode. Pri T približno $200\,^{\circ}\mathrm{C}$ je razmerje gostot med 0.9 in 0.95. Dodatnemu povečanju temperature sledi izrazit padec gostote. Pri T približno $400\,^{\circ}\mathrm{C}$ gostota lesa pade na približno 20% prvotne vrednosti. Pri T nad $400\,^{\circ}\mathrm{C}$ ostane gostota materiala praktično nespremenjena.

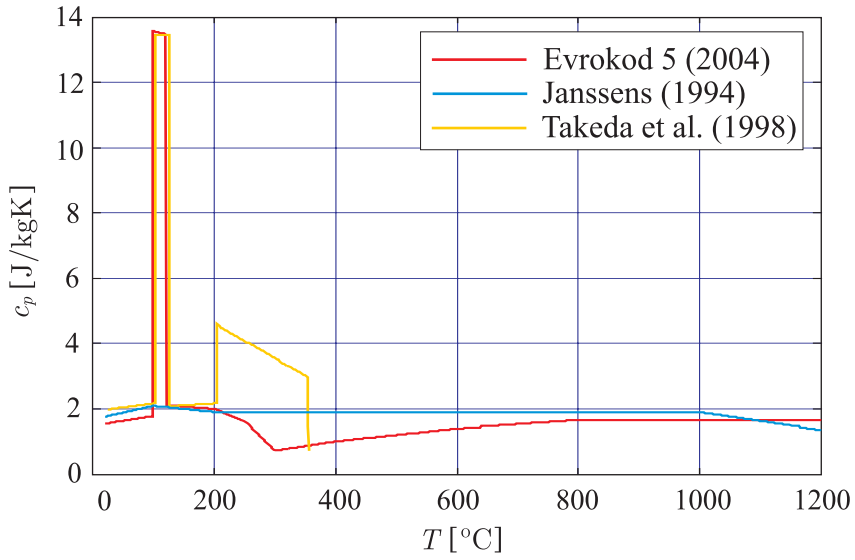

Slika 2.5: Specifična toplota lesa c_p v odvisnosti od temperature T.
Figure 2.5: Specific heat c_p of wood as a function of temperature T.

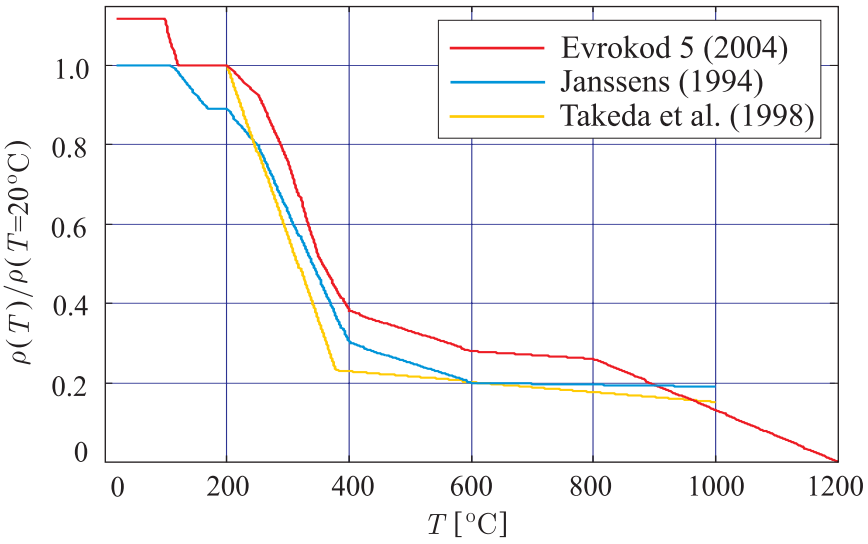

Slika 2.6: Gostota lesa ρ v odvisnosti od temperature T.
Figure 2.6: Density ρ of wood as a function of temperature T.

2.6 Računski primeri

Z računskimi primeri prikažemo učinkovitost in primernost v disertaciji predstavljenega matematičnega modela oglenenja za analizo obnašanja lesenih nosilcev pri požaru. Računske primere smo razdelili vsebinsko v dve skupini.

V prvi skupini primerjamo predstavljeni matematični model oglenenja z različnimi empiričnimi modeli enodimenzionalnega oglenenja, ki so predlagani v literaturi. Poleg tega predstavljeni model primerjamo tudi z eksperimentalnimi rezultati, ki jih je predstavil Fredlund (1988, 1993). Na koncu izvedemo tudi parametrično analizo, s katero analiziramo vpliv izbranih parametrov na hitrost oglenenja.

V drugi skupini predstavljeni matematični model oglenenja uporabimo za analizo oglenenja dvodimenzionalnih homogenih prečnih prerezov. Poleg homogenih prerezov obravnavamo tudi slojevite prereze. V primeru slednjih izračunamo razporeditev temperature pri različnih časih požarne obtežbe. Dobljeno razporeditev temperature po prečnem prerezu dvoslojnega lesenega nosilca potrebujemo v drugem delu disertacije pri mehanski analizi kompozitnih nosilcev pri sočasnem delovanju zunanje statične mehanske obtežbe in obtežbe požara.

2.6.1 Enodimenzionalno oglenenje lesenih nosilcev

2.6.1.1 Primerjava z empiričnimi modeli

V literaturi obstaja mnogo empiričnih modelov za določitev hitrosti enodimenzionalnega oglenenja lesenih nosilcev. Uporabni so za različne vrste požarne obtežbe (standardna, nestandardna in konstantna). Velika večina empiričnih modelov je bila razvita na osnovi eksperimentalnih rezultatov lesenih nosilcev, podvrženih standardni požarni obtežbi ISO 834 (1999) in ASTM E119 (1976).

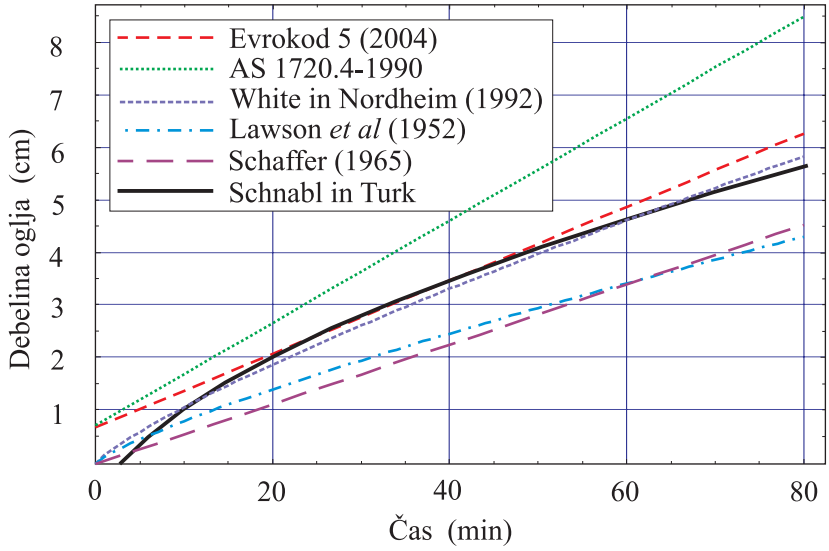

Slika 2.7: Primerjava različnih enodimenzionalnih modelov oglenenja lesa.
Figure 2.7: Comparison of different charring models.

Zaradi tega se odločimo, da v disertaciji predstavljeni matematični model oglenenja primerjamo z empiričnimi modeli oglenenja v primeru standardne požarne obtežbe. Empirični modeli upoštevajo konstantne materialne karakteristike lesa in se med seboj ločijo glede na število parametrov, ki vplivajo na hitrost oglenenja (glej poglavje Empirični modeli oglenenja). Pri računu smo upoštevali enodimenzionalno oglenenje smrekovega nosilca debeline d, ki je izpostavljen standardni požarni obtežbi ISO 834 (1999). Materialne podatke omenjenega smrekovega nosilca sta podala Chang in Weng (2000) in so naslednji:

$$T_0 = 20°\mathrm{C},\ \ w_0 = 13°\mathrm{M},\ \ w_A = 4°\mathrm{M}, \rho = 370\ \mathrm{kg/m^3},\ \ k_{\mathrm{les}} = 0.12\ \ k_{\mathrm{oglje}} = 0.15\ \mathrm{W/(m\,K)},$$
$$D_M = 2.2 \times 10^{-8}\ \mathrm{kg/(m\,s\,°M)},\ \ h_{LV} = 2500\ \mathrm{kJ/kg},\ \ h_c = 22.5\ \mathrm{W/(m^2\,K)},\ \ \varepsilon = 0,3,$$
$$c_{p\,\mathrm{les}} = 1530\mathrm{J/(kg\,K)},\ \ c_{p\,\mathrm{oglje}} = 1050\ \mathrm{J/(kg\,K)},\ \ c_m = 0.01\ \mathrm{kg/(kg\,°M)},\ \ \delta = 2.0\ °\mathrm{M/K},$$
$$h_m = 2.5 \times 10^{-6}, \mathrm{d} = 0.3\ \mathrm{m},\ \ \gamma = 0. \tag{2.64}$$

Primerjavo modelov prikazuje slika 2.7. Velika večina modelov (Schaffer (1965), Evrokod 5 (2004), AS 1720.4 (1990)) predlaga konstantno hitrost oglenenja. Uporaba oziroma upoštevanje konstantnega oglenenja je pripravna, a ne odraža dejanskega obnašanja lesa. Nelinerni model oglenenja so razvili Lawson *et al.* (1952) ter White in Nordheim (1992). Iz primerjave različnih modelov je razvidno, da se v večini primerov razlike med posameznimi modeli s časom povečujejo. Razlika v debelini oglja, ki jo predlagata avstralski standard AS 1720.4 (1990) in Schaffer (1965), je po 80-ih minutah skoraj 100%. Opaziti je izredno dobro ujemanje predlaganega modela z modeloma, ki ju predlagajo Evrokod 5 (2004) ter White in Nordheim (1992). S slike 2.7 se tudi vidi, da empirični modeli, ki jih primerjamo, predpostavljajo začetek oglenenja ob nastopu požarne obtežbe. To seveda ne predstavlja dejanskega stanja. V našem modelu je upoštevano, da les začne ogleneti, ko temperatura doseže temperaturo pirolize ($300\,^{\circ}\mathrm{C}$). To se zgodi približno 3 minute po začetku požara.

2.6.1.2 Primerjava z eksperimentalnimi rezultati

V literaturi ni mnogo objav podatkov oziroma rezultatov eksperimentalnega opazovanja oglenenja lesenih nosilcev pri požaru.

Eden redkih primerov eksperimentalnega analiziranja lesenih nosilcev pri požaru predstavlja delo švedskega raziskovalca Fredlunda (1988, 1993). Eksperimentalno in numerično je obravnaval primer smrekovega nosilca začetne vsebnosti vlage 14.5%. Z dodatnimi eksperimenti je določil temperaturno odvisne termomehanske lastnosti lesa pri visokih temperaturah (Fredlund, 1988). Temperaturno odvisne lastnosti materiala, ki jih podaja Fredlund (1988), smo upoštevali pri izračunu oglenenja z našim matematičnim modelom. Primerjava rezultatov je podana na sliki 2.8.

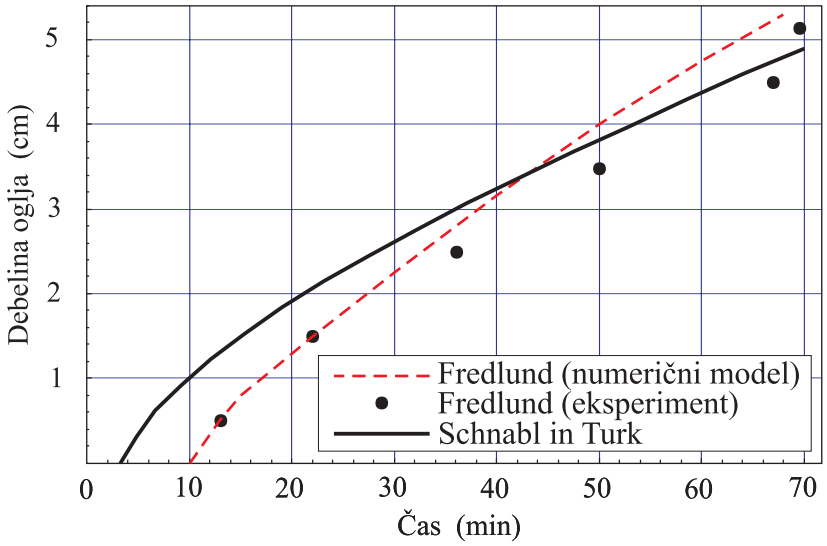

Slika 2.8: Primerjava numeričnih in eksperimentalnih rezultatov debeline oglja smrekovih nosilcev začetne vlažnosti 14.5%.
Figure 2.8: Comparison of experimental and numerical results for penetration of the char layer as a function of time for spruce with initial moisture content of 14.5%.

Primerjava pokaže, da se modela razlikujeta predvsem glede časa, ko les začne ogleneti, kar je lahko posledica različne definicije začetka oglenenja. Fredlund (1988, 1993) nastanek oglja definira kot stanje, kjer specifična gostota lesa pade pod 300 kg/m^3, medtem ko v našem primeru oglje nastane, ko les doseže temperaturo $300\,^{\circ}\mathrm{C}$. Kljub temu se razlike s časom zmanjšujejo do približno 45-ih minut, ko je debelina oglja v obeh primerih enaka. Primerjava z eksperimentalnimi rezultati je v obeh primerih dobra. Na

začetku je model Fredlunda bližje rezultatom eksperimenta, po 45 minutah pa model Fredlunda očitno precenjuje hitrost oglenenja.

2.6.1.3 Parametrična študija

Matematični model oglenenja lesa lahko uporabimo za parametrično analizo, s katero ugotavljamo vpliv različnih parametrov na hitrost oglenenja. V sklopu izvedene parametrične analize smo analizirali vpliv začetne vlažnosti w_0 in specifične gostote lesa ρ na obnašanje lesenih nosilcev pri standardnem požaru. V ta namen smo za različne vrednosti začetne vlage in specifične gostote lesa izračunali debelino oglja pri različnih časih požarne obtežbe. Vpliv začetne vlažnosti lesa na hitrost oglenenja je prikazana na sliki 2.9.

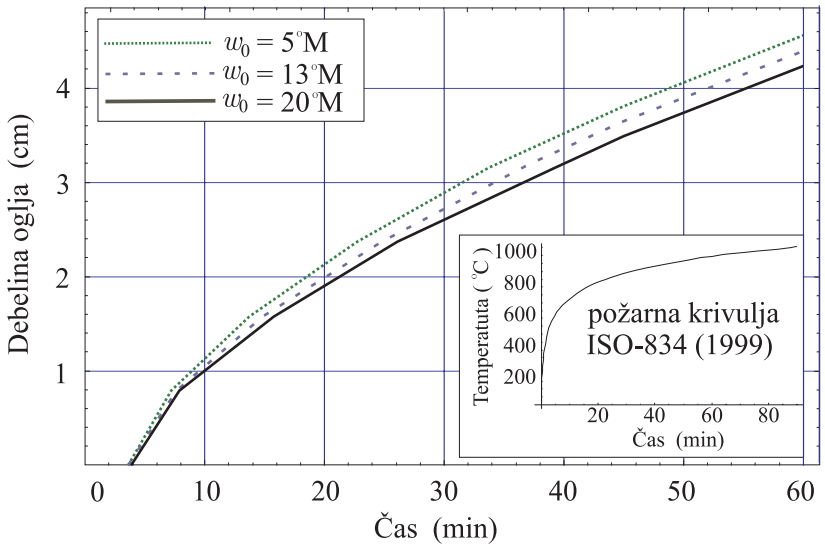

Slika 2.9: Vpliv začetne vlažnosti lesa na hitrost oglenenja.
Figure 2.9: Numerical results for penetration of the char layer as a function of time for different initial moisture contents.

Iz slike 2.9 je razvidno, da se z večanjem začetne vlažnosti lesa hitrost oglenenja zmanjšuje, medtem ko se čas začetka oglenenja povečuje. Hitrost oglenenja je pričakovano največja v primeru suhega lesa ($w_0 \approx 5\,°\mathrm{M}$). Razlika debelin oglja v primeru suhega lesa in lesa začetne vlažnosti 20% znaša po eni uri približno 0.4 cm. Vpliv vlage je najbolj izrazit v prvih 30-ih minutah. Čas potreben za dosego določene debeline oglja je v primeru različnih vlažnosti zelo različen. Na primer, za enako debelino oglja (približno 3 cm), potrebuje suh les okoli 8 minut manj kot les z začetno vlažnostjo $20\,°\mathrm{M}$. Omenjeni časovni zamik bistveno vpliva na nosilnost lesenih nosilcev. Glede na povedano, lahko zaključimo, da ima vlažnost lesa pomemben vpliv na hitrost oglenenja.

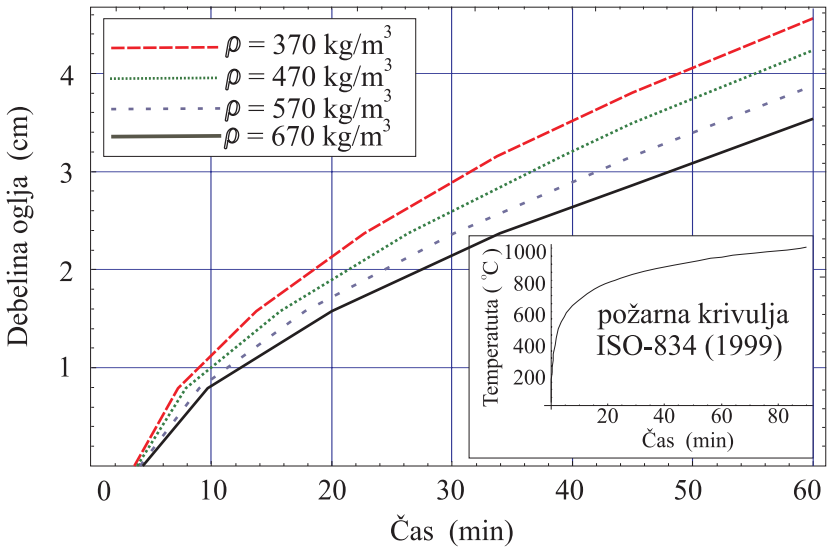

Slika 2.10: Vpliv gostote materiala na hitrost oglenenja.
Figure 2.10: Numerical results for penetration of the char layer as a function of time for different densities of wood.

Vpliv gostote lesa ρ na oglenenje prikazuje slika 2.10. Vidimo, da ima gostota lesa pomemben vpliv na hitrost oglenenja. Les z višjo gostoto začne ogleneti kasneje in ogleni počasneje kot les z nižjo gostoto. Razlike v debelini oglja se v primeru različnih gostot lesa s časom povečujejo. Pri času 60 min, je debelina zoglenelega lesa z $\rho \approx 370$ kg/m^3 približno za 35% večja, kot v primeru, ko je $\rho \approx 670$ kg/m^3.

2.6.2 Dvodimenzionalno oglenenje lesenih nosilcev

2.6.2.1 Homogeni leseni prerez

Obravnavamo oglenenje homogenega lesenega nosilca, ki je izpostavljen standardnemu požaru ISO 834 (1999) s treh strani, medtem ko je zgornja stran nosilca toplotno in vlažnostno izolirana. Začetni prečni prerez nosilca je pravokotne oblike dimenzij 10×15 cm. Prečni prerez nosilca diskretiziramo z ekvidistantno diferenčno mrežo 30×45 točk. Uporabimo enake materialne lastnosti kot pri enodimenzionalnem primeru. Rezultati simulacije izpostavljenosti požaru pri časih 1.2, 10, 20 in 30 minut so prikazani na slikah 2.11.

Ker so vogali izpostavljeni prehodu toplote in vlage z dveh različnih strani, je oglenenje najhitrejše v vogalih. Zato se oglenenje prečnega prereza vedno začne prav v vogalih. Pojavi se tako imenovani zaokrožitveni efekt, ki ima za posledico spreminjanje oblike prečnega prereza, ki kmalu po začetku gorenja ni več pravokoten.

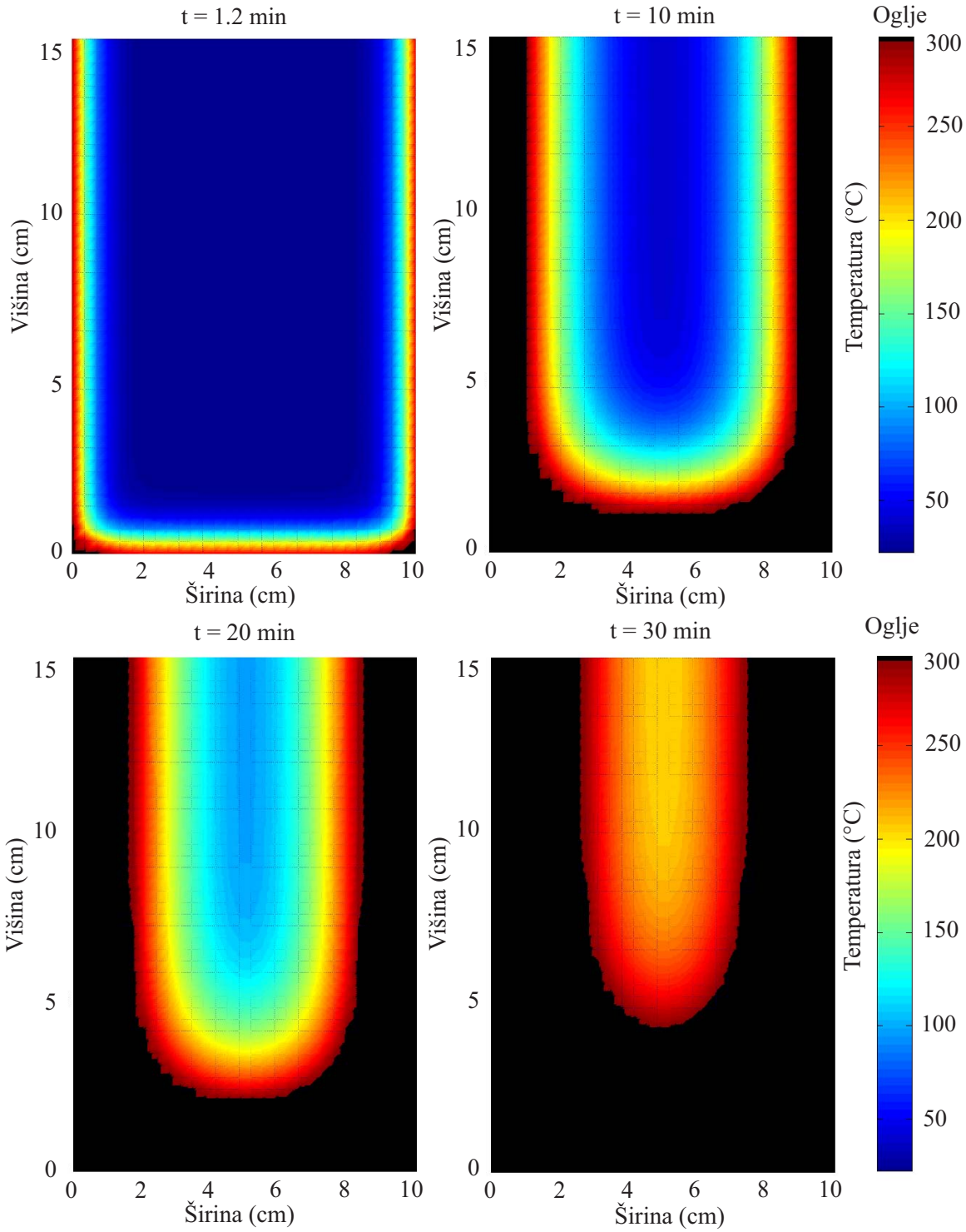

Slika 2.11: Porazdelitev temperature po prečnem prerezu smrekovega nosilca začetne vsebnosti vlage 13% in degradacija lesa v oglje pri 1.2, 10-ih, 20-ih in 30-ih minutah.

Figure 2.11: Temperature distribution in cross-section of spruce beam with initial moisture content of 13% and the transformation of wood into char at 1.2, 10, 20 and 30 minutes.

2.6.2.2 Dvoslojni leseni prerez

Obravnavamo oglenenje dvoslojnega kompozitnega simetričnega lesenega nosilca začetne temperature $T_0 = 20\,^{\circ}\mathrm{C}$ in začetne vlažnosti $w_0 = 13\,^{\circ}\mathrm{M}$, ki je izpostavljen standardnemu požaru ISO 834 (1999) s treh strani (glej sliko 2.12, a). Slojeviti nosilec sestavljata spodnji (a) in zgornji sloj (b), ki sta iz lesa različnih materialnih lastnosti. Materialne karakteristike so razen karakteristik, ki jih podajamo na sliki 2.12, enake, kot v podpoglavju Primerjava z empiričnimi modeli (2.64). Dodatno predpostavimo, da je sloj b na levem in desnem robu vlažnostno povsen neprepusten, medtem ko stik med slojema modeliramo kot povsem prepusten za toploto in vlago.

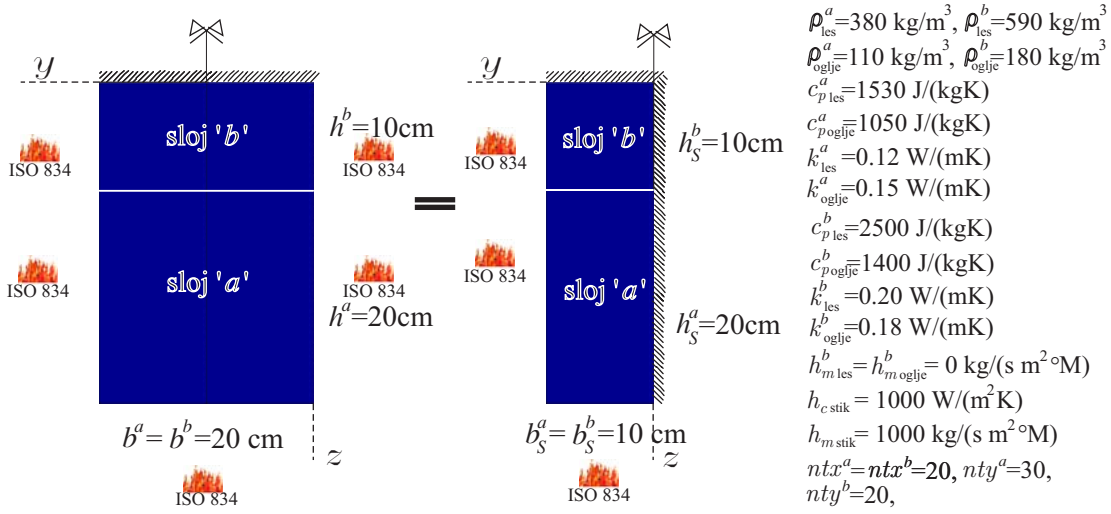

Slika 2.12: Geometrija, obtežba in materialne lastnosti dvoslojnega lesenega prereza.
Figure 2.12: Cross-section of the two-layer composite wooden beam and its equivalent symmetrical part.

Dimenzije na začetku simetričnega pravokotnega prečnega prereza posameznega sloja so $b^a/h^a = 20 \times 20$ cm oziroma $b^b/h^b = 20 \times 10$ cm. S slike 2.12 vidimo, da je tako izbran prečni prerez dvoslojnega kompozitnega nosilca geometrijsko in materialno simetričen glede na navpično ravnino simetrije $y = 0$. Poleg tega je simetrična tudi obtežba s požarom. Zaradi geometrijske in materialne simetrije in simetrije delujoče obtežbe, lahko prečni prerez razpolovimo na dva, po obliki in vrsti robnih pogojev, popolnoma enaka dela. Del prereza, ki leži na simetrijski osi, moramo podpreti (izolirati) tako, da bodo sprememba temperature in vlage ter toplotni in vlažnostni tok v smeri pravokotno na simetrijsko ravnino enaki nič. To pa pomeni, da moramo omenjeni del prereza povsem toplotno in vlažnostno izolirati (glej sliko 2.12b). Upoštevanje simetrije je računsko zelo ugodno. Upoštevamo lahko gostejšo mrežo. Na ta način izboljšamo natančnost rešitev. Dimenzije obravnavanega prereza so z upoštevanjem simetrije naslednje $b^a_S/h^a_S = 10 \times 20$ cm oziroma $b^b_S/h^b_S = 10 \times 10$ cm. Prečna prereza slojev v nadaljevanju diskretiziramo z ekvidistantno mrežo diferenčnih točk $ntx^a \times nty^a = 20 \times 30$, oziroma $ntx^b \times nty^b = 20 \times 20$. Opazovano časovno obdobje ($t = 60$ min) razdelimo na enake intervale (d$t = 5$s), pri tem pa upoštevamo čisto implicitno metodo ($t_b = 1$).

Časovni potek temperature in oglenenja po prerezu obravnavanega dvoslojnega kompozitnega nosilca pri časih $t = 1, 5, 10, 20, 30, 40, 50$ in 60 min, prikazujemo na sliki 2.13. Meja med lesom in ogljem je definirana s temperaturno izotermo $T = 300\,^{\circ}\mathrm{C}$. Opazimo lahko, da so temperaturni gradienti v bližini meje med lesom in ogljem zelo veliki. Ta nenaden skok oziroma padec temperature je posledica relativno majhne toplotne prevodnosti lesa in oglja. Oglenenje je tako najhitrejše na začetku. Ker ima oglje dobre toplotno izolativne lastnosti, se z razvojem plasti oglja hitrost oglenenja postopoma zmanjšuje. Zaradi

omenjenih izolativnih lastnosti lesa in oglja, ostane temperatura notranjih nosilnih delov prereza, kljub visokim temperaturam požara, relativno nizka.

S slike 2.13 oziroma 2.14 vidimo, da je oglenenje spodnjega sloja v primerjavi z zgornjim bistveno hitrejše. Rezultat je pričakovan, saj je gostota in specifična toplota spodnjega sloja dosti manjša od gostote zgornjega sloja. Gostota in specifična toplota lesa imata namreč pomemben vpliv na hitrost oglenenja lesa, (slika 2.10). Oglenenje se začne približno v 4. minuti požara, začne pa se najprej v spodnjem vogalu spodnjega sloja. Po 10-ih minutah začne ogleneti tudi zgornji sloj. Posledica hitrejšega oglenenja v vogalih je znani zaokrožitveni efekt, ki s časom spreminja obliko prečnega prereza. Začetni pravokotni prečni prerez dvoslojnega kompozitnega nosilca kmalu po nastopu oglenenja ni več pravokoten.

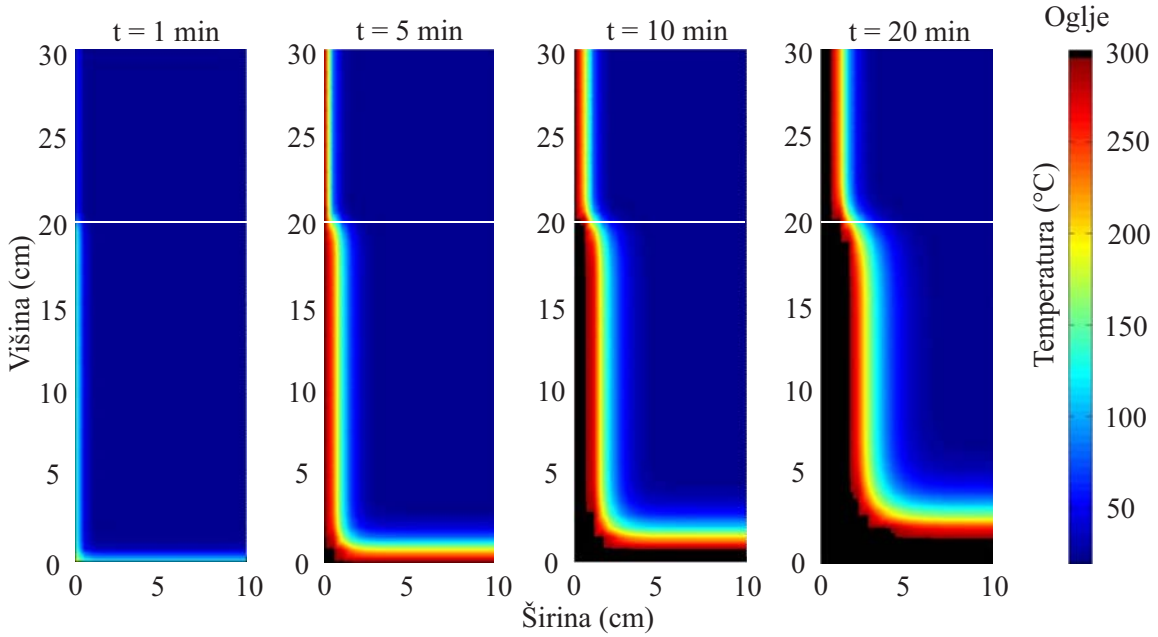

Slika 2.13: Porazdelitev temperature in oglenenje po prečnem prerezu dvoslojnega kompozitnega lesenega nosilca pri $t = 1, 5, 10$ in 20 min.

Figure 2.13: Temperature distribution in the cross-section of two-layer composite beam and the transformation of wood into char at $t = 1, 5, 10$ and 20 minutes.

Izračunano temperaturno polje in razporeditev oglja po prečnem prerezu bomo v nadaljevanju uporabili pri določitvi napetostnega in deformacijskega stanja dvoslojnega kompozitnega nosilca pri hkratnem delovanju statične in požarne obtežbe.

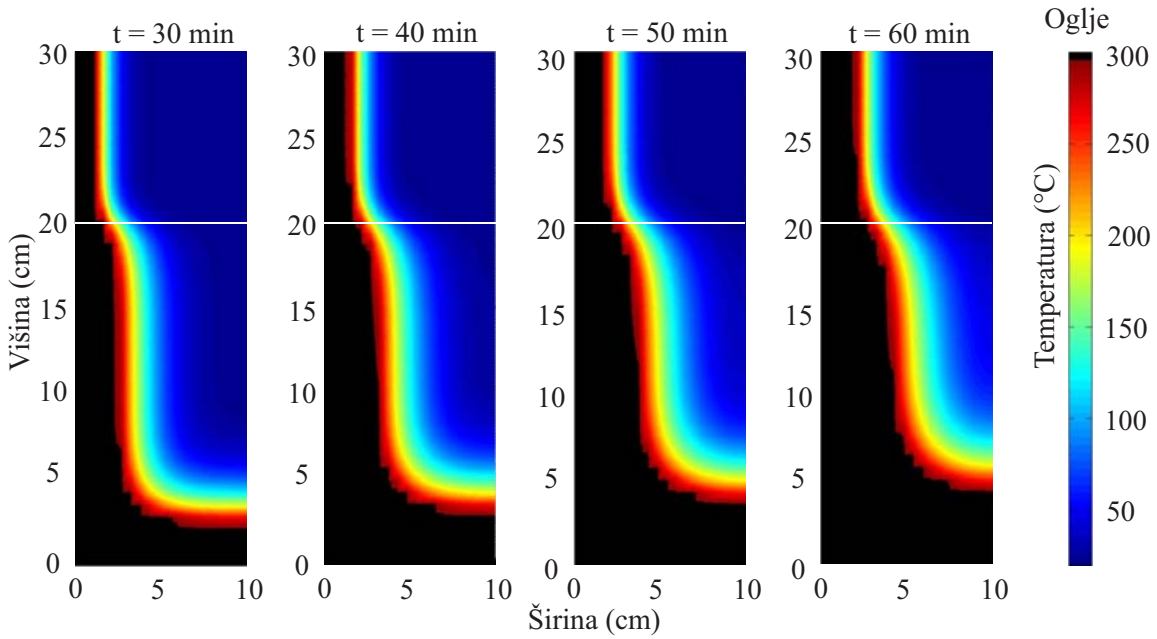

Slika 2.14: Porazdelitev temperature in oglenenje po prečnem prerezu dvoslojnega kompozitnega lesenega nosilca pri $t = 30, 40, 50$ in 60 min.

Figure 2.14: Temperature distribution in the cross-section of two-layer composite beam and the transformation of wood into char at $t = 30, 40, 50$ and 60 minutes.

3 ANALIZA KOMPOZITNIH NOSILCEV

3.1 Osnovne enačbe kompozitnih nosilcev

V tem poglavju predstavimo osnovne enačbe, ki opisujejo mehansko obnašanje kompozitnih nosilcev z upoštevanjem zdrsa med sloji. Osnovni algebrajsko–diferencialni sistem enačb kompozitnega nosilca sestavljajo kinematične, ravnotežne, konstitutivne in vezne enačbe ter pripadajoči statični in kinematični robni pogoji posameznih slojev. Predstavljena formulacija kompozitnega nosilca z upoštevanjem zdrsa med sloji je osnovana na kinematično (ali geometrijsko) točni Reissnerjevi teoriji ravninskih nosilcev (Reissner, 1972) za vsak sloj kompozitnega nosilca posebej. Le-ta opisuje membransko, strižno in upogibno deformiranje ravninskih nosilcev pri poljubnih končnih pomikih, rotacijah, vzdolžnih ter strižnih deformacijah. Upošteva tudi Timoshenkovo hipotezo o ravnih prečnih prerezih. Ta predpostavka določa, da ravninski prečni prerezi, pravokotni na nedeformirano referenčno os nosilca, ostanejo ravninski tudi po deformiranju, a ne več pravokotni na referenčno os nosilca. Upošteva tudi, da je prečni prerez nosilca v svoji ravnini absolutno tog, kar pomeni, da se oblika in velikost prečnega prereza med deformiranjem ne spreminjata. Poleg omenjenih predpostavk, formulacija kompozitnega nosilca z upoštevanjem zdrsa med sloji upošteva še dodatno predpostavko, da sloja lahko drsita drug po drugem ne moreta pa se razmakniti ali prodreti drug v drugega. Formulacija ni omejena s številom slojev.

3.1.1 Kinematične enačbe

Definicijsko območje ravninskega kompozitnega nosilca določa množica točk $\mathcal{B} = \bigcup_{i=1}^{i=N_{\mathrm{sl}}} \mathcal{B}^i \subset \mathbb{R}^3$. Pri tem $(\mathcal{B}^i)$ predstavlja definicijsko območje sloja i, ki je definirano s predpisom

$$\mathcal{B}^i = \mathcal{C}^i \times \mathcal{A}^i = \{(x^i, y^i, z^i) \,|\, x^i \in \mathcal{C}^i, (y^i, z^i) \in \mathcal{A}^i\} \tag{3.1}$$

kjer je $\mathcal{C}^i = [0, L]$ referenčna (v splošnem ne nujno težiščna) os posameznega sloja, $\mathcal{A}^i$ je konstantni simetrični prečni prerez sloja, N_{sl} pa število slojev kompozitnega nosilca, (slika 3.1). Množici $\mathcal{B}$ ($\mathcal{B}^i$) rečemo tudi domena nosilca (sloja) ali referenčna konfiguracija. Zaradi enostavnosti izberemo, da referenčna konfiguracija nosilca (sloja) sovpada s konfiguracijo kompozitnega nosilca $\mathcal{B}$ (sloja $\mathcal{B}^i$) v nedeformiranem stanju. Na ta način vse enačbe zapišemo skladno z Lagrangevim (začetnim) opisom. Deformiranje kompozitnega nosilca analiziramo v ravnini (X, Z) nepomičnega kartezičnega evklidskega (ambientnega) prostora $\mathbb{R}^3 = \{(X, Y, Z)\}$, ki je napet na ortonormirano kanonsko bazo $\{\mathbf{E}_X, \mathbf{E}_Y, \mathbf{E}_Z = \mathbf{E}_X \times \mathbf{E}_Y\}$. Referenčna os ravnega nedeformiranega kompozitnega nosilca je skupna vsem slojem. Predpostavimo, da sovpada z osjo X prostorskega koordinatnega sistema. Oblika prečnih prerezov posameznih slojev je poljubna, a simetrična glede na koordinatno ravnino $Y = 0$. V nedeformiranem stanju se prostorske koordinate (X^i, Y^i, Z^i) posameznega sloja ujemajo z njegovimi materialnimi koordinatami (x^i, y^i, z^i).

Pri izpeljavi osnovnih enačb se izkaže (Čas, 2004), da je referenčno os posameznih slojev najprimerneje parametrizirati z vpeljavo materialnih koordinat $x^i \in \mathcal{I}_l^i \cup \mathcal{I}^i \cup \mathcal{I}_d^i = [0, L]$, kjer $\mathcal{I}^i$ predstavlja definicijsko območje na stiku slojev i in $i+1$. $\mathcal{I}_l^i, \mathcal{I}_d^i$ predstavljata definicijski območji levega in desnega previsa sloja i. Koordinata x^{i+1} določa začetno koordinato delca sloja $i+1$, ki je v deformirani legi v kontaktu z delcem sloja i, s koordinato x^i. Povezavo materialnih koordinat x^i in x^{i+1} prikazuje slika 3.1.

Deformirana lega kompozitnega nosilca je znana, če poznamo lego vsake točke (x^i, y^i, z^i) sloja ($\mathcal{B}^i$) v koordinatnem sistemu (X, Y, Z). Definirana je z vektorsko preslikavo

$$\mathbf{R}^i : \mathcal{B}^i \longrightarrow \mathbf{R}^i(\mathcal{B}^i) \subset \mathbb{R}^3. \tag{3.2}$$

S predpisom (3.2) je podan krajevni vektor poljubne točke (x^i, y^i, z^i) posameznega sloja glede na izhodišče prostorskega koordinatnega sistema $\{X, Y, Z\}$. Krajevni vektor točke $(x^i, y^i, z^i) \in \mathcal{C}^i \times \mathcal{A}^i$ lahko zapišemo kot

$$\mathbf{R}^i(x^i, y^i, z^i) = \mathbf{r}_0^i(x^i) + \mathbf{u}^i(x^i) + \rho^i(x^i, y^i, z^i). \tag{3.3}$$

V (3.3) in v vseh nadaljnjih izrazih, oznake $(\bullet)^i$ pomenijo, da količina $(\bullet)$ pripada sloju i. Z $\mathbf{r}_0^i(x^i) = x\mathbf{E}_X$ smo označili krajevni vektor poljubne točke referenčne osi sloja. Nadalje smo z $\mathbf{u}^i(x^i) = u^i(x^i)\mathbf{E}_X + w^i(x^i)\mathbf{E}_Z$ označili vektor pomikov referenčne osi, kjer $u^i(x^i)$ ter $w^i(x^i)$ določata pomika točk referenčne osi sloja v smeri koordinatnih osi X in Z. Deformirano lego poljubne točke prereza glede na referenčno os v skladu s Timoshenkovo hipotezo o prečnih prerezih izrazimo s krajevnim vektorjem $\rho^i(x^i, y^i, z^i) = y^i\mathbf{e}_y^i(x^i) + z^i\mathbf{e}_z^i(x^i)$, kjer $\{\mathbf{e}_x^i(x^i), \mathbf{e}_y^i(x^i), \mathbf{e}_z^i(x^i)\}$ določajo materialno bazo zavrtenega prečnega prereza. $\mathbf{e}_x^i(x^i)$ je normalni, $\mathbf{e}_z^i(x^i)$ pa tangentni vektor na deformirano ravnino prereza sloja. Zveza med materialno in prostorsko bazo se glasi

$$\mathbf{e}_x^i(x^i) = \cos\varphi^i(x^i)\mathbf{E}_X - \sin\varphi^i(x^i)\mathbf{E}_Z, . \tag{3.4}$$

$$\mathbf{e}_y^i(x^i) = \mathbf{E}_Y, \tag{3.5}$$

$$\mathbf{e}_z^i(x^i) = \sin\varphi^i(x^i)\mathbf{E}_X + \cos\varphi^i(x^i)\mathbf{E}_Z, \tag{3.6}$$

kjer je $\varphi^i(x^i)$ zasuk (rotacija) prečnega prereza sloja, ki v splošnem, zaradi strižne deformacije prereza, ni enaka naklonu deformirane referenčne osi sloja. Geometrijska upodobitev baznih vektorjev $\mathbf{E}_X, \mathbf{E}_Z, \mathbf{e}_x(x^i)$ in $\mathbf{e}_z(x^i)$ je prikazana na sliki 3.1.

Konfiguracija (3.2) oziroma (3.3) se z upoštevanjem (3.4)–(3.6) glasi

$$\mathbf{R}^i(x^i, y^i, z^i) = \big(x^i + u^i(x^i) + z^i\sin\varphi^i(x^i)\big)\mathbf{E}_X + \big(w^i(x^i) + z^i\cos\varphi^i(x^i)\big)\mathbf{E}_Z + y^i\mathbf{E}_Y, \tag{3.7}$$

oziroma v komponentni obliki

$$X^i(x^i, y^i, z^i) = x^i + u^i(x^i) + z^i\sin\varphi^i(x^i), \tag{3.8}$$

$$Y^i(x^i, y^i, z^i) = y^i, \tag{3.9}$$

$$Z^i(x^i, y^i, z^i) = w^i(x^i) + z^i\cos\varphi^i(x^i). \tag{3.10}$$

Iz (3.7) oziroma (3.8)–(3.10) se vidi, da je konfiguracija sloja (3.3) popolnoma določena s tremi funkcijami $u^i(x^i), w^i(x^i)$ ter $\varphi^i(x^i)$. Ker $u^i(x^i), w^i(x^i)$ in $\varphi^i(x^i)$ natanko določajo geometrijo sloja, jih v nadaljevanju imenujemo tudi geometrijske količine.

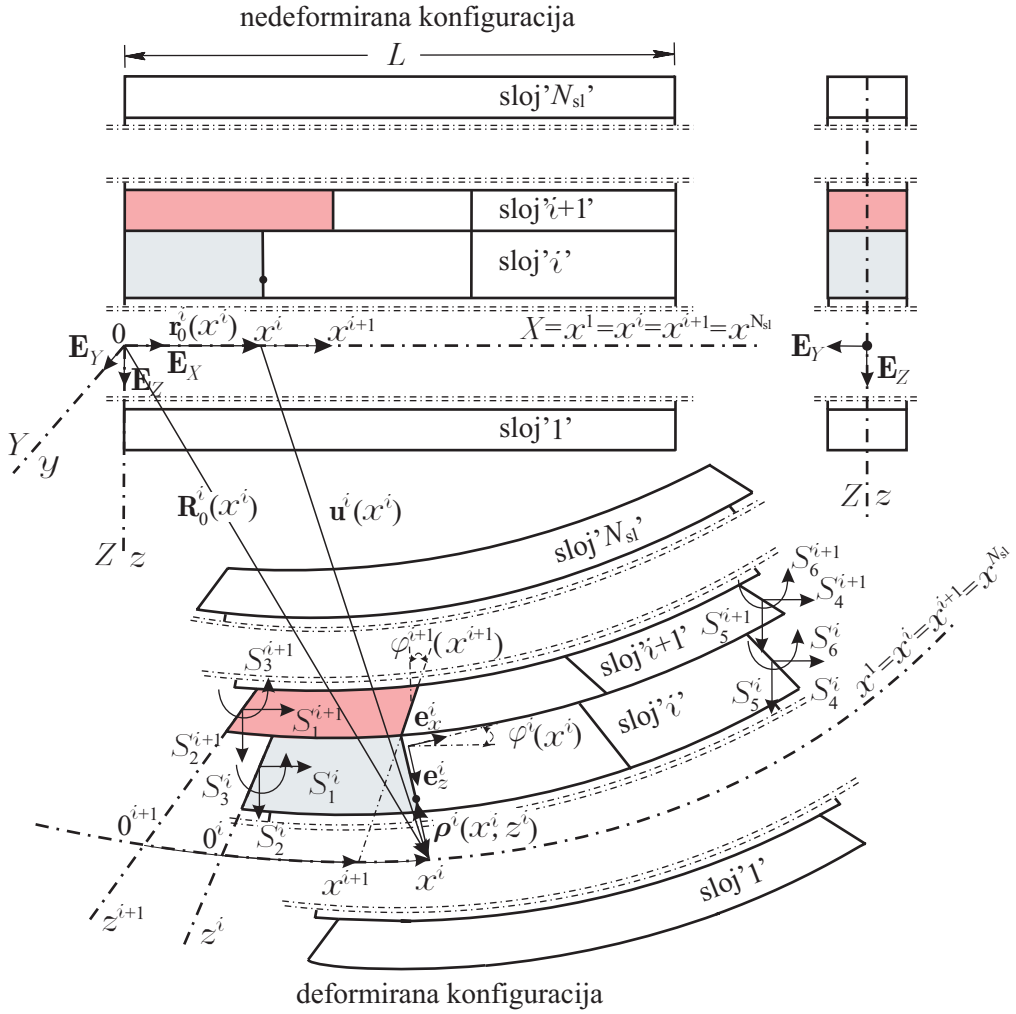

Slika 3.1: Nedeformirana in deformirana konfiguracija kompozitnega nosilca.
Figure 3.1: Undeformed and deformed configuration of the multi-layered composite beam.

S konfiguracijo nosilca (sloja) je definirano tudi njegovo deformirano stanje. Poleg geometrijskih količin zato potrebujemo tudi deformacijske količine. Preslikava 3.2 tako ni poljubna. Vežejo jo geometrijske vezne enačbe, ki predstavljajo mankajoči člen med geometrijskimi in deformacijskimi količinami. V primeru ravninskih nosilcev je zvezo prvi podal Reissner (1972). V tem primeru govorimo o Reissnerjevi teoriji ravninskih nosilcev. Za vsak posamezen sloj kompozitnega nosilca so zveze med geometrijskimi in deformacijskimi količinami določene z Reissnerjevima kinematičnima enačbama:

$x^i \in \mathcal{I}_l^i \cup \mathcal{I}^i \cup \mathcal{I}_d^i$:

$$\frac{\mathrm{d}\mathbf{R}_0^i(x^i)}{\mathrm{d}x^i} = \big(1+\varepsilon^i(x^i)\big)\mathbf{e}_x^i(x^i) + \gamma^i(x^i)\mathbf{e}_z^i(x^i), \tag{3.11}$$

$$\frac{\mathrm{d}\boldsymbol{\varphi}^i(x^i)}{\mathrm{d}x^i} = \kappa^i(x^i)\mathbf{e}_y^i(x^i), \tag{3.12}$$

oziroma v komponentni obliki

$$1+\frac{\mathrm{d}u^i(x^i)}{\mathrm{d}x^i}-\big(1+\varepsilon^i(x^i)\big)\cos\varphi^i(x^i)-\gamma^i(x^i)\sin\varphi^i(x^i)=0, \tag{3.13}$$

$$\frac{\mathrm{d}w^i(x^i)}{\mathrm{d}x^i}+\big(1+\varepsilon^i(x^i)\big)\sin\varphi^i(x^i)-\gamma^i(x^i)\cos\varphi^i(x^i)=0, \tag{3.14}$$

$$\frac{\mathrm{d}\varphi^i(x^i)}{\mathrm{d}x^i}-\kappa^i(x^i)=0. \tag{3.15}$$

Z $\mathbf{R}_0^i(x^i)=\mathbf{r}_0^i(x^i)+\mathbf{u}^i(x^i)$ smo označili krajevni vektor deformirane referenčne osi, s $\boldsymbol{\varphi}^i(x^i)$ pa vektor rotacije prečnega prereza sloja. V enačbah (3.11–3.15) predstavlja $\gamma^i(x^i)$ strižno deformacijo; $\varepsilon^i(x^i)>-1$ je specifična vzdolžna deformacija materialnega vlakna in sicer v smeri pripadajoče energijsko konjugirane osne sile sloja. Funkcija $\varepsilon^i(x^i)$ predstavlja tudi specifično spremembo dolžine referenčne osi deformiranega sloja, a le v primeru, ko je strižna deformacija $\gamma^i(x^i)=0$. Podobno predstavlja upogibna deformacija $\kappa^i(x^i)$ pravo ukrivljenost referenčne osi deformiranega sloja le kadar je $\varepsilon^i(x^i)=0$ (Vratanar in Saje, 1998). V nadaljevanju jo zato imenujemo psevdoukrivljenost. Specifična sprememba dolžine poljubnega materialnega vlakna prečnega prereza posameznega sloja kompozitnega nosilca je po Timoshenkovi hipotezi o prečnih prerezih naslednja

$$D^i(x^i,z^i)=\varepsilon^i(x^i)+z^i\kappa^i(x^i),\qquad (i=1,2,\ldots,N_{\mathrm{sl}}). \tag{3.16}$$

Enačbe (3.11–3.15) predstavljajo kinematične enačbe na stiku med posameznimi sloji. Pri računanju kompozitnih konstrukcij z upoštevanjem zdsa med sloji pa moramo poznati tudi enačbe previsov kompozitnega nosilca. Kinematične enačbe previsov so povsem enake enačbam (3.11–3.15), le definicijsko območje funkcij je potrebno spremeniti. Definicijsko območje na stiku $\mathcal{I}^i$ zamenjamo z definicijskim območjem previsov $\mathcal{I}_l^i$ in $\mathcal{I}_d^i$. Za dvoslojne nosilce so kinematične enačbe previsov ter različne možne kombinacije definicijskih območij geometrijskih (kinematičnih) in deformacijskih funkcij podane v (Čas, 2004).

3.1.2 Ravnotežne enačbe

Z ravnotežnimi enačbami povežemo notranje statične količine kompozitnega nosilca z zunanjo obtežbo, ki predstavlja vpliv ambientnega prostora (okolice) na kompozitni nosilec. Kot smo že omenili, na kompozitni nosilec $\mathcal{B}$ oziroma na posamezen sloj $\mathcal{B}^i$ v splošnem učinkujeta dve vrsti obtežb: koncentrirana in zvezna obtežba. Zvezna nadomestna linijska obtežba $\boldsymbol{p}^i(x^i)=p_X^i(x^i)\mathbf{E}_X+p_Z^i(x^i)\mathbf{E}_Z$ ter linijski moment $\boldsymbol{m}^i(x^i)=m_Y^i(x^i)\mathbf{E}_Y$ delujeta na nekem podintervalu intervala $[0,L]$, medtem ko koncentrirana obtežba S_j^i učinkuje le na njegovem robu $x^i=0$ ter $x^i=L$. V našem primeru predpostavimo, da obtežbi $\boldsymbol{p}^i(x^i)$ in $\boldsymbol{m}^i(x^i)$ delujeta na deformirani referenčni osi sloja in da sta merjeni na nedeformirano dolžino kompozitnega nosilca.

Kompozitni nosilec obravnavamo kot unijo ločenih nosilcev (slojev). Posledica medsebojnega delovanja slojev je, da je posamezen sloj zaradi stika z sosednjima slojema obtežen vzdolž referenčne osi $x^i\in\mathcal{I}^i$ tudi s t.i. nadomestno kontaktno linijsko obtežbo

$$\begin{aligned}\boldsymbol{q}^i(x^i)=&q_x^i(x^i)\mathbf{e}_x^i(x^i)+q_z^i(x^i)\mathbf{e}_z^i(x^i)=\\ =&\Big(q_{x,j-1}^i(x^i)+q_{x,j}^i(x^i)\Big)\mathbf{e}_x^i(x^i)+\Big(q_{z,j-1}^i(x^i)+p_{z,j}^i(x^i)\Big)\mathbf{e}_z^i(x^i)=\\ =&q_X^i(x^i)\mathbf{E}_X+q_Z^i(x^i)\mathbf{E}_Z,=\\ =&\Big(q_{X,j-1}^i(x^i)+q_{X,j}^i(x^i)\Big)\mathbf{E}_X+\Big(q_{Z,j-1}^i(x^i)+p_{Z,j}^i(x^i)\Big)\mathbf{E}_Z,\end{aligned} \tag{3.17}$$

in nadomestnim kontaktnim linijskim momentom

$$\begin{aligned}\boldsymbol{h}^i(x^i) =& h_y^i(x^i)\mathbf{e}_y^i(x^i) = \Big(h_{y,j-1}^i(x^i) + h_{x,j}^i(x^i)\Big)\mathbf{e}_y^i(x^i) = \Big(z_{j-1}q_{x,j-1}^i(x^i) + z_j q_{x,j}^i(x^i)\Big)\mathbf{e}_y^i(x^i) = \\ =& h_Y^i(x^i)\mathbf{E}_Y = \Big(h_{y,j-1}^i(x^i) + h_{x,j}^i(x^i)\Big)\mathbf{E}_y = \\ =& \Big[\Big(z_{j-1}q_{X,j-1}^i(x^i) + z_j q_{X,j}^i(x^i)\Big)\cos\varphi^i(x^i) - \Big(z_{j-1}q_{Z,j-1}^i(x^i) + z_j q_{Z,j}^i(x^i)\Big)\sin\varphi^i(x^i)\Big]\mathbf{E}_y,\end{aligned} \tag{3.18}$$

kjer na primer $q_{X,j-1}^i(x^i)$ oziroma $q_{X,j}^i(x^i)$ predstavljata komponenti kontaktne linijske obtežbe $\boldsymbol{q}^i(x^i)$ sloja i zaradi stika le tega s spodnjim $(i-1)$ oziroma zgornjim slojem $(i+1)$. Pri tem smo z indeksom j $(j = i = 1, \ldots, N_{\text{sl}};\ j \neq N_{\text{sl}})$ označili stik sloja i z zgornjim slojem $i+1$. Z z_{j-1} in z_j smo označili ročici komponent kontaktne linijske obtežbe $\boldsymbol{q}^i(x^i)$, ki delujeta v spodnjem in zgornjem stiku. Podobno kot za zunanjo linijsko obtežbo $\boldsymbol{p}^i(x^i)$ in moment $\boldsymbol{m}^i(x^i)$, tudi za kontaktno linijsko obtežbo $\boldsymbol{q}^i(x^i)$ in moment $\boldsymbol{h}^i(x^i)$ predpostavimo, da sta merjena na nedeformirano dolžino referenčne osi kompozitnega nosilca.

Definicijsko območje funkcij, ki nastopajo v ravnotežnih enačbah, je podobno kot pri kinematičnih enačbah sestavljeno iz treh medsebojno povezanih intervalov: za sloj i je $x^i \in \mathcal{I}_l^i \cup \mathcal{I}^i \cup \mathcal{I}_d^i = [0, L]$.

Ravnotežne enačbe posameznega sloja kompozitnega nosilca predstavljata vektorski diferencialni enačbi prvega reda (Simo, 1985)

$$\frac{\mathrm{d}\mathbf{N}^i(x^i)}{\mathrm{d}x^i} + \boldsymbol{p}^i(x^i) + \boldsymbol{q}^i(x^i) = \mathbf{0}, \tag{3.19}$$

$$\frac{\mathrm{d}\mathbf{M}^i(x^i)}{\mathrm{d}x^i} + \frac{\mathrm{d}\mathbf{R}_0^i(x^i)}{\mathrm{d}x^i} \times \mathbf{N}^i(x^i) + \boldsymbol{m}^i(x^i) + \boldsymbol{h}^i(x^i) = \mathbf{0}. \tag{3.20}$$

V enačbah (3.19) in (3.20) predstavljata vektorski funkciji $\mathbf{N}^i(x^i)$ in $\mathbf{M}^i(x^i)$ posplošeni notranji sili v deformirani referenčni osi posameznega sloja kompozitnega nosilca. Zapisani v komponentni obliki glede na materialno in prostorsko bazo se glasita

$$\boldsymbol{N}^i(x^i) = \mathcal{N}^i(x^i)\mathbf{e}_x^i(x^i) + \mathcal{Q}^i(x^i)\mathbf{e}_z^i(x^i) = \mathcal{R}_X^i(x^i)\mathbf{E}_E + \mathcal{R}_Z^i(x^i)\mathbf{E}_Z, \tag{3.21}$$

$$\mathbf{M}^i(x^i) = \mathcal{M}_y^i(x^i)\mathbf{e}_y(x^i) = \mathcal{M}_Y^i(x^i)\mathbf{E}_Y. \tag{3.22}$$

Komponenti rezultante notranjih sil $\mathcal{N}^i(x^i)$ in $\mathcal{Q}^i(x^i)$ v (3.21) predstavljata ravnotežno osno in ravnotežno prečno silo sloja i v smeri baznih vektorjev materialnega koordinatnega sistema $\mathbf{e}_x^i(x^i)$ in $\mathbf{e}_z^i(x^i)$. Na tem mestu moramo poudariti, da vektor $\mathbf{e}_x^i(x^i)$ ni tangenten na deformirano referenčno os, temveč pravokoten na prečni prerez, slika 3.2. Vektor $\mathbf{e}_x^i(x^i)$ postane tangenten na referenčno os šele ob predpostavki, da so strižne deformacije enake nič ($\gamma^i(x^i) = 0$). Podobno $\mathcal{M}_y^i(x^i) \equiv \mathcal{M}_Y^i(x^i)$ pomeni ravnotežni upogibni moment sloja i. $\mathcal{R}_X^i(x^i)$ ter $\mathcal{R}_Z^i(x^i)$ sta komponenti rezultante notranji sil, zapisani glede na prostorsko bazo $\mathbf{E}_X$, $\mathbf{E}_Z$. Geometrijski pomen posameznih komponent, zapisanih v materialni in prostorski bazi, je razviden iz slike 3.2.

Zveze med $\mathcal{N}^i(x^i)$, $\mathcal{Q}^i(x^i)$ ter $\mathcal{R}_X^i(x^i)$, $\mathcal{R}_Z^i(x^i)$ so opisane tudi z izrazi:

$$\mathcal{N}^i(x^i) = \mathcal{R}_X^i(x^i)\cos\varphi^i(x^i) - \mathcal{R}_Z^i(x^i)\sin\varphi^i(x^i), \tag{3.23}$$

$$\mathcal{Q}^i(x^i) = \mathcal{R}_X^i(x^i)\sin\varphi^i(x^i) + \mathcal{R}_Z^i(x^i)\cos\varphi^i(x^i). \tag{3.24}$$

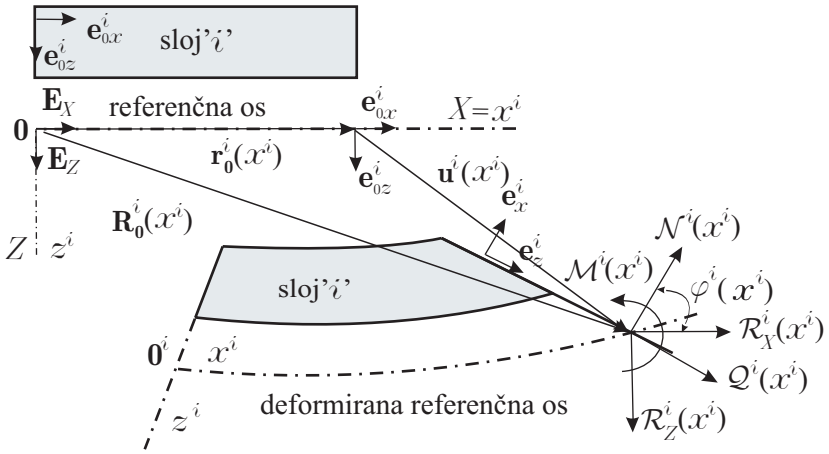

Slika 3.2: Komponente notranjih sil glede na materialni $\left(\mathbf{e}_x^i, \mathbf{e}_z^i\right)$ in prostorski $(\mathbf{E}_X, \mathbf{E}_Z)$ koordinatni sistem.
Figure 3.2: Internal forces in the material $\left(\mathbf{e}_x^i, \mathbf{e}_z^i\right)$ and spatial $(\mathbf{E}_X, \mathbf{E}_Z)$ coordinate system.

Z vstavitvijo izrazov (3.21) in (3.22) v enačbe (3.19–3.20) in upoštevanjem (3.13) in (3.14) dobimo ravnotežne enačbe za posamezen sloj kompozitnega nosilca. Zapisane glede na prostorske bazne vektorje $\mathbf{E}_X$, $\mathbf{E}_Y$ in $\mathbf{E}_Z$, so na intervalu $x^i \in \mathcal{I}^i$ naslednje

$$\frac{\mathrm{d}\mathcal{R}_X^i(x^i)}{\mathrm{d}x^i} + p_X^i(x^i) + q_{X,j-1}^i(x^i) + q_{X,j}^i(x^i) = 0, \tag{3.25}$$

$$\frac{\mathrm{d}\mathcal{R}_Z^i(x^i)}{\mathrm{d}x^i} + p_Z^i(x^i) + q_{Z,j-1}^i(x^i) + q_{Z,j}^i(x^i) = 0, \tag{3.26}$$

$$\begin{aligned}&\frac{\mathrm{d}\mathcal{M}^i(x^i)}{\mathrm{d}x^i} - \left(1+\varepsilon^i(x^i)\right)\mathcal{Q}^i(x^i) + \gamma^i(x^i)\mathcal{N}^i(x^i) + m_Y^i(x^i) + \\ &+\Big(z_{j-1}q_{X,j-1}^i(x^i) + z_j q_{X,j}^i(x^i)\Big)\cos\varphi^i(x^i) - \Big(z_{j-1}q_{Z,j-1}^i(x^i) + z_j q_{Z,j}^i(x^i)\Big)\sin\varphi^i(x^i) = 0.\end{aligned} \tag{3.27}$$

Če pri zapisu enačb (3.25–3.27) upoštevamo zvezi (3.23–3.24), dobimo ravnotežne enačbe sloja zapisane v celoti v odvisnosti od ravnotežne osne sile $\mathcal{N}^i(x^i)$, ravnotežne prečne sile $\mathcal{Q}^i(x^i)$ ter ravnotežnega upogibnega momenta $\mathcal{M}^i(x^i)$ sloja kompozitnega nosilca:

$$\frac{\mathrm{d}\left(\mathcal{N}^i(x^i)\cos\varphi^i(x^i) + \mathcal{Q}^i(x^i)\sin\varphi^i(x^i)\right)}{\mathrm{d}x^i} + p_X^i(x^i) + q_{X,j-1}^i(x^i) + q_{X,j}^i(x^i) = 0, \tag{3.28}$$

$$\frac{\mathrm{d}\left(-\mathcal{N}^i(x^i)\cos\varphi^i(x^i) + \mathcal{Q}^i(x^i)\sin\varphi^i(x^i)\right)}{\mathrm{d}x^i} + p_Z^i(x^i) + q_{Z,j-1}^i(x^i) + q_{Z,j}^i(x^i) = 0, \tag{3.29}$$

$$\begin{aligned}&\frac{\mathrm{d}\mathcal{M}^i(x^i)}{\mathrm{d}x^i} - \left(1+\varepsilon^i(x^i)\right)\mathcal{Q}^i(x^i) + \gamma^i(x^i)\mathcal{N}^i(x^i) + m_Y^i(x^i) + \\ &+\Big(z_{j-1}q_{X,j-1}^i(x^i) + z_j q_{X,j}^i(x^i)\Big)\cos\varphi^i(x^i) - \Big(z_{j-1}q_{Z,j-1}^i(x^i) + z_j q_{Z,j}^i(x^i)\Big)\sin\varphi^i(x^i) = 0.\end{aligned} \tag{3.30}$$

V enačbah (3.17–3.18) in (3.25–3.30) smo kontaktno linijsko obtežbo opisali v prostorskem $\{\mathbf{E}_X, \mathbf{E}_Z\}$, in materialnem $\{\mathbf{e}_x^i(x^i), \mathbf{e}_z^i(x^i)\}$ koordinatnem sistemu. Ker pa bomo konstitutivni zakon stika, ki ga

vpeljemo v nadaljevanju, izrazili s komponentami linijske kontaktne obtežbe v naravnem $\{\mathbf{e}_t^i(x^i), \mathbf{e}_n^i(x^i)\}$ koordinatnem sistemu, izrazimo nadomestno linijsko kontaktno obtežbo $\boldsymbol{q}^i(x^i)$ v smereh omenjenega koordinatnega sistema $\{\mathbf{e}_t^i(x^i), \mathbf{e}_n^i(x^i)\}$.

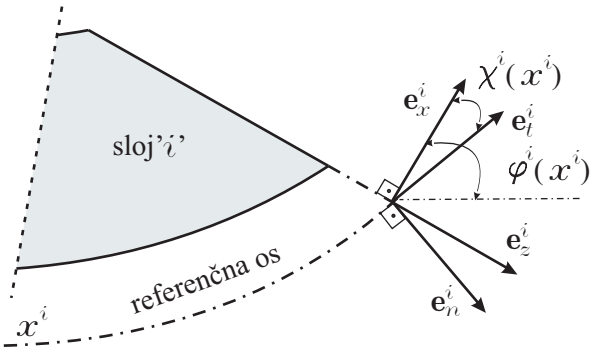

Slika 3.3: Geometrijska upodobitev baznih vektorjev $\mathbf{e}_x^i(x^i)$, $\mathbf{e}_z^i(x^i)$, $\mathbf{e}_t^i(x^i)$, $\mathbf{e}_n^i(x^i)$.
Figure 3.3: A geometric representation of base vectors $\mathbf{e}_x^i(x^i)$, $\mathbf{e}_z^i(x^i)$, $\mathbf{e}_t^i(x^i)$, $\mathbf{e}_n^i(x^i)$.

V ta namen definiramo ortogonalni preslikavi $\mathbf{T}^i_{\varphi^i-\chi^i}(x^i)$= span$\{\mathbf{E}_X, \mathbf{E}_Z\} \longrightarrow$ span$\{\mathbf{e}_t^i(x^i), \mathbf{e}_n^i(x^i)\}$ in $\mathbf{T}^i_{\chi^i}(x^i)$= span$\{\mathbf{e}_x^i(x^i), \mathbf{e}_z^i(x^i)\} \longrightarrow$ span$\{\mathbf{e}_t^i(x^i), \mathbf{e}_n^i(x^i)\}$, ki definirata lego vektorske baze $\{\mathbf{e}_t^i(x^i)$, $\mathbf{e}_n^i(x^i)\}$ glede na bazo $\{\mathbf{E}_X, \mathbf{E}_Z\}$, oziroma glede na $\{\mathbf{e}_x^i(x^i), \mathbf{e}_z^i(x^i)\}$. Kota rotacije sta $\varphi^i(x^i)-\chi^i(x^i)$ in $\chi^i(x^i)$, slika 3.3. S preslikavama $\mathbf{T}^i_{\varphi^i-\chi^i}(x^i)$ ter $\mathbf{T}^i_{\chi^i}(x^i)$ lahko komponente linijske kontaktne obtežbe $\boldsymbol{q}^i(x^i)$ izrazimo glede na bazi $\{\mathbf{E}_X, \mathbf{E}_Z\}$ ter $\{\mathbf{e}_t^i(x^i), \mathbf{e}_n^i(x^i)\}$ kot

$$\boldsymbol{q}^i(x^i)\Big|_{\{\mathbf{e}_t^i,\mathbf{e}_n^i\}} = \mathbf{T}^i_{\varphi^i-\chi^i}(x^i)\boldsymbol{q}^i(x^i)\Big|_{\{\mathbf{E}_X,\mathbf{E}_Z\}} = \mathbf{T}^i_{\chi^i}(x^i)\boldsymbol{q}^i(x^i)\Big|_{\{\mathbf{e}_x^i,\mathbf{e}_z^i\}} \tag{3.31}$$

oziroma v komponenti obliki v stiku j kot

$$\begin{aligned}\begin{bmatrix} q^i_{t,j}(x^i) \\ q^i_{n,j}(x^i) \end{bmatrix} &= \begin{bmatrix} \cos\big(\varphi^i(x^i)-\chi^i(x^i)\big) & -\sin\big(\varphi^i(x^i)-\chi^i(x^i)\big) \\ \sin\big(\varphi^i(x^i)-\chi^i(x^i)\big) & \cos\big(\varphi^i(x^i)-\chi^i(x^i)\big) \end{bmatrix} \begin{bmatrix} q^i_{X,j}(x^i) \\ q^i_{Z,j}(x^i) \end{bmatrix} = \\ &= \begin{bmatrix} \cos\chi^i(x^i) & \sin\chi^i(x^i) \\ -\sin\chi^i(x^i) & \cos\chi^i(x^i) \end{bmatrix} \begin{bmatrix} q^i_{x,j}(x^i) \\ q^i_{z,j}(x^i) \end{bmatrix}.\end{aligned} \tag{3.32}$$

Ravnotežne enačbe (3.25–3.27) lahko s transformacijo (3.32) zapišemo še drugače

$$\begin{aligned}&\frac{\mathrm{d}\mathcal{R}^i_X(x^i)}{\mathrm{d}x^i} + p^i_X(x^i) + \\ &+\Big(q^i_{t,j-1}(x^i) + q^i_{t,j}(x^i)\Big)\cos\big(\varphi^i(x^i)-\chi^i(x^i)\big) + \Big(q^i_{n,j-1}(x^i) + q^i_{n,j}(x^i)\Big)\sin(\varphi^i(x^i) - \chi^i(x^i)) = 0,\end{aligned} \tag{3.33}$$

$$\begin{aligned}&\frac{\mathrm{d}\mathcal{R}^i_Z(x^i)}{\mathrm{d}x^i} + p^i_Z(x^i) - \\ &-\Big(q^i_{t,j-1}(x^i) + q^i_{t,j}(x^i)\Big)\sin\big(\varphi^i(x^i)-\chi^i(x^i)\big) + \Big(q^i_{n,j-1}(x^i) + q^i_{n,j}(x^i)\Big)\cos(\varphi^i(x^i) - \chi^i(x^i)) = 0,\end{aligned} \tag{3.34}$$

$$\frac{\mathrm{d}\mathcal{M}^i(x^i)}{\mathrm{d}x^i} - \left(1+\varepsilon^i(x^i)\right)\mathcal{Q}^i(x^i) + \gamma^i(x^i)\mathcal{N}^i(x^i) + m_Y^i(x^i) + \Big(z_{j-1}q_{t,j-1}^i(x^i) + z_j q_{t,j}^i(x^i)\Big)$$
$$\Big(\cos\varphi^i(x^i)\cos(\varphi^i(x^i)-\chi^i(x^i)) + \sin\varphi^i(x^i)\sin(\varphi^i(x^i)-\chi^i(x^i))\Big) + \Big(z_{j-1}q_{n,j-1}^i(x^i) + z_j q_{n,j}^i(x^i)\Big)$$
$$\Big(\cos\varphi^i(x^i)\sin(\varphi^i(x^i)-\chi^i(x^i)) - \sin\varphi^i(x^i)\cos(\varphi^i(x^i)-\chi^i(x^i))\Big) = 0. \tag{3.35}$$

Analogno kinematičnim enačbam (3.11–3.13), so tudi ravnotežne enačbe na desnem in levem previsu sloja i enake enačbam (3.25–3.27) in (3.28–3.30). V tem primeru je potrebno spremeniti le definicijsko območje funkcij, ki nastopajo v enačbah. Definicijsko območje stika $\mathcal{I}^i$ zamenjamo z definicijskima območjema previsov $\mathcal{I}_l^i$ in $\mathcal{I}_d^i$.

3.1.3 Konstitutivne enačbe

Ambienti prostor (okolica) deluje na kompozitni nosilec $\mathcal{B}$ preko zunanje obtežbe. Posledica je deformiranje kompozitnega nosilca. Nosilec se deformiranju upira tako, da so ravnotežne količine vedno enake konstitutivnim. Konstitutivne enačbe tako predstavljajo vez med ravnotežnim napetostnim prostorom z elementi $\{\mathcal{N}^i(x^i), \mathcal{Q}^i(x^i), \mathcal{M}^i(x^i)\}$ in deformacijskim prostorom z elementi $\{\varepsilon^i(x^i), \gamma^i(x^i), \kappa^i(x^i)\}$. Poleg tega moramo vpeljati tudi konstitutivni napetostni prostor z elementi $\{\mathcal{N}_\mathrm{c}^i(x^i), \mathcal{Q}_\mathrm{c}^i(x^i), \mathcal{M}_\mathrm{c}^i(x^i)\}$, kjer $\mathcal{N}_\mathrm{c}^i(x^i)$ predstavlja konstitutivno osno silo, $\mathcal{Q}_\mathrm{c}^i(x^i)$ konstitutivno prečno silo in $\mathcal{M}_\mathrm{c}^i(x^i)$ konstitutivni upogibni moment posameznega sloja. Paziti moramo, da so konstitutivne sile in momenti definirani v istem koordinatnem sistemu kot ravnotežne sile in momenti, tj. v našem primeru v materialni bazi $\{\mathbf{e}_x^i(x^i), \mathbf{e}_y^i(x^i), \mathbf{e}_z^i(x^i)\}$. Kot smo že omenili, s konstitutivnimi enačbami zahtevamo, da so vzdolž referenčne osi sloja i, $x^i \in [0, L]$, ravnotežne statične količine enake konstitutivnim količinam. Konstitutivne količine so v direktni zvezi s prvim Piola-Kirchoffovim napetostnim tenzorjem. Po privzetih predpostavkah ravninskega nosilca v prečnem prerezu sloja i učinkujeta fizikalna normalna σ_c^i in fizikalna strižna τ_c^i napetost:

$$\sigma_\mathrm{c}^i(x^i, y^i, z^i) = \mathcal{F}^i\Big(x^i, y^i, z^i, \varepsilon^i(x^i), \kappa^i(x^i), T^i(x^i, y^i, z^i), w^i(x^i, y^i, z^i)\Big) \tag{3.36}$$

in

$$\tau_\mathrm{c}^i(x^i, y^i, z^i) = \mathcal{G}^i\Big(x^i, y^i, z^i, \gamma^i(x^i), T^i(x^i, y^i, z^i), w^i(x^i, y^i, z^i)\Big). \tag{3.37}$$

V splošnem sta funkciji $\mathcal{F}^i$ in $\mathcal{G}^i$ poljubni in ju določimo eksperimentalno za vsak uporabljeni material posebej. S tako splošnim materialnim modelom lahko opišemo elastično, hiperelastično, plastično in tudi termeraturno-viskozno obnašanje materialov. Z upoštevanjem konstitutivnih materialnih zvez (3.36–3.37) definiramo konstitutivne količine prereza sloja i z naslednjimi izrazi:

$$\mathcal{N}_\mathrm{c}^i(x^i) = \int_{\mathcal{A}^i} \sigma_\mathrm{c}^i(x^i, y^i, z^i)\mathrm{d}\mathcal{A}^i = \int_{\mathcal{A}^i} \mathcal{F}^i\Big(x^i, y^i, z^i, \varepsilon^i(x^i), \kappa^i(x^i), T^i(x^i, y^i, z^i), w^i(x^i, y^i, z^i)\Big)\mathrm{d}A^i, \tag{3.38}$$

$$\mathcal{Q}_\mathrm{c}^i(x^i) = \int_{\mathcal{A}^i} \tau_\mathrm{c}^i(x^i, y^i, z^i)\mathrm{d}\mathcal{A}^i = \int_{\mathcal{A}^i} \mathcal{G}^i\Big(x^i, y^i, z^i, \gamma^i(x^i), T^i(x^i, y^i, z^i), w^i(x^i, y^i, z^i)\Big)\mathrm{d}A^i \tag{3.39}$$

$$\mathcal{M}_\mathrm{c}^i(x^i) = \int_{\mathcal{A}^i} z^i\sigma_\mathrm{c}^i(x^i, y^i, z^i)\mathrm{d}\mathcal{A}^i = \int_{\mathcal{A}^i} z^i\mathcal{F}^i\Big(x^i, y^i, z^i, \varepsilon^i(x^i), \kappa^i(x^i), T^i(x^i, y^i, z^i), w^i(x^i, y^i, z^i)\Big)\mathrm{d}A^i \tag{3.40}$$

$\mathcal{N}_{\mathrm{c}}^i(x^i), \mathcal{Q}_{\mathrm{c}}^i(x^i), \mathcal{M}_{\mathrm{c}}^i(x^i)$ so funkcije istih argumentov kot fizikalni napetosti σ_{c}^i in τ_{c}^i. Konsistentno ravnotežje v poljubnem prečnem prerezu sloja i je tako zagotovljeno, če je

$$\mathcal{N}^i(x^i) = \mathcal{N}_{\mathrm{c}}^i\Big(x^i, \varepsilon^i(x^i), \kappa^i(x^i), T^i(x^i, y^i, z^i), w^i(x^i, y^i, z^i)\Big), \tag{3.41}$$

$$\mathcal{Q}^i(x^i) = \mathcal{Q}_{\mathrm{c}}^i\Big(x^i, \gamma^i(x^i), T^i(x^i, y^i, z^i), w^i(x^i, y^i, z^i)\Big), \tag{3.42}$$

$$\mathcal{M}^i(x^i) = \mathcal{M}_{\mathrm{c}}^i\Big(x^i, \varepsilon^i(x^i), \kappa^i(x^i), T^i(x^i, y^i, z^i), w^i(x^i, y^i, z^i)\Big), \tag{3.43}$$

za vsak $x^i \in [0, L]$. Enačbe (3.41–3.42) predstavljajo konstitutivne enačbe prečnega prereza sloja i.

3.1.4 Vezne enačbe

Vezne enačbe določajo pogoje, s katerimi povežemo posamezne sloje kompozitnega nosilca v celoto. Kot smo že uvodoma omenili, posamezni sloji lahko drsijo drug po drugem, ne morejo pa se razmakniti ali prodreti drug v drugega. Ta pogoj izrazimo z zahtevo

$$\mathbf{R}^i(x^i, y^i = 0, z^i = z_j) = \mathbf{R}^{i+1}(x^{i+1}, y^{i+1} = 0, z^{i+1} = z_j) \qquad (i = j = 1, 2, \ldots, N_{\mathrm{sl}} - 1), \tag{3.44}$$

kjer $\mathbf{R}^i(x^i, y^i = 0, z^i = z_j)$ in $\mathbf{R}^{i+1}(x^{i+1}, y^{i+1} = 0, z^{i+1} = z_j)$ pomenita krajevna vektorja krivulje, ki opisuje deformirano stično ploskev med slojema i in $i + 1$. z_j predstavlja razdaljo med krivuljo, ki opisuje nedeformirano stično ploskev in nedeformirano referenčno os kompozitnega nosilca, glej sliko 3.1. Zahtevo (3.44) lahko z enačbo (3.7) zapišemo tudi v komponentni obliki, in sicer

$$x^i + u^i(x^i) + z_j \sin\varphi^i(x^i) = x^{i+1} + u^{i+1}(x^{i+1}) + z_j \sin\varphi^{i+1}(x^{i+1}), \tag{3.45}$$

$$w^i(x^i) + z_j \cos\varphi^i(x^i) = w^{i+1}(x^{i+1} + z_j \cos\varphi^{i+1}(x^{i+1})). \tag{3.46}$$

Enačbi (3.45–3.46) predstavljata kinematični vezni enačbi sloja i: $x^i \subset \mathcal{I}^i = [0, L] \cap (\mathcal{I}_l^i \cup \mathcal{I}_d^i)$, oziroma sloja $i + 1$: $x^{i+1} \subset \mathcal{I}^{i+1} = [0, L] \cap (\mathcal{I}_l^{i+1} \cup \mathcal{I}_d^{i+1})$.

Pri deformiranju kompozitnega nosilca se v splošnem pojavijo zdrsi (zamiki) na stiku slojev. Ker do sedaj zdrsa $\Delta_j^i(x^i)$ med delcema slojev i in $i + 1$ z materialnima koordinatama x^i in x^{i+1} še nismo definirali, to storimo zdaj. Z upoštevanjem zveze (3.44) oziroma (3.45)–(3.46) definiramo zdrs $\Delta_j^i(x^i)$ preprosto kot razliko materialnih koordinat tistih dveh delcev sloja i ter $i + 1$, ki sta v j-tem stiku v kontaktu. Dobljeni izraz za zdrs se glasi

$$\Delta_j^i(x^i) = x^i - x^{i+1} = u^i(x^i) - u^{i+1}(x^{i+1}) + z_j\Big(\sin\varphi^i(x^i) - \sin\varphi^{i+1}(x^{i+1})\Big). \tag{3.47}$$

Geometrijski pomen zdrsa $\Delta_j^i(x^i)$ prikazuje slika 3.4. S slike 3.4 lahko zdrs $\Delta_j^i(x^i)$ izrazimo z deformacijskima količinama $e_*^i(x^i)$ ter $e_*^{i+1}(x^{i+1})$, ki predstavljata specifični spremembi dolžin materialnih vlaken krivulje stika med slojema i ter $i + 1$:

$$\Delta_j^i(x^i) + s_*^{i+1}(x^i) = \Delta_j^i(0) + s_*^i(x^i). \tag{3.48}$$

Z upoštevanjem izrazov za izračun infinitezimalne spremembe dolžine krivulje stika

$$\mathrm{d}s_*^i(x^i) = \big(1 + e_*^i(x^i)\big)\mathrm{d}x^i \tag{3.49}$$

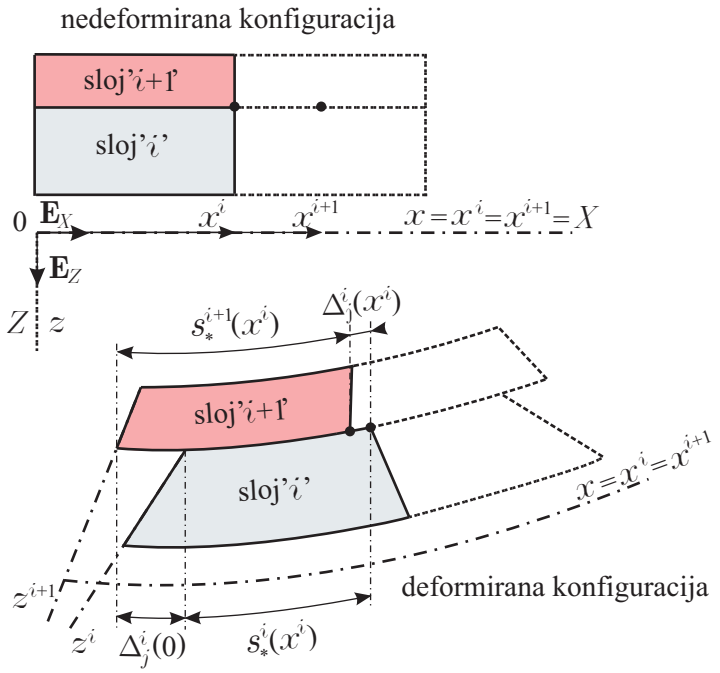

Slika 3.4: Geometrijski pomen zdrsa $\Delta_j^i(x^i)$ med slojema i in $i+1$ kompozitnega nosilca.

Figure 3.4: A geometric representation of interlayer slip $\Delta_j^i(x^i)$ between the layer i and $i+1$ of the composite beam.

in

$$\mathrm{d}s_*^{i+1}(x^i) = \big(1 + e_*^{i+1}(x^i)\big)\mathrm{d}x^i \tag{3.50}$$

lahko enačbo za zdrs (3.48) zapišemo tudi drugače

$$\Delta_j^i(x^i) = \Delta_j^i(0) + \int_0^{x^i} \big(e_*^i(\xi) - e_*^{i+1}(\xi)\big)\mathrm{d}\xi. \tag{3.51}$$

V enačbi (3.51) lahko $e_*^i(x^i)$ in $e_*^{i+1}(x^i)$ nadomestimo z deformacijskimi količinami referenčne osi posameznega sloja. V ta namen uporabimo izraza (Reissner, 1972), ki povezujeta specifično spremembo referenčne osi nosilca $e(x)$ z deformacijskimi količinami referenčne osi

$$\varepsilon(x) = \big(1 + e(x)\big)\cos\chi(x) - 1, \tag{3.52}$$

$$\gamma(x) = \big(1 + e(x)\big)\sin\chi(x). \tag{3.53}$$

S posplošitvijo na kompozitne nosilce in upoštevanjem (3.16) v (3.52) namesto $\varepsilon(x)$, dobimo po kratki izpeljavi naslednja izraza

$$e_*^i(x^i) = \Big(1 + \varepsilon^i(x^i) + z_j\kappa^i(x^i)\Big)\cos\chi^i(x^i) + \gamma^i(x^i)\sin\chi^i(x^i) - 1, \tag{3.54}$$

$$e_*^{i+1}(x^i) = \Big(1 + \varepsilon^{i+1}(x^i) + z_j\kappa^{i+1}(x^i)\Big)\cos\chi^{i+1}(x^i) + \gamma^{i+1}(x^i)\sin\chi^{i+1}(x^i) - 1. \tag{3.55}$$

Z vstavitvijo izrazov (3.54) in (3.55) v (3.51) dobimo enačbo za izračun zdrsa $\Delta_j^i(x^i)$ v odvisnosti od deformacijskih količin $\varepsilon^i(x^i)$, $\varepsilon^{i+1}(x^i)$, $\gamma^i(x^i)$, $\gamma^{i+1}(x^i)$, $\kappa^i(x^i)$, $\kappa^{i+1}(x^i)$ ter zasukov $\chi^i(x^i)$, $\chi^{i+1}(x^i)$.

$$\begin{aligned}\Delta_j^i(x^i) =&\Delta_j^i(0) + \int_0^{x^i} \Big(\big(1 + \varepsilon^i(\xi) + z_j\kappa^i(\xi)\big)\cos\chi^i(\xi) + \gamma^i(\xi)\sin\chi^i(\xi) - \\ &- \big(1 + \varepsilon^{i+1}(\xi) + z_j\kappa^{i+1}(\xi)\big)\cos\chi^{i+1}(\xi) + \gamma^{i+1}(\xi)\sin\chi^{i+1}(\xi)\Big)\mathrm{d}\xi.\end{aligned} \tag{3.56}$$

Enačbo zdrsa (3.48) oziroma (3.51) lahko zapišemo tudi drugače:

$$\Delta_j^i(x^i) = \int_{x^i}^{x^{i+1}(x^i)} \big(1 + e_*^{i+1}(\xi)\big)\mathrm{d}\xi, \tag{3.57}$$

oziroma z upoštevanjem zveze (3.55) kot

$$\Delta_j^i(x^i) = \int_{x^i}^{x^{i+1}(x^i)} \Big(\big(1 + \varepsilon^{i+1}(\xi) + z_j\kappa^{i+1}(\xi)\big)\cos\chi^{i+1}(\xi) + \gamma^{i+1}(\xi)\sin\chi^{i+1}(\xi)\Big)\mathrm{d}\xi. \tag{3.58}$$

Podobno kot smo zapisali izraz za zdrs $\Delta_j^i(x^i)$, lahko zapišemo tudi izraz za zdrs $\Delta_j^{i+1}(x^{i+1})$, ki predstavlja zdrs med delcema slojev i in $i+1$ z materialnima koordinatama x^{i+1}, kot

$$\begin{aligned}\Delta_j^{i+1}(x^{i+1}) &= \int_{x^i}^{x^{i+1}(x^i)} \big(1 + e_*^i(\xi)\big)\mathrm{d}\xi = \\ &= \int_{x^i(i+1)}^{x^{i+1}} \Big(1 + \varepsilon^i(\xi) + z_j\kappa^i(\xi)\Big)\cos\chi^i(\xi) + \gamma^i(\xi)\sin\chi^i(\xi)\mathrm{d}\xi\end{aligned} \tag{3.59}$$

Vezni enačbi (3.47) ali (3.56) povsem določata konstitutivni zakon stika.

3.1.5 Konstitutivni zakon stika

Kompozitne konstrukcije sestavljajo posamezni deli (sloji), ki so s pomočjo različnih veznih sredstev povezani v celoto. Uporaba veznih sredstev se razlikuje glede na vrsto uporabljenega materiala in zahtevane stopnje povezanosti slojev. Le-ti so lahko povezani togo, delno (podajno) ali pa so povsem nepovezani. Absolutno toge povezave slojev značilnih kompozitnih konstrukcij, ki nastopajo v gradbeništvu, ni mogoče zagotoviti. Lahko se ji le približamo z uporabo izredno togih veznih sredstev. V splošnem pa je povezava med sloji podajna. Posledično se v vseh fazah obremenitve pojavijo zamiki na stiku med sloji. Pri modeliranju kompozitnih nosilcev se moramo zavedati, da je stik oziroma povezanost slojev ključnega pomena pri določitvi napetostnega in deformacijskega stanja obravnavanih nosilcev.

Stik oziroma povezavo slojev običajno obravnavamo kot kontaktni problem. Veda, ki se ukvarja s kontaktom oziroma trenjem med telesi se imenuje tribologija (gr. beseda *tribos* pomeni trenje). Pri tako imenovanem tribološkem kontaktu medsebojno delujeta vsaj dve telesi (površini), ki sta v medsebojnem relativnem gibanju. Posledica sta normalna in tangencialna kontaktna napetost. Predstavljata dodatno obremenitev sloja v stiku. Analiza dejanskih triboloških sistemov (kontaktov), kjer je prisotna tako normalna, kot tudi tangencialna obremenitev, je možna z uporabo superpozicije dveh enostavnejših problemov, čiste normalne in čiste tangencialne obremenitve. Pogoji, ki karakterizirajo stik, se tako

običajno delijo na pogoje, ki opisujejo kontakt v normalni smeri in pogoje, ki opisujejo kontakt v tangentni smeri na stično ploskev. V literaturi obstaja veliko različnih formulacij stika v normalni smeri skupaj s tribološkimi zakoni v tangencialni smeri (Wriggers, 1999), (Jonhson, 1987), (Rabinowicz, 1995), (Kalker, 1990), itd. Med najpreprostejšimi in največkrat uporabljenimi je Signorinijev model stika z upoštevanjem kvazistatičnega modela trenja po Coulombovem zakonu (Raous, 1999), (Renaud in Feng, 2003), (Fernandez in Sofonea, 2002), itd. Omenjeni model stika spada v skupino unilateralnih stikov. Osnovna predpostavka omenjene skupine stikov je, da deformabilna telesa, ki so v kontaktu s poljubnim togim telesom, ne morejo prodreti vanj.

V nadaljevanju na kratko opišemo Signorinijev model stika z upoštevanjem Coulombovega zakona trenja.

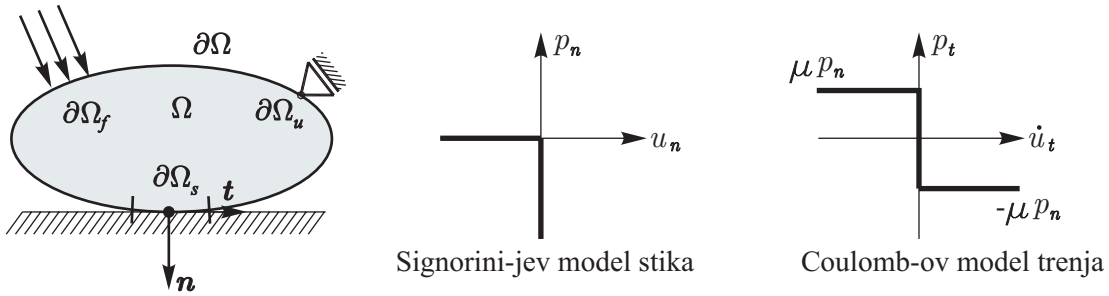

Slika 3.5: (a) Kontakt telesa s togo podlago; (b) Signorinijev model stika; (c) Coulombov zakon trenja.
Figure 3.5: (a) Contact with a rigid obstacle, (b) a Signorini's contact law, (c) a Coulomb friction law.

V ta namen obravnavamo poljubno deformabilno telo Ω, ki je v kontaktu s togim telesom oziroma podlago. Rob deformabilnega telesa definiramo kot $\partial\Omega = \partial\Omega_f \cup \partial\Omega_u \cup \partial\Omega_s$. Z Ω_f (Ω_u) označimo območje $\partial\Omega$ kjer je predpisana obtežba (pomiki), s $\partial\Omega_s$ pa začetno območje stika deformabilnega telesa s togo podlago. Definiramo tudi zvezno kontaktno napetost $\boldsymbol{p} = p_t\boldsymbol{t} + p_n\boldsymbol{n}$ ter vektor pomikov $\boldsymbol{u} = u_t\boldsymbol{t} + u_n\boldsymbol{n}$ dotikališčnih točk območja $\partial\Omega_s$. Pri tem sta $\boldsymbol{t}$ in $\boldsymbol{n}$ enotska vektorja v smeri tangente in normale na rob $\partial\Omega$. Z upoštevanjem modela stika (slika 3.5) (a) ter Coulombovega zakona trenja, ki ga prikazuje slika 3.5 (b), je Signorinijev kontaktni problem opisan z naslednjimi pogoji:

1. če $u_n < 0 \longrightarrow p_n = 0$ ni kontakta,
2. če $\boldsymbol{u} = \boldsymbol{0}$ in $|p_t| \leq k_t\,|p_n|$ kontakt–lepenje,
3. če $u_t \neq 0$ in $|p_t| = k_t\,|p_n|$ kontakt–drsenje,

kjer smo z k_t označili Coulombov koeficient trenja. V primeru 2, koeficient k_t imenujemo tudi koeficient lepenja.

Pri opisu modela kontakta se do sedaj nismo spraševali o obliki in lastnostih kontaktne površine. Realne kontaktne površine niso idealno gladke, temveč so hrapave. To pomeni, da je kontaktna površina dveh teles zmanjšana na zelo majhen del navidezne kontaktne površine, pri čemer je realna kontaktna površina sestavljena iz mikrokontaktov med posameznimi vrščki hrapavosti kontaktnih teles, slika 3.6.

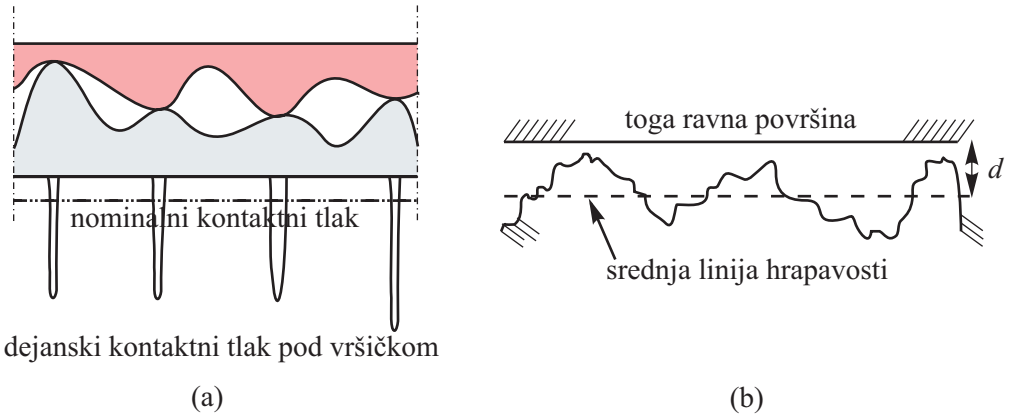

Slika 3.6: (a) Realna kontaktna površina in porazdelitev kontaktnega tlaka, (b) kontakt dveh hrapavih površin, predstavljen s kontaktom hrapave deformabilne površine in ravne toge površine.

Figure 3.6: (a) A real contact surface and a distribution of contact pressure, (b) contact interface represented by the contact between a rough deformable surface and a rigid flat obstacle.

Kontaktne napetosti, ki nastopijo v posameznem mikrokontaktu so lahko zelo visoke, kar ima lahko za posledico pojav lokalne plastične deformacije, slika 3.6 (a). Za natančno formulacijo realnega kontaktnega problema potrebujemo poleg izračuna dejanske kontaktne površine tudi vrednosti materialnih konstant ter koeficient trenja v vsaki točki kontaktne površine. Vse te količine je izredno težko natančno določiti. Kontakt dveh hrapavih površin zato običajno predstavimo s kontaktom hrapave deformabilne površine telesa in ravne toge plošče, slika 3.6 (b), materialne lastnosti pa predpostavimo oziroma povzamemo iz literature. Na sliki 3.6 (b), predstavlja d začetno razdaljo predpostavljene srednje linije hrapavosti od toge ravne površine. S tako definirano količino lahko razširimo Signorinijev model stika na kontaktno površino, ki se spreminja z obremenitvijo telesa. To storimo preprosto z zamenjavo pogoja $u_n \leq 0$ s pogojem $u_n \leq d$. Omenimo le še, da v literaturi obstaja cela vrsta empiričnih in analitičnih konstitutivnih modelov stika (Wriggers, 1999), ki poleg naštetega upoštevajo še adhezijo, vpliv nivoja obtežbe na velikost in obliko kontaktne površine itd.

Poleg materialnih lastnosti posameznih slojev opisanih z enačbami (3.41–3.43), ima na nosilnost in togost slojevitih konstrukcij z upoštevanjem zdrsa med sloji pomembno vlogo tudi konstitutivna zveza stične površine med sloji. Točna formulacija konstitutivnega modela stika je zato izredno pomembna in tudi zelo zahtevna naloga. Mehanske in toplotne lastnosti materialov se v kontaktih nesprestano spreminjajo. Pri vsakem nivoju obremenitve moramo poznati dejanske količine najrazličnejših parametrov, ki vplivajo na obnašanje stika. S splošnim konstitutivnim zakonom stika tako povežemo komponente vektorja kontaktne napetosti s parametri stika. Splošna oblika konstitutivnega zakona stika vzdolž referenčne osi kompozitnega nosilca je tako

$$q^i_{t,j}(x^i) = \mathcal{H}^i_{t,j}(x^i, q^i_{n,j}(x^i), \Delta^i_{t,j}(x^i), T^i(x^i, y^i, z^i), w^i(x^i, y^i, z^i), \ldots), \tag{3.60}$$

$$q^i_{n,j}(x^i) = \mathcal{H}^i_{n,j}(x^i, \Delta^i_{n,j}(x^i), T^i(x^i, y^i, z^i), w^i(x^i, y^i, z^i), \ldots), \tag{3.61}$$

kjer smo z $\Delta^i_{t,j}(x^i)$ in $\Delta^i_{n,j}(x^i)$ označili zdrs v tangentni smeri in razmak med sloji v normalni smeri na referenčno krivuljo j-tega stika. Z enačbama (3.60–3.61) povežemo tangencialno $q^i_{t,j}(x^i)$ in normalno

komponento $q^i_{n,j}(x^i)$ linijske kontaktne obtežbe $\boldsymbol{q}^i_j(x^i)$ z značilnimi količinami na stiku med posameznimi sloji.

Zaradi predpostavke, da sloji lahko drsijo drug po drugem, ne morejo pa se razmakniti oziroma prodreti drug v drugega, v nadaljevanju obravnavamo le konstitutivni zakon (3.60). Določitev konstitutivne zveze (3.60) je izredno zahtevna. Konstitutivno funkcijo $\mathcal{H}^i_{t,j}$ običajno določimo eksperimentalno s tako imenovanim testom *push-out*, slika 3.7. Na ta način, za različne vrste stikov (oziroma veznih sredstev) in drugih parametrov stika, določimo razmerje med obtežbo in zdrsom. Poenostavljen konstitutivni zakon (3.60) ima tako obliko

$$q^i_{t,j}(x^i) = \mathcal{H}^i_{t,j}\big(x^i, \Delta^i_{t,j}(x^i)\big). \tag{3.62}$$

Pogosto konstitutivni zakon (3.62) imenujemo tudi zveza *strižni tok-zamik*. Z njim lahko opišemo večino načinov izvedb stika med sloji kompozitnega nosilca, ki nastopajo v praksi. Najenostavnejši in pri analizi kompozitnih nosilcev najbolj uporabljeni je linearen konstitucijski model stika

$$q^i_{t,j}(x^i) = K^i_j \Delta^i_{t,j}(x^i). \tag{3.63}$$

Koeficient K^i_j v (3.63) imenujemo koeficient togosti stika. V skladu z zahtevo (3.44) z uporabo tretjega Newtonovega zakona o akciji in reakciji ter relacije (3.62) izpeljemo povezavo med komponentama kontaktne linijske obtežbe sloja i in i+1 v j-tem stiku deformiranega kompozitnega nosilca

$$q^i_{t,j}(x^i) + q^{i+1}_{t,j}(x^{i+1}) = 0, \tag{3.64}$$

$$q^i_{n,j}(x^i) + q^{i+1}_{n,j}(x^{i+1}) = 0. \tag{3.65}$$

Z uporabo konstitutivnega zakona (3.62) se izkaže, da velja v ravnotežni deformirani legi kompozitnega

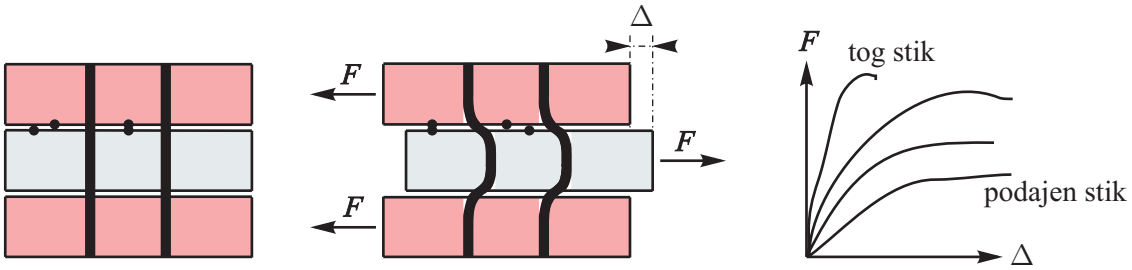

Slika 3.7: Eksperimentalno določanje lastnosti veznih sredstev uporabljenih v stiku.
Figure 3.7: Experimental determination of the interlayer connection properties.

nosilca neenakost:

$$q^i_{t,j}(x^i) + q^{i+1}_{t,j}(x^{i+1}) \neq 0. \tag{3.66}$$

Tako vpeljan konstitutivni zakon (3.62) pa je lahko nekoliko dvoumen, če ne upoštevamo dejstva, da smo pač vpeljali tak konstitutivni zakon, da sta delca, ki solegata v deformirani legi, v kontaktu le v normalni in ne tudi v tangencialni smeri na krivuljo stika.

3.1.6 Robni pogoji

Poleg osnovnega algebrajsko-diferencialnega sistema enačb kompozitnega nosilca z upoštevanjem zdrsa med sloji (3.11–3.12), (3.19–3.20), (3.41–3.43), (3.60) ter (3.45)-(3.46), (3.47), (3.57) in (3.65), potrebujemo za njegovo rešitev tudi pripadajoče robne pogoje. V splošnem se robni pogoji delijo na naravne (Neumannove) in bistvene (Dirchletove). O naravnih ali Neumannovih robnih pogojih govorimo

tedaj, kadar so robni pogoji posledica predpisanih robnih sil, medtem ko bistveni ali Dirchletovi robni pogoji izhajajo iz predpisanih geometrijskih količin na robovih. Znano je, da robni pogoji v splošnem ne določajo enolične rešitve sistema enačb kompozitnega nosilca (npr. če so predpisani le naravni robni pogoji, tj. Neumannov problem). Robni pogoji zato običajno niso samo Neumannovi ali Dirchletovi. V tem primeru govorimo o mešanih robnih pogojih. Definicijski območji naravnih in bistvenih robnih pogojev se medsebojno izključujeta, kar pomeni, da je v robni točki za vsako prostostno stopnjo lahko predpisan le en robni pogoj, naravni ali bistveni. Robni pogoji za posamezni sloj kompozitnega nosilca se glasijo

$$\begin{array}{lll} \mathcal{R}^i_X(0) - S^i_1 = 0 & \text{ali} & u^i(0) = u^i_1, \\ \mathcal{R}^i_Z(0) - S^i_2 = 0 & \text{ali} & w^i(0) = u^i_2, \\ \mathcal{M}^i(0) - S^i_3 = 0 & \text{ali} & \varphi^i(0) = u^i_3, \\ \mathcal{R}^i_X(L) - S^i_4 = 0 & \text{ali} & u^i(L) = u^i_4, \\ \mathcal{R}^i_Z(L) - S^i_5 = 0 & \text{ali} & w^i(L) = u^i_5, \\ \mathcal{M}^i(L) - S^i_6 = 0 & \text{ali} & \varphi^i(L) = u^i_6. \end{array} \tag{3.67}$$

Z robnimi pogoji je formulacija robnega problema nelinearnega kompozitnega nosilca z upoštevanjem zdrsa povsem določena. Osnovni algebrajsko-diferencialni sistem enačb zaradi preglednosti zapišemo v oknu 3.1.

3.1.7 Poenostavljene teorije kompozitnih nosilcev

V nadaljevanju z vpeljavo določenih predpostavk izpeljemo različne poenostavljene teorije kompozitnih nosilcev z upoštevanjem zdrsa med sloji.

3.1.7.1 Linearizirana teorija kompozitnih nosilcev

Pri večini konstrukcij, ki nastopajo v gradbeništvu, so pomiki in zasuki ter deformacije majhni v primerjavi z dimenzijami konstrukcije. To pomeni, da lahko ravnotežne enačbe v večini primerov upoštevamo na nedeformiranem stanju konstrukcije. V takem primeru pravimo, da rešujemo problem kompozitnega nosilca po teoriji prvega reda. Enačbe kompozitnega nosilca po teoriji prvega reda najlažje dobimo z linearizacijo nelinearnega diferencialnega operatorja $\boldsymbol{f}$, v katerem so združene enačbe (3.89–3.107). Vse neznane funkcije združimo v vektor neznanih funkcij

$$\boldsymbol{g} = \Big(u^i(x^i), w^i(x^i), \varphi^i(x^i), \varepsilon^i(x^i), \gamma^i(x^i), \kappa^i(x^i), \mathcal{R}^i_X(x^i), \mathcal{R}^i_Z(x^i), \mathcal{M}^i(x^i), q^i_{t,j}(x^i), q^i_{n,j}(x^i), \dots\Big), \tag{3.68}$$

ki ga pogosto imenujemo tudi vektor posplošenih kooordinat problema. Pri tem točko, v kateri robni problem kompozitnega nosilca lineariziramo, označimo s prečko nad simbolom. Torej se točka linearizacije glasi

$$\overline{\boldsymbol{g}} = \Big(\overline{u}^i(x^i), \overline{w}^i(x^i), \overline{\varphi}^i(x^i), \overline{\varepsilon}^i(x^i), \overline{\gamma}^i(x^i), \overline{\kappa}^i(x^i), \overline{\mathcal{R}}^i_X(x^i), \overline{\mathcal{R}}^i_Z(x^i), \overline{\mathcal{M}}^i(x^i), \overline{q}^i_{t,j}(x^i), \overline{q}^i_{n,j}(x^i), \dots\Big). \tag{3.69}$$

Čeprav je točka $\overline{\boldsymbol{g}}$ (3.69) poljubna, se bomo v nadaljevanju omejili na trivialno ravnotežno točko $\overline{\boldsymbol{g}} = \boldsymbol{0}$. Trivialni ravnotežni točki rečemo tudi nedeformirano stanje. Preidimo sedaj k linearizaciji. Linearizacija robnega problema kompozitnega nosilca z upoštevanjem zdrsa med sloji temelji na Fréchetovem odvodu $\boldsymbol{F}$ preslikav $\boldsymbol{f}$, ki ga imenujemo tudi smerni odvod (Marsden in Huges, 1983):

$$\boldsymbol{F}\Big(x^i, \overline{\boldsymbol{g}}, \frac{\mathrm{d}\overline{\boldsymbol{g}}}{\mathrm{d}x^i}\Big)\boldsymbol{g} = \frac{\mathrm{d}}{\mathrm{d}\varepsilon}\bigg|_{\varepsilon=0} \boldsymbol{f}\Big(x^i, \overline{\boldsymbol{g}} + \varepsilon\boldsymbol{g}, \frac{\mathrm{d}\overline{\boldsymbol{g}}}{\mathrm{d}x^i} + \varepsilon\frac{\mathrm{d}\boldsymbol{g}}{\mathrm{d}x^i}\Big). \tag{3.70}$$

Fréchetov odvod (3.70) v mehaniki konstrukcij imenujemo tangentna (togostna ali podajnostna) matrika. Linearizacija funkcij $\boldsymbol{f}$ okoli poljubne ravnotežne točke $\overline{\boldsymbol{g}}$ in v smeri vektorja $\boldsymbol{g}$ je tako z upoštevanjem (3.70) naslednja:

$$\boldsymbol{L}_{\overline{g}}(\boldsymbol{f},\boldsymbol{g}) = \boldsymbol{f}\Big(x^i, \overline{\boldsymbol{g}}, \frac{\mathrm{d}\overline{\boldsymbol{g}}}{\mathrm{d}x^i}\Big) + \boldsymbol{F}\Big(x^i, \overline{\boldsymbol{g}}, \frac{\mathrm{d}\overline{\boldsymbol{g}}}{\mathrm{d}x^i}\Big)\boldsymbol{g}. \tag{3.71}$$

Robni problem (3.89–3.107) moremo pisati v krajši obliki kot $\boldsymbol{f}\Big(x^i, \boldsymbol{g}, \frac{\mathrm{d}\boldsymbol{g}}{\mathrm{d}x^i}\Big) = 0$. Od tod in z upoštevanjem, da linearizirano okoli nedeformirane lege $\overline{\boldsymbol{g}} = \boldsymbol{0}$, dobimo linearizirani robni problem kompozitnega nosilca zapisan v sledeči obliki

$$\boldsymbol{F}\Big(x^i, \overline{\boldsymbol{g}} = \boldsymbol{0}, \frac{\mathrm{d}\overline{\boldsymbol{g}}}{\mathrm{d}x^i} = \boldsymbol{0}\Big)\boldsymbol{g} = \boldsymbol{0}. \tag{3.72}$$

Z rešitvijo (3.72) lahko v okolici ravnotežne točke $\overline{\boldsymbol{g}} = \boldsymbol{0}$ (nedeformirano stanje) sklepamo na lastnosti rešitve nelinearnega sistema (3.89–3.107). Z linearizacijo smo nelinearni robni problem kompozitnega nosilca z upoštevanjem zdrsa med sloji prevedli na linearnega. Kot rezultat dobimo sistem linearnih diferencialnih in algebrajskih enačb (3.108–3.126), ki ga lažje obvladujemo. V komponentni obliki ga zapišemo v oknu 3.2.

Na koncu omenimo še, da kljub temu, da smo upoštevali majhnost pomikov in zasukov posameznih slojev, velikosti zdrsov med sloji ostajajo poljubno velike. Inženirsko predpostavko o majhnosti zdrsov med sloji bomo upoštevali v nadaljevanju.

3.1.7.2 Teorija majhnih zdrsov

V gradbeništvu imamo običajno opravka s kompozitnimi konstrukcijami, pri katerih uporaba veznih sredstev kot so žeblji, mozniki, itd. pogojuje relativno majhne zdrse med posameznimi sloji. Vpeljava predpostavke o majhnih zdrsih je pri analizi kompozitnih nosilcev inženirsko povsem upravičena. To predpostavko potrjujejo tudi opazovanja obnašanja kompozitnih nosilcev pri eksperimentih, kakor tudi pri njihovi vsakdanji uporabi v praksi. Omenjeno predpostavko zapišemo kot

$$\Delta_j^i(x^i) \cong \Delta_j^{i+1}(x^{i+1}) = \Delta_j(x^i), \tag{3.73}$$

kar pomeni, da sta zdrsa dveh slojev $\Delta_j^i(x^i)$ in $\Delta_j^{i+1}(x^{i+1})$ v stiku j praktično enako velika. Posledično to pomeni, da je vpliv previsov na deformiranje kompozitnega nosilca zanemarljiv, torej $\mathcal{I}_l^i \cong \mathcal{I}_d^i \cong 0$ ter $\mathcal{I}_l^{i+1} \cong \mathcal{I}_d^{i+1} \cong 0$. Dolžina stične ploskve med slojema je približno enaka začetni dolžini kompozitnega nosilca. Definicijsko območje kinematičnih, deformacijskih in ravnotežnih količin kompozitnega nosilca je tako za vse sloje približno enako celotni dolžini kompozitnega nosilca $\mathcal{I}^i \cong \mathcal{I}^{i+1} \in [0, L]$. To pomeni, da lahko vse količine poljubnega sloja zapišemo v odvisnosti od materialne kooordinate referenčnega sloja. Izbira referenčnega sloja je poljubna. Če materialno koordinato referenčnega sloja označimo z x^i, potem za vse količine preostalih slojev velja $(\bullet)^{i+1}(x^{i+1}) \cong (\bullet)^{i+1}(x^i)$, na primer $w^{i+1}(x^{i+1}) \cong w^{i+1}(x^i)$, $\mathcal{Q}^{i+1}(x^{i+1}) \cong \mathcal{Q}^{i+1}(x^i)$, itd. Ker velja slednje tudi za komponente linijske kontaktne obtežbe, iz (3.64) in (3.65) sledi

$$q_{t,j}^i(x^i) + q_{t,j}^{i+1}(x^{i+1}) = 0 \longrightarrow q_{t,j}^i(x^i) = -q_{t,j}^{i+1}(x^i) = q_{t,j}(x^i) \tag{3.74}$$

$$q_{n,j}^i(x^i) + q_{n,j}^{i+1}(x^{i+1}) = 0 \longrightarrow q_{n,j}^i(x^i) = -q_{n,j}^{i+1}(x^i) = q_{n,j}(x^i) \tag{3.75}$$

Z upoštevanjem izrazov (3.64) ter (3.74) lahko poenostavljen konstitutivni zakon stika (3.62) pišemo v preprostejši obliki

$$q_{t,j}(x^i) = \mathcal{H}_j\big(x^i, \Delta_j(x^i)\big). \tag{3.76}$$

Skladno z opisanimi predpostavkami se osnovne enačbe kompozitnega nosilca z upoštevanjem zdrsa med sloji nekoliko poenostavijo. Enačbe kompozitnega nosilca, kjer velikosti pomikov, zasukov in deformacij posameznih slojev niso omejene, zdrsi pa so majhni, dobimo z upoštevanjem poenostavitev (3.73-3.76) v sistemu enačb (3.89–3.107). Združene jih zapišemo v oknu 3.3.

3.1.7.3 Timoshenkov kompozitni nosilec (teorija prvega reda in teorija majhnih zdrsov)

Enačbe kompozitnega nosilca, po teoriji prvega reda v primeru majhnih zdrsov, dobimo z upoštevanjem predpostavk (3.73–3.76) v sistemu lineariziranih enačb kompozitnega nosilca (3.108–3.126). Zapišemo jih v oknu 3.4.

3.1.7.4 Bernoullijev kompozitni nosilec (teorija prvega reda in teorija majhnih zdrsov)

Enačbe (3.89–3.158), ki smo jih izpeljali v prejšnjih razdelkih, določajo različne Timoshenkove teorije kompozitnih nosilcev z upoštevanjem zdrsa med sloji. Ena izmed glavnih lastnosti omenjenih teorij je, da upoštevajo vpliv strižnih deformacij na pomike in zdrse kompozitnih nosilcev. Vpliv strižnih deformacij je pomembno upoštevati predvsem pri kratkih nosilcih. V primeru vitkih nosilcev, kjer je razmerje med višino in dolžino nosilca majhno (manj kot 0.1), je napaka, ki jo naredimo, če zanemarimo vpliv strižnih deformacij, majhna. Tedaj lahko upoštevamo, da je strižna deformacija posameznega sloja kompozitnega nosilca zanemarljivo majhna, tj. $\gamma^i(x^i) \cong 0$. Z upoštevanjem zadnje predpostavke v (3.89–3.107) po krajši izpeljavi dobimo naslednje zveze (Čas, 2004):

$$\tan\varphi^i(x^i) = \tan\varphi^{i+1}(x^{i+1}) \longrightarrow \varphi^i(x^i) = \varphi^{i+1}(x^{i+1}), \tag{3.77}$$

$$\kappa^{i+1}(x^{i+1}) = \frac{1+\varepsilon^{i+1}(x^{i+1})}{1+\varepsilon^i(x^i)}\kappa^i(x^i), \tag{3.78}$$

$$\frac{\mathrm{d}x^{i+1}}{\mathrm{d}x^i} = \frac{1+\varepsilon^{i+1}(x^{i+1})}{1+\varepsilon^i(x^i)}. \tag{3.79}$$

Ker upoštevamo, da so pomiki, zasuki, deformacije ter zdrsi majhne količine, dobimo iz (3.78) in (3.79) povezavo med psevdoukrivljenostima referenčnih osi dveh sosednjih slojev kompozitnega nosilca

$$\frac{\mathrm{d}x^{i+1}}{\mathrm{d}x^i} \cong 1 \longrightarrow \kappa^{i+1}(x^{i+1}) \cong \kappa^{i+1}(x^i) \cong \kappa^i(x^i) \overset{\text{predpostavka}}{\longrightarrow} \kappa(x^i) = \kappa^i(x^i) = \kappa^{i+1}(x^i), \tag{3.80}$$

ter njunimi navpičnimi pomiki in zasuki

$$w^i(x^i) \cong w^{i+1}(x^{i+1}) \cong w^{i+1}(x^i) \overset{\text{predpostavka}}{\longrightarrow} w(x^i) = w^i(x^i) = w^{i+1}(x^i), \tag{3.81}$$

$$\varphi^i(x^i) \cong \varphi^{i+1}(x^{i+1}) \cong \varphi^{i+1}(x^i) \overset{\text{predpostavka}}{\longrightarrow} \varphi(x^i) = \varphi^i(x^i) = \varphi^{i+1}(x^i), \tag{3.82}$$

Če predpostavke oziroma nove oznake (3.80–3.82) vstavimo v sistem (3.143)-(3.158) se izkaže, da lahko namesto enačb (3.144–3.145) upoštevamo samo enačbi za skupen pomik $w(x^i)$ in zasuk $\varphi(x^i)$ kompozitnega nosilca:

$$\frac{\mathrm{d}w(x^i)}{\mathrm{d}x^i} + \varphi(x^i) = 0, \tag{3.83}$$

$$\frac{\mathrm{d}\varphi(x^i)}{\mathrm{d}x^i} - \kappa(x^i) = 0. \tag{3.84}$$

Zaradi (3.83) in (3.84) lahko vpeljemo skupno prečno silo $\mathcal{Q}(x^i)$ in skupni upogibni moment $\mathcal{M}(x^i)$ kompozitnega nosilca. Zato se poenostavijo tudi pripadajoče ravnotežne enačbe

$$\mathcal{Q}(x^i) = \sum_{i=1}^{\mathrm{N_{sl}}} \mathcal{Q}^i(x^i) \quad \longrightarrow \quad \frac{\mathrm{d}\mathcal{Q}(x^i)}{\mathrm{d}x^i} + \sum_{i=1}^{\mathrm{N_{sl}}} p_Z^i(x^i) = 0, \tag{3.85}$$

oziroma

$$\mathcal{M}(x^i) = \sum_{i=1}^{\mathrm{N_{sl}}} \mathcal{M}^i(x^i) \quad \longrightarrow \quad \frac{\mathrm{d}\mathcal{M}(x^i)}{\mathrm{d}x^i} - \mathcal{Q}(x^i) + \sum_{i=1}^{\mathrm{N_{sl}}} m_Y^i(x^i) = 0, \tag{3.86}$$

ter nekateri kinematični in statični robni pogoji

$$\begin{array}{rcl}
\mathcal{N}^i(0) - S_1^i = 0 & \text{ali} & u^i(0) = u_1^i, \\
\mathcal{Q}(0) - \sum_{i=1}^{N_{\mathrm{sl}}} S_2^i = 0 & \text{ali} & w(0) = u_2, \\
\mathcal{M}(0) - \sum_{i=1}^{N_{\mathrm{sl}}} S_3^i = 0 & \text{ali} & \varphi(0) = u_3, \\
\mathcal{N}^i(L) - S_4^i = 0 & \text{ali} & u^i(L) = u_4^i, \\
\mathcal{Q}(L) - \sum_{i=1}^{N_{\mathrm{sl}}} S_5^i = 0 & \text{ali} & w(L) = u_5, \\
\mathcal{M}(L) - \sum_{i=1}^{N_{\mathrm{sl}}} S_6^i = 0 & \text{ali} & \varphi(L) = u_6.
\end{array} \tag{3.87}$$

Napetostno in deformacijsko stanje geometrijsko linearnega Bernoullijevega kompozitnega nosilca z upoštevanjem majhnih zdrsov med sloji je tako določeno z dvema nepovezanima diferencialno algebrajskima sistemoma enačb (3.162–3.172) in (3.173–3.178). Izpeljava je trivialna zato jo tu ne prikažemo. Podana je v (Čas, 2004). Zaradi nazornosti oba sistema enačb prikažemo v oknu 3.5. Omeniti velja, da je posebnost reševanja opisanega sistema enačb (3.162–3.178) za določitev napetostnega in deformacijskega stanja kompozitnega nosilca v tem, da normalne komponente $q_{n,j}(x^i)$ linijske kontaktne obtežbe $\boldsymbol{q}$ niso osnovne neznanke problema. Ko rešimo osnovni sistem (3.162–3.172), jih določimo z rešitvijo dodatnega sistema (3.173–3.178), oziroma sistema

$$\begin{bmatrix}
1 & 0 & 0 & \dots & 0 & 0 \\
-1 & 1 & 0 & \dots & 0 & 0 \\
0 & -1 & 1 & \dots & 0 & 0 \\
\vdots & \vdots & \vdots & \ddots & \vdots & \vdots \\
0 & 0 & 0 & -1 & 1 & 0 \\
0 & 0 & 0 & 0 & -1 & 1
\end{bmatrix}
\begin{Bmatrix}
q_{n,1}(x^i) \\ q_{n,2}(x^i) \\ q_{n,3}(x^i) \\ \vdots \\ q_{n,N_{\mathrm{sl}}-2}(x^i) \\ q_{n,N_{\mathrm{sl}}-1}(x^i)
\end{Bmatrix}
= -
\begin{Bmatrix}
\frac{\mathrm{d}\mathcal{Q}^1(x^i)}{\mathrm{d}x^i} + p_Z^1(x^i) \\
\frac{\mathrm{d}\mathcal{Q}^2(x^i)}{\mathrm{d}x^i} + p_Z^2(x^i) \\
\frac{\mathrm{d}\mathcal{Q}^3(x^i)}{\mathrm{d}x^i} + p_Z^3(x^i) \\
\vdots \\
\frac{\mathrm{d}\mathcal{Q}^{N_{\mathrm{sl}}-2}(x^i)}{\mathrm{d}x^i} + p_Z^{N_{\mathrm{sl}}-2}(x^i) \\
\frac{\mathrm{d}\mathcal{Q}^{N_{\mathrm{sl}}-1}(x^i)}{\mathrm{d}x^i} + p_Z^{N_{\mathrm{sl}}-1}(x^i)
\end{Bmatrix}. \tag{3.88}$$

Okno 3.1: Robni problem kompozitnega nosilca v komponentni obliki

Za $x^i \in \mathcal{I}_l^i \cup \mathcal{I}^i \cup \mathcal{I}_d^i = [0, L]$:

- $(i = j = 1, \ldots, N_{\text{sl}};\ j \neq N_{\text{sl}})$ in $q_{t,0}^1(x^i) = q_{n,0}^1(x^i) = 0$

kinematične enačbe

$$1 + \frac{\mathrm{d}u^i(x^i)}{\mathrm{d}x^i} - \big(1 + \varepsilon^i(x^i)\big)\cos\varphi^i(x^i) - \gamma^i(x^i)\sin\varphi^i(x^i) = 0, \tag{3.89}$$

$$\frac{\mathrm{d}w^i(x^i)}{\mathrm{d}x^i} + \big(1 + \varepsilon^i(x^i)\big)\sin\varphi^i(x^i) - \gamma^i(x^i)\cos\varphi^i(x^i) = 0, \tag{3.90}$$

$$\frac{\mathrm{d}\varphi^i(x^i)}{\mathrm{d}x} - \kappa^i(x^i) = 0, \tag{3.91}$$

ravnotežne enačbe

$$\frac{\mathrm{d}\mathcal{R}_X^i(x^i)}{\mathrm{d}x^i} + p_X^i(x^i) + \\ + \Big(q_{t,j-1}^i(x^i) + q_{t,j}^i(x^i)\Big)\cos\big(\varphi^i(x^i) - \chi^i(x^i)\big) + \Big(q_{n,j-1}^i(x^i) + q_{n,j}^i(x^i)\Big)\sin(\varphi^i(x^i) - \chi^i(x^i)) = 0, \tag{3.92}$$

$$\frac{\mathrm{d}\mathcal{R}_Z^i(x^i)}{\mathrm{d}x^i} + p_Z^i(x^i) - \\ - \Big(q_{t,j-1}^i(x^i) + q_{t,j}^i(x^i)\Big)\sin\big(\varphi^i(x^i) - \chi^i(x^i)\big) + \Big(q_{n,j-1}^i(x^i) + q_{n,j}^i(x^i)\Big)\cos(\varphi^i(x^i) - \chi^i(x^i)) = 0, \tag{3.93}$$

$$\mathcal{N}^i(x^i) = \mathcal{R}_X^i(x^i)\cos\varphi^i(x^i) - \mathcal{R}_Z^i(x^i)\sin\varphi^i(x^i), \tag{3.94}$$

$$\mathcal{Q}^i(x^i) = \mathcal{R}_X^i(x^i)\sin\varphi^i(x^i) + \mathcal{R}_Z^i(x^i)\cos\varphi^i(x^i), \tag{3.95}$$

$$\frac{\mathrm{d}\mathcal{M}^i(x^i)}{\mathrm{d}x^i} - \big(1 + \varepsilon^i(x^i)\big)\mathcal{Q}^i(x^i) + \gamma^i(x^i)\mathcal{N}^i(x^i) + m_Y^i(x^i) + \Big(z_{j-1}q_{t,j-1}^i(x^i) + z_j q_{t,j}^i(x^i)\Big) \\ \Big(\cos\varphi^i(x^i)\cos(\varphi^i(x^i) - \chi^i(x^i)) + \sin\varphi^i(x^i)\sin(\varphi^i(x^i) - \chi^i(x^i))\Big) + \Big(z_{j-1}q_{n,j-1}^i(x^i) + z_j q_{n,j}^i(x^i)\Big) \\ \Big(\cos\varphi^i(x^i)\sin(\varphi^i(x^i) - \chi^i(x^i)) - \sin\varphi^i(x^i)\cos(\varphi^i(x^i) - \chi^i(x^i))\Big) = 0. \tag{3.96}$$

konstitutivne enačbe

$$\mathcal{N}^i(x^i) = \mathcal{N}_{\text{c}}^i\Big(x^i, \varepsilon^i(x^i), \kappa^i(x^i), T^i(x^i, y^i, z^i), w^i(x^i, y^i, z^i)\Big), \tag{3.97}$$

$$\mathcal{Q}^i(x^i) = \mathcal{Q}_{\text{c}}^i\Big(x^i, \gamma^i(x^i), T^i(x^i, y^i, z^i), w^i(x^i, y^i, z^i)\Big) \tag{3.98}$$

$$\mathcal{M}^i(x^i) = \mathcal{M}_{\text{c}}^i\Big(x^i, \varepsilon^i(x^i), \kappa^i(x^i), T^i(x^i, y^i, z^i), w^i(x^i, y^i, z^i)\Big) \tag{3.99}$$

pripadajoči naravni (Neumannovi) in bistveni (Dirichletovi) robni pogoji

$$\begin{array}{lll} \mathcal{R}_X^i(0) - S_1^i = 0 & \text{ali} & u^i(0) = u_1^i, \\ \mathcal{R}_Z^i(0) - S_2^i = 0 & \text{ali} & w^i(0) = u_2^i, \\ \mathcal{M}^i(0) - S_3^i = 0 & \text{ali} & \varphi^i(0) = u_3^i, \\ \mathcal{R}_X^i(L) - S_4^i = 0 & \text{ali} & u^i(L) = u_4^i, \\ \mathcal{R}_Z^i(L) - S_5^i = 0 & \text{ali} & w^i(L) = u_5^i, \\ \mathcal{M}^i(L) - S_6^i = 0 & \text{ali} & \varphi^i(L) = u_6^i. \end{array} \tag{3.100}$$

- $(i = j = 1, \ldots, N_{\text{sl}} - 1)$

posplošene vezne enačbe

$$x^i + u^i(x^i) + z_j\sin\varphi^i(x^i) = x^{i+1} + u^{i+1}(x^{i+1}) + z_j\sin\varphi^{i+1}(x^{i+1}), \tag{3.101}$$

$$w^i(x^i) + z_j\cos\varphi^i(x^i) = w^{i+1}(x^{i+1}) + z_j\cos\varphi^{i+1}(x^{i+1}), \tag{3.102}$$

$$\Delta_j^i(x^i) = x^{i+1} - x^i = u^i(x^i) - u^{i+1}(x^{i+1}) + z_j\Big(\sin\varphi^i(x^i) - \sin\varphi^{i+1}(x^{i+1})\Big), \tag{3.103}$$

$$\Delta_j^{i+1}(x^{i+1}) = \int_{x^i(i+1)}^{x^{i+1}} \Big(1 + \varepsilon^i(\xi) + z_j\kappa^i(\xi)\Big)\cos\chi^i(\xi) + \gamma^i(\xi)\sin\chi^i(\xi)\mathrm{d}\xi, \tag{3.104}$$

$$q_{n,j}^i(x^i) - q_{n,j}^{i+1}(x^{i+1}) = 0, \tag{3.105}$$

$$q_{t,j}^i(x^i) = \mathcal{H}_{t,j}^i(x^i, q_{n,j}^i(x^i), \Delta_j^i(x^i), T^i(x^i, y^i, z^i), w^i(x^i, y^i, z^i)), \tag{3.106}$$

$$q_{t,j}^{i+1}(x^{i+1}) = \mathcal{H}_{t,j}^{i+1}(x^{i+1}, q_{n,j}^{i+1}(x^{i+1}), \Delta_j^{i+1}(x^{i+1}), T^{i+1}(x^{i+1}, y^{i+1}, z^{i+1}), w^{i+1}(x^{i+1}, y^{i+1}, z^{i+1})), \tag{3.107}$$

Osnovne neznanke problema so:

$u^i(x^i), w^i(x^i), \varphi^i(x^i), \varepsilon^i(x^i), \gamma^i(x^i), \kappa^i(x^i), \mathcal{R}_X^i(x^i), \mathcal{R}_Z^i(x^i), \mathcal{M}^i(x^i), q_{t,j}^i(x^i), q_{n,j}^i(x^i), \Delta_j^i(x^i), x^i$

Okno 3.2: Linearizirani robni problem kompozitnega nosilca v komponentni obliki

Za $x^i \in \mathcal{I}_l^i \cup \mathcal{I}^i \cup \mathcal{I}_d^i = [0, L]$:

- $(i = j = 1, \ldots, N_{\mathrm{sl}};\ j \neq N_{\mathrm{sl}})$ in $q_{t,0}^1(x^i) = q_{n,0}^1(x^i) = 0$

kinematične enačbe

$$\frac{\mathrm{d}u^i(x^i)}{\mathrm{d}x^i} - \varepsilon^i(x^i) = 0, \tag{3.108}$$

$$\frac{\mathrm{d}w^i(x^i)}{\mathrm{d}x^i} + \varepsilon^i(x^i) - \gamma^i(x^i) = 0, \tag{3.109}$$

$$\frac{\mathrm{d}\varphi^i(x^i)}{\mathrm{d}x} - \kappa^i(x^i) = 0, \tag{3.110}$$

ravnotežne enačbe

$$\frac{\mathrm{d}\mathcal{R}_X^i(x^i)}{\mathrm{d}x^i} + p_X^i(x^i) + q_{t,j-1}^i(x^i) + q_{t,j}^i(x^i) = 0, \tag{3.111}$$

$$\frac{\mathrm{d}\mathcal{R}_Z^i(x^i)}{\mathrm{d}x^i} + p_Z^i(x^i) q_{n,j-1}^i(x^i) + q_{n,j}^i(x^i) = 0, \tag{3.112}$$

$$\mathcal{N}^i(x^i) = \mathcal{R}_X^i(x^i), \tag{3.113}$$

$$\mathcal{Q}^i(x^i) = \mathcal{R}_Z^i(x^i), \tag{3.114}$$

$$\frac{\mathrm{d}\mathcal{M}^i(x^i)}{\mathrm{d}x^i} - \mathcal{Q}^i(x^i) + m_Y^i(x^i) + z_{j-1} q_{t,j-1}^i(x^i) + z_j q_{t,j}^i(x^i) = 0. \tag{3.115}$$

konstitutivne enačbe

$$\mathcal{N}^i(x^i) = \mathcal{N}_{\mathrm{c}}^i\Big(x^i, \varepsilon^i(x^i), \kappa^i(x^i), T^i(x^i, y^i, z^i), w^i(x^i, y^i, z^i)\Big), \tag{3.116}$$

$$\mathcal{Q}^i(x^i) = \mathcal{Q}_{\mathrm{c}}^i\Big(x^i, \gamma^i(x^i), T^i(x^i, y^i, z^i), w^i(x^i, y^i, z^i)\Big) \tag{3.117}$$

$$\mathcal{M}^i(x^i) = \mathcal{M}_{\mathrm{c}}^i\Big(x^i, \varepsilon^i(x^i), \kappa^i(x^i), T^i(x^i, y^i, z^i), w^i(x^i, y^i, z^i)\Big) \tag{3.118}$$

pripadajoči naravni (Neumannovi) in bistveni (Dirichletovi) robni pogoji

$$\begin{array}{lll} \mathcal{R}_X^i(0) - S_1^i = 0 & \text{ali} & u^i(0) = u_1^i, \\ \mathcal{R}_Z^i(0) - S_2^i = 0 & \text{ali} & w^i(0) = u_2^i, \\ \mathcal{M}^i(0) - S_3^i = 0 & \text{ali} & \varphi^i(0) = u_3^i, \\ \mathcal{R}_X^i(L) - S_4^i = 0 & \text{ali} & u^i(L) = u_4^i, \\ \mathcal{R}_Z^i(L) - S_5^i = 0 & \text{ali} & w^i(L) = u_5^i, \\ \mathcal{M}^i(L) - S_6^i = 0 & \text{ali} & \varphi^i(L) = u_6^i. \end{array} \tag{3.119}$$

- $(i = j = 1, \ldots, N_{\mathrm{sl}} - 1)$

posplošene vezne enačbe

$$x^i + u^i(x^i) + z_j \varphi^i(x^i) = x^{i+1} + u^{i+1}(x^{i+1}) + z_j \varphi^{i+1}(x^{i+1}), \tag{3.120}$$

$$w^i(x^i) = w^{i+1}(x^{i+1}), \tag{3.121}$$

$$\Delta_j^i(x^i) = x^{i+1} - x^i = u^i(x^i) - u^{i+1}(x^{i+1}) + z_j\Big(\varphi^i(x^i) - \varphi^{i+1}(x^{i+1})\Big), \tag{3.122}$$

$$\Delta_j^{i+1}(x^{i+1}) = \int_{x^i(i+1)}^{x^{i+1}} \Big(1 + \varepsilon^i(\xi) + z_j \kappa^i(\xi)\Big)\cos\chi^i(\xi) + \gamma^i(\xi)\sin\chi^i(\xi)\mathrm{d}\xi, \tag{3.123}$$

$$q_{n,j}^i(x^i) - q_{n,j}^{i+1}(x^{i+1}) = 0, \tag{3.124}$$

$$q_{t,j}^i(x^i) = \mathcal{H}_{t,j}^i(x^i, q_{n,j}^i(x^i), \Delta_j^i(x^i), T^i(x^i, y^i, z^i), w^i(x^i, y^i, z^i)), \tag{3.125}$$

$$q_{t,j}^{i+1}(x^{i+1}) = \mathcal{H}_{t,j}^{i+1}(x^{i+1}, q_{n,j}^{i+1}(x^{i+1}), \Delta_j^{i+1}(x^{i+1}), T^{i+1}(x^{i+1}, y^{i+1}, z^{i+1}), w^{i+1}(x^{i+1}, y^{i+1}, z^{i+1})), \tag{3.126}$$

Osnovne neznanke problema so:
$u^i(x^i), w^i(x^i), \varphi^i(x^i), \varepsilon^i(x^i), \gamma^i(x^i), \kappa^i(x^i), \mathcal{R}_X^i(x^i), \mathcal{R}_Z^i(x^i), \mathcal{M}^i(x^i), q_{t,j}^i(x^i), q_{n,j}^i(x^i), \Delta_j^i(x^i), x^i$

Okno 3.3: Robni problem kompozitnega nosilca v komponentni obliki (teorija majhnih zdrsov)

Za $x \cong x^i = \mathcal{I}^i = [0, L]$:

- $(i = j = 1, \ldots, N_{\mathrm{sl}};\ j \neq N_{\mathrm{sl}})$ in $q^1_{t,0}(x^i) = q^1_{n,0}(x^i) = 0$

kinematične enačbe

$$1 + \frac{\mathrm{d}u^i(x^i)}{\mathrm{d}x^i} - \big(1 + \varepsilon^i(x^i)\big)\cos\varphi^i(x^i) - \gamma^i(x^i)\sin\varphi^i(x^i) = 0, \tag{3.127}$$

$$\frac{\mathrm{d}w^i(x^i)}{\mathrm{d}x^i} + \big(1 + \varepsilon^i(x^i)\big)\sin\varphi^i(x^i) - \gamma^i(x^i)\cos\varphi^i(x^i) = 0, \tag{3.128}$$

$$\frac{\mathrm{d}\varphi^i(x^i)}{\mathrm{d}x^i} - \kappa^i(x^i) = 0, \tag{3.129}$$

ravnotežne enačbe

$$\frac{\mathrm{d}\mathcal{R}^i_X(x^i)}{\mathrm{d}x^i} + p^i_X(x^i) + \\ + \Big(q_{t,j-1}(x^i) + q_{t,j}(x^i)\Big)\cos\big(\varphi^i(x^i) - \chi^i(x^i)\big) + \Big(q_{n,j-1}(x^i) + q_{n,j}(x^i)\Big)\sin(\varphi^i(x^i) - \chi^i(x^i)) = 0, \tag{3.130}$$

$$\frac{\mathrm{d}\mathcal{R}^i_Z(x^i)}{\mathrm{d}x} + p^i_Z(x^i) - \\ - \Big(q_{t,j-1}(x^i) + q_{t,j}(x^i)\Big)\sin\big(\varphi^i(x^i) - \chi^i(x^i)\big) + \Big(q_{n,j-1}(x^i) + q_{n,j}(x^i)\Big)\cos(\varphi^i(x^i) - \chi^i(x^i)) = 0, \tag{3.131}$$

$$\mathcal{N}^i(x) = \mathcal{R}_X(x^i)\cos\varphi^i(x^i) - \mathcal{R}^i_Z(x^i)\sin\varphi^i(x^i), \tag{3.132}$$

$$\mathcal{Q}^i(x) = \mathcal{R}_X(x^i)\sin\varphi^i(x^i) + \mathcal{R}^i_Z(x^i)\cos\varphi^i(x^i), \tag{3.133}$$

$$\frac{\mathrm{d}\mathcal{M}^i(x^i)}{\mathrm{d}x^i} - \big(1 + \varepsilon^i(x^i)\big)\mathcal{Q}^i(x^i) + \gamma^i(x^i)\mathcal{N}^i(x^i) + m^i_Y(x^i) + \Big(z_{j-1}q_{t,j-1}(x^i) + z_j q_{t,j}(x^i)\Big) \\ \Big(\cos\varphi^i(x^i)\cos(\varphi^i(x^i) - \chi^i(x^i)) + \sin\varphi^i(x^i)\sin(\varphi^i(x^i) - \chi^i(x^i))\Big) + \Big(z_{j-1}q_{n,j-1}(x^i) + z_j q_{n,j}(x^i)\Big) \\ \Big(\cos\varphi^i(x^i)\sin(\varphi^i(x^i) - \chi^i(x^i)) - \sin\varphi^i(x^i)\cos(\varphi^i(x^i) - \chi^i(x^i))\Big) = 0. \tag{3.134}$$

konstitutivne enačbe

$$\mathcal{N}^i(x^i) = \mathcal{N}^i_{\mathrm{c}}\Big(x^i, \varepsilon^i(x^i), \kappa^i(x^i), T^i(x^i, y^i, z^i), w^i(x^i, y^i, z^i)\Big), \tag{3.135}$$

$$\mathcal{Q}^i(x^i) = \mathcal{Q}^i_{\mathrm{c}}\Big(x, \gamma^i(x), T^i(x^i, y^i, z^i), w^i(x^i, y^i, z^i)\Big) \tag{3.136}$$

$$\mathcal{M}^i(x^i) = \mathcal{M}^i_{\mathrm{c}}\Big(x^i, \varepsilon^i(x^i), \kappa^i(x^i), T^i(x^i, y^i, z^i), w^i(x^i, y^i, z^i)\Big) \tag{3.137}$$

pripadajoči naravni (Neumannovi) in bistveni (Dirichletovi) robni pogoji

$$\begin{array}{lll} \mathcal{R}^i_X(0) - S^i_1 = 0 & \text{ali} & u^i(0) = u^i_1, \\ \mathcal{R}^i_Z(0) - S^i_2 = 0 & \text{ali} & w^i(0) = u^i_2, \\ \mathcal{M}^i(0) - S^i_3 = 0 & \text{ali} & \varphi^i(0) = u^i_3, \\ \mathcal{R}^i_X(L) - S^i_4 = 0 & \text{ali} & u^i(L) = u^i_4, \\ \mathcal{R}^i_Z(L) - S^i_5 = 0 & \text{ali} & w^i(L) = u^i_5, \\ \mathcal{M}^i(L) - S^i_6 = 0 & \text{ali} & \varphi^i(L) = u^i_6. \end{array} \tag{3.138}$$

- $(i = j = 1, \ldots, N_{\mathrm{sl}} - 1)$

posplošene vezne enačbe

$$x^i + u^i(x^i) + z_j\sin\varphi^i(x^i) = x^{i+1} + u^{i+1}(x^i) + z_j\sin\varphi^{i+1}(x^i), \tag{3.139}$$

$$w^i(x^i) + z_j\cos\varphi^i(x^i) = w^{i+1}(x^i) + z_j\cos\varphi^{i+1}(x^i), \tag{3.140}$$

$$\Delta_j(x^i) = u^i(x^i) - u^{i+1}(x^i) + z_j\Big(\sin\varphi^i(x^i) - \sin\varphi^{i+1}(x^i)\Big), \tag{3.141}$$

$$q_{t,j}(x^i) = \mathcal{H}_j\big(x^i, \Delta_j(x^i)\big), \tag{3.142}$$

Osnovne neznanke problema so:
$u^i(x^i), w^i(x^i), \varphi^i(x^i), \varepsilon^i(x^i), \gamma^i(x^i), \kappa^i(x^i), \mathcal{R}^i_X(x^i), \mathcal{R}^i_Z(x^i), \mathcal{M}^i(x^i), q_{t,j}(x^i), q_{n,j}(x^i), \Delta_j(x^i), x^{i+1}$

Okno 3.4: Linearizirani robni problem kompozitnega nosilca v komponentni obliki (teorija majhnih zdrsov)

Za $x^i \in \cup\mathcal{I}^i = [0, L]$: **OSNOVNI SISTEM ENAČB:**

- $(i = j = 1, \ldots, N_{\mathrm{sl}};\ j \neq N_{\mathrm{sl}})$ in $q^1_{t,0}(x^i) = q^1_{n,0}(x^i) = 0$

kinematične enačbe

$$\frac{\mathrm{d}u^i(x^i)}{\mathrm{d}x^i} - \varepsilon^i(x^i) = 0, \tag{3.143}$$

$$\frac{\mathrm{d}w^i(x^i)}{\mathrm{d}x^i} + \varphi^i(x^i) - \gamma^i(x^i) = 0, \tag{3.144}$$

$$\frac{\mathrm{d}\varphi^i(x^i)}{\mathrm{d}x^i} - \kappa^i(x^i) = 0, \tag{3.145}$$

ravnotežne enačbe

$$\frac{\mathrm{d}\mathcal{R}^i_X(x^i)}{\mathrm{d}x^i} + p^i_X(x^i) + q_{t,j-1}(x^i) - q_{t,j}(x^i) = 0, \tag{3.146}$$

$$\frac{\mathrm{d}\mathcal{R}^i_Z(x^i)}{\mathrm{d}x^i} + p^i_Z(x^i) - q_{n,j-1}(x^i) + q_{n,j}(x^i) = 0, \tag{3.147}$$

$$\mathcal{N}^i(x^i) = \mathcal{R}^i_X(x^i), \tag{3.148}$$

$$\mathcal{Q}^i(x^i) = \mathcal{R}^i_Z(x^i), \tag{3.149}$$

$$\frac{\mathrm{d}\mathcal{M}^i(x^i)}{\mathrm{d}x^i} - \mathcal{Q}^i(x^i) + m^i_Y(x^i) + z_{j-1}q_{t,j-1}(x^i) - z_j q_{t,j}(x^i) = 0, \tag{3.150}$$

konstitutivne enačbe

$$\mathcal{N}^i(x^i) = \mathcal{N}^i_{\mathrm{c}}\Big(x^i, \varepsilon^i(x^i), \kappa^i(x^i), T^i(x^i, y^i, z^i), w^i(x^i, y^i, z^i)\Big) \tag{3.151}$$

$$\mathcal{Q}^i(x^i) = \mathcal{Q}^i_{\mathrm{c}}\Big(x^i, \gamma^i(x^i), T^i(x^i, y^i, z^i), w^i(x^i, y^i, z^i)\Big) \tag{3.152}$$

$$\mathcal{M}^i(x^i) = \mathcal{M}^i_{\mathrm{c}}\Big(x^i, \varepsilon^i(x^i), \kappa^i(x^i), T^i(x^i, y^i, z^i), w^i(x^i, y^i, z^i)\Big) \tag{3.153}$$

pripadajoči naravni (Neumannovi) in bistveni (Dirichletovi) robni pogoji

$$\begin{array}{lll} \mathcal{R}^i_X(0) - S^i_1 = 0 & \text{ali} & u^i(0) = u^i_1, \\ \mathcal{R}^i_Z(0) - S^i_2 = 0 & \text{ali} & w^i(0) = u^i_2, \\ \mathcal{M}^i(0) - S^i_3 = 0 & \text{ali} & \varphi^i(0) = u^i_3, \\ \mathcal{R}^i_X(L) - S^i_4 = 0 & \text{ali} & u^i(L) = u^i_4, \\ \mathcal{R}^i_Z(L) - S^i_5 = 0 & \text{ali} & w^i(L) = u^i_5, \\ \mathcal{M}^i(L) - S^i_6 = 0 & \text{ali} & \varphi^i(L) = u^i_6. \end{array} \tag{3.154}$$

- $(i = j = 1, \ldots, N_{\mathrm{sl}} - 1)$

posplošene vezne enačbe

$$\Delta_j(x^i) = u^i(x^i) - u^{i+1}(x^i) + z_j\Big(\varphi^i(x^i) - \varphi^{i+1}(x^i)\Big), \tag{3.155}$$

$$q_{t,j}(x^i) = \mathcal{H}_j(x^i, \Delta_j(x^i)), \tag{3.156}$$

$$w^i(x^i) = w^{i+1}(x^i). \tag{3.157}$$

Neznanke osnovnega sistema so:
$u^i(x^i), w(x^i), \varphi(x^i), \varepsilon^i(x^i), \gamma^i(x^i), \kappa^i(x^i), \mathcal{N}^i(x^i), \mathcal{Q}(x^i), \mathcal{M}(x^i), \Delta_j(x^i), q_{t,j}(x^i), q_{n,j}(x^{i+1})$

DODATNI SISTEM ENAČB:

- $(i = j = 1, \ldots, N_{\mathrm{sl}} - 1)$

$$x^i + u^i(x^i) + z_j\varphi^i(x^i) = x^{i+1} + u^{i+1}(x^i) + z_j\varphi^{i+1}(x^i), \tag{3.158}$$

- $(i = 1, \ldots, N_{\mathrm{sl}})$

$$\mathcal{N}(x^i) = \sum_{i=1}^{N_{\mathrm{sl}}} \mathcal{N}^i(x^i), \tag{3.159}$$

$$\mathcal{Q}(x^i) = \sum_{i=1}^{N_{\mathrm{sl}}} \mathcal{Q}^i(x^i), \tag{3.160}$$

$$\mathcal{M}(x^i) = \sum_{i=1}^{N_{\mathrm{sl}}} \mathcal{M}^i(x^i). \tag{3.161}$$

Neznanke dodatnega sistema so: $x^{i+1}(x^i), \mathcal{N}(x^i), \mathcal{Q}(x^i), \mathcal{M}(x^i)$

Okno 3.5: Linearizirani robni problem Bernoullijevega kompozitnega nosilca v komponentni obliki (teorija majhnih zdrsov)

Za $x^i \in \cup\mathcal{I}^i = [0, L]$: **OSNOVNI SISTEM ENAČB:**

- $(i = j = 1, \ldots, N_{\text{sl}};\ j \neq N_{\text{sl}})$ in $q^1_{t,0}(x^i) = q^1_{n,0}(x^i) = 0$

kinematične enačbe

$$\frac{\mathrm{d}u^i(x^i)}{\mathrm{d}x^i} - \varepsilon^i(x^i) = 0, \tag{3.162}$$

$$\frac{\mathrm{d}w(x^i)}{\mathrm{d}x^i} + \varphi(x^i) = 0, \tag{3.163}$$

$$\frac{\mathrm{d}\varphi(x^i)}{\mathrm{d}x^i} - \kappa(x^i) = 0, \tag{3.164}$$

ravnotežne enačbe

$$\frac{\mathrm{d}\mathcal{N}^i(x^i)}{\mathrm{d}x^i} + p^i_X(x^i) + q_{t,j-1}(x^i) + q_{t,j}(x^i) = 0, \tag{3.165}$$

$$\frac{\mathrm{d}\mathcal{Q}(x^i)}{\mathrm{d}x^i} + \sum_{i=1}^{N_{\text{sl}}} p^i_Z(x^i) = 0, \tag{3.166}$$

$$\mathcal{M}(x^i) = \sum_{i=1}^{N_{\text{sl}}} \mathcal{M}^i(x^i) \quad \longrightarrow \quad \frac{\mathrm{d}\mathcal{M}(x^i)}{\mathrm{d}x^i} - \mathcal{Q}(x^i) + \sum_{i=1}^{N_{\text{sl}}} m^i_Y(x^i) = 0, \tag{3.167}$$

konstitutivne enačbe

$$\mathcal{N}^i(x^i) = \mathcal{N}^i_{\text{c}}\Big(x^i, \varepsilon^i(x^i), \kappa(x^i), T^i, w^i\Big), \tag{3.168}$$

$$\sum_{i=1}^{i=N_{\text{sl}}} \mathcal{M}^i(x^i) = \sum_{i=1}^{i=N_{\text{sl}}} \mathcal{M}^i_{\text{c}}\Big(x^i, \varepsilon^i(x^i), \kappa(x^i), T^i, w^i\Big) \quad \longrightarrow \quad \mathcal{M}(x^i) = \mathcal{M}_{\text{c}}\Big(x^i, \varepsilon^i(x^i), \kappa(x^i), T^i, w^i\Big) \tag{3.169}$$

pripadajoči naravni (Neumannovi) in bistveni (Dirichletovi) robni pogoji

$$\begin{array}{rcl}
\mathcal{N}^i(0) - S^i_1 = 0 & \text{ali} & u^i(0) = u^i_1, \\
\mathcal{Q}(0) - \sum_{i=1}^{N_{\text{sl}}} S^i_2 = 0 & \text{ali} & w(0) = u_2, \\
\mathcal{M}(0) - \sum_{i=1}^{N_{\text{sl}}} S^i_3 = 0 & \text{ali} & \varphi(0) = u_3, \\
\mathcal{N}^i(L) - S^i_4 = 0 & \text{ali} & u^i(L) = u^i_4, \\
\mathcal{Q}(L) - \sum_{i=1}^{N_{\text{sl}}} S^i_5 = 0 & \text{ali} & w(L) = u_5, \\
\mathcal{M}(L) - \sum_{i=1}^{N_{\text{sl}}} S^i_6 = 0 & \text{ali} & \varphi(L) = u_6.
\end{array} \tag{3.170}$$

- $(i = j = 1, \ldots, N_{\text{sl}} - 1)$

posplošene vezne enačbe

$$\Delta_j(x^i) = u^i(x^i) - u^{i+1}(x^i), \tag{3.171}$$

$$q_{t,j}(x^i) = \mathcal{H}_j(x^i, \Delta_j(x^i)), \tag{3.172}$$

Neznanke osnovnega sistema so: $u^i(x^i), w(x^i), \varphi(x^i), \varepsilon^i(x^i), \kappa^i(x^i), \mathcal{N}^i(x^i), \mathcal{Q}(x^i), \mathcal{M}(x^i), \Delta_j(x^i), q_{t,j}(x^i)$

DODATNI SISTEM ENAČB:

- $(i = j = 1, \ldots, N_{\text{sl}} - 1)$

$$x^i + u^i(x^i) = x^{i+1} + u^{i+1}(x^i) \quad \longrightarrow \quad x^{i+1}(x^i) = x^i + \Delta_j(x^i), \tag{3.173}$$

- $(i = j = 1, \ldots, N_{\text{sl}};\ j \neq N_{\text{sl}})$

$$\mathcal{Q}(x^i) = \sum_{i=1}^{N_{\text{sl}}} \mathcal{Q}^i(x^i), \tag{3.174}$$

$$\mathcal{M}(x^i) = \sum_{i=1}^{N_{\text{sl}}} \mathcal{M}^i(x^i), \tag{3.175}$$

$$\frac{\mathrm{d}\mathcal{Q}^i(x^i)}{\mathrm{d}x^i} + p^i_Z(x^i) + q_{n,j-1}(x^i) + q_{n,j}(x^i) = 0, \tag{3.176}$$

$$\frac{\mathrm{d}\mathcal{M}^i(x^i)}{\mathrm{d}x^i} - \mathcal{Q}^i(x^i) + m^i_Y(x^i) + z_{j-1} q_{t,j-1}(x^i) + z_j q_{t,j}(x^i) = 0, \tag{3.177}$$

$$\mathcal{M}^i(x^i) = \mathcal{M}^i_{\text{c}}(x^i). \tag{3.178}$$

Neznanke dodatnega sistema so: $x^{i+1}(x^i), q_{n,j}(x^i), \mathcal{Q}^i(x^i), \mathcal{M}^i(x^i)$

3.2 Analitično reševanje

3.2.1 Pregled literature

Začetki teorije kompozitnih nosilcev z upoštevanjem zdrsa med sloji segajo v štirideseta leta prejšnjega stoletja. Potem, ko so številni raziskovalci tistega časa (natančen pregled med leti 1920 in 1958 podaja Viest (1960)) z eksperimentalnim opazovanjem mostnih nosilcev potrdili delno povezanost med posameznimi sloji kompozitnega nosilca, se je na Švedskem, v Švici in v Združenih državah Amerike, neodvisno druga od druge, razvilo kar nekaj teorij delne povezanosti slojev kompozitnih nosilcev. Temeljile so na predpostavkah linearno elastičnega materiala in Bernoullijeve hipoteze o ravnih prečnih prerezih. Najbolj znana med njimi je teorija, ki jo je leta 1943 razvil in leta 1951 s sodelavci objavil Newmark (1951). S teoretično analizo je podal zaključene izraze za zdrs, deformacije in navpične pomike dvoslojnih nosilcev iz različnega materiala. Rezultate so primerjali z eksperimentalnimi rezutati pomanjšanih modelov dvoslojnih nosilcev iz jekla in betona in dvoslojnih nosilcev iz jekla in betona v naravni velikosti. Analitične rezultate so primerjali tudi z rezultati testov ”push-out”. Primerjava je pokazala dobro ujemanje med analitičnimi in eksperimentalmimi rezultati. Poleg tega so ugotovili, da so zamiki med slojema obravnavanega nosilca zanemarljivo majhni. Zaključili so, da je za inženirsko analizo sovprežnih nosilcev dovolj natančen standardni račun z upoštevanjem togega stika med sloji. Toda kasneje se je izkazalo, da so obravnavali relativno togo povezane nosilce, kjer je bil zdrs med sloji zelo majhen. Z nadaljnjimi raziskavami so raziskovalci ugotovili, da ima zdrs med slojema pomemben vpliv na obnašanje kompozitnih nosilcev.

Pozneje sta Goodman in Popov (1968, 1969) pokazala, da so vse do tedaj razvite teorije dale praktično enake rezultate. Poleg tega sta med prvimi izpeljala analitične izraze za linearno obnašanje lesenih troslojnih prostoležečih kompozitnih nosilcev, sestavljenih iz enakih slojev in obremenjenih s točkovno obtežbo. Rezultate sta primerjala z eksperimentom. Validacija je pokazala zelo dobro ujemanje rezultatov. Med prvimi sta tudi prikazala postopek za upoštevanje nelinearnega obnašanja veznega sredstva. Dvoslojne nosilce iz jekla in betona je obravnaval tudi Adekola (1968), ki je analizo prostoležečih kompozitnih nosilcev razširil z upoštevanjem navpičnega razmaka in trenja med sloji. V svojem delu je opozoril na težavno določitev modula podlage in področja negativnega razmaka (kompresije) med sloji. Plum in Horne (1975) sta predstavila približne in analitične rešitve dvoslojnih kontinuirnih nosilcev, obremenjenih s točkovnimi silami. Približne rešitve, ki so bile lažje obvladljive, sta izpeljala z metodo rotacije členka. V bližini prijemališča točkovne sile, kjer je koncentracija deformacije zdrsa največja, sta dodala členek s katerim sta povečala deformabilnost prereza. Ugotovila sta tudi, da je šibka točka analize določitev modula stika. Namesto določitve modula stika s pomočjo testa ”push-out”, sta predlagala določitev modula stika neposredno iz testa dejanskega kompozitnega nosilca. Prostoležeče lamelirane nosilce z upoštevanjem zdrsa med sloji sta obravnavala Suzuki in Chang (1979). Zdrs med sloji sta modelirala malo drugače. Togost stika sta zamenjala s koeficientom trenja. Zdrs nastopi šele, ko je v stiku dosežena kritična strižna napetost. V numeričnem primeru sta pokazala uporabo predlagane metode v primeru lameliranih, heterogenih superprevodnih magnetov fuzijskih reaktorjev. Kristek in Studnička (1982) sta s pomočjo izvedene parametrične analize v primeru prostoležečih dvoslojnih nosilcev iz betona in jekla, predlagala poenostavljene enačbe in izraze primerne za praktično uporabo. Rešitev Goodman in Popova (1968, 1969) je uporabna samo v primeru simetričnih prečnih prerezov. Razširitev na nesimetrične prečne prereze je predstavil McCutheon (1986). Izpeljal je preproste izraze troslojnih lesenih prostoležečih nosilcev. Pri tem je predpostavil, da je togost srednjega sloja dosti večja od togosti ostalih dveh slojev. Analitične izraze za določitev navpičnih pomikov linearno elastičnih troslojnih prostoležečih nosilcev brez upoštevanja zadnje predpostavke sta izpeljala Chui in Barclay (1998). Primerjava z McCutheon (1986) je pokazala, da je izmerjena togost vedno manjša od izračunane. Odstopanje pripišejo strižnemu vplivu deformacije lesa, kajti McCutheon (1986) je testiral relativno kratke nosilce,

pri katerih vpliv strižne deformacije pogosto ni zanemarljiv v primerjavi z vplivom upogiba in zdrsa med sloji. Chui in Barclay (1998) nista upoštevala vpliva strižne deformacije na navpične pomike, zato ni presenetljivo, da so le-ti manjši od tistih, ki jih je izmeril McCutheon (1986).

Nekateri avtorji so analizirali tudi uklon kompozitnih nosilcev z upoštevanjem zdrsa med sloji. Rassam in Goodman (1970, 1971) sta analizirala uklon linearno elastičnih troslojnih lesenih kompozitnih stebrov. Izpeljala sta analitične izraze in predlagala projektne diagrame, ki nadomeščajo uporabo empiričnih formul. Uklon lesenih kompozitnih elementov je analiziral tudi Kamiya (1987). Analiziral je leseni steber, ki je z žeblji povezan z leseno oblogo. Uklonske sile različno podprtih dvoslojnih kompozitnih nosilcev izpeljeta tudi Girhammar in Gopu (1993). Dvoslojne nosilce analizirata s t.i. modificirano teorijo drugega reda, ki še vedno predstavlja geometrijsko poenostavljeno teorijo nosilcev, a je bolj natančna kot teorija prvega reda. Poleg uklonskih sil izpeljeta tudi analitične izraze za kinematične in statične količine prostoležečga kompozitnega nosilca po teoriji prvega reda in modificirani teoriji drugega reda. Nadalje sta Girhammar and Pan (1993) predstavila točne in približne rešitve dinamično obremenjenih Euler-Bernoullijevih kompozitnih nosilcev z zdrsom med sloji. Razvita točna dinamična analiza kompozitnih nosilcev je osnovana na točni statični analizi, ki sta jo predstavila Girhammar in Gopu (1993). Dodatno sta upoštevala, da ni trenja in dušenja. Analizirala sta vpliv zdrsa na lastne frekvence nosilca. Analitične rešitve dobita le za preproste načine obtežbe in podpiranja. Za praktično uporabo razvijeta poenostavljeno metodo. Jasim in Ali (1997) ter Jasim (1999) na osnovi analitične rešitve prostoležečega nosilca, obremenjenega s točkovno obtežbo, razvijeta za dimenzioniranje zelo priročne izraze. Rezultate prikažeta v obliki projektnih diagramov za račun navpičnih pomikov. Veliko število parametrov, ki vplivajo na navpične pomike, zajameta v brezdimenzionalnih parametrih. Diagrami so uporabni za vse vrste obtežb, geometrije in materiala. Podobno Jasim (1997) in Jasim in Atalla (1999) izpeljejo oziroma prikažejo projektne diagrame za račun navpičnih pomikov kontinuirnih kompozitnih nosilcev. Rešitve kontiniurnih nosilcev določijo s superpozicijo rešitev prostoležečih kompozitnih nosilcev. Betti in Gjelsvik (1995) upoštevata, da sta sloja dvoslojnega elastičnega nosilca povezana s tankim slojem. Izvedeta parametrične analize. Navpične pomike normalizirata glede na pomike nosilca s togo povezanimi sloji. Poudarita pomen drsne podpore med sloji kot povečanje togosti celotnega nosilca. Cosenza in Pecce (2001) ter Nguyen, Oehlers in Bradford (2001) podobno kot Adekola (1968) obravnavajo delno povezanost v dveh pravokotnih smereh. Cosenza in Pecce (2001) poudarita pomen normalne kontaktne napetosti v stiku, ki je v analizi kompozitnih nosilcev večkrat zanemarjena. Med pregledom literature smo zasledili tudi težnjo nekaterih avtorjev po razvoju preprostih računskih postopkov. Omenimo avtorje kot so Wang (1998), Seracino, Oehlers in Yeo (2001) ter Nie in Cai (2003). Ti avtorji so podali poenostavljene izraze za račun navpičnih pomikov sovprežnih nosilcev iz jekla in betona. Velikosti navpičnih pomikov določijo s sklepanjem iz razporeditve pomikov togo povezanih kompozitnih nosilcev. Nekateri avtorji so pri analizi kompozitnih nosilcev upoštevali tudi časovno spreminjajoče se pojave, kot so lezenje in krčenje. Ranzi in Bradford (2003, 2006) sta podala zaključene izraze vpliva deformacije krčenja na mehansko obnašanje različno podprtih dvoslojnih nosilcev. V okviru doktorskega dela smo (Schnabl it et al., 2006) razširili teorijo troslojnih prostoležečih nosilcev, ki so jih predhodno obravnavali Goodman in Popov (1968, 1969), McCutheon (1986) ter Chui in Barclay (1998), na kontinuirne troslojne nosilce.

Pregled računskih postopkov in različne možne izvedbe upogibno obremenjenih kompozitnih nosilcev iz lesa in betona predstavita Van der Linden (1999) ter Dias (2005). Zelo natančen pregled literature s področja analize kompozitnih nosilcev z upoštevanjem zdrsa med sloji do leta 1997 sta v svojem prispevku podala Leon in Viest (1998).

Vse zgoraj omenjene teorije kompozitnih nosilcev z upoštevanjem zdrsa med sloji so izpeljane na osnovi klasične ali inženirske Euler-Bernoullijeve teorije upogiba, pri kateri zanemarimo vpliv strižne deforma-

cije. Omenjena predpostavka temelji na predpostavki, da prerezi, ki so pred nastopom deformacije ravni in pravokotni na nedeformirano referenčno os nosilca ostanejo takšni tudi po njej. Posledica omenjene predpostavke je nična strižna deformacija oziroma neskončna strižna togost prečnega prereza. V realnosti material, ki bi imel takšne lastnosti seveda ne obstaja. Iz tega sledi, da je uporaba klasične teorije v nekaterih primerih vprašljiva. Tak primer so kratki in debeli (visoki) nosilci.

Prvi, ki je v teorijo upogiba nosilcev vključil tudi vpliv strižne deformacije je bil ukrajinski raziskovalec Timoshenko (1921). Vpliv strižne deformacije je upošteval kot dodaten zasuk prečnega prereza. Na ta način je predpostavil, da je strižna deformacija konstantna po višini prereza. V literaturi je teorija dobro znana kot Timoshenkova teorija upogiba. V sedemdesetih letih prejšnjega stoletja je na ta način strižno deformacijo v svoj model vključil tudi Reissner (1972). Potreba po natančnejši določitvi razporeda in velikosti strižnih napetosti po prerezu (posebno v letalski in vesoljski industriji) je vodila do izpeljave bolj natančnih iterativnih strižnih teorij višjih redov. Naj omenimo le nekaj avtorjev kot so Soldatos in Watson (1997), Matsunaga (2002), Gorik (2003), Piskunov in Grinevitskii (20004), itd. Začetni približek pri strižnih teorijah višjih redov je analogen Euler-Bernoullijevi teoriji nosilcev, prva iteracija pa običajno Timoshenkovi teoriji upogiba. Ker v okviru zahtevane natančnosti višje iteracije pri analizi konstrukcij, ki nastopajo v gradbeništvu, ne vplivajo pomembno na rezultate, pregled literature s področja strižnih teorij višjih redov ni namen tega dela. Obravnavali bomo le prvo iteracijo strižnih metod oziroma Timoshenkovo teorijo upogiba.

V literaturi analitičnih rešitev dvoslojnih nosilcev z upoštevanjem strižnih deformacij posameznih slojev in zdrsa nismo našli. Zato so objave (Schnabl *et al.*, 2005, 2006, 2007) na to temo pomemben del doktorskega dela. V teh prispevkih z izpeljano analitično rešitvijo izvedemo parametrično analizo, s katero pokažemo, da ima v nekaterih primerih strižna deformacija prereza pomemben vpliv na mehansko obnašanje kompozitnih nosilcev z upoštevanjem zdrsa med sloji.

3.2.2 Bernoullijev kompozitni nosilec

V tem podpoglavju bomo obravnavali Bernoullijev kompozitni nosilec z upoštevanjem majhnih zdrsov in sicer po teoriji prvega reda. Enačbe, ki opisujejo mehansko obnašanje omenjenega nosilca smo prikazali v oknu 3.5, enačbe (3.162–3.178). Predstavimo algoritem reševanja, s katerim analizo prostoležečih troslojnih kompozitnih nosilcev preprosto razširimo na kontinuirne troslojne kompozitne nosilce. Analitične rezultate prostoležečega troslojnega kompozitnega nosilca najprej primerjamo z rezultati, ki sta jih predstavila Goodman and Popov (1968) ter rezultati, dobljenimi z uporabo empiričnih enačb, ki so predlagane v Evrokodu 5 (2004). V nadaljevanju prikažemo analizo troslojnih kontinuirnih kompozitnih nosilcev z upoštevanjem zdrsa med sloji.

3.2.2.1 Algoritem reševanja

Izkaže se, da lahko sistem enačb Bernoullijevega kompozitnega nosilca (3.162–3.178) preprosto rešimo, če le poznamo izraze za zdrse med posameznimi sloji. Postopek reševanja je sestavljen iz naslednjega zaporedja korakov. V prvem koraku z integracijo ravnotežnih enačb (3.166) in (3.167) določimo skupno ravnotežno prečno silo $\mathcal{Q}(x^i)$ in skupni ravnotežni upogibni moment $\mathcal{M}(x^i)$ kompozitnega nosilca

$$\mathcal{Q}(x^i) = \mathcal{Q}(0) - \int_0^{x^i} \left(\sum_{i=1}^{N_{\mathrm{sl}}} p_Z^i(\xi) \right) \mathrm{d}\xi, \tag{3.179}$$

$$\mathcal{M}(x^i) = \mathcal{M}(0) + \int_0^{x^i} \left(\mathcal{Q}(x^i) - \sum_{i=1}^{N_{\mathrm{sl}}} m_Y^i(\xi) \right) \mathrm{d}\xi. \tag{3.180}$$

V drugem koraku z dvakratnim odvajanjem enačbe (3.171) po vzdolžni koordinati x^i in upoštevanjem kinematične enačbe (3.162), izpeljemo diferencialne enačbe za zdrs

$$\frac{\mathrm{d}^2\Delta_j(x^i)}{\mathrm{d}{x^i}^2} = \frac{\mathrm{d}\varepsilon^i(x^i)}{\mathrm{d}x^i} - \frac{\mathrm{d}\varepsilon^{i+1}(x^i)}{\mathrm{d}x^i}. \tag{3.181}$$

Odvode specifičnih vzdolžnih deformacij $\dfrac{\mathrm{d}\varepsilon^i(x^i)}{\mathrm{d}x^i}$ in $\dfrac{\mathrm{d}\varepsilon^{i+1}(x^i)}{\mathrm{d}x^i}$ v (3.181) določimo z odvajanjem in invertiranjem konstitucijskih enačb (3.168–3.169), ki imajo v primeru linearno elastičnega materiala in stacionarnega temperaturnega in vlažnostnega stanja naslednjo obliko

$$\mathcal{N}(x^i) = \mathcal{N}_{\mathrm{c}}^i(x^i) = C_{11}^i\varepsilon^i(x^i) + C_{12}^i\kappa(x^i), \tag{3.182}$$

$$\mathcal{M}(x^i) = \mathcal{M}_{\mathrm{c}}(x^i) = \sum_{i=1}^{N_{\mathrm{sl}}} C_{21}^i\varepsilon^i(x^i) + \sum_{i=1}^{N_{\mathrm{sl}}} C_{22}^i\kappa(x^i). \tag{3.183}$$

Poleg linearno elastičnega materiala predpostavimo tudi linearni konstitucijski model stika

$$q_{t,j}(x^i) = K_j\Delta_j(x^i), \tag{3.184}$$

kjer s K_j označimo linearni koeficient togosti stika j. V nadaljevanju z rešitvijo odvajanih in invertiranih enačb (3.182–3.183) dobimo

$$\left\{\begin{array}{c} \dfrac{\mathrm{d}\varepsilon^1(x^i)}{\mathrm{d}x^i} \\ \dfrac{\mathrm{d}\varepsilon^2(x^i)}{\mathrm{d}x^i} \\ \vdots \\ \dfrac{\mathrm{d}\varepsilon^{N_{\mathrm{sl}}}(x^i)}{\mathrm{d}x^i} \\ \dfrac{\mathrm{d}\kappa(x^i)}{\mathrm{d}x^i} \end{array}\right\} = \boldsymbol{C}^{-1} \left\{\begin{array}{c} \dfrac{\mathrm{d}\mathcal{N}^1(x^i)}{\mathrm{d}x^i} \\ \dfrac{\mathrm{d}\mathcal{N}^2(x^i)}{\mathrm{d}x^i} \\ \vdots \\ \dfrac{\mathrm{d}\mathcal{N}^{N_{\mathrm{sl}}}(x^i)}{\mathrm{d}x^i} \\ \dfrac{\mathrm{d}\mathcal{M}(x^i)}{\mathrm{d}x^i} \end{array}\right\}. \tag{3.185}$$

$\boldsymbol{C}$ predstavlja konstitucijsko matriko materialnih konstant in $\boldsymbol{C}^{-1}$ njeno inverzno ali recipročno matriko

$$\boldsymbol{C}^{-1} = \begin{bmatrix} C_{11}^1 & 0 & \dots & C_{12}^1 \\ 0 & C_{11}^2 & \dots & C_{12}^2 \\ \vdots & \vdots & \ddots & \vdots \\ C_{21}^1 & C_{21}^2 & \dots & C_{22}^1 + \ldots + C_{22}^{\mathrm{N_{sl}}} \end{bmatrix}^{-1} = \begin{bmatrix} D_{11} & 0 & \dots & D_{1,N_{\mathrm{sl}}+1} \\ 0 & D_{22} & \dots & D_{2,N_{\mathrm{sl}}+1} \\ \vdots & \vdots & \ddots & \vdots \\ D_{N_{\mathrm{sl}}+1,1} & D_{N_{\mathrm{sl}}+1,2} & \dots & D_{N_{\mathrm{sl}}+1,N_{\mathrm{sl}}+1} \end{bmatrix}. \tag{3.186}$$

Z zaporednim vstavljanjem enačb (3.185), (3.165), (3.167) in (3.184) v enačbo (3.181), dobimo sistem linearnih navadnih diferencialnih enačb drugega reda s konstantnimi koeficienti za zdrse med sloji kompozitnega nosilca

$$A_j\Delta_{j-1} + \Delta_j'' + B_j\Delta_j + C_j\Delta_{j+1} = f_j, \tag{3.187}$$

kjer so A_j, B_j, C_j in f_j konstante, ki jih določimo z naslednjimi izrazi

$$\begin{gathered} A_j = K_{j-1}D_{ii}, \quad B_j = -K_j(D_{ii} + D_{i+1,i+1}), \quad C_j = K_{j+1}D_{i+1,i+1}, \\ f_j = -D_{ii}\,p_X^i + D_{i+1,i+1}\,p_X^{i+1} + (D_{i,N_{\mathrm{sl}}+1} - D_{i+1,N_{\mathrm{sl}}+1})\left(\mathcal{Q} - \sum_{i=1}^{N_{\mathrm{sl}}} m_Y^i(x^i)\right). \end{gathered} \tag{3.188}$$

Sistem navadnih diferencialnih enačb (3.187) lahko enolično rešimo, če poznamo pripadajoče robne pogoje. V tem primeru so to vrednosti zdrsov na robu $x^i = 0$ in $x^i = L$ kompozitnega nosilca. Analitično rešitev sistema (3.187) dobimo z uporabo računalniškega programa MATHEMATICA (Wolfram, 2003). Ko poznamo vrednosti zdrsov med sloji kompozitnega nosilca, lahko enačbe osnovnega sistema (3.162–3.172) preprosto rešimo. Najprej iz ravnotežja vozlišč določimo robne vrednosti zasukov in pomikov z rešitvijo linearnega sistema enačb

$$\boldsymbol{K}_T\, \boldsymbol{u} = \boldsymbol{g}. \tag{3.189}$$

Enačbo (3.189) imenujemo tudi enačba konstrukcije, kjer $\boldsymbol{K}_T$ predstavlja togostno matriko konstrukcije, $\boldsymbol{u}$ je vektor neznanih robnih pomikov in zasukov in $\boldsymbol{g}$ je obtežni vektor. Ko poznamo robne vrednosti pomikov in zasukov, lahko izračunamo robne vrednosti ravnotežnih sil. Z znanimi vrednostmi robnih sil in pomikov je rešitev osnovnega sistema (3.162–3.172) za neznane funkcije $u^i(x^i), w(x^i), \varphi(x^i)$, $\varepsilon^i(x^i), \kappa^i(x^i), \mathcal{N}^i(x^i), \mathcal{Q}(x^i), \mathcal{M}(x^i), \Delta_j(x^i), q_{t,j}(x^i)$ znana. Na koncu rešimo še dodatni sistem (3.173–3.178), ki predstavlja sistem enačb za naslednje neznane funkcije: $x^{i+1}(x^i), q_{n,j}(x^i), \mathcal{Q}^i(x^i), \mathcal{M}^i(x^i)$. Normalne kontaktne napetosti $g_{n,j}$ določimo z rešitvijo sistema (3.88).

3.2.2.2 Primeri

Z računskimi primeri ilustriramo učinkovitost predstavljenega računskega postopka za točno analizo napetostnega in deformacijskega obnašanja linearno elastičnih troslojnih prostoležečih in kontinuirnih kompozitnih nosilcev z upoštevanjem delne povezanosti slojev. Poleg tega so prikazane rešitve uporabne za oceno natančnosti in učinkovitosti na novo razvitih numeričnih formulacij opisa troslojnih kompozitnih nosilcev. V ta namen obravnavamo dva računska primera:

1. troslojni prostoležeči leseni nosilec,
2. troslojni kontiniurni leseni nosilec preko dveh polj.

3.2.2.2.1 Troslojni prostoležeči leseni nosilec

Točno rešitev geometrijsko in materialno linearnih kompozitnih nosilcev pogosto zasledimo v literaturi: Newmark *et al.* (1951), Adekola (1968), Jasim (1997), Wang (1998), Ranzi in Bradford (2006), itd. Rešitev je običajno podana za dvoslojne nosilce. Točne rešitve troslojnih prostoležečih nosilcev podajajo Goodman in Popov (1968), Rassam in Goodman (1971), McCutheon (1986) ter Chiu in Barclay (1998).

Veljavnost in učinkovitost predstavljenega računskega postopka za določitev točne rešitve troslojnih nosilcev z upoštevanjem zdrsa med sloji prikažemo s primerjavo med navpičnimi pomiki, izračunanimi s predstavljenim postopkom in navpičnimi pomiki, izračunanimi z enačbami Goodman in Popova (1968) ter empiričnimi formulami, ki jih predlaga Evrokod 5 (2004). Navpične pomike na sredini razpona prostoležečega nosilca primerjamo za dva različna obtežna primera in sicer:

- za nosilec, ki je obremenjen s točkovno silo P na sredini razpona in
- za nosilec, ki je obremenjen z enakomerno zvezno linijsko obtežbo p_Z.

Geometrijski in materialni podatki ter podatki o obtežbi so prikazani na sliki 3.8.

V preglednicah 3.1 in 3.2 so prikazani prispevki k navpičnim pomikom zaradi podajne povezave med sloji. Rezultati so prikazani za zelo podajne stike ($K = 0.01$ kN/cm^2) pa vse do zelo togih stikov ($K = 100$ kN/cm^2). Primerjava rezultatov pokaže, da so rezultati matematičnega modela, ki sta ga

predstavila Goodman in Popov (1968) identični našim rezultatom za obe vrsti obremenitve. Ker se rezultati Goodman in Popova (1968) dobro ujemajo z eksperimenti, ki sta jih opravila, lahko sklepamo, da je naša predstavljena formulacija ustrezna za opis napetostnega in deformacijskega stanja troslojnih nosilcev v območju obremenitev nosilca v stanju uporabnosti.

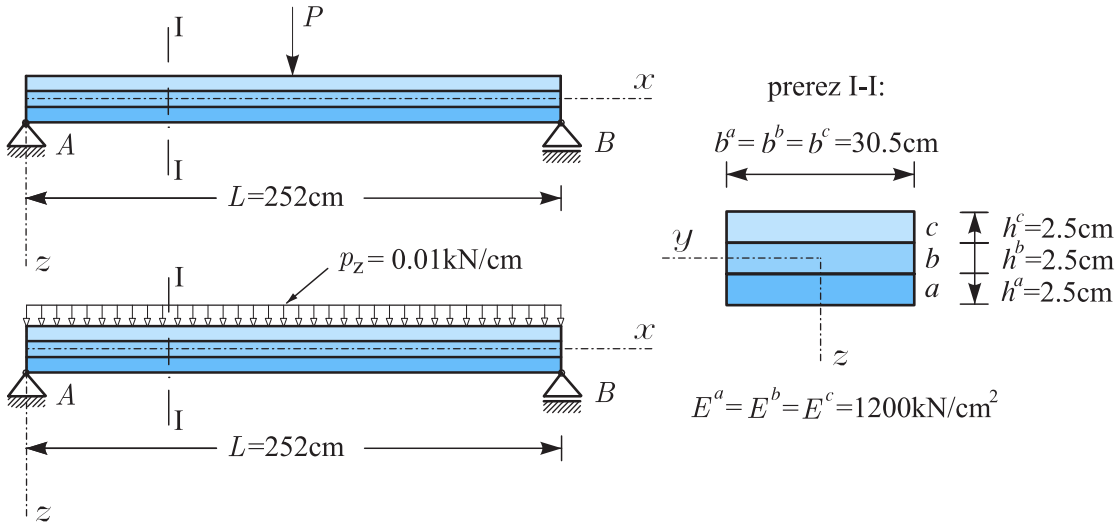

Slika 3.8: Geometrija, obtežba in materialne karakteristike enostavno podprtega troslojnega prostoležečega nosilca.

Figure 3.8: The geometric, material and loading data of simply supported three-layer beam.

Preglednica 3.1: Enostavno podprt prostoležeči troslojni nosilec, obremenjen s točkovno silo P. Prispevki podajne povezave k navpičnim pomikom v cm za različne togosti stika, $K = K^{ab} = K^{bc}$. Navpični pomik homogenega nosilca je 0.246 cm.

Table 3.1: Simply supported three-layer beam subjected to the point load P. The contribution of the flexible connection to the vertical deflections in cm as a function of slip modulus, $K = K^{ab} = K^{bc}$. Deflection of a solid beam is 0.246 cm.

$P = 1$ kN				
K [kN/cm^2]	Goodman in Popov (1968) [cm]	disertacija [cm]	EC 5 (2004) [cm]	EC 5 (2004) relativna napaka [%]
0.01	1.953	1.953	1.953	−0.01
0.1	1.852	1.852	1.852	−0.08
0.5	1.506	1.506	1.499	0.39
1	1.222	1.222	1.212	0.76
2	0.899	0.899	0.877	1.45
3	0.701	0.701	0.686	2.06
4	0.579	0.579	0.564	2.62
5	0.494	0.494	0.479	3.12
10	0.287	0.287	0.273	5.13
100	0.035	0.035	0.031	13.56

Analitični rezultati prispevkov k navpičnim pomikom zaradi podajne povezave med sloji troslojnega nosilca, obremenjenega s točkovno silo na sredini, so za majhne vrednosti togosti stika ($K < 1$ kN/cm^2) praktično enaki prispevkom po Evrokodu 5 (2004), čeprav so empirične formule podane v Evrokodu 5 (2004) namenjene le za račun navpičnih pomikov nosilcev obremenjenih z zvezno linijsko obtežbo, ki povzroča kvadratično in kubično razporeditev upogibnih momentov vzdolž nosilca. Za večje togosti stikov so pomiki po Evrokodu 5 (2004) nekoliko manjši. Empirične formule za račun navpičnih pomikov slojevitih nosilcev, ki so podane v Evrokodu 5 (2004), so uporabne tudi za račun navpičnih pomikov nosilcev, ki so obremenjeni s točkovno silo. V tem primeru smo nekoliko na nevarni strani, saj so tako izračunani pomiki nekoliko manjši od točno izračunanih.

V primeru obremenitve slojevitega nosilca z zvezno linijsko obtežbo p_Z so navpični pomiki oziroma prispevki k navpičnim pomikom zaradi podajne povezave praktično enaki za vse togosti stikov, glej preglednico 3.2. Razlike so zelo majhne in so večje za večje togosti stikov. V primeru zelo toge povezave med sloji, kjer je $K = 100$ kN/cm^2, je relativna napaka po Evrokodu 5 (2004) izračunanih pomikov v primerjavi s točnimi navpičnimi pomiki 2.52%.

Preglednica 3.2: Enostavno podprt prostoležeči troslojni nosilec, obremenjen z enakomerno zvezno linijsko obtežbo p_Z. Prispevki podajne povezave k navpičnim pomikom v cm za različne togosti stika, $K = K^{ab} = K^{bc}$. Navpični pomik homogenega nosilca je 0.386 cm.

Table 3.2: Simply supported three-layer beam subjected to the uniform load p_Z. The contribution of the flexible connection to the vertical deflections in cm as a function of slip modulus, $K = K^{ab} = K^{bc}$. Deflection of a solid beam is 0.386 cm.

$p_Z = 1$ kN/m				
K [kN/cm^2]	Goodman in Popov (1968) [cm]	disertacija [cm]	EC 5 (2004) [cm]	EC 5 (2004) relativna napaka [%]
0.01	3.069	3.069	3.069	0.00
0.1	2.907	2.907	2.908	0.02
0.5	2.355	2.355	2.357	0.10
1	1.902	1.902	1.906	0.20
2	1.373	1.373	1.378	0.37
3	1.073	1.073	1.079	0.52
4	0.881	0.881	0.887	0.66
5	0.747	0.747	0.753	0.78
10	0.423	0.423	0.429	1.24
100	0.048	0.048	0.049	2.52

Primerjava prispevkov k navpičnim pomikom zaradi podajne povezave med sloji v preglednici 3.2 pokaže, da so lahko prispevki v primeru zelo podajne povezave med sloji tudi do 8-krat večji od navpičnih pomikov nosilca s togo povezanimi sloji, kjer je navpični pomik 0.386 cm.

Povezanost slojev bistveno vpliva tudi na razpored in velikosti ostalih kinematičnih in statičnih količin. Velikosti in razpored vzdolžnih normalnih napetosti σ_{xx} v prerezu na sredini razpona troslojnega prostoležečega nosilca obremenjenega z točkovno silo P za različne togosti stikov prikazujemo na sliki 3.9.

Razpored vzdolžnih napetosti σ_{xx} je po višini slojevitega nosilca odsekoma linearen. Maksimalne vrednosti napetosti v posameznem sloju naraščajo z manjšanjem togosti stika in so lahko občutno večje kot v primeru homogenega nosilca, kjer je $K = \infty$. V primeru zelo podajne povezanosti slojev se napetosti v posameznem sloju spreminjajo od tlačnih napetosti na zgornji strani sloja do nateznih napetosti na spodnji strani sloja.

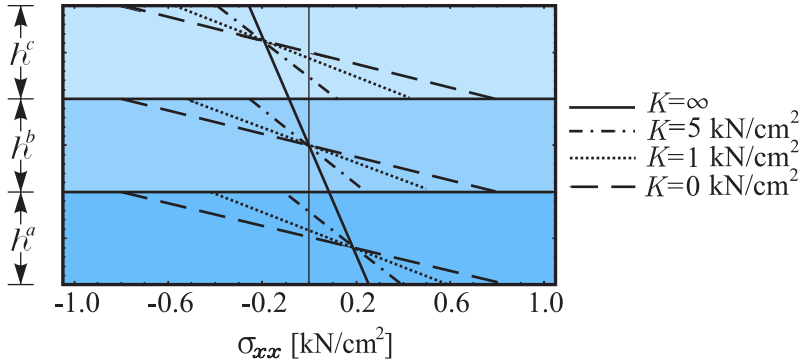

Slika 3.9: Razpored vzdolžnih normalnih napetosti σ_{xx} po višini prečnega prereza enostavno podprtega troslojnega nosilca obremenjenega s točkovno silo P na sredini razpona.

Figure 3.9: Simply supported three-layer beam subjected to point load P. The distribution of the normal stresses σ_{xx} over the cross-section.

3.2.2.2.2 Troslojni kontinuirni leseni nosilec preko dveh polj

Namen tega računskega primera je razširitev analize troslojnih prostoležečih nosilcev na troslojne kontinuirne nosilce. V ta namen obravnavamo troslojni kontinuirni nosilec preko dveh polj. Za obravnavani kontinuirni nosilec prikažemo točne rešitve napetostnega in deformacijskega stanja. Posamezni sloji so izdelani iz lesa različne kakovosti. Označeni so s trdnostnimi razredi skladno z Evrokodom 5 (2004). Togost stika med slojema a in b je $K^{ab} = 3$ kN/cm^2 ter med b in c pa $K^{bc} = 0.01$ kN/cm^2. Kontinuirni nosilec je obremenjen v obeh poljih z enakomerno zvezno linijsko obtežbo $p_Z = 0.01$ kN/cm. Geometrijski in materialni podatki ter podatki o obtežbi so podani na sliki 3.10.

Neznane vozliščne vrednosti pomikov in zasukov izračunamo z enačbo konstrukcije (3.189). V ta namen kontinuirni nosilec razdelimo na elemente. Za vsak element rešimo osnovni sistem enačb (3.162–3.172). Vrednosti vozliščnih pomikov in zasukov podajamo v preglednici 3.3. Pomiki so podani v centimetrih in zasuki v radianih.

Preglednica 3.3: Vozliščne vrednosti pomikov in zasukov troslojnega kontinuirnega lesenega nosilca preko dveh polj, obremenjenega z zvezno linijsko obtežbo p_Z.

Table 3.3: Nodal displacements and rotations of the three-layer continuous wooden beam over two spans subjected to the uniform load p_Z.

u_b^A	u_c^A	φ^A	u_a^B	$u_b^B = u_c^B$	φ^B	u_a^C	u_b^C	u_c^C	φ^C
-0.064	-0.151	-0.011	-0.065	-0.065	0	-0.131	-0.067	0.021	0.012

Z znanimi vozliščnimi vrednostmi pomikov in zasukov lahko izračunamo vozliščne vrednosti osnih in prečnih sil ter upogibnih momentov slojev a, b in c. Vrednosti neničelnih količin so podane v preglednici 3.4.

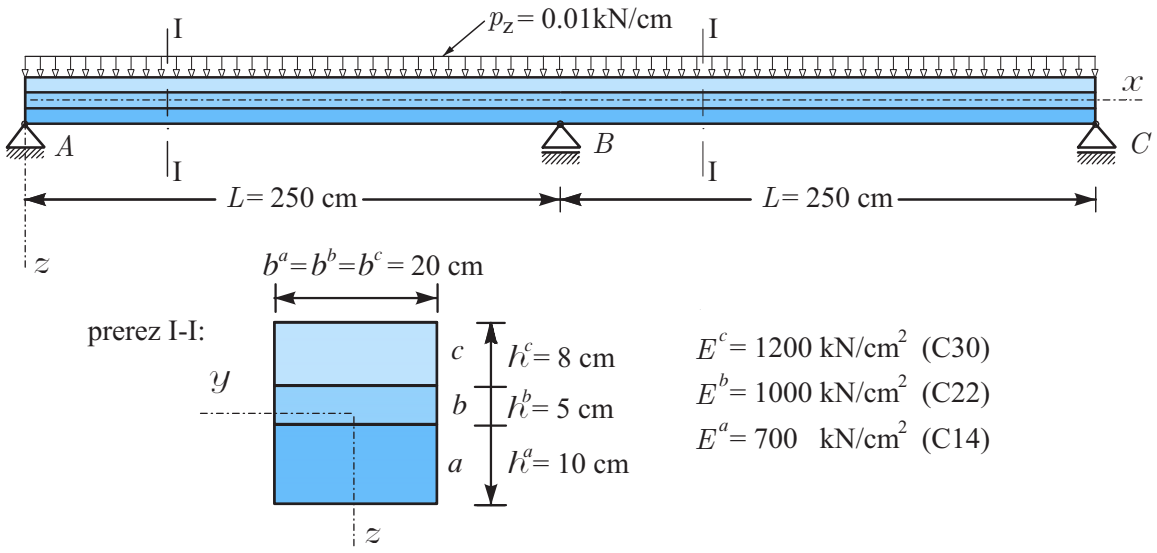

Slika 3.10: Geometrijski in materialni podatki ter podatki o obtežbi troslojnega kontinuirnega lesenega nosilca preko dveh polj.

Figure 3.10: The geometric, material and loading data of continuous three-layer beam over two spans.

Preglednica 3.4: Vozliščne vrednosti osnih in prečnih sil ter upogibnih momentov v vozliščih A in B troslojnega kontinuirnega lesenega nosilca preko dveh polj, obremenjenega z zvezno linijsko obtežbo p_Z.

Table 3.4: Nodal internal forces at nodes A and B of the three-layer continuous wooden beam over two spans subjected to the uniform load p_Z.

Vozlišče A	Vozlišče B				
$\mathcal{Q}_{e1}(0)$	$\mathcal{N}^a_{e2}(0)$	$\mathcal{N}^b_{e2}(0)$	$\mathcal{N}^c_{e2}(0)$	$\mathcal{Q}_{e2}(0)$	$\mathcal{M}_{e2}(0)$
9.53 kN	−5.38 kN	5.39 kN	−0.01 kN	15.47 kN	−743.04 kNcm

Poleg vozliščnih vrednosti posameznih količin prikažemo tudi velikosti in porazdelitev izbranih količin vzdolž kontinuirnega nosilca. Na sliki 3.11 so prikazani diagrami zdrsov Δ^{ab} in Δ^{bc} ter ravnotežnih količin $\mathcal{N}$, $\mathcal{Q}$ in $\mathcal{M}$ vzdolž referenčne osi troslojnega kontinuirnega nosilca. Iz slike 3.11(a) je razvidno, da so zdrsi največji na mestih skrajnih podpor.

Diagrama Δ^{ab} in Δ^{bc} sta praktično enaka. Osni sili spodnjega a in zgornjega sloja c sta enako veliki a nasprotno usmerjeni, medtem ko je osna sila srednjega sloja b zanemarljivo majhna, glej sliko 3.11(b). Rezultanta osnih sil je tako očitno enaka nič ($\mathcal{N} = \mathcal{N}^a + \mathcal{N}^b + \mathcal{N}^c = 0$). Kadar je $\mathcal{N}^a$ natezna je $\mathcal{N}^c$ tlačna in obratno. Drugače kot pri osnih silah so upogibni momenti in prečne sile posameznih slojev vedno enako predznačeni, glej sliki 3.11(c) in 3.11(d). Njihove velikosti so približno sorazmerne z upogibno togostjo posameznega sloja. Največji del prečne sile in upogibnega momenta prevzame najbolj tog sloj a, medtem ko je strižna in upogibna nosilnost vmesnega sloja b relativno majhna.

Spreminjanje zamika med slojema a in b (Δ^{ab}), navpičnega pomika (w), normalne komponente kontaktne napetosti med slojema b in c (p_n^{bc}) ter upogibnega momenta sloja c ($\mathcal{M}^c$) vzdolž referenčne osi v odvisnosti od togosti stika prikazujemo na sliki 3.12. Iz slike 3.12 je očitno, da ima koeficient togosti

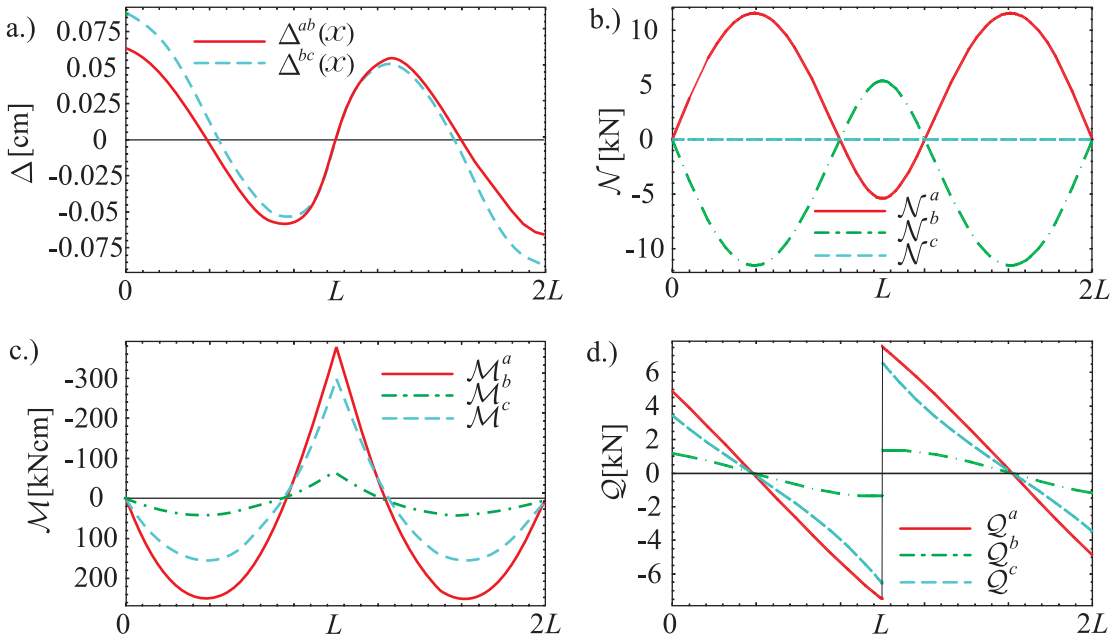

Slika 3.11: Porazdelitev zdrsov Δ^{ab} in Δ^{bc} ter ravnotežnih količin $\mathcal{N}$, $\mathcal{Q}$ in $\mathcal{M}$ posameznega sloja vzdolž referenčne osi troslojnega kontinuirnega nosilca.

Figure 3.11: Distribution of Δ^{ab}, Δ^{bc} and $\mathcal{N}, \mathcal{Q}$ in $\mathcal{M}$ in layers along the span of continuous three-layer beam over two spans.

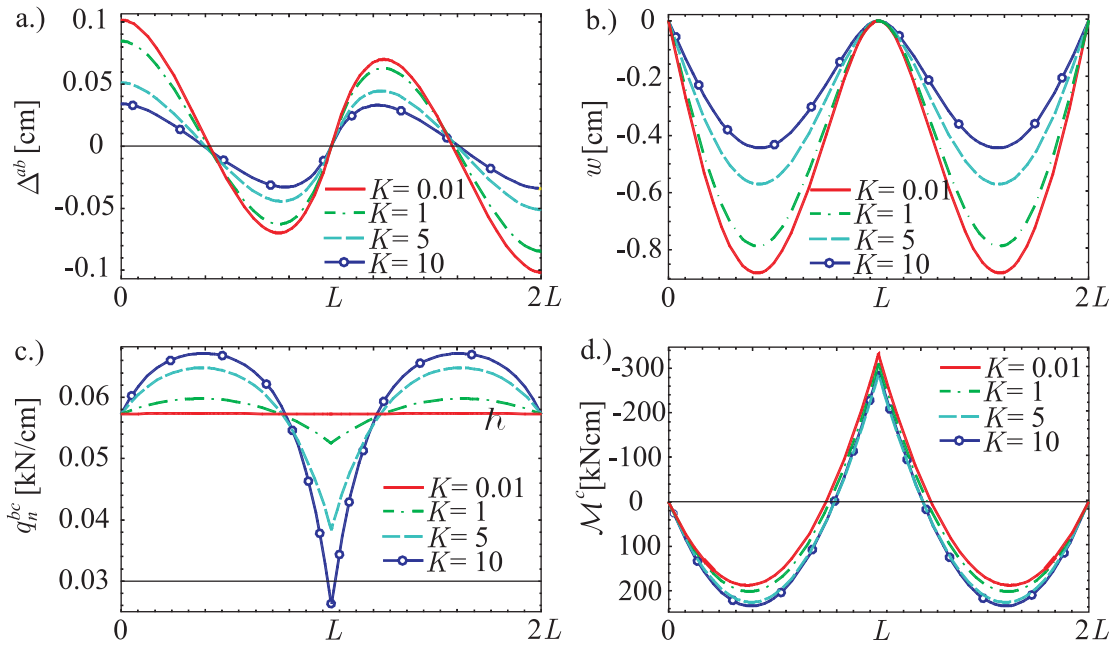

Slika 3.12: Porazdelitev zdrsa Δ^{ab}, navpičnega pomika w, normalne komponente kontaktne napetosti p_n^{bc} ter upogibnega momenta $\mathcal{M}^c$ vzdolž referenčne osi troslojnega kontinuirnega nosilca v odvisnosti od togosti stika $K = K^{ab} = K^{bc}$.

Figure 3.12: Distribution of Δ^{ab}, w, p_n^{bc}, and $\mathcal{M}^c$ along the span of the continuous three-layer beam as a function of different values of the interlayer slip moduli, $K = K^{ab} = K^{bc}$.

stika pomemben vpliv na statične in kinematične količine. Δ^{ab} in w sta manjša za večje koeficiente zdrsa K, medtem ko sta p_n^{bc} in $\mathcal{M}^c$ za večje koeficiente togosti stika med sloji večja.

3.2.3 Timoshenkov slojeviti nosilec

V tem podpoglavju bomo obravnavali Timoshenkov kompozitni nosilec z upoštevanjem majhnih zdrsov po teoriji prvega reda. Enačbe, ki opisujejo napetostno in deformacijsko stanje Timoshenkovega kompozitnega nosilca smo prikazali v oknu 5.4. V nadaljevanju bomo predstavili algoritem analitičnega reševanja enačb omenjenega nosilca. Z znanimi analitičnimi rešitvami bomo nato izvedli parametrično analizo s katero bomo študirali vpliv različnih parametrov na mehansko obnašanje kompozitnega nosilca.

3.2.3.1 Algoritem reševanja

Podobno kot v primeru Bernoullijevega kompozitnega nosilca lahko tudi v primeru Timoshenkovega kompozitnega nosilca sistem osnovnih enačb (3.143–3.157) preprosto rešimo, če le poznamo izraze za zdrse in normalne kontaktne napetosti med posameznimi sloji. Postopek reševanja je sestavljen iz naslednjega zaporedja matematičnih operacij. V prvem koraku dvakrat odvajamo enačbi (3.155) in (3.157) po vzdolžni koordinati x^i. Z upoštevanjem kinematičnih enačb (3.143–3.145) izpeljemo diferencialne enačbe za zdrse in psevdoukrivljenosti

$$\frac{\mathrm{d}^2\Delta_j(x^i)}{\mathrm{d}{x^i}^2} = \frac{\mathrm{d}\varepsilon^i(x^i)}{\mathrm{d}x^i} - \frac{\mathrm{d}\varepsilon^{i+1}(x^i)}{\mathrm{d}x^i} + z_j\Big(\frac{\mathrm{d}\kappa^i(x^i)}{\mathrm{d}x^i} - \frac{\mathrm{d}\kappa^{i+1}(x^i)}{\mathrm{d}x^i}\Big), \tag{3.190}$$

$$\kappa^{i+1}(x^i) = \kappa^i(x^i) - \frac{\mathrm{d}\gamma^i(x^i)}{\mathrm{d}x^i} + \frac{\mathrm{d}\gamma^{i+1}(x^i)}{\mathrm{d}x^i}. \tag{3.191}$$

Odvode deformacijskih količin v enačbah (3.190) in (3.191) določimo z odvajanjem in invertiranjem konstitucijskih enačb (3.151–3.153), ki imajo v primeru linearno elastičnega materiala in stacionarnega temperaturnega in vlažnostnega stanja naslednjo obliko

$$\mathcal{N}^i(x^i) = \mathcal{N}_{\mathrm{c}}^i(x^i) = E^iA^i\varepsilon^i(x^i) + E^iS^i\kappa^i(x^i) = C_{11}^i\varepsilon^i(x^i) + C_{12}^i\kappa^i(x^i), \tag{3.192}$$

$$\mathcal{Q}^i(x^i) = \mathcal{Q}_{\mathrm{c}}^i(x^i) = k_yG^iA^i\gamma^i(x^i) = C_{33}^i\gamma^i(x^i), \tag{3.193}$$

$$\mathcal{M}^i(x^i) = \mathcal{M}_{\mathrm{c}}^i(x^i) = E^iS^i\varepsilon^i(x^i) + E^iJ^i\kappa^i(x^i) = C_{21}^i\varepsilon^i(x^i) + C_{22}^i\kappa^i(x^i), \tag{3.194}$$

kjer smo s $C_{11}^i, C_{12}^i, \ldots, C_{33}^i$ označili osno, strižno in upogibno togost sloja. E^i in G^i sta elastični in strižni modul sloja i, A^i je ploščina prečnega prereza sloja, S^i in J^i pa sta statični in vztrajnostni momoment prečnega prereza sloja glede na referenčno os kompozitnega nosilca. Ker v našem modelu predpostavimo konstantno strižno deformacijo po prečnem prerezu, v enačbi upoštevamo korekcijski faktor k_y, ki ga je predstavil Cowper (1966). V primeru pravokotnih prečnih prerezov in izotropnega materiala je $k_y = 5/6$. Poleg linearno elastičnega materiala predpostavimo tudi linearni konstitucijski model stika

$$q_{t,j}(x^i) = K_j\Delta_j(x^i), \tag{3.195}$$

kjer s K_j označimo linearni koeficient togosti stika j. V nadaljevanju z rešitvijo odvajanih in invertiranih enačb (3.192–3.194) dobimo

$$\left\{ \begin{array}{c} \dfrac{\mathrm{d}\varepsilon^i(x^i)}{\mathrm{d}x^i} \\ \dfrac{\mathrm{d}\gamma^i(x^i)}{\mathrm{d}x^i} \\ \dfrac{\mathrm{d}\kappa^i(x^i)}{\mathrm{d}x^i} \end{array} \right\} = \boldsymbol{C}_i^{-1} \left\{ \begin{array}{c} \dfrac{\mathrm{d}\mathcal{N}^i(x^i)}{\mathrm{d}x^i} \\ \dfrac{\mathrm{d}\mathcal{Q}^i(x^i)}{\mathrm{d}x^i} \\ \dfrac{\mathrm{d}\mathcal{M}^i(x^i)}{\mathrm{d}x^i} \end{array} \right\}. \tag{3.196}$$

$\boldsymbol{C}_i$ predstavlja konstitucijsko matriko materialnih konstant sloja i in $\boldsymbol{C}_i^{-1}$ njeno inverzno ali recipročno matriko

$$\boldsymbol{C}_i^{-1} = \begin{bmatrix} C_{11}^i & 0 & C_{12}^i \\ 0 & C_3^i & 0 \\ C_{21}^i & 0 & C_{22}^i \end{bmatrix}^{-1} = \begin{bmatrix} D_{11}^i & 0 & D_{12}^i \\ 0 & C_3^i & 0 \\ D_{21}^i & 0 & D_{22}^i \end{bmatrix}. \tag{3.197}$$

Enačbe (3.196) vstavimo v (3.190) in (3.191). Odvode ravnotežnih količin izrazimo preko ravnotežnih enačb (3.146–3.147) in (3.150) s komponentami kontaktne napetosti $\boldsymbol{q}(x^i)$ in zunanje obtežbe $\boldsymbol{p}(x^i)$ in $\boldsymbol{m}(x^i)$ posameznega sloja. S ponovnim odvajanjem obeh enačb po vzdolžni koordinati x^i in upoštevanjem ravnotežne enačbe (3.147), dobimo sistem linearnih navadnih diferencialnih enačb drugega reda s konstantnimi koeficienti za zdrse in normalne kontaktne napetosti med sloji kompozitnega nosilca

$$A_j\Delta'_{j-1} + \Delta'''_j + B_j\Delta'_j + C_j\Delta'_{j+1} + D_j q_{n,j-1} + E_j q_{n,j} + F_j q_{n,j+1} = f_j, \tag{3.198}$$

$$G_j\Delta'_{j-1} + H_j\Delta'_j + I_j\Delta'_{j+1} + J_j q''_{n,j-1} + L_j q''_{n,j} + M_j q''_{n,j+1} + N_j q_{n,j-1} + O_j q_{n,j} + P_j q_{n,j+1} = g_j, \tag{3.199}$$

kjer so $A_j, B_j, C_j, D_j, E_j, F_j, G_j, H_j, I_j, J_j, L_j, M_j, N_j, O_j, P_j$ konstante ter f_j in g_j desne strani, ki jih določimo z izrazi

$$\begin{aligned}
A_j &= K_{j-1}\Big(-D_{11}^i + z_{j-1}D_{21}^i + z_j(D_{12}^i - z_{j-1}D_{22}^i)\Big), \\
B_j &= z_jK_j\Big(D_{12}^i + D_{12}^{i+1} + z_j(D_{22}^i + D_{22}^{i+1})\Big) - K_j\Big(D_{11}^i + D_{11}^{i+1} + z_j(D_{21}^i + D_{21}^{i+1})\Big), \\
C_j &= K_{j+1}\Big(D_{11}^{i+1} + z_jD_{21}^{i+1} - z_j(D_{12}^{i+1} + z_jD_{22}^{i+1})\Big), \quad D_j = -D_{12}^i - z_jD_{22}^i, \\
E_j &= \Big(D_{12}^i + D_{12}^{i+1} + z_j(D_{22}^i + D_{22}^{i+1})\Big), \quad F_j = -D_{12}^{i+1} - z_jD_{22}^{i+1}, \quad G_j = K_{j-1}(D_{12}^i - z_{j-1}D_{22}^i), \\
H_j &= K_j\Big(-D_{12}^i - D_{12}^{i+1} + z_j(D_{22}^i + D_{22}^{i+1})\Big), \quad I_j = K_{j+1}(D_{12}^{i+1} - z_{j+1}D_{22}^{i+1}), \quad J_j = D_{33}^i, \\
L_j &= -(D_{33}^i + D_{33}^{i+1}), \quad M_j = D_{33}^{i+1}, \quad N_j = -D_{22}^i, \quad O_j = (D_{22}^i + D_{22}^{i+1}), \quad P_j = -D_{22}^{i+1}, \\
f_j &= -(D_{12}^i + z_jD_{22}^i)\,p_Z^i + (D_{12}^{i+1} + z_jD_{22}^{i+1})\,p_Z^{i+1}, \quad g_j = D_{22}^i\,p_Z^i - D_{22}^{i+1}\,p_Z^{i+1}.
\end{aligned} \tag{3.200}$$

Pri izpeljavi enačb (3.198–3.200) smo upoštevali, da je posamezni sloj kompozitnega nosilca obremenjen samo s konstantno linijsko zunanjo obtežbo p_X^i, p_Z^i in momentom m_Y^i.

Sistem navadnih diferencialnih enačb (3.198) in (3.199) lahko enolično rešimo, če poznamo pripadajoče robne pogoje. Robni pogoji so vrednosti zdrsov in njihovih prvih dveh odvodov na robu ter vrednosti normalnih kontaktnih napetosti in njihovih prvih odvodov na robu $x^i = 0$ kompozitnega nosilca. Analitično

rešitev sistema (3.198–3.199) dobimo z uporabo računalniškega programa MATHEMATICA (Wolfram, 2003). Ko poznamo vrednosti zdrsov in kontaktnih napetosti med sloji kompozitnega nosilca, lahko enačbe osnovnega sistema (3.143–3.157) preprosto rešimo. Najprej iz ravnotežja vozlišč določimo robne vrednosti zasukov in pomikov z rešitvijo linearnega sistema enačb

$$\boldsymbol{K}_T\,\boldsymbol{u} = \boldsymbol{g}. \tag{3.201}$$

Kot smo že povedali enačbo (3.201) imenujemo enačba konstrukcije, kjer $\boldsymbol{K}_T$ predstavlja togostno matriko konstrukcije, $\boldsymbol{u}$ je vektor neznanih robnih pomikov in zasukov in $\boldsymbol{g}$ je obtežni vektor. Ko poznamo robne vrednosti pomikov in zasukov lahko izračunamo robne vrednosti ravnotežnih sil. Z znanimi vrednostmi robnih sil in pomikov je rešitev sistema enačb (3.143–3.157) za neznane funkcije $u^i(x^i), w(x^i), \varphi(x^i), \varepsilon^i(x^i), \gamma^i(x^i), \kappa^i(x^i)$, $\mathcal{N}^i(x^i)$ $\mathcal{Q}(x^i), \mathcal{M}(x^i), \Delta_j(x^i), q_{t,j}(x^i), q_{n,j}(x^i)$ znana. Na koncu rešimo še dodatni sistem (3.158–3.161), ki predstavlja sistem enačb za naslednje neznane funkcije: $x^{i+1}(x^i), \mathcal{N}(x^i), \mathcal{Q}(x^i), \mathcal{M}(x^i)$.

3.2.3.2 Primer

Z računskim primerom predstavimo učinkovitost matematičnega modela oziroma njegovo analitično rešitev za točno analizo mehanskega obnašanja geometrijsko in materialno linearnih ravninskih kompozitnih nosilcev z upoštevanjem strižne deformacije prečnega prereza in zdrsa med sloji. Z izvedeno parametrično analizo analiziramo vpliv strižne deformacije prečnega prereza na statične in kinematične količine posameznega sloja dvoslojnega kompozitnega nosilca.

3.2.3.2.1 Dvoslojni nosilec z upoštevanjem strižne deformacije prereza

V okviru računskega primera izvedemo parametrično študijo, s katero analiziramo vpliv različnih parametrov, kot so togost stika K, razmerje upogibne in strižne togosti E/G, razmerje dolžine proti višini nosilca oziroma sloja L/h itd., na izbrane statične in kinematične količine dvoslojnega prostoležečega Timoshenkovega nosilca obremenjenega z zvezno linijsko obtežbo p_Z (glej sliko 3.13) ter dobljene rezultate primerjamo z rešitvami, ki jih dobimo z uporabo klasične upogibne teorije kompozitnih nosilcev.

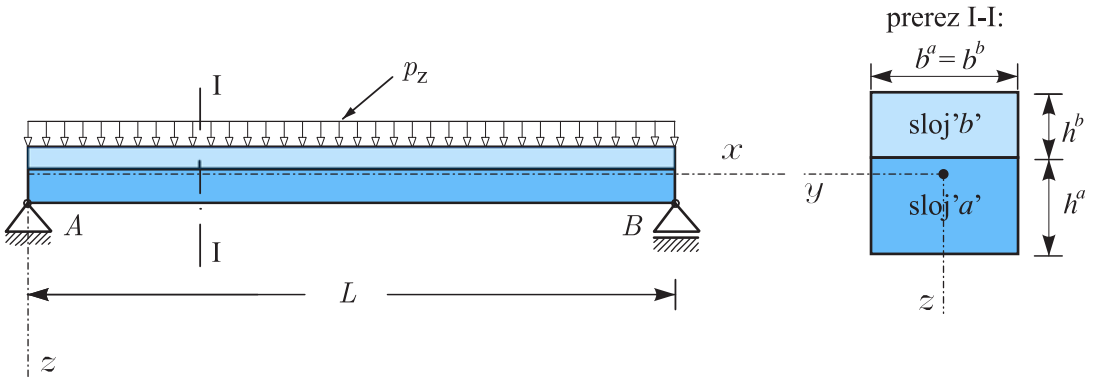

Slika 3.13: Geometrija in obtežba enostavno podprtega dvoslojnega prostoležečega Timoshenkovega nosilca.

Figure 3.13: The descriptive geometric and loading data of simply supported two-layer Timoshenko beam.

Poseben poudarek smo posvetili določitvi vpliva strižne deformacije prečnega prereza na navpične pomike kompozitnega nosilca. V ta namen primerjamo izračunane navpične pomike na sredini razpona prostoležečega kompozitnega nosilca, ki jih izračunamo po Timoshenkovi teoriji (w_T) in pomiki, izračunanimi po klasični Euler-Bernoullijevi teoriji (w_B) kompozitnih nosilcev.

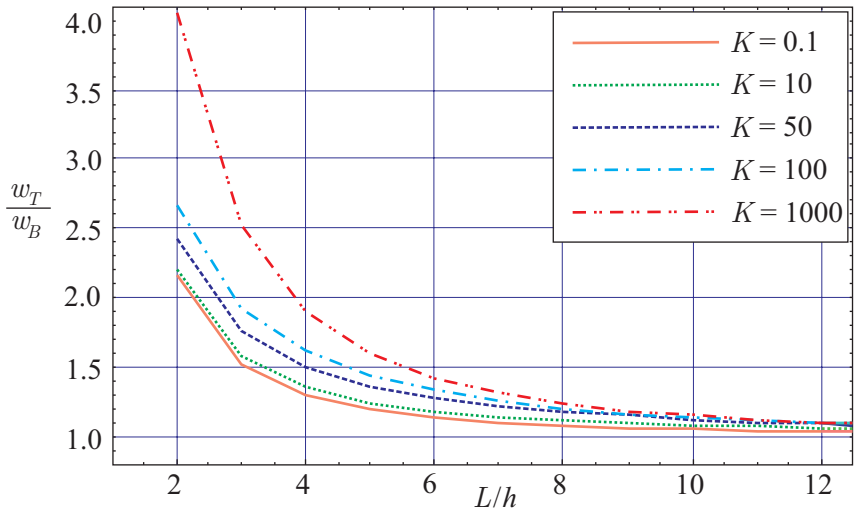

Slika 3.14: Vpliv strižne deformacije na navpične pomike lesenega dvoslojnega prostoležečega nosilca z $E/G = 16$ za različne vrednosti K in L/h.

Figure 3.14: Influence of slip modulus K and L/h ratios on vertical deflections for $E/G = 16$.

Pomike primerjamo za različne togosti stika K in različna razmerja med dolžino in višino kompozitnega nosilca L/h ter za različne vrste materiala, ki ga opišemo z razmerjem upogibne in strižne togosti E/G. Rezultate prikažemo grafično z diagrami 3.14, 3.15, 3.16 ter numerično s preglednico 3.5.

Vpliv strižne deformacije prereza v primeru lesenega nosilca, kjer je razmerje $E/G = 16$, prikazuje slika 3.14. Vpliv je prikazan za različne togosti stika K in različna razmerja L/h. Očitno je, da vpliv strižne deformacije raste z večanjem togosti K in manjšanjem razmerja L/h. Vpliv strižne deformacije tudi v primeru vitkih nosilcev $(L/h = 10)$ z relativno togo povezanimi sloji $(K > 50\mathrm{kN/cm^2})$ ni zanemarljiv in je večji od 13%. Vpliv je še večji pri krajših nosilcih $(L/h = 5)$, kjer za različne togosti stika K znaša od 19.2% do 59.5%.

Analizirali smo tudi vpliv izbire materiala (E/G) na velikost vpliva strižne deformacije prečnega prereza na navpične pomike dvoslojnega prostoležečega nosilca. Navpične pomike smo izračunali za različna razmerja (E/G). Slika 3.15 prikazuje vpliv striga za relativno podajne povezave $(K = 0.1\mathrm{kN/cm^2})$, medtem ko slika 3.16 prikazuje vpliv v primeru relativno toge povezave med sloji $(K = 100\mathrm{kN/cm^2})$. Izkaže se, da vpliv strižne deformacije pri razmerjih $E/G \geq 16$ ni zanemarljiv, kar še posebej velja za relativno toge povezave z velikim koeficientom stika K. Vpliv striga je od 15.4% za $L/h = 10$ pa do več kot 250% v primeru kratkih nosilcev z $L/h = 3$.

V primeru izotropnega materiala z $(E/G) = 2.68$ (jeklo, aluminij, baker, itd.) znaša vpliv striga za različne togosti stika $0.001\mathrm{kN/cm^2} \leq K \leq 1000\mathrm{kN/cm^2}$ pri razmerju $L/h = 5$ od 0.3% do 8.3%. Za take nosilce je v večini primerov vpliv striga zanemarljiv z izjemo zelo kratkih nosilcev $(L/h \leq 3)$ in zelo togih stikov.

Pri nosilcih iz steklenih vlaken z $E/G = 8.67$ in $L/h \geq 10$ je vpliv striga manjši od 8.4%. Vpliv postane pomemben pri $L/h \leq 5$ kjer znaša od 10.4% do 32.9%. Rezultati za anizotropen lesen nosilec z $E/G \simeq 20$ so podobni rezultatom za leseni nosilec z $E/G = 16$, ki smo ga že analizirali. Poleg tega smo izračunali vpliv strižne deformacije na navpične pomike za material, ki nima realnih materialnih lastnosti, npr. $E/G = 100$. V primeru $10 \leq L/h \leq 20$, znaša vpliv striga za $K = 0.01\mathrm{kN/cm^2}$ od 10.4% do 32.9%, medtem ko je za $K = 100\mathrm{kN/cm^2}$ od 20.4% do 62.3%.

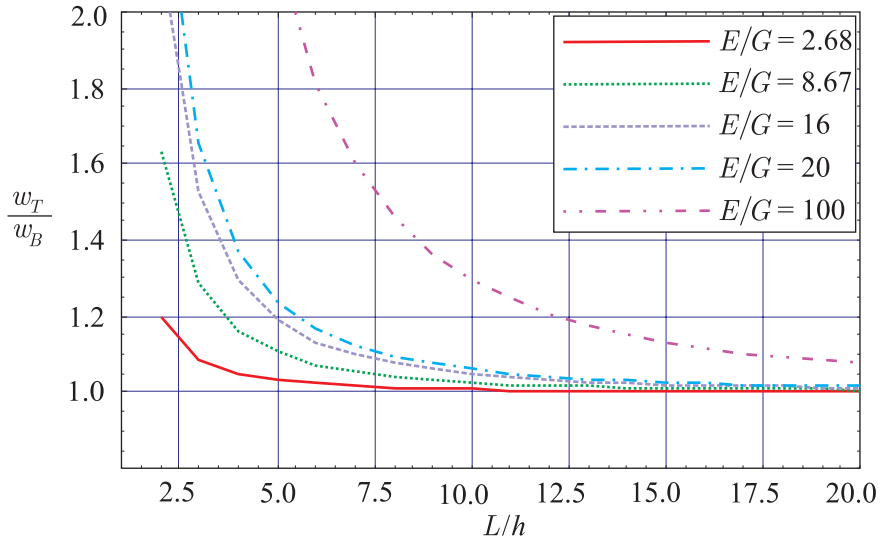

Slika 3.15: Vpliv strižne deformacije na navpične pomike dvoslojnega prostoležečega nosilca s $K = 0.01\text{kN/cm}^2$ za različne vrednosti E/G in L/h.

Figure 3.15: Influence of E/G and L/h ratios on vertical deflections for $K = 0.01\text{kN/cm}^2$.

Preglednica 3.5: Vpliv strižne deformacije prečnega prereza na navpične pomike (w_T/w_B) za različne vrednosti parametrov K, E/G in L/h.

Table 3.5: Influence of K, E/G, and L/h on vertical deflections (w_T/w_B).

	E/G=2.68			E/G=8.67			E/G=16		
$K\,[\text{kN/cm}^2]$	I	II	III	I	II	III	I	II	III
0.001	1.090	1.032	1.008	1.287	1.104	1.026	1.524	1.192	1.048
0.01	1.090	1.032	1.008	1.287	1.104	1.026	1.524	1.192	1.048
0.1	1.090	1.032	1.008	1.288	1.105	1.027	1.524	1.192	1.049
1	1.091	1.033	1.008	1.293	1.110	1.032	1.529	1.197	1.054
10	1.092	1.034	1.010	1.341	1.152	1.056	1.581	1.244	1.087
50	1.098	1.040	1.014	1.494	1.237	1.075	1.767	1.370	1.128
100	1.105	1.046	1.017	1.603	1.274	1.080	1.931	1.445	1.139
1000	1.182	1.083	1.024	1.875	1.329	1.084	2.534	1.595	1.154

I: $L/h = 3$ II: $L/h = 5$ III: $L/h = 10$

Poleg vpliva strižne deformacije na navpične pomike kompozitnega nosilca smo analizirali tudi vpliv strižne deformacije prereza na druge statične in kinematične količine, kot so $\Delta, q_n, \varepsilon^a, \mathcal{N}^a$, itd. Izbrane količine smo v primeru lesenega nosilca z $E/G = 16$ izračunali za različne vrednosti parametrov L/h in K. Rezultate predstavimo grafično na slikah 3.17 in 3.18 ter z vrednostmi v preglednici 3.6. Rezultate v primeru podajne povezave med sloji ($K = 0.1\text{kN/cm}^2$) prikazuje slika 3.17, v primeru toge povezave

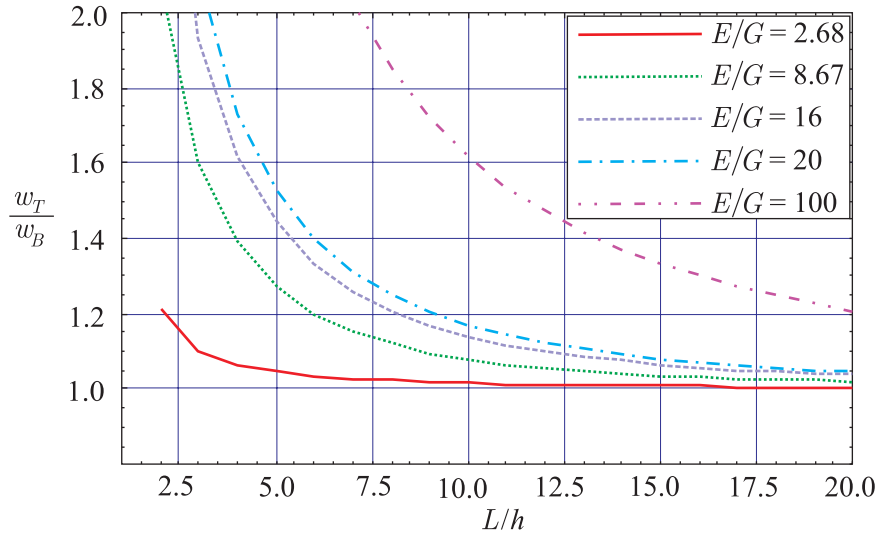

Slika 3.16: Vpliv strižne deformacije na navpične pomike dvoslojnega prostoležečega nosilca s $K = 100\mathrm{kN/cm^2}$ za različne vrednosti E/G in L/h.

Figure 3.16: Influence of E/G and L/h ratios on vertical deflections for $K = 100\mathrm{kN/cm^2}$.

med sloji ($K = 100\mathrm{kN/cm^2}$) pa slika 3.18. Izbrane količine smo izračunali z različnima teorijama kompozitnih nosilcev. Z oznako $(\bullet)_B$ označimo količine, ki jih izračunamo z Euler-Bernoullijevim modelom kompozitnih nosilcev z zdrsom med sloji, medtem ko z $(\bullet)_T$ označimo količine izračunane s Timoshenkovim modelom kompozitnih nosilcev.

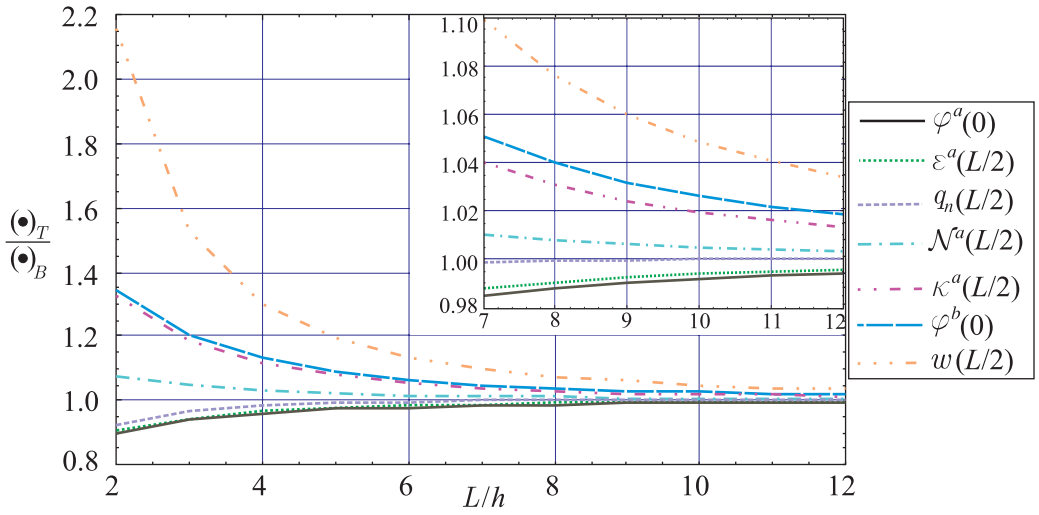

Slika 3.17: Vpliv strižne deformacije na izbrane količine lesenega dvoslojnega prostoležečega nosilca z $E/G = 16$ in $K = 0.01\mathrm{kN/cm^2}$ za različne vrednosti L/h.

Figure 3.17: Static and kinematic quantities as a function of L/h for $E/G = 16$ and $K = 0.01\mathrm{kN/cm^2}$.

Zanimivo je, da je vpliv strižne deformacije prečnega prereza na različne količine različen. Nekatere količine, kot so $w, \varphi^b, \kappa^b, \mathcal{N}^a$ se povečajo, medtem ko se druge, npr. $q_n, \varepsilon^a, \varphi^a$, zmanjšajo v primerjavi s količinami izračunanimi s klasičnim Euler-Bernoullijevim modelom kompozitnega nosilca.

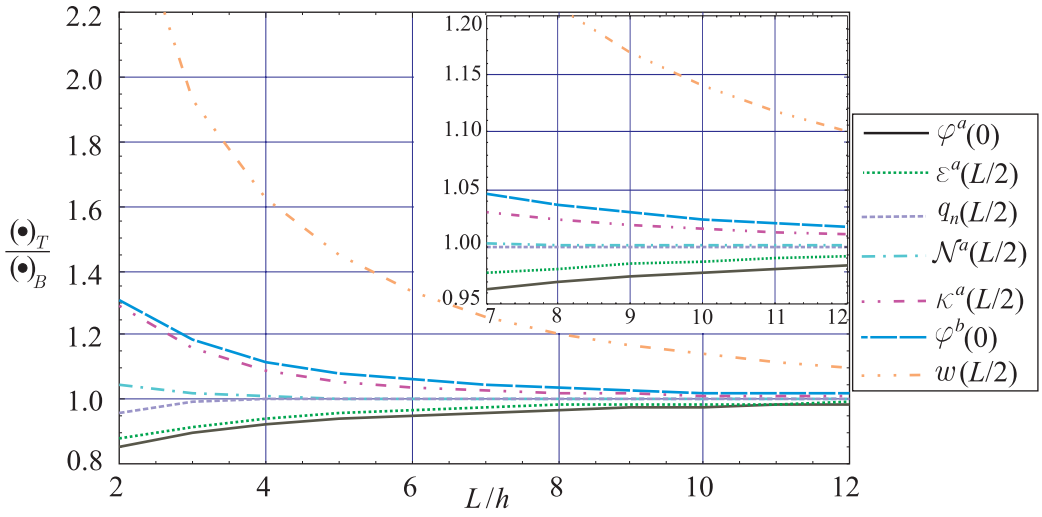

Slika 3.18: Vpliv strižne deformacije na izbrane količine lesenega dvoslojnega prostoležečega nosilca z $E/G = 16$ in $K = 100\mathrm{kN/cm}^2$ za različne vrednosti L/h.

Figure 3.18: Static and kinematic quantities as a function of L/h for $E/G = 16$ and $K = 100\mathrm{kN/cm}^2$.

Vpliv strižne deformacije na povečanje $\varphi^b(0)$ je v primeru $K = 0.1\mathrm{kN/cm}^2$ in $L/h = 3$ približno 25%, medtem ko je v primeru $L/h = 5$ samo še 1.2%. Na drugi strani je vpliv na zmanjšanje $\varepsilon^b(L/2)$ v primeru $K = 100\mathrm{kN/cm}^2$ in $L/h = 3$ okrog -10.3% ter pri $L/h = 10$ samo še -2.2%.

Preglednica 3.6: Vpliv strižne deformacije na statične in kinematične količine za različne vrednosti parametrov K in L/h pri $E/G = 16$.

Table 3.6: Static and kinematic quantities as functions of K and L/h for $E/G = 16$.

	$K = 0.1\,\mathrm{kN/cm}^2$			$K = 100\,\mathrm{kN/cm}^2$		
$(\bullet)_T/(\bullet)_B$	I	II	III	I	II	III
$w(L/2)$	1.524	1.192	1.049	1.931	1.445	1.139
$\Delta(0)$	1.046	1.020	1.006	1.026	1.012	1.005
$\varphi^a(0)$	0.939	0.973	0.992	0.919	0.960	0.988
$\varphi^b(0)$	1.250	1.092	1.026	1.185	1.083	1.030
$\kappa^a(L/2)$	0.944	0.977	0.994	0.927	0.969	0.992
$\kappa^b(L/2)$	1.188	1.077	1.020	1.156	1.059	1.015
$\mathcal{N}^a(L/2)$	1.044	1.019	1.005	1.022	1.007	1.001
$\varepsilon^a(L/2)$	0.944	0.977	0.994	0.897	0.942	0.978
$q_n(L/2)$	0.968	0.994	1.000	1.993	1.004	1.001

I: $L/h = 3$ II: $L/h = 5$ III: $L/h = 10$

Opazimo tudi, da ima strižna deformacija za različne togosti stika različen vpliv na različne količine. Nekatere količine se z večanjem togosti stika K povečujejo (npr. $w(L/2), q_n(L/2)$), druge zmanjšujejo (npr. $\Delta(0), \varphi^b(L/2), \kappa^b(L/2), \mathcal{N}^a$, itd.) v primerjavi s količinami, izračunanimi s klasično teorijo kompozitnih nosilcev. Slika 3.19 prikazuje vpliv strižne deformacije na razmerje vzdolžnih in normalnih kontaktnih napetosti lesenega kompozitnega nosilca z razmerjem $E/G = 16$ za različne K in L/h.

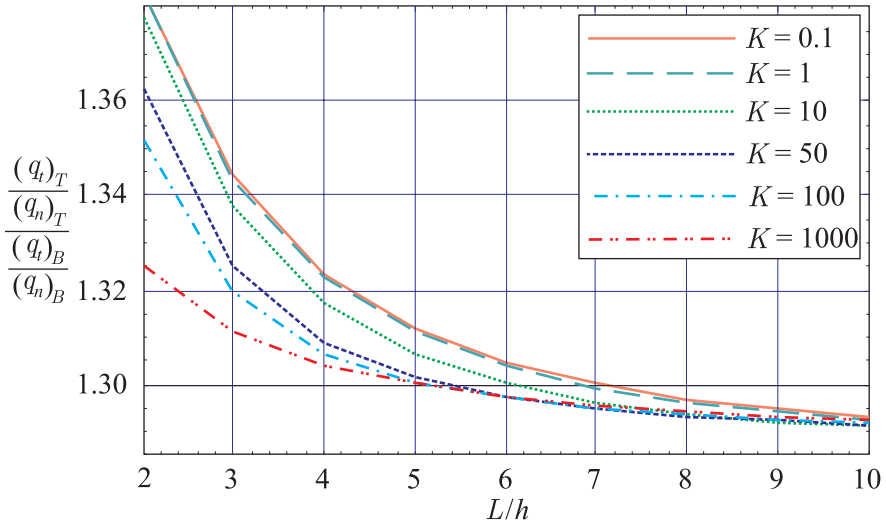

Slika 3.19: Vpliv strižne deformacije prečnega prereza na razmerje vzdolžnih in normalnih kontaktnih napetosti za različne K in L/h v primeru lesenega kompozitnega nosilca z $E/G = 16$.

Figure 3.19: Ratio of tangential and normal tractions as a function of L/h for $E/G = 16$ and different K's.

Iz slike 3.19 je razvidno, da je vpliv strižne deformacije na razmerje kontaktnih napetosti q_t/q_n velik tudi v primeru vitkih nosilcev. Pri razmerju $L/h = 10$ je približno 29%. Vpliv je večji za bolj podajne povezave med sloji. Poleg tega iz slike 3.20 vidimo, da je razmerje vzdolžnih kontaktnih napetosti proti normalnim v primeru Timoshenkovega nosilca večje za bolj vitke nosilce in bolj toge povezave med sloji. V primeru vitkega nosilca z razmerjem $L/h = 20$ in $K = 1000\mathrm{kN/cm^2}$ so vzdolžne napetosti približno 20-krat večje od normalnih kontaktnih napetosti. V primeru $L/h = 20$ in $K = 0.1\mathrm{kN/cm^2}$ so večje le še 1.5-krat.

V okviru parametrične študije smo analizirali tudi vpliv razmerja višin posameznih slojev h^a/h^b na navpične pomike w in prečne sile $\mathcal{Q}$ dvoslojnega lesenega prostoležečega kompozitnega nosilca. V ta namen smo za različne vrednosti h^a/h^b ter K izračunali navpične pomike na sredini $w(L/2)$ in prečne sile na začetku $\mathcal{Q}(0)$ kompozitnega nosilca. Rezultati so za navpične pomike prikazani na sliki 3.21.

Parametrična študija pokaže, da je vpliv strižne deformacije na navpične pomike vedno najmanjši, kadar imata sloja približno enako višino, kadar je razmerje $h^a/h^b \simeq 1$. Iz slike 3.21 vidimo, da je vpliv manjši za manjše vrednosti K. V primeru podajne povezave, ko je $K \leq 1\mathrm{kN/cm^2}$, je lahko vpliv tudi do 4-krat manjši kot v primeru relativno toge povezave, ko je $K = 1000\mathrm{kN/cm^2}$.

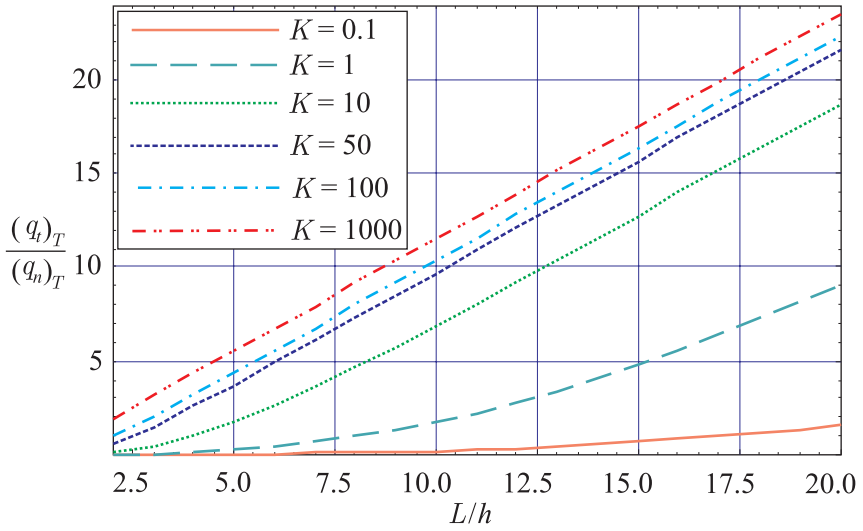

Slika 3.20: Vpliv strižne deformacije prečnega prereza na razmerje vzdolžnih in normalnih kontaktnih napetosti po Timoshenku za različne K in L/h v primeru lesenega kompozitnega nosilca z $E/G = 16$.

Figure 3.20: Ratio of tangential and normal tractions as a function of L/h for $E/G = 16$ and different K's.

Vpliv strižne deformacije na prečne sile posameznega sloja prikažemo za različne togosti stika K in različna razmerja višin posameznih slojev h^a/h^b s slikami 3.22, 3.23 in 3.24. Primerjava prečnih sil $\mathcal{Q}^a$ in $\mathcal{Q}^b$ pokaže, da je vpliv strižne deformacije, podobno kot pri navpičnih pomikih, najmanjši v primeru, ko sta sloja približno enakih višin, takrat je $h^a/h^b \simeq 1$.

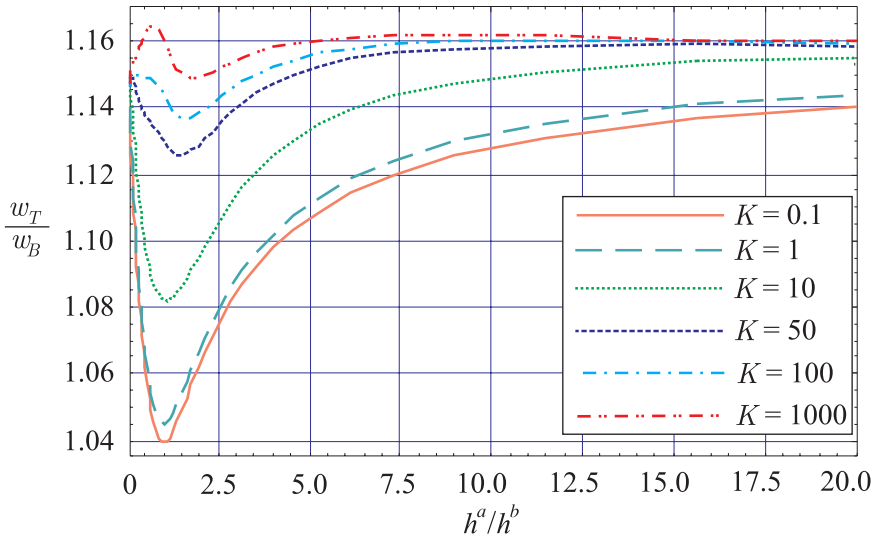

Slika 3.21: Vpliv strižne deformacije prečnega prereza na navpične pomike w za različne K in h^a/h^b v primeru lesenega kompozitnega nosilca z $E/G = 16$ in $L/h = 10$.

Figure 3.21: Vertical deflections as a function of h^a/h^b for $L/h = 10$ and $E/G = 16$ and different K's.

Izkaže se, da so lahko prečne sile v sloju, ki je zelo tanek v primerjavi z drugim slojem, v primeru podajnega stika ($K \leq 1\mathrm{kN/cm^2}$), tudi do 2.5-krat večje, kot so prečne sile v tem sloju, izračunane po klasični upogibni teoriji kompozitnih nosilcev z upoštevanjem zdrsa med sloji. V primeru zelo toge

povezave ($K \geq 1000\mathrm{kN/cm^2}$) je vpliv strižne deformacije na prečne sile zanemarljiv. Izjema so nosilci, kjer je zgornji sloj b, zelo tanek v primerjavi z spodnjim slojem a. V tem primeru, so lahko prečne sile $\mathcal{Q}^a$, tudi do 2-krat manjše, kot so prečne sile $\mathcal{Q}^b$.

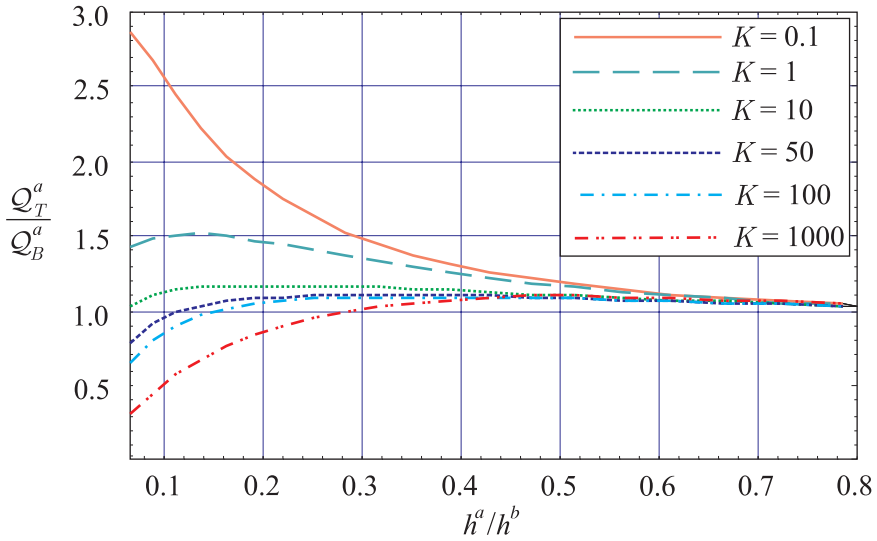

Slika 3.22: Vpliv strižne deformacije prečnega prereza na prečne sile $\mathcal{Q}^a$ za različne K in h^a/h^b v primeru lesenega kompozitnega nosilca z $E/G = 16$.

Figure 3.22: Shear force $\mathcal{Q}^a$ as a function of h^a/h^b for $L/h = 10$ and $E/G = 16$ and different K's.

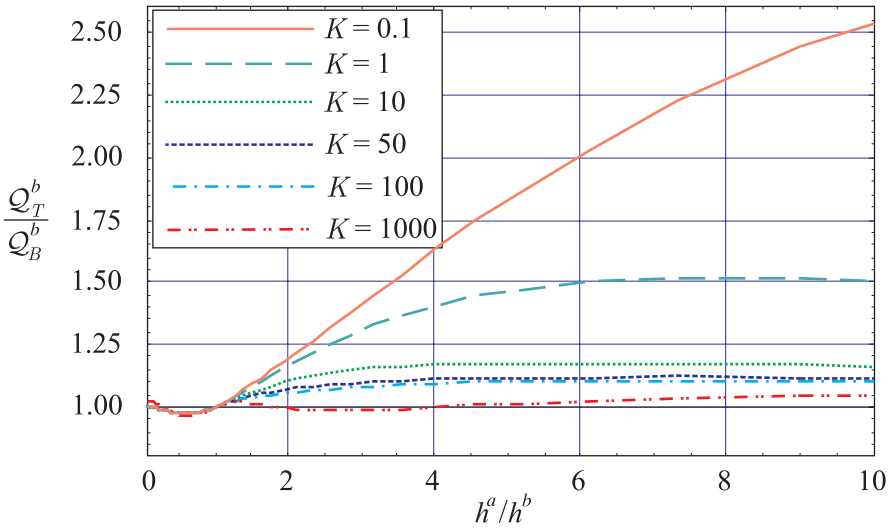

Slika 3.23: Vpliv strižne deformacije prečnega prereza na prečne sile $\mathcal{Q}^b$ za različne K in h^a/h^b v primeru lesenega kompozitnega nosilca z $E/G = 16$.

Figure 3.23: Shear force $\mathcal{Q}^b$ as a function of h^a/h^b for $L/h = 10$ and $E/G = 16$ and different K's.

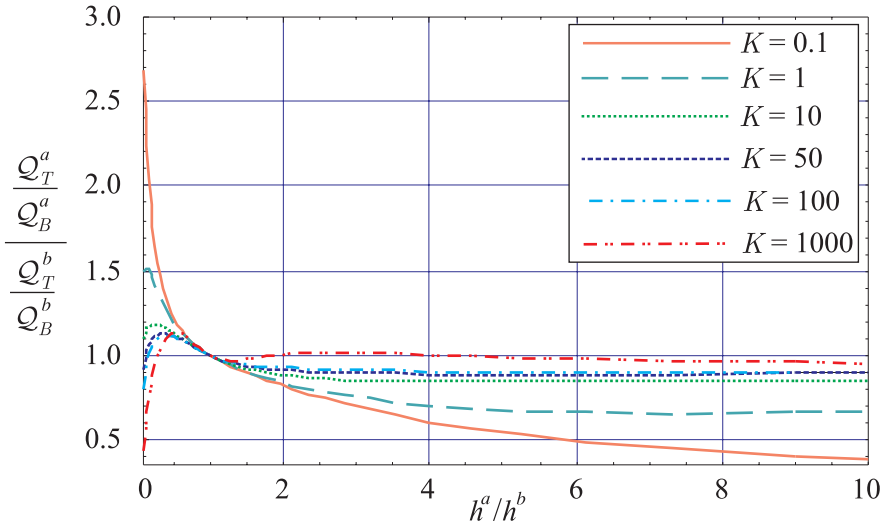

Slika 3.24: Vpliv strižne deformacije prečnega prereza na razmerje prečnih sil $\mathcal{Q}^a/\mathcal{Q}^b$ za različne K in h^a/h^b v primeru lesenega kompozitnega nosilca z $E/G = 16$.

Figure 3.24: Shear force ratio $\mathcal{Q}^a/\mathcal{Q}^b$ for $L/h = 10$ and $E/G = 16$ and different K's.

V nadaljevanju primerjamo uporabo različnih modelov za račun navpičnih pomikov ravninskih nosilcev. Navpične pomike lesenega dvoslojnega nosilca z $E/G = 16$ in $L/h = 10$ izračunamo z uporabo različnih modelov oziroma formul: (1) empirične enačbe, ki jih predlaga Evrokod 5 (2004), (2) Euler-Bernoullijev model z in brez upoštevanja zdrsa in (3) Timoshenkov model z in brez upoštevanja zdrsa. Primerjavo navpičnih pomikov različnih modelov za različne togosti stika K prikazujeta slika 3.25 in preglednica 3.7.

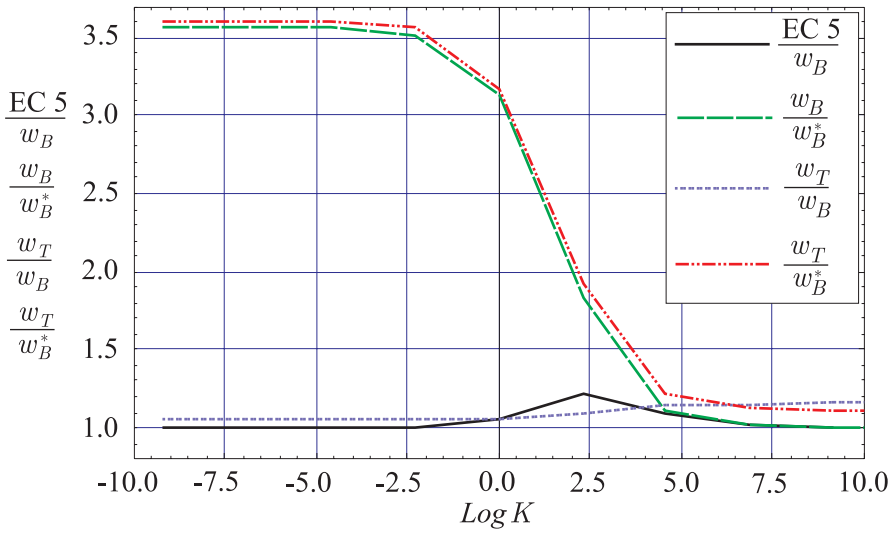

Slika 3.25: Primerjava navpičnih pomikov w za različne togosti stika K in različne modele nosilcev.

Figure 3.25: Comparisons of vertical deflections calculated by different beam models, for different K's with $L/h = 10$ and $E/G = 16$.

Iz slike 3.25 vidimo, da togost stika K v primeru dokaj podajnih stikov $(0.001\text{kN/cm}^2 \leq K \leq 0.1\text{kN/cm}^2)$ nima vpliva na prispevek strižne deformacije k navpičnim pomikom. Vpliv zdrsa na navpične pomike (w_B/w_B^*) razumljivo pada z naraščanjem togosti stika. V primeru zelo togega stika

($K > 1000\mathrm{kN/cm^2}$) ima vpliv na navpične pomike samo strižna deformacija. V tem primeru znaša razlika med navpičnimi pomiki po Timoshenku in Bernoulliju le 1.2%. Pomiki po Evrokodu 5 (2004) se dobro ujemajo s pomiki po Bernoulliju (w_{EC5}/w_B) za togosti stika $0.001\mathrm{kN/cm^2} < K < 10\mathrm{kN/cm^2}$ in $100\mathrm{kN/cm^2} < K < 1000\mathrm{kN/cm^2}$. Večje odstopanje je zaslediti na intervalu $10\mathrm{kN/cm^2} < K < 100\mathrm{kN/cm^2}$, kjer so pomiki po Evrokodu 5, tudi do 25% večji od pomikov po Bernoulliju.

Preglednica 3.7: Primerjava navpičnih pomikov za različne vrednosti parametrov K in različne modele nosilcev.
Table 3.7: Vertical deflections calculated by different beam models for different K's with $L/h = 10$ and $E/G = 16$.

K	EC 5	w_B^*	w_B	w_T^*	w_T	$\frac{\mathrm{EC5}}{w_B}$	$\frac{w_T}{w_B}$	$\frac{w_B}{w_B^*}$	$\frac{w_T}{w_T^*}$	$\frac{w_T}{w_B^*}$
$\left[\frac{\mathrm{kN}}{\mathrm{cm^2}}\right]$	[cm]	[cm]	[cm]	[cm]	[cm]					
0.001	3.875	1.085	3.875	1.252	4.062	1.000	1.048	3.571	3.243	3.743
0.01	3.872	1.085	3.869	1.252	4.057	1.000	1.048	3.566	3.239	3.738
0.1	3.845	1.085	3.818	1.252	4.005	1.007	1.049	3.518	3.197	3.691
1	3.602	1.085	3.391	1.252	3.573	1.062	1.054	3.125	2.853	3.293
10	2.427	1.085	1.982	1.252	2.154	1.225	1.087	1.826	1.720	1.985
50	1.526	1.085	1.325	1.252	1.494	1.153	1.128	1.221	1.193	1.377
100	1.326	1.085	1.230	1.252	1.379	1.096	1.139	1.115	1.101	1.270
1000	1.111	1.085	1.098	1.252	1.267	1.012	1.154	1.012	1.012	1.168

* brez zdrsa

Analiza različnih modelov računanja nosilcev pokaže, da so modeli, ki upoštevajo delno povezavo med sloji, zelo pomembni za natančno napoved velikosti navpičnih pomikov kompzitnih nosilcev še posebno v primeru zelo podajnih povezav, kjer je $0.001\mathrm{kN/cm^2} < K < 1\mathrm{kN/cm^2}$. Primerjavi w_B/w_B^* in w_T/w_T^* pokažeta, da so lahko pomiki nosilcev z delno povezanimi sloji tudi do 3.5-krat večji od pomikov nosilcev s togo povezanimi sloji. Vidimo, da je potrebno model z upoštevanjem zdrsa med sloji upoštevati tudi za togosti stika $K > 50\mathrm{kN/cm^2}$. Iz primerjave w_T/w_B je razvidno, da je vpliv strižne deformacije na navpične pomike tudi do 15.4%.

Analizirali smo tudi vpliv togosti stika K na porazdelitev napetosti po višini dvoslojnega lesenega nosilca z $E/G = 10$ ter $L/h = 10$ in z upoštevanjem delne povezanosti slojev. Za različne togosti stika K smo izračunali glavne vzdolžne normalne napetosti σ_{xx} v prečnem prerezu na sredini razpona nosilca in tangencialne strižne napetosti σ_{xz} v prečnem prerezu na začetnem robu
nosilca, glej sliko 3.26.

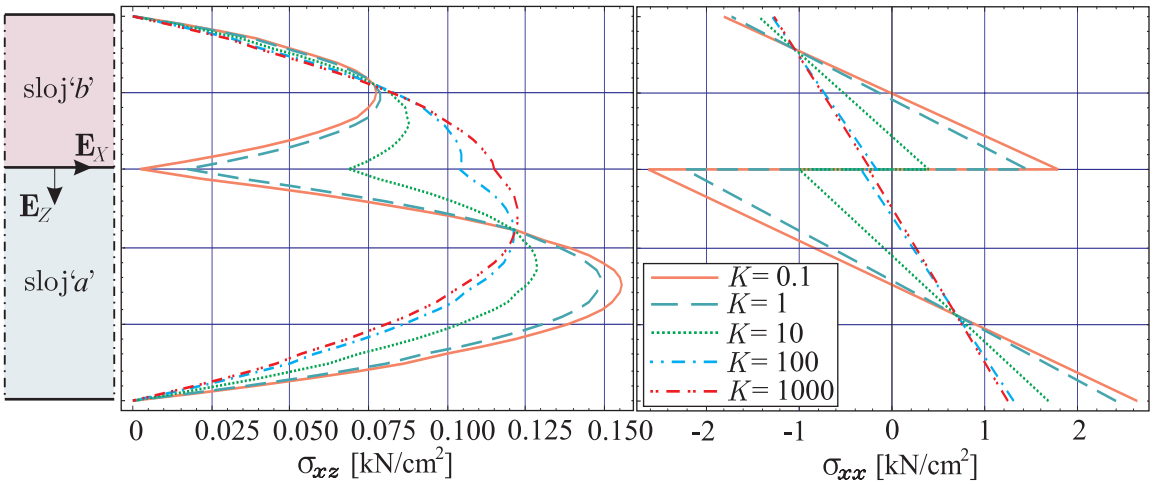

Slika 3.26: Vpliv togosti stika K na velikost in razporeditev normalnih σ_{xx} in strižnih σ_{xz} napetosti po višini prečnega prereza dvoslojnega lesenega nosilca z $E/G = 16$ in $E/h = 10$.

Figure 3.26: The distribution of normal and tangential stresses over the cross section for different K's.

Po višini prereza kompozitnega nosilca dobimo odsekoma linearno razporeditev normalnih napetosti in kvadratično razporeditev strižnih napetosti. Vidimo, da ima vpliv togosti stika K zelo pomemben vpliv na velikost in razpored strižnih in normalnih napetosti po prerezu. V primeru zelo podajnih stikov so maksimalne strižne in normalne napetosti dosti večje od napetosti, ki jih dobimo z upoštevanjem klasičnega modela nosilcev s togo povezanimi sloji. Strižne napetosti σ_{xz} so v primeru zelo podajnih stikov tudi za 25% večje od napetosti homogenega nosilca togo povezanimi sloji. Razlike v primeru normalnih napetostih σ_{xx} so še večje.

3.3 Numerično reševanje

3.3.1 Pregled literature

V dostopni tehnični literaturi obstaja veliko število člankov in drugih prispevkov s področja numeričnega reševanja problemov kompozitnih nosilcev, sestavljenih iz različnih materialov in z upoštevanjem zdrsa med sloji. V nadaljevanju na kratko opišemo pregled literature na tem področju.

Eden prvih raziskovalcev, ki je numerično obravnaval kompozitne nosilce je bil Thompson s sodelavci (1975). Na osnovi predhodno razvitega modela za elastično analizo sestavljenih lesenih nosilcev je izdelal računalniški program *FEAFLO*, ki temelji na metodi končnih elementov. Program je nekaj let kasneje razširil Wheat *et al.* (1983), in sicer tako, da omogoča modeliranje nelinearnega zakona stika. S sodelavci je ugotovil, da so rezultati nelinearne analize bistveno natančnejši, kot rezultati linearne analize. Razlike so še posebej opazne v primeru nosilcev, ki so obremenjeni z zvezno obtežbo. Roberts (1985) je eden redkih avtorjev, ki je pri analizi kompozitnih nosilcev uporabil metodo končnih diferenc. V veliki večini primerov so avtorji analizirali nosilce iz jekla in betona. Tako je Oven *et al.* (1997) obravnaval geometrijsko in materialno nelinearne sovprežne nosilce. Rezultate za prostoležeči in kontinuirni nosilec je primerjal z eksperimentalnimi rezultati, ki jih je dobil iz literature. Poroča o dobrem ujemanju rezultatov. V nadaljevanju so Salari in Spacone ter sodelavci (1998) obravnavali kompozitne nosilce z metodo končnih elementov, ki je osnovana na aproksimaciji notranjih sil. Stik med sloji so modelirali z zvezno razporejenimi vzmetmi. Končni element so primerjali z elementi osnovanimi na aproksimaciji

pomikov. S predstavljenim numeričnim primerom so pokazali prednosti njihovega končnega elementa v primerjavi z ostalimi. Manfredi in Pecce (1998) sta obravnavala armiranobetonske nosilce, pri katerih sta upoštevala zdrs armature. Vpliv ciklične obtežbe na obnašanje sovprežnega nosilca sta z mešano metodo končnih elementov obravnavala Ayoub in Filippou (2000). Leta 2001 sta Salari in Spacone (2001) model linearnega stika Salari *et al.* (1998) razširila na nelinearni stik. Pri tem sta ponovno uporabila metodo končnih elementov osnovano na aproksimaciji notranji sil. Podobno metodo je pri svojem delu uporabil Ayoub (2001, 2005). Pri tem je stik med sloji modeliral s tankim slojem. Pri analizi je zanemaril trenje in ločitev slojev. Dall'Asta in Zona (2002, 2004a, 2004b) sta predstavila različne metode končnih elementov za analizo kompozitnih nosilcev iz jekla in betona. Študirala sta natančnost in konvergenco različnih razvitih končnih elementov, ki se med seboj ločijo glede stopnje interpolacijskih polinomov, s katerimi aproksimirajo neznane funkcije. Opozorila sta na prisotnost blokiranja zdrsa in psevdoukrivljenosti slojev v primeru velikih togosti stika. Vzrok blokiranja pripišeta nekonsistenti interpolaciji vzdolžnih in navpičnih pomikov. Za rešitev problema blokiranja predlagata ustrezno izbiro interpolacijskih nastavkov za polje pomikov. Faela *et al.* (2002, 2003) predlaga tako imenovano direktno metodo, pri kateri aproksimacija neznanih pomikov ni potrebna. Direktno metodo uporabi pri analizi kontiniurnih kompozitnih nosilcev tudi Ranzi *et al.* (2004). Uporabo metode končnih elementov v primeru prednapetih sovprežnih nosilcev prikažeta Dall'Asta in Zona (2005) in Zona (2005). Pri tem upoštevata zdrs zunanjega kabla, zanemarita pa trenje med kablom in betonom. Zona *et al.* (2006) izvede tudi občutljivostno analizo kontinuirnih sovprežnih nosilcev, s katero analizira vpliv različnih parametrov na mehansko obnašanje obravnavanih konstrukcij. Ranzi *et al.* (2006) ter Gara *et al.* (2006) sta poleg zdrsa upoštevala tudi ločitev slojev. Pri tem uporabita tri različne metode končnih elementov. Podobno kot Dall'Asta in Zona (2004a 2004b), tudi onadva poročata o blokiranju zdrsa med sloji ter psevdoukrivljenosti posameznih slojev. Materialno nelinearno analizo sovprežnih nosilcev predstavi tudi Čas s sodelavci (2004b). Pri tem uporabi metodo končnih elementov, ki temelji na aproksimaciji deformacij. Schbnabl *et al.* (2007) izpelje na osnovi deformacijske metode končnih elementov končni element s katerim upošteva vpliv strižne deformacije posameznega sloja na mehansko obnašanje kompozitnega nosilca. Pri tem vsak sloj modelira s Timoshenkovo teorijo nosilcev. Izvede tudi parametrično študijo, s katero pokaže, v katerih primerih vpliv striga ni zanemarljiv. Čas (2004) predstavi geometrijsko in materialno nelinearni model kompozitnih nosilcev z upoštevanjem poljubnih zdrsov med sloji. Predpostavka o majhnih zdrsih je namreč osnovna predpostavka oziroma omejitev vseh ostalih modelov kompozitnih nosilcev. Aplikacijo modela z upoštevanjem majhnih zdrsov prikaže Čas *et al.* (2004a). Primer uklona lesenih stebrov obravnava Čas *et al.* (2007). Z dinamiko sovprežnih nosilcev z upoštevanjem zdrsa med sloji se je ukvarjal Sapountzakis (2004).

Nekateri raziskovalci so analizirali tudi reološko obnašanje kompozitnih nosilcev z upoštevanjem zdrsa med sloji. Dezi in Tarantino (1993a, 1993b) sta analizirala krčenje in lezenje sovprežnih kontinuirnih nosilcev. Podobno sta reološke pojave v primeru sovprežnih nosilcev z delno povezavo med sloji študirala Kwak in Seo (2000, 2002). Fragiacomo in Ceccotti (2005, 2006a, 2006b) sta predstavila metodo končnih elementov za reološko analizo kompozitnih nosilcev iz lesa in betona. Pri tem sta upoštevala mehanosorptivno lezenje, krčenje in nabrekanje materiala, itd. S požarno analizo kompozitnih nosilcev so se ukvarjali Huang *et al.* (1999), Elghazouli *et al.* (2000). Elghazouli *et al.* (2000) je obravnaval sovprežne nosilce pri požaru. Rezultate, ki jih je dobil z uporabo metode končnih elementov je primerjal z eksperimentalnimi rezultati. Tudi Huang *et al.* (1999) je obravnaval sovprežne nosilce z metodo končnih elementov. Izdelal je model za nelinearno analizo tridimenzionalnih nosilcev.

3.3.2 Diskretizacija. Metoda končnih elementov

Točne rešitve enačb, ki opisujejo napetostno in deformacijsko stanje kompozitnih nosilcev z upoštevanjem zdrsa med sloji, v splošnem ne poznamo. Analitične rešitve lahko dobimo le v izjemno preprostih

primerih linearno elastičnega materiala in preproste geometrije ter robnih pogojev. V vseh ostalih primerih je reševanje možno le z uporabo približnih numeričnih metod, kot so metoda končnih razlik, metoda končnih elementov, metoda robnih elementov, metoda končnih volumnov, itd. V nalogi se odločimo za uporabo metode končnih elementov.

Osrednja naloga poglavja je tako diskretizacija robnega problema kompozitnega nosilca z upoštevanjem zdrsa med sloji. Z razliko od metode končnih razlik, kjer aproksimiramo osnovne enačbe, pri metodi končnih elementov aproksimiramo rešitev osnovnih enačb. To pomeni, da aproksimiramo neznane funkcije, ki enolično določajo napetostno in deformacijsko stanje kompozitnega nosilca. S tem sistem diferencialnih enačb, ki določajo robni problem kompozitnga nosilca, nadomestimo s sistemom algebrajskih enačb.

Odločimo se, da bomo diskretizirali enačbe lineariziranega robnega problema (3.143-3.157). Ker je rezultat linearizacije linearna teorija kompozitnih nosilcev z upoštevanjem majhnih zdrsov, se pri izpeljavi diskretiziranih enačb nosilca brez izgube splošnosti izognemo pisanju funkcijskih argumentov.

3.3.2.1 Izrek o virtualnem delu

Enačbe kompozitnega nosilca lahko namesto v strogi obliki (3.143–3.157), pišemo v šibki oziroma variacijski obliki. Tedaj je ravnotežje določeno z minimumom funkcionala, ki ga v mehaniki imenujemo izrek o virtualnem delu. Omenjeni izrek zahteva, da je virtualno delo notranjih sil enako virtualnemu delu zunanjih sil. Ravnotežje v tem primeru določa naslednji izraz (Planinc, 1998),

$$\int_{\mathcal{V}} \boldsymbol{S} : \delta \boldsymbol{E} \, \mathrm{d}V = \int_{\mathcal{V}} \boldsymbol{v} \cdot \delta \boldsymbol{u} \, \mathrm{d}V + \int_{\mathcal{S}} \boldsymbol{p} \cdot \delta \boldsymbol{u} \, \mathrm{d}S, \tag{3.202}$$

kjer je z δ označena variacija, $\boldsymbol{v}$ in $\boldsymbol{p}$ sta vektorja specifične prostorninske oziroma površinske obtežbe, $\boldsymbol{S}$ je drugi Piola-Kirchhoffov napetostni tenzor; $\boldsymbol{E}$ je Green-Lagrangev tenzor deformacij in $\boldsymbol{u}$ je vektor pomikov. V komponentni obliki ima izraz (3.202) v primeru kompozitnega nosilca naslednjo obliko

$$\begin{aligned}
&\sum_{i=1}^{N_{\mathrm{sl}}} \left(\int_0^L (\mathcal{N}^i \, \delta\varepsilon^i + \mathcal{Q}^i \, \delta\gamma^i + \mathcal{M}^i \, \delta\kappa^i) \mathrm{d}x \right) = \sum_{i=1}^{N_{\mathrm{sl}}} \left(\int_0^L (p_X^i + q_{t,j-1} - q_{t,j}) \delta u^i \mathrm{d}x \right) + \\
&\sum_{i=1}^{N_{\mathrm{sl}}} \left(\int_0^L (p_Z^i - q_{n,j-1} + q_{n,j}) \delta w^i \mathrm{d}x \right) + \sum_{i=1}^{N_{\mathrm{sl}}} \left(\int_0^L (m_Y^i - z_j q_{t,j} + z_{j-1} q_{t,j-1}) \delta\varphi^i \mathrm{d}x \right) + \\
&+ \sum_{i=1}^{N_{\mathrm{sl}}} \sum_{k=1}^{6} S_k^i \delta u_k^i.
\end{aligned} \tag{3.203}$$

V izrazu (3.203) količine δu^i, δw^i in $\delta\varphi^i$ označujejo virtualne spremembe pomikov in zasukov referenčne osi slojev, medtem ko $\delta\varepsilon^i$, $\delta\gamma^i$ in $\delta\kappa^i$ predstavljajo virtualne spremembe deformacijskih količin. $\delta u_k^i \, (i = 1, \ldots, 6)$ so virtualne spremembe robnih pomikov in zasukov:

$$\delta u_1^i = \delta u^i(0), \;\; \delta u_2^i = \delta w^i(0), \;\; \delta u_3^i = \delta\varphi^i(0), \;\; \delta u_4^i = \delta u^i(L), \;\; \delta u_5^i = \delta w^i(L), \;\; \delta u_6^i = \delta\varphi^i(L). \tag{3.204}$$

Z $S_k^i \, (i = 1, \ldots, 6)$ smo označili vozliščne sile in momente.

3.3.2.2 Modificirani izrek o virtualnem delu

Z namenom izpeljave diskretnih posplošenih enačb kompozitnega nosilca v nadaljevanju uporabimo modificirani izrek o virtualnem delu, (Planinc, 1998). Če predpostavimo, da je kinematičnim enačbam

(3.151–3.153) identično zadoščeno, lahko ravnotežne količine v (3.203) zamenjamo s konstitutivnimi. Po zamenjavi dobimo

$$\begin{aligned}\delta W = &\sum_{i=1}^{N_{\mathrm{sl}}}\left(\int_0^L (\mathcal{N}_c^i\,\delta\varepsilon^i + \mathcal{Q}_c^i\,\delta\gamma^i + \mathcal{M}_c^i\,\delta\kappa^i)\mathrm{d}x\right) - \sum_{i=1}^{N_{\mathrm{sl}}}\left(\int_0^L (p_X^i + q_{t,j-1} - q_{t,j})\delta u^i \mathrm{d}x\right) - \\ &- \sum_{i=1}^{N_{\mathrm{sl}}}\left(\int_0^L (p_Z^i - q_{n,j-1} + q_{n,j})\delta w^i \mathrm{d}x\right) - \sum_{i=1}^{N_{\mathrm{sl}}}\left(\int_0^L (m_Y^i - z_j q_{t,j} + z_{j-1} q_{t,j-1})\delta\varphi^i \mathrm{d}x\right) - \\ &- \sum_{i=1}^{N_{\mathrm{sl}}}\sum_{k=1}^{6} S_k^i \delta u_k^i = 0.\end{aligned} \tag{3.205}$$

Kinematične in deformacijske količine v (3.205) med seboj niso neodvisne. Povezane so preko kinematičnih enačb (3.143 – –(3.145). To pomeni, da so v primeru posameznega sloja, od šestih funkcij $\varepsilon^i, \gamma^i, \kappa^i, u^i, w^i, \varphi^i$ neodvisne le tri. Glede na izbiro neodvisnih funkcij delimo različne metode končnih elementov. Če za neodvisne funkcije izberemo pomike sloja (u^i, w^i, φ^i), pravimo da metoda končnih elementov temelji na aproksimaciji pomikov. Taka metoda je zelo pogosto uporabljena. Poleg tega nekateri raziskovalci izberejo za neodvisne funkcije poljubno kombinacijo neodvisnih funkcij. Taki metodi pravimo mešana metoda. Obe metodi sta v določenih primerih podvrženi različnim numeričnim problemom oziroma blokiranju. Najbolj znano je strižno blokiranje v primeru Timoshenkovih nosilcev. V disertaciji se zato lotimo pristopa, ki ga predlaga Planinc (1998). V tem primeru se za neodvisne funkcije izbere deformacijske količine. Dobra lastnost tako razvitih končnih elementov je neobčutljivost na kakršnokoli blokiranje (strižno, membransko, itd) ter konsistentno upoštevanje ravnotežnih pogojev.

Izpeljava končnega elementa poteka v grobem takole. Funkcional (3.205) razširimo s kinematičnimi enačbami (3.143 – –3.145) v smislu problema vezanega ekstrema, poznanega v variacijskem računu. V ta namen jih najprej pomnožimo z Lagrangevimi množitelji $\mathcal{R}_1^i$, $\mathcal{R}_2^i$ ter $\mathcal{M}^i$. Tako pomnožene kinematične enačbe integriramo po referenčni osi kompozitnega nosilca. Dobljene izraze variiramo po vseh spremenljivkah. Integrale, ki jih dobimo $\int_0^L \mathcal{R}_1^i \delta u^{i\prime}\mathrm{d}x$, $\int_0^L \mathcal{R}_2^i w^{i\prime}\mathrm{d}x$ ter $\int_0^L \mathcal{M}^i \varphi^{i\prime}\mathrm{d}x$, integriramo po delih in prištejemo k principu virtualnega dela (3.205). Simbol $'$ pomeni odvod po vzdolžni koordinati. Razširjen princip virtualnega dela ima obliko

$$\begin{aligned}\delta W_r = &\sum_{i=1}^{N_{\mathrm{sl}}}\left(\int_0^L \Big((\mathcal{N}_c^i - \mathcal{R}_1^i)\,\delta\varepsilon^i + (\mathcal{Q}_c^i - \mathcal{R}_2^i)\,\delta\gamma^i + (\mathcal{M}_c^i - \mathcal{M}^i)\,\delta\kappa^i\Big)\mathrm{d}x\right) - \\ &- \sum_{i=1}^{N_{\mathrm{sl}}}\left(\int_0^L (\mathcal{R}_1^{i\prime} + p_X^i + q_{t,j-1} - q_{t,j})\delta u^i \mathrm{d}x\right) - \sum_{i=1}^{N_{\mathrm{sl}}}\left(\int_0^L (\mathcal{R}_2^{i\prime} + p_Z^i - q_{n,j-1} + q_{n,j})\delta w^i \mathrm{d}x\right) - \\ &- \sum_{i=1}^{N_{\mathrm{sl}}}\left(\int_0^L (\mathcal{M}^{i\prime} - \mathcal{R}_2^i + m_Y^i - z_j q_{t,j} + z_{j-1} q_{t,j-1})\delta\varphi^i \mathrm{d}x\right) - \sum_{i=1}^{N_{\mathrm{sl}}}\left(\int_0^L (u^{i\prime} - \varepsilon^i)\delta\mathcal{R}_1^i \mathrm{d}x\right) - \\ &- \sum_{i=1}^{N_{\mathrm{sl}}}\left(\int_0^L (w^{i\prime} + \varphi^i - \gamma^i)\delta\mathcal{R}_2^i \mathrm{d}x\right) - \sum_{i=1}^{N_{\mathrm{sl}}}\left(\int_0^L (\varphi^{i\prime} - \kappa^i)\delta\mathcal{M}^i \mathrm{d}x\right) - \\ &- \sum_{i=1}^{N_{\mathrm{sl}}}\Big(\Big(S_1^i + \mathcal{R}_1^i(0)\Big)\delta u_1^i - \Big(S_2^i + \mathcal{R}_2^i(0)\Big)\delta u_2^i - \Big(S_3^i + \mathcal{M}^i(0)\Big)\delta u_3^i\Big) - \\ &- \sum_{i=1}^{N_{\mathrm{sl}}}\Big(\Big(S_4^i - \mathcal{R}_1^i(L)\Big)\delta u_4^i - \Big(S_5^i - \mathcal{R}_2^i(L)\Big)\delta u_5^i - \Big(S_6^i - \mathcal{M}^i(L)\Big)\delta u_6^i\Big) = 0.\end{aligned} \tag{3.206}$$

Variacije $\delta\varepsilon^i, \delta\gamma^i, \delta\kappa^i, \delta u^i, \delta w^i, \delta\varphi^i$, $\delta\mathcal{R}_1^i, \delta\mathcal{R}_2^i, \delta\mathcal{M}^i$ so v funkcionalu (3.206) neodvisne funkcije. Podobno predstavljajo $\delta u_1^i, \delta u_2^i, \delta u_3^i, \delta u_4^i, \delta u_5^i, \delta u_6^i$ poljubne neodvisne diskretne vrednosti na robu elementa. Z upoštevanjem osnovnega pravila variacijskega računa, ki pravi, da so koeficienti pri poljubnih neodvisnih variacijah enaki nič, dobimo Euler-Lagrangeve enačbe kompozitnega nosilca:

$x \in [0, L]$, $i = j = 1, \ldots, N_{\mathrm{sl}}$:

konstitutivne enačbe:

$$f_1^i(\varepsilon^i, \kappa^i) = \mathcal{N}_c^i - \mathcal{R}_1^i = 0, \tag{3.207}$$

$$f_2^i(\gamma^i) = \mathcal{Q}_c^i - \mathcal{R}_2^i = 0, \tag{3.208}$$

$$f_3^i(\varepsilon^i, \kappa^i) = \mathcal{M}_c^i - \mathcal{M}^i = 0, \tag{3.209}$$

kinematične enačbe:

$$f_4^i(\varepsilon^i, u^{i\prime}) = u^{i\prime} - \varepsilon^i = 0, \tag{3.210}$$

$$f_5^i(\gamma^i, w^{i\prime}, \varphi^i) = w^{i\prime} + \varphi^i - \gamma^i = 0, \tag{3.211}$$

$$f_6^i(\kappa^i, \varphi^{i\prime}) = \varphi^{i\prime} - \kappa^i = 0, \tag{3.212}$$

ravnotežne enačbe:

$$f_7^i(\mathcal{R}_1^{i\prime}, \lambda) = \mathcal{R}_1^{i\prime} + p_X^i + q_{t,j-1} - q_{t,j} = 0, \tag{3.213}$$

$$f_8^i(\mathcal{R}_2^{i\prime}, q_{n,j}, q_{n,j-1}, \lambda) = \mathcal{R}_2^{i\prime} + p_Z^i - q_{n,j-1} + q_{n,j} = 0, \tag{3.214}$$

$$f_9^i(\mathcal{M}^{i\prime}, \mathcal{R}_2^i, \lambda) = \mathcal{M}^{i\prime} - \mathcal{R}_2^i + m_Y^i - z_j q_{t,j} + z_{j-1} q_{t,j-1} = 0, \tag{3.215}$$

ter pripadajoči naravni (statični) in bistveni (kinematični) robni pogoji:

$x = 0$:

$$S_1^i + \mathcal{R}_1^i(0) = 0 \qquad \text{ali} \qquad u^i(0) = u_1^i, \tag{3.216}$$

$$S_2^i + \mathcal{R}_2^i(0) = 0 \qquad \text{ali} \qquad w^i(0) = u_2^i, \tag{3.217}$$

$$S_3^i + \mathcal{M}^i(0) = 0 \qquad \text{ali} \qquad \varphi^i(0) = u_3^i, \tag{3.218}$$

$x = L$:

$$S_4^i - \mathcal{R}_1^i(L) = 0 \qquad \text{ali} \qquad u^i(L) = u_4^i, \tag{3.219}$$

$$S_5^i - \mathcal{R}_2^i(L) = 0 \qquad \text{ali} \qquad w^i(L) = u_5^i, \tag{3.220}$$

$$S_6^i - \mathcal{M}^i(L) = 0 \qquad \text{ali} \qquad \varphi^i(L) = u_6^i. \tag{3.221}$$

Napetostno in deformacijsko stanje kompozitnega nosilca poleg Euler-Lagrangevih enačb (3.207–3.221) sestavljajo tudi posplošene vezne enačbe (3.155–3.157), ki določajo pogoje povezanosti posameznih slojev v kompozitni nosilec:

$x \in [0, L]$, $i = j = 1, \ldots, N_{\mathrm{sl}} - 1$:

$$\Delta_j = u^i - u^{i+1} + z_j\Big(\varphi^i - \varphi^{i+1}\Big), \tag{3.222}$$

$$q_{t,j}(x) = \mathcal{H}_j(x, \Delta_j), \tag{3.223}$$

$$w^i = w^{i+1}. \tag{3.224}$$

Sistem Euler-Lagrangevih enačb kompozitnega nosilca (3.207–3.221) sestavlja skupaj s posplošenimi veznimi enačbami (3.222–3.224) pri izbrani referenčni obtežbi in obtežnem faktorju λ sistem $12N_{\mathrm{sl}} - 3$

enačb za določitev prav toliko neznank. Poleg neznanih funkcij $\varepsilon^i, \gamma^i, \kappa^i, u^i, w^i, \varphi^i, \mathcal{R}_1^i, \mathcal{R}_2^i, \mathcal{M}^i$ so neznanke tudi normalne kontaktne napetosti v stiku $q_{n,j}$, $(j = 1, \ldots, N_{\mathrm{sl}})$.

V nadaljevanju lahko sistem enačb (3.207–3.224) še nekoliko poenostavimo. Z upoštevanjem vezne enačbe (3.224) sledi, da velja tudi $\delta w = \delta w^i = \delta w^{i+1}$. Če to upoštevamo v razširjenem izreku o virtualnem delu (3.206), dobimo po krajši izpeljavi naslednji sistem modificiranih Euler-Lagrangevih enačb kompozitnega nosilca:

$x \in [0, L]$, $i = j = 1, \ldots, N_{\mathrm{sl}}$:

konstitutivne enačbe:

$$f_1^i(\varepsilon^i, \kappa^i) = \mathcal{N}_c^i - \mathcal{R}_1^i = 0, \tag{3.225}$$

$$f_2^i(\varepsilon^n, \kappa^n, \gamma^i) = \mathcal{Q}_c^i - \mathcal{R}_2 + \sum_{n \neq i}^{N_{\mathrm{sl}}} (\mathcal{M}_c^{n\prime} - m_Y^n + z_n q_{t,n} - z_{n-1} q_{t,n-1}) = 0, \tag{3.226}$$

$$f_3^i(\varepsilon^i, \kappa^i) = \mathcal{M}_c^i - \mathcal{M}^i = 0, \tag{3.227}$$

kinematične enačbe:

$$f_4^i(\varepsilon^i, u^{i\prime}) = u^{i\prime} - \varepsilon^i = 0, \tag{3.228}$$

$$f_5(\gamma^i, w', \varphi^i) = w' + \varphi^i - \gamma^i = 0, \tag{3.229}$$

$$f_6^i(\kappa^i, \varphi^{i\prime}) = \varphi^{i\prime} - \kappa^i = 0, \tag{3.230}$$

ravnotežne enačbe:

$$f_7^i(\mathcal{R}_1^{i\prime}, \lambda) = \mathcal{R}_1^{i\prime} + p_X^i + q_{t,j-1} - q_{t,j} = 0, \tag{3.231}$$

$$f_8(\mathcal{R}_2', \lambda) = \mathcal{R}_2' + \sum_{i=1}^{N_{\mathrm{sl}}} p_Z^i = 0, \tag{3.232}$$

$$f_9^i(\mathcal{M}^{i\prime}, \mathcal{Q}_c^i, \lambda) = \mathcal{M}^{i\prime} + \mathcal{Q}_c^i + m_Y^i - z_j q_{t,j} + z_{j-1} q_{t,j-1} = 0, \tag{3.233}$$

ter pripadajoči naravni (statični) in bistveni (kinematični) robni pogoji:

$x = 0$:

$$S_1^i + \mathcal{R}_1^i(0) = 0 \quad \text{ali} \quad u^i(0) = u_1^i, \tag{3.234}$$

$$\sum_{i=1}^{\mathrm{N_{sl}}} S_2^i + \mathcal{R}_2(0) = 0 \quad \text{ali} \quad w(0) = u_2, \tag{3.235}$$

$$S_3^i + \mathcal{M}^i(0) = 0 \quad \text{ali} \quad \varphi^i(0) = u_3^i, \tag{3.236}$$

$x = L$:

$$S_4^i - \mathcal{R}_1^i(L) = 0 \quad \text{ali} \quad u^i(L) = u_4^i, \tag{3.237}$$

$$\sum_{i=1}^{\mathrm{N_{sl}}} S_5^i - \mathcal{R}_2(L) = 0 \quad \text{ali} \quad w(L) = u_5, \tag{3.238}$$

$$S_6^i - \mathcal{M}^i(L) = 0 \quad \text{ali} \quad \varphi^i(L) = u_6^i. \tag{3.239}$$

Poleg modoficiranih Euler-Lagrangevih enačb (3.225–3.239) imamo seveda še vedno tudi posplošene vezne enačbe (3.240–3.242), ki določajo pogoje povezanosti posameznih slojev v kompozitni nosilec:

$x \in [0, L]$, $i = j = 1, \ldots, N_{\mathrm{sl}} - 1$:

$$\Delta_j = u^i - u^{i+1} + z_j \left(\varphi^i - \varphi^{i+1} \right), \tag{3.240}$$

$$q_{t,j}(x) = \mathcal{H}_j(x, \Delta_j), \tag{3.241}$$

$$w = w^i = w^{i+1}. \tag{3.242}$$

Z rešitvijo kinematičnih (3.228–3.230) ter ravnotežnih (3.231–3.233) enačb lahko izrazimo kinematične in ravnotežne spremenljivke samo z deformacijskimi količinami (glej Planinc (1998)). Na ta način postane funkcional razširjenega izreka o virtualnem delu (3.206) odvisen samo od deformacijskih količin $\varepsilon^i, \gamma^i, \kappa^i$ ter statičnih robnih vrednosti $\mathcal{R}_1^i(0), \mathcal{R}_2(0), \mathcal{M}^i(0), \mathcal{R}_1^i(L), \mathcal{R}_2(L)$ in $\mathcal{M}^i(L)$. Z rešenimi kinematičnimi enačbami lahko med seboj povežemo robne pomike in zasuke. Na ta način lahko nosilec geometrijsko umestimo v prostor (konstrukcijo). Če tako izražene kinematične enačbe prištejemo k razširjenemu funkcionalu virtualnega dela kompozitnega nosilca (3.206), dobimo tako imenovani modificirani izrek o virtualnem delu:

$$\begin{aligned}
\delta W^* = &\sum_{i=1}^{N_{\mathrm{sl}}} \left(\int_0^L \left((\mathcal{N}_c^i - \mathcal{R}_1^i)\, \delta\varepsilon^i + (\mathcal{M}_c^i - \mathcal{M}^i)\, \delta\kappa^i \right) \mathrm{d}x \right) - \sum_{i=1}^{N_{\mathrm{sl}}} \left(\left(\varphi^i(L) - \varphi^i(0) - \int_0^L \kappa^i \mathrm{d}x \right) \delta\mathcal{M}^i \right) - \\
&\sum_{i=1}^{N_{\mathrm{sl}}} \left(\int_0^L \left(\mathcal{Q}_c^i - \mathcal{R}_2 + \sum_{n \neq i}^{\mathrm{N_{sl}}} (\mathcal{M}_c^{n\prime} - m_Y^n + z_n q_{t,n} - z_{n-1} q_{t,n-1})\, \delta\gamma^i \right) \mathrm{d}x \right) - \\
&- \sum_{i=1}^{N_{\mathrm{sl}}} \left(\left(u^i(L) - u^i(0) - \int_0^L \varepsilon^i \mathrm{d}x \right) \delta\mathcal{R}_1^i \right) - \sum_{i=1}^{N_{\mathrm{sl}}} \left(\left(w(L) - w(0) - \int_0^L (\varphi^i - \gamma^i) \mathrm{d}x \right) \delta\mathcal{R}_2^i \right) - \\
&- \sum_{i=1}^{N_{\mathrm{sl}}} \left(\left(S_1^i + \mathcal{R}_1^i(0) \right) \delta u_1^i - \left(\sum_{i=1}^{N_{\mathrm{sl}}} S_2^i + \mathcal{R}_2(0) \right) \delta u_2 - \left(S_3^i + \mathcal{M}^i(0) \right) \delta u_3^i \right) - \\
&- \sum_{i=1}^{N_{\mathrm{sl}}} \left(\left(S_4^i - \mathcal{R}_1^i(L) \right) \delta u_4^i - \left(\sum_{i=1}^{\mathrm{N_{sl}}} S_5^i - \mathcal{R}_2(L) \right) \delta u_5 - \left(S_6^i - \mathcal{M}^i(L) \right) \delta u_6^i \right) = 0.
\end{aligned} \tag{3.243}$$

Značilnost funkcionala δW^* (3.243) je, da v njem kot edine neznane funkcije nastopajo le deformacijske količine $\varepsilon^i, \gamma^i, \kappa^i$. Vse ostale spremenljivke nastopajo v funkcionalu le s svojimi robnimi vrednostmi.

3.3.2.3 Galerkinova metoda končnih elementov

Ker v variacijskem problemu, ki je formuliran s funkcionalom modificiranega virtualnega dela δW^* (3.243), kot osnovne neznane funkcije nastopajo le deformacijske količine, si pri reševanju pomagamo z aproksimacijo deformacij in njihovih variacij. Kompozitni nosilec začetne dolžine L razdelimo v splošnem na $N_\varepsilon^i - 1$, $N_\gamma^i - 1$ in $N_\kappa^i - 1$ različno dolgih odsekov. To storimo z izbiro N_ε^i,N_γ^i oziroma N_κ^i v splošnem poljubno razporejenih točk. Pri izpeljavi predpostavimo, da je število točk v vsakem sloju enako, tj, $N_\varepsilon = N_\varepsilon^i$, $N_\gamma = N_\gamma^i$ in $N_\kappa = N_\kappa^i$. Neznane funkcije $\varepsilon^i, \gamma^i, \kappa^i$ aproksimiramo z Lagrangevimi polinomi $P_{n_\varepsilon}(x)\,(n_\varepsilon = 1, \ldots, N_\varepsilon)$, $P_{n_\gamma}(x)\,(n_\gamma = 1, \ldots, N_\gamma)$, $P_{n_\kappa}(x)\,(n_\kappa = 1, \ldots, N_\kappa)$. Variacije neznanih funkcij $\delta\varepsilon^i, \delta\gamma^i, \delta\kappa^i$ lahko aproksimiramo z enakimi ali različnimi interpolacijskimi nastavki kot neznane funkcije. V nalogi izberemo za aproksimacijo variacij znano Dirac δ-funkcijo (Reddy, 1986). Metoda končnih elementov, ki temelji na aproksimaciji tako izbranih interpolacijskih nastavkov se imenuje Petrov-Galerkinova kolokacijska metoda končnih elementov. Tudi izbira kolokacijskih točk je v splošnem poljubna. Odločimo se, da sta lega in število kolokacijskih točk enaka točkam skozi katere potekajo Lagrangevi polinomi. Interpolacijski nastavki neznanih funkcij in njihovih variacij so tako naslednji:

$$\varepsilon^i(x) \approx \sum_{n=1}^{N_\varepsilon} P_{n_\varepsilon}(x)\, \varepsilon_n^i, \qquad \delta\varepsilon^i(x) \approx \delta(x - x_i), \tag{3.244}$$

$$\gamma^i(x) \approx \sum_{n=1}^{N_\gamma} P_{n_\gamma}(x)\,\gamma_n^i, \qquad \delta\gamma^i(x) \approx \delta(x-x_i), \tag{3.245}$$

$$\kappa^i(x) \approx \sum_{n=1}^{N_\kappa} P_{n_\kappa}(x)\,\kappa_n^i, \qquad \delta\kappa^i(x) \approx \delta(x-x_i), \tag{3.246}$$

Diskretne vrednosti $\varepsilon_n^i, \gamma_n^i, \kappa_n^i$ predstavljajo vrednosti interpoliranih neznanih funkcij v izbranih interpolacijskih točkah; x_i pa je lega kolokacijske točke. Z vstavitvijo interpolacijskih nastavkov (3.244–3.246) v (3.243) in upoštevanjem osnovne leme variacijskega računa dobimo sistem diskretnih posplošenih ravnotežnih enačb končnega elementa kompozitnega nosilca v naslednji obliki

$$f_{(i-1)N_\varepsilon+n_\varepsilon} = \left(\mathcal{N}_c^i - \mathcal{R}_1^i\right)\Big|_{x=x_{n_\varepsilon}} = 0 \qquad n_\varepsilon = 1,\ldots,N_\varepsilon \tag{3.247}$$

$$f_{N_{\mathrm{sl}}N_\varepsilon+(i-1)N_\gamma+n_\gamma} = \left(\mathcal{Q}_c^i - \mathcal{R}_2 + \sum_{n\neq i}^{N_{\mathrm{sl}}} (\mathcal{M}_c^{n\prime} - m_Y^n + z_n q_{t,n} - z_{n-1} q_{t,n-1})\right)\Big|_{x=x_{n_\gamma}} = 0 \qquad n_\gamma = 1,\ldots,N_\gamma \tag{3.248}$$

$$f_{N_{\mathrm{sl}}(N_\varepsilon+N_\gamma)+(i-1)N_\kappa+n_\kappa} = \left(\mathcal{M}_c^i - \mathcal{M}^i\right)\Big|_{x=x_{n_\kappa}} = 0 \qquad n_\kappa = 1,\ldots,N_\kappa \tag{3.249}$$

$$f_{N_{\mathrm{sl}}(N_\varepsilon+N_\gamma+N_\kappa)+i} = u^i(L) - u^i(0) - \sum_{n=1}^{N_\varepsilon} P_{n_\varepsilon}^*(x)\,\varepsilon_n^i = 0 \tag{3.250}$$

$$f_{N_{\mathrm{sl}}(N_\varepsilon+N_\gamma+N_\kappa+1)+1} = w(L) - w(0) + \varphi^i(0)L + \sum_{n=1}^{N_\kappa} P_{n_\kappa}^{**}(x)\,\kappa_n^i - \sum_{n=1}^{N_\gamma} P_{n_\gamma}^*(x)\,\gamma_n^i = 0 \tag{3.251}$$

$$f_{N_{\mathrm{sl}}(N_\varepsilon+N_\gamma+N_\kappa+1)+1+i} = \varphi^i(L) - \varphi^i(0) - \sum_{n=1}^{N_\kappa} P_{n_\kappa}^*(x)\,\kappa_n^i = 0 \tag{3.252}$$

$$f_{N_{\mathrm{sl}}(N_\varepsilon+N_\gamma+N_\kappa+2)+1+i} = S_1^i + \mathcal{R}_1^i(0) = 0 \tag{3.253}$$

$$f_{N_{\mathrm{sl}}(N_\varepsilon+N_\gamma+N_\kappa+3)+2} = \sum_{i=1}^{N_{\mathrm{sl}}} S_2^i + \mathcal{R}_2(0) = 0 \tag{3.254}$$

$$f_{N_{\mathrm{sl}}(N_\varepsilon+N_\gamma+N_\kappa+3)+2+i} = S_3^i + \mathcal{M}^i(0) = 0 \tag{3.255}$$

$$f_{N_{\mathrm{sl}}(N_\varepsilon+N_\gamma+N_\kappa+4)+2+i} = S_4^i - \mathcal{R}_1^i(0) + \int_0^L (p_X^i + q_{t,j-1} - q_{t,j})\mathrm{d}x = 0 \tag{3.256}$$

$$f_{N_{\mathrm{sl}}(N_\varepsilon+N_\gamma+N_\kappa+5)+3} = \sum_{i=1}^{N_{\mathrm{sl}}} S_5^i - \mathcal{R}_2(0) + \int_0^L p_Z^i \mathrm{d}x = 0 \tag{3.257}$$

$$f_{N_{\mathrm{sl}}(N_\varepsilon+N_\gamma+N_\kappa+5)+3+i} = S_6^i - \mathcal{M}^i(0) - \int_0^L (\mathcal{Q}_c^i + m_Y^i - z_j q_{t,j} + z_{j-1} q_{t,j-1})\mathrm{d}x = 0 \tag{3.258}$$

kjer so

$$P^{**}_{n_\kappa}(x) = \int_0^L \Big(\int_0^L P_{n_\kappa}(\xi)\mathrm{d}\xi \Big)\mathrm{d}\xi \qquad P^{*}_{n_\kappa}(x) = \int_0^L P_{n_\kappa}(\xi)\mathrm{d}\xi, \ \text{itd.} \tag{3.259}$$

Sistem posplošenih diskretnih ravnotežnih enačb (3.247–3.258) predstavlja pri dani zunanji obtežbi sistem $N_{\mathrm{sl}}(N_\varepsilon + N_\gamma + N_\kappa + 6) + 3$ algebrajskih enačb za $N_{\mathrm{sl}}(N_\varepsilon + N_\gamma + N_\kappa + 6) + 3$ neznank. Med neznankami je $N_{\mathrm{sl}}(N_\varepsilon + N_\gamma + N_\kappa + 2) + 1$ notranjih prostostnih stopenj $\varepsilon^i, \gamma^i, \kappa^i, \mathcal{R}_1^i(0), \mathcal{R}_2(0), \mathcal{M}^i(0)$, in $4N_{\mathrm{sl}}+2$ zunanjih prostostnih stopenj končnega elementa $u^i(0), w(0), \varphi^i(0), u^i(L), w(L), \varphi^i(L)$. Integrale v enačbah (3.256–3.258) izvrednotimo z numerično integracijo. V nadaljevanju notranje prostostne stopnje $\varepsilon^i, \gamma^i, \kappa^i, \mathcal{R}_1^i(0), \mathcal{R}_2(0), \mathcal{M}^i(0)$ kondenziramo s postopkom numerične kondenzacije na nivoju elementa, zunanje prostostne stopnje $u^i(0), w(0), \varphi^i(0), u^i(L), w(L), \varphi^i(L)$ pa združimo v enačbo konstrukcije (Zienkiewicz in Taylor, 1991)

$$\boldsymbol{G}(\boldsymbol{x}, \boldsymbol{\lambda}) = \boldsymbol{R}(\boldsymbol{x}) - \boldsymbol{P}(\boldsymbol{\lambda}) = \boldsymbol{0}. \tag{3.260}$$

Vektor $\boldsymbol{x}$ je vektor posplošenih pomikov oziroma vektor vozliščnih (robnih) pomikov in zasukov končnih elementov. $\boldsymbol{\lambda}$ je vektor obtežnih faktorjev konstrukcije.

3.3.3 Osnovne enačbe kompozitnega nosilca pri času t^{s+1}

V tem poglavju prikažemo enačbe, ki jih potrebujemo za določitev napetostnega in deformacijskega stanja kompozitnih konstrukcij pri hkratnem delovanju zunanje statične in požarne obtežbe. Mehanski odziv kompozitnega nosilca pri časovno spreminjajoči vlažnostno-temperaturni obremenitvi bomo določili z uporabo končnega elementa kompozitnega nosilca, ki smo ga izpeljali v poglavju Diskretizacija in Metoda končnih elementov. Celotni časovni interval v katerem analiziramo odziv konstrukcije $[t_{\mathrm{zac}}, t_{kon}]$, razdelimo na časovne podintervale $[t^s, t^{s+1}]$. Odziv konstrukcije pri času t^{s+1} izračunamo s posplošenimi ravnotežnimi enačbami (3.247–3.258), ki jih zaradi časovne odvisnosti pišemo v inkrementni obliki na naslednji način

$$f^{s+1}_{(i-1)N_\varepsilon + n_\varepsilon} = \Big(\mathcal{N}_c^{i,s+1} - \mathcal{R}_1^{i,s+1} \Big)\Big|_{x=x_{n_\varepsilon}} = 0, \qquad n_\varepsilon = 1, \ldots, N_\varepsilon, \tag{3.261}$$

$$f^{s+1}_{N_{\mathrm{sl}}N_\varepsilon + (i-1)N_\gamma + n_\gamma} = \Big(\mathcal{Q}_c^{i,s+1} - \mathcal{R}_2^{s+1} + \sum_{n\neq i}^{\mathrm{N_{sl}}} (\mathcal{M}_c^{n\prime,s+1} - m_Y^{n,s+1} + z_n q_{t,n}^{s+1} - z_{n-1} q_{t,n-1}^{s+1}) \Big)\Big|_{x=x_{n_\gamma}} = 0, \quad n_\gamma = 1, \ldots, N_\gamma, \tag{3.262}$$

$$f^{s+1}_{N_{\mathrm{sl}}(N_\varepsilon+N_\gamma) + (i-1)N_\kappa + n_\kappa} = \Big(\mathcal{M}_c^{i,s+1} - \mathcal{M}^{i,s+1} \Big)\Big|_{x=x_{n_\kappa}} = 0, \qquad n_\kappa = 1, \ldots, N_\kappa, \tag{3.263}$$

$$f^{s+1}_{N_{\mathrm{sl}}(N_\varepsilon+N_\gamma+N_\kappa)+i} = u^{i,s+1}(L) - u^{i,s+1}(0) - \sum_{n=1}^{N_\varepsilon} P^*_{n_\varepsilon}(x)\, \varepsilon_n^{i,s+1} = 0, \tag{3.264}$$

$$f^{s+1}_{N_{\mathrm{sl}}(N_\varepsilon+N_\gamma+N_\kappa+1)+1} = w^{s+1}(L) - w^{s+1}(0) + \varphi^{i,s+1}(0)L + \sum_{n=1}^{N_\kappa} P^{**}_{n_\kappa}(x)\, \kappa_n^{i,s+1} - \sum_{n=1}^{N_\gamma} P^*_{n_\gamma}(x)\, \gamma_n^{i,s+1} = 0, \tag{3.265}$$

$$f^{s+1}_{N_{\mathrm{sl}}(N_\varepsilon+N_\gamma+N_\kappa+1)+1+i} = \varphi^{i,s+1}(L) - \varphi^{i,s+1}(0) - \sum_{n=1}^{N_\kappa} P^*_{n_\kappa}(x)\, \kappa_n^{s+1} = 0, \tag{3.266}$$

$$f^{s+1}_{N_{\mathrm{sl}}(N_\varepsilon+N_\gamma+N_\kappa+2)+1+i} = S_1^{i,s+1} + \mathcal{R}_1^{i,s+1}(0) = 0, \tag{3.267}$$

$$f^{s+1}_{N_{\mathrm{sl}}(N_\varepsilon+N_\gamma+N_\kappa+3)+2} = \sum_{i=1}^{N_{\mathrm{sl}}} S_2^{i,s+1} + \mathcal{R}_2^{s+1}(0) = 0, \tag{3.268}$$

$$f^{s+1}_{N_{\mathrm{sl}}(N_\varepsilon+N_\gamma+N_\kappa+3)+2+i} = S_3^{i,s+1} + \mathcal{M}^{i,s+1}(0) = 0, \tag{3.269}$$

$$f^{s+1}_{N_{\mathrm{sl}}(N_\varepsilon+N_\gamma+N_\kappa+4)+2+i} = S_4^{i,s+1} - \mathcal{R}_1^{i,s+1}(0) + \int_0^L (p_X^{i,s+1} + q_{t,j-1}^{s+1} - q_{t,j}^{s+1})\mathrm{d}x = 0, \tag{3.270}$$

$$f^{s+1}_{N_{\mathrm{sl}}(N_\varepsilon+N_\gamma+N_\kappa+5)+3} = \sum_{i=1}^{N_{\mathrm{sl}}} S_5^{i,s+1} - \mathcal{R}_2^{s+1}(0) + \int_0^L p_Z^{i,s+1}\mathrm{d}x = 0, \tag{3.271}$$

$$f^{s+1}_{N_{\mathrm{sl}}(N_\varepsilon+N_\gamma+N_\kappa+5)+3+i} = S_6^{i,s+1} - \mathcal{M}^{i,s+1}(0) - \int_0^L (\mathcal{Q}_c^{i,s+1} + m_Y^{i,s+1} - z_j q_{t,j}^{s+1} + z_{j-1} q_{t,j-1}^{s+1})\mathrm{d}x = 0, \tag{3.272}$$

Sistem posplošenih diskretnih ravnotežnih enačb (3.261–3.272) predstavlja pri dani zunanji obtežbi sistem $N_{\mathrm{sl}}(N_\varepsilon + N_\gamma + N_\kappa + 6) + 3$ algebrajskih enačb za $N_{\mathrm{sl}}(N_\varepsilon + N_\gamma + N_\kappa + 6) + 3$ neznank. Med neznankami je $N_{\mathrm{sl}}(N_\varepsilon + N_\gamma + N_\kappa + 2) + 1$ notranjih prostostnih stopenj $\varepsilon^{i,s+1}, \gamma^{i,s+1}, \kappa^{i,s+1}, \mathcal{R}_1^{i,s+1}(0)$, $\mathcal{R}_2^{s+1}(0), \mathcal{M}^{i,s+1}(0)$ in $4N_{\mathrm{sl}} + 2$ zunanjih prostostnih stopenj končnega elementa $u^{i,s+1}(0), w^{s+1}(0)$, $\varphi^{i,s+1}(0), u^{i,s+1}(L), w^{s+1}(L), \varphi^{i,s+1}(L)$. Integrale v enačbah (3.270–3.272) izvrednotimo z numerično integracijo. V nadaljevanju notranje prostostne stopnje $\varepsilon^{i,s+1}$, $\gamma^{i,s+1}$, $\kappa^{i,s+1}$, $\mathcal{R}_1^{i,s+1}(0)$, $\mathcal{R}_2^{s+1}(0)$, $\mathcal{M}^{i,s+1}(0)$ kondenziramo s postopkom numerične kondenzacije na nivoju elementa, zunanje prostostne stopnje $u^{i,s+1}(0), w^{s+1}(0), \varphi^{i,s+1}(0), u^{i,s+1}(L), w^{s+1}(L), \varphi^{i,s+1}(L)$ pa združimo v enačbo konstrukcije (Zienkiewicz in Taylor, 1991)

$$\boldsymbol{G}(\boldsymbol{x}^{s+1}, \boldsymbol{\lambda}^{s+1}, T^{s+1}, w^{s+1}, t^{s+1}) = \boldsymbol{0}. \tag{3.273}$$

Vektor $\boldsymbol{x}^{s+1}$ je vektor posplošenih pomikov oziroma vektor vozliščnih (robnih) pomikov in zasukov končnih elementov pri času t^{s+1}. $\boldsymbol{\lambda}^{s+1}$ je vektor obtežnih faktorjev konstrukcije pri času t^{s+1}. T^{s+1} in w^{s+1} pa sta temperaturno polje in polje vlažnosti po elementu pri času t^{s+1}.

3.3.4 Mehanske lastnosti lesa pri visokih temperaturah

Če hočemo določiti mehanski odziv slojevitih kompozitnih nosilcev pri hkratnem delovanju statične mehanske obtežbe in obtežbe požara moramo poznati mehanske lastnosti lesa pri visokih temperaturah. Mehanske lastnosti lesa so odvisne od temperature, vsebnosti vlage, hitrosti oglenenja in orientacije materialnih vlaken. Znano je, da se mehanske lastnosti (togost in trdnost) lesa z višanjem temperature slabšajo (zmanjšujejo). Z višanjem temperature del vode izpareva, medtem ko ostala voda prodira v notranjost prereza. Zvišanje vsebnosti vlage notranjega dela prereza zmanjšuje trdnost in togost lesa. Podobno oglenenje lesa zmanjšuje velikost prečnega prereza in s tem hitrejšo porušitev elementa. Običajno je trdnost lesa pri temperaturi vnetišča zanemarljiva. Les je ortotropen material, zato je upoštevanje orientacije materialnih vlaken pomembno. Trdnost in togost lesa v vzdolžni prečni smeri sta različna.

V nadaljevanju prikažemo modul elastičnosti v smeri materialnih vlaken v odvisnosti od temperature lesa, kot ga predlagajo različni avtorji, (glej sliko 3.27). V vseh primerih se modul elastičnosti z višanjem

temperature zmanjšuje. Največje zmanjšanje elastičnega modula predvideva Evrokod 5 (2004). Pri $T = 100°\mathrm{C}$ predvidi zmanjšanje elastičnega modula za od $50 - 60\%$, medtem ko je pri $T = 300°\mathrm{C}$ enak nič. V primeru lesa začetne vlažnosti $0 - 12\%$, Preusser poroča, da se elastični modul počasi manjša do $T \approx 180 - 200°\mathrm{C}$, medtem ko je nad to temperaturo padec elastičnega modula hitrejši. Schaffer in Nyman predvidevata linearno zmanjševanje elastičnega modula do temperature oglenenja $T = 300°\mathrm{C}$ in drastičen padec elastičnega modula nad to temperaturo.

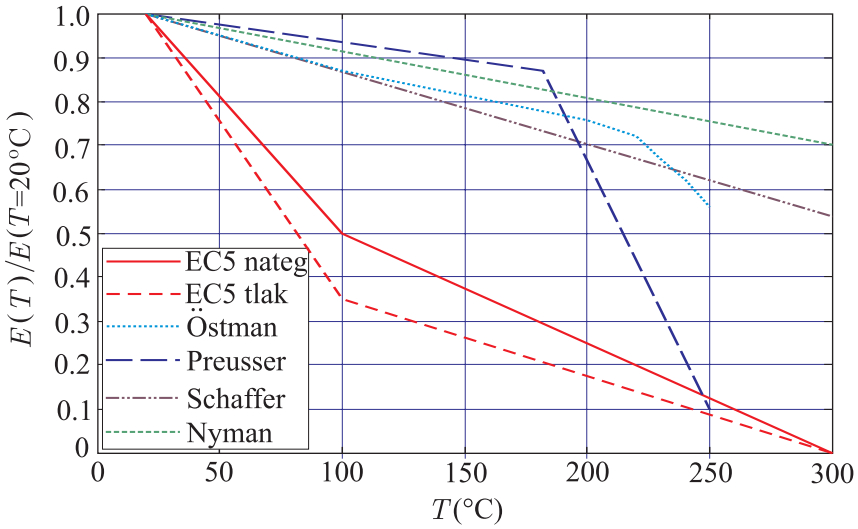

Slika 3.27: Reducirani elastični modul lesa $\dfrac{E(T)}{E(T = 20°\mathrm{C})}$ v odvisnosti od temperature T.

Figure 3.27: Mechanical properties (a reduced modulus of elasticity $\dfrac{E(T)}{E(T = 20°\mathrm{C})}$) at elevated temperatures of the two-layer beam proposed by various researchers.

3.3.5 Računski primeri

Z računskimi primeri prikažemo učinkovitost v disertaciji predstavljenega računskega postopka za določitev napetostnega in deformacijskega stanja slojevitih kompozitnih nosilcev z upoštevanjem delne povezanosti slojev in oglenenja pri sočasnem delovanju statične obtežbe in požara. Računske primere razdelimo v dve skupini.

V prvi skupini obravnavamo dvoslojni Timoshenkov nosilec z upoštevanjem strižne deformacije prereza pri stacionarnem stanju temperature in vlage. Najprej analiziramo točnost, učinkovitost ter konvergenco razvitih končnih elementov za določitev mehanskega stanja slojevitih kompozitnih nosilcev. Numerične rešitve, ki jih dobimo z izbiro različnih tipov in števila končnih elementov, primerjamo z rezultati točne rešitve obravnavanega kompozitnega nosilca. Poleg točnosti in konvergence pokažemo, da so predlagani končni elementi odporni na različne vrste blokiranja. S tem potrdimo, da so razviti končni elementi primerni za analizo mehanskega stanja slojevitih kompozitnih nosilcev z upoštevanjem strižne deformacije prereza in zdrsa med sloji.

V drugi skupini obravnavamo dvoslojni kompozitni nosilec, ki je poleg zunanje statične obtežbe obremenjen tudi s standardno požarno obtežbo. Mehanski odziv kompozitnega nosilca na časovno spreminjajočo požarno obtežbo določimo z uporabo v disertaciji razvitih končnih elementov. Poleg tega analiziramo vpliv oglenenja lesa na časovni razvoj izbranih kinematičnih količin. Z upoštevanjem pogoja,

ki določa požarno odpornost nosilcev, določimo predviden čas do porušitve konstrukcije. Na ta način prikažemo uporabnost predlaganega matematičnega modela za določitev mehanskega odziva (požarne odpornosti) slojevitih kompozitnih nosilcev pri hkratnem delovanju zunanje statične obtežbe in požara ter upoštevanjem delne povezanosti med sloji ter oglenenja lesa.

3.3.5.1 Slojevit nosilec z upoštevanjem strižne deformacije prereza

V tem računskem primeru prikažemo uporabo izpeljane družine končnih elementov za določitev mehanskega stanja kompozitnih nosilcev z upoštevanjem zdrsa med sloji in strižne deformacije prečnega prereza. Pri tem predpostavimo, da je kompozitni nosilec obremenjen s statično obtežbo in da se nahaja v okolju s stalno temperaturo in vlažnostjo. Zaradi stacionarnosti temperaturnega in vlažnostnega stanja lahko za določitev mehanskega obnašanja kompozitnega nosilca uporabimo posplošene diskretne ravnotežne enačbe (3.247–3.258).

Obravnavamo dva preprosta a nazorna računska primera:

- prostoležeči dvoslojni Timoshenkov kompozitni nosilec dolžine L,
- kontinuirni Timoshenkov kompozitni nosilec preko dveh polj.

V obeh primerih sta nosilca obremenjena s konzervativno zvezno linijsko obtežbo p_Z. Geometrijski in materialni podatki ter podatki o obtežbi so prikazani na slikah 3.28 in 3.32. Prečni prerezi posameznih slojev so v vseh primerih pravokotni. Ker upoštevamo konstantno strižno deformacijo moremo uporabiti Cowper-jev korekcijski faktor k_S, ki je v primeru pravokotnega prečnega prereza enak $5/6$, (Cowper, 1966).

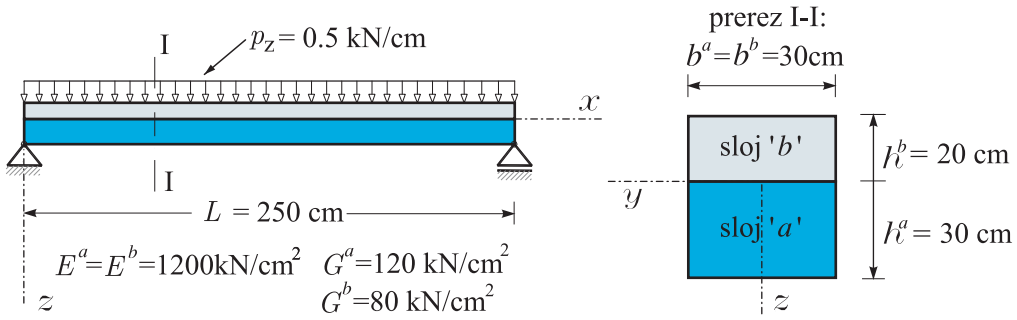

Slika 3.28: Geometrijski in materialni podatki ter podatki o obtežbi dvoslojnega prostoležečega Timoshenkovega kompozitnega nosilca.

Figure 3.28: The descriptive geometric, material and loading data of the simply supported two-layer Timoshenko composite beam.

Točnost, učinkovitost ter konvergenco razvitih končnih elementov smo preverili tako, da smo z uporabo različnih tipov (različna stopnja interpolacije) končnih elementov izračunali navpične pomike na sredini razpona $w(L/2)$ in zdrse med sloji na robu nosilca $\Delta(0)$, ter jih primerjali s točno rešitvijo. Za točno rešitev smo izbrali rešitev, ki jo dobimo z uporabo 1000 elementov E_0. Z E_0 smo označili končni element, pri katerem vse neznane funkcije aproksimiramo s konstantnim interpolacijskim nastavkom. Na ta način smo analizirali vpliv stopnje interpolacijskih polinomov (Lagrangevi interpolacijski polinomi), števila končnih elementov ter pozicijo izbranih kolokacijskih točk $\{x_1, x_2, \ldots, x_n\}$ na približno numerično rešitev dvoslojnega Timoshenkovega kompozitnega nosilca.

Lega kolokacijskih točk je v splošnem poljubna. Odločili smo se, da v nalogi analiziramo vpliv lege kolokacijskih točk, ki so po elementu porazdeljene ekvidistantno (E), po Lobattu (L), Gaussu (G) in Chebyshevu (C). Za tako izbrane kolokacijske točke smo za različno število končnih elementov in različne stopenje interpolacijskih polinomov izračunali $w(L/2)$, $\Delta(0)$ in razliko med ravnotežnim $\mathcal{M}^a$ in konstitucijskim upogibnim momentom $\mathcal{M}_c^a$. Velikost razlike med $\mathcal{M}^a$ in $\mathcal{M}_c^a$ kontroliramo preko norme L_2 njune razlike, tj. $||\mathcal{M}_c - \mathcal{M}||_2$. Način in stopnjo numerične integracije smo vselej izbrali tako, da je bila integracija točna. To je tudi razlog, da nismo analizirali tudi vpliva stopnje integracije na izbrane rezultate. Rezultati so prikazani v preglednicah 3.8–3.11.

Preglednica 3.8: Primerjava numeričnih rezultatov s točno rešitvijo. Kompozitni nosilec smo analizirali z enim končnim elementom E_1, E_2, E_3, E_4 in E_5.

Table 3.8: The comparison of numerical results for one element E_1, E_2, E_3, E_4 and E_5 with the exact solution.

n_e	d.o.i.	tip elementa	$w^a(L/2)$	$\Delta(0)$	$\|\mathcal{M}_{\mathrm{C}}^a - \mathcal{M}^a\|_2$
1	0	E/L/G/C	0.290 643	0.116 257	$1.78210 \cdot 10^{4}$
1	1	E/L	0.033 613	0.002 988	$2.83842 \cdot 10^{4}$
		G	0.225 855	0.079 659	$1.18826 \cdot 10^{4}$
		C	0.178 063	0.060 640	$1.34222 \cdot 10^{4}$
1	2	E/L	0.270 938	0.077 249	$1.93548 \cdot 10^{-10}$
		G	0.270 972	0.077 287	$4.32163 \cdot 10^{-10}$
		C	0.270 959	0.077 273	$3.18158 \cdot 10^{-10}$
1	3	E	0.270 988	0.077 271	$3.56716 \cdot 10^{-10}$
		L	0.271 028	0.077 289	$2.29257 \cdot 10^{-10}$
		G	0.270 996	0.077 288	$3.25371 \cdot 10^{-10}$
		C	0.271 005	0.077 286	$3.31368 \cdot 10^{-10}$
1	4	E	0.270 993	**0.077 293**	$1.87862 \cdot 10^{-10}$
		L	0.270 993	**0.077 293**	$2.89523 \cdot 10^{-10}$
		G	0.270 993	**0.077 293**	$2.34103 \cdot 10^{-10}$
		C	0.270 993	0.077 540	$3.30434 \cdot 10^{-10}$
1	5	E	**0.271 026**	**0.077 293**	$1.42962 \cdot 10^{-10}$
		L	**0.271 026**	**0.077 293**	$2.29257 \cdot 10^{-10}$
		G	**0.271 026**	**0.077 293**	$1.23514 \cdot 10^{-10}$
		C	**0.271 026**	**0.077 293**	$2.82211 \cdot 10^{-10}$
Točna rešitev			**0.271 026**	**0.077 293**	**0**

n_e–število elementov, d.o.i.–stopnja interpolacije
E–ekvidistantno, L–Lobatto, G–Gauss, C–Chebyshev

Dvoslojni prostoležeči Timoshenkov nosilec smo modelirali z $1, 2, 4, 8, 10, 20, 50, 100$ in 1000 končnimi elementi različnih stopenj $(1, 2, \ldots, 5)$ interpolacijskih polinomov . Označili smo jih z $E_0, E_1, E_2, \ldots$, E_5. Pri uporabi le enega elementa E_0 ali E_1 je napaka izračunanih $w(L/2)$ in $\Delta(0)$ precejšnja. Z večanjem števila elementov se napaka manjša, toda konvergenca k točni rešitvi je kljub temu relativno počasna.

Z večanjem stopnje interpolacijskih polinomov je napaka manjša in hitrost konvergence večja. Iz preglednic 3.8–3.11 je razvidno, da je za točnost rezultatov na 6 decimalnih mest potrebno uporabiti: 2 elementa E_4, 4 elemente E_3, 8 ali 10 elementov E_2, 1000 elementov E_0 ali na drugi strani samo 1 element E_5.

Preglednica 3.9: Primerjava numeričnih rezultatov s točno rešitvijo. Kompozitni nosilec smo analizirali z dvema končnima elementoma E_0, E_1, E_2, E_3 in E_4 in štirimi končnimi elementi E_0 in E_1.

Table 3.9: The comparison of numerical results for two and four elements E_0, E_1, E_2, E_3 and E_4 with the exact solution.

n_e	d.o.i.	tip elementa	$w^a(L/2)$	$\Delta(0)$	$\|\mathcal{M}_C - \mathcal{M}\|_2$
2	0	E/L/G/C	0.246 928	0.086 513	$1.72959 \cdot 10^4$
2	1	E/L	0.215 860	0.060 491	$1.00353 \cdot 10^4$
		G	0.263 520	0.079 511	$4.20113 \cdot 10^3$
		C	0.251 622	0.074 765	$4.74548 \cdot 10^3$
2	2	E/L	0.271 029	0.077 288	$2.87028 \cdot 10^{-10}$
		G	0.271 014	0.077 290	$2.31795 \cdot 10^{-10}$
		C	0.271 020	0.077 290	$4.21815 \cdot 10^{-10}$
2	3	E	0.271 031	0.077 290	$4.54423 \cdot 10^{-10}$
		L	0.271 033	0.077 291	$3.35126 \cdot 10^{-10}$
		G	0.271 034	0.077 291	$3.24815 \cdot 10^{-10}$
		C	0.271 033	0.077 291	$2.86409 \cdot 10^{-10}$
2	4	E	**0.271 026**	**0.077 293**	$3.96382 \cdot 10^{-10}$
		L	**0.271 026**	**0.077 293**	$5.54296 \cdot 10^{-10}$
		G	**0.271 026**	**0.077 293**	$4.08983 \cdot 10^{-10}$
		C	**0.271 026**	**0.077 293**	$6.22722 \cdot 10^{-10}$
4	0	E/L/G/C	0.264 388	0.079 038	$1.2927 \cdot 10^4$
4	1	E/L	0.251 631	0.074 756	$3.54803 \cdot 10^3$
		G	0.263 518	0.079 501	$1.48532 \cdot 10^3$
		C	0.260 547	0.078 315	$1.67778 \cdot 10^3$
Točna rešitev			**0.271 026**	**0.077 293**	**0**

n_e–število elementov, d.o.i.–stopnja interpolacije
E–ekvidistantno, L–Lobatto, G–Gauss, C–Chebyshev

Različna izbira pozicije in vrste kolokacijskih točk pokaže, da so rezultati za različne izbire zelo podobni. Rezultati pri različnih izbirah lege kolokacijskih točk so praktično enaki za elemente E_2-E_5, medtem ko se razlikujejo za elemente E_1. Pri izbiri zadnjih, se uporaba Gaussove sheme kolokacijskih točk izkaže za najprimernejšo. Iz preglednic 3.8–3.11 je razvidno, da se norma $||\mathcal{M}_c - \mathcal{M}||_2$ z večanjem števila elementov in stopnje interpolacijskih funkcij enakomerno zmanjšuje. Zaključimo lahko, da je numerična rešitev dvoslojnega Timoshenkovega kompozitnega nosilca, dobljena z uporabo predstavljene družine končnih elementov, konvergentna k točni rešitvi.

Naslednja dobra lastnost predstavljene družine končnih elementov je, da so povsem odporni na vse vrste blokiranja. Znano je, da je pomanjklivost nekaterih končnih elementov tako imenovano blokiranje (ang. locking). Znani primeri blokiranja so strižno blokiranje v primeru homogenih Timoshenkovih nosilcev, membransko blokiranje v primeru ukrivljenih nosilcev, itd. V primeru kompozitnih nosilcev je najbolj znano blokiranje zdrsa med sloji. Blokiranje zdrsa je posebej izrazito, kadar je togost stika zelo velika. Dall'Asta in Zona (2004a, 2004b) poročata, da se v primeru velikih togosti stika pojavijo oscilacije zdrsov.

Preglednica 3.10: Primerjava numeričnih rezultatov s točno rešitvijo. Kompozitni nosilec smo analizirali s štirimi končnimi elementi E_2 in E_3 ter osmimi in destimi končnimi elementi E_0, E_1 in E_2.

Table 3.10: The comparison of numerical results for four elements E_2 and E_3 and eight and ten elements E_0, E_1 in E_2 with the exact solution.

n_e	d.o.i.	tip elementa	$w^a(L/2)$	$\Delta(0)$	$\|\mathcal{M}_C - \mathcal{M}\|_2$
4	2	E/L	0.271 023	0.077 291	$5.11367 \cdot 10^{-10}$
		G	0.271 021	0.077 291	$7.05474 \cdot 10^{-10}$
		C	0.271 022	0.077 291	$6.60154 \cdot 10^{-10}$
4	3	E	**0.271 026**	**0.077 293**	$1.03876 \cdot 10^{-10}$
		L	**0.271 026**	**0.077 293**	$3.65277 \cdot 10^{-10}$
		G	**0.271 026**	**0.077 293**	$4.67220 \cdot 10^{-10}$
		C	**0.271 026**	**0.077 293**	$4.07509 \cdot 10^{-10}$
8	0	E/L/G/C	0.268 728	0.077 167	$9.26026 \cdot 10^{3}$
8	1	E/L	0.260 549	0.078 315	$1.25442 \cdot 10^{3}$
		G	0.263 519	0.079 501	$5.25141 \cdot 10^{2}$
		C	0.262 776	0.079 204	$5.93185 \cdot 10^{2}$
8	2	E/L	**0.271 026**	**0.077 293**	$6.92304 \cdot 10^{-10}$
		G	**0.271 026**	**0.077 293**	$7.45907 \cdot 10^{-10}$
		C	**0.271 026**	**0.077 293**	$1.01180 \cdot 10^{-10}$
10	0	E/L/G/C	0.269 248	0.0769 432	$8.29534 \cdot 10^{3}$
10	1	E/L	0.261 619	0.078 742	$8.9758 \cdot 10^{2}$
		G	0.263 519	0.079 501	$3.7576 \cdot 10^{2}$
		C	0.263 044	0.079 312	$4.2445 \cdot 10^{2}$
10	2	E/L	**0.271 026**	**0.077 293**	$4.14354 \cdot 10^{-10}$
		G	**0.271 026**	**0.077 293**	$6.45604 \cdot 10^{-10}$
		C	**0.271 026**	**0.077 293**	$1.01005 \cdot 10^{-10}$
Točna rešitev			**0.271 026**	**0.077 293**	**0**

n_e–število elementov, d.o.i.–stopnja interpolacije
E–ekvidistantno, L–Lobatto, G–Gauss, C–Chebyshev

Preglednica 3.11: Primerjava numeričnih rezultatov različnega števila končnih elementov E_0 s točno rešitvijo.

Table 3.11: The comparison of numerical results for constant interpolation with the exact solution.

n_e	d.o.i.	tip elementa	$w^a(L/2)$	$\Delta(0)$	$\|\mathcal{M}_C - \mathcal{M}\|_2$
20	0	E/L/G/C	0.269 942	0.077 187	$5.87765 \cdot 10^{2}$
50	0	E/L/G/C	0.270 457	0.077 278	$3.71945 \cdot 10^{-2}$
100	0	E/L/G/C	0.271 013	0.077 286	$2.31448 \cdot 10^{-7}$
1000	0	E/L/G/C	**0.271 026**	**0.077 293**	$1.31255 \cdot 10^{-10}$
Točna rešitev			**0.271 026**	**0.077 293**	**0**

n_e–število elementov, d.o.i.–stopnja interpolacije
E–ekvidistantno, L–Lobatto, G–Gauss, C–Chebyshev

Z namenom prikazati, da predstavljeni končni elementi niso podvrženi blokiranju zdrsa, smo zdrs med slojema izračunali za velike in majhne togosti stika (slika 3.29 in 3.30).

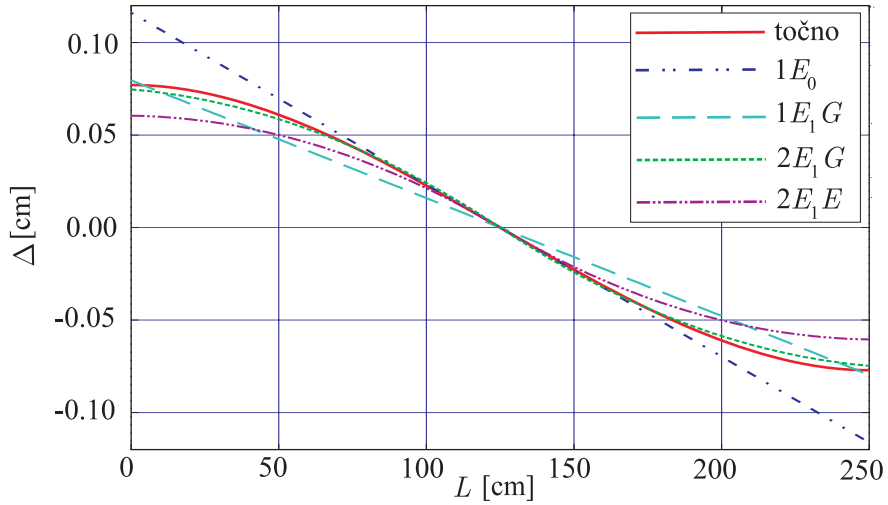

Slika 3.29: Razporeditev zdrsov vzdolž prostoležečega Timoshenkovega kompozitnega nosilca s togostjo stika $K = 0.243$ kN/cm^2 za različne izbire kolokacijskih točk, stopnje interpolacije in števila končnih elementov.

Figure 3.29: The distribution of interlayer slip over the span of a simply supported two-layer Timoshenko composite beam for $K = 0.243$ kN/cm^2.

Prikazujemo le rezultate za 1 in 2 elementa nizke stopnje interpolacijskih polinomov (npr. $1E_1/G$ pomeni 1 element E_1 s kolokacijskimi točkami, ki so razporejene v skladu z Gauss-ovimi integracijskimi točkami). Vsi ostali rezultati, ki v slikah 3.29 in 3.30 niso prikazani, praktično sovpadajo s točno rešitvijo zdrsa med sloji. Zaključimo lahko, da predstavljeni končni elementi ne izkazujejo blokiranja oziroma oscilacij zdrsa.

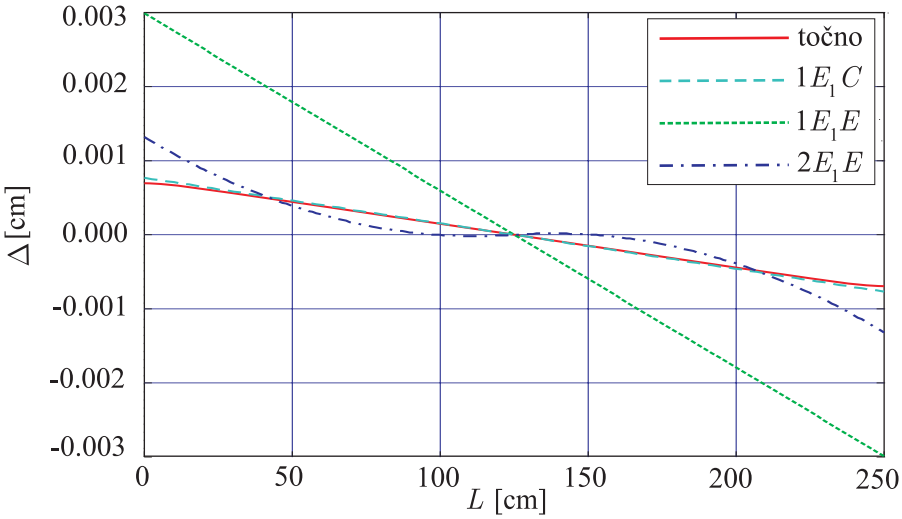

Slika 3.30: Razporeditev zdrsov vzdolž prostoležečega Timoshenkovega kompozitnega nosilca s togostjo stika $K = 2430$ kN/cm^2 za različne izbire kolokacijskih točk, stopnje interpolacije in števila končnih elementov.

Figure 3.30: The distribution of interlayer slip over the span of a simply supported two-layer Timoshenko composite beam for $K = 2430$ kN/cm^2.

V nadaljevanju pokažemo, da obravnavani končni elementi tudi strižno ne blokirajo. Navpične pomike Timoshenkovega kompozitnega nosilca (w_T), primerjamo z navpičnimi pomiki (w_B), ki jih izračunamo po Euler-Bernoullijevi teoriji kompozitnih nosilcev z upoštevanjem zdrsa med sloji. Navpične pomike primerjamo za različna razmerja dolžine proti višini kompozitnega nosilca (L/h), različno število elementov, različno stopnjo interpolacijskih polinomov in različno izbiro kolokacijskih točk. S slike 3.31 je razvidno, da v primeru, ko postane nosilec relativno dolg (vitek), rezultati Timoshenkovega modela konvergirajo k rezultatom Bernoullijevega modela. Podobno kot v primeru blokiranja zdrsa, lahko zaključimo, da predlagani končni elementi ne izkazujejo strižnega blokiranja.

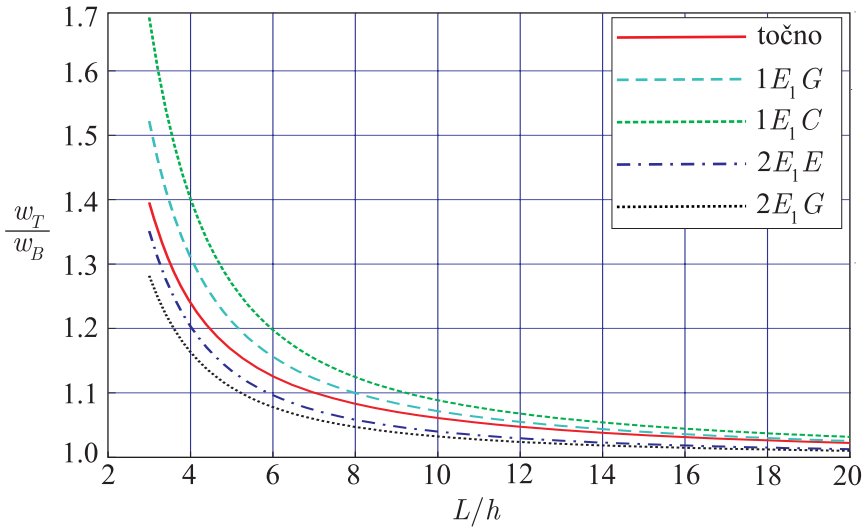

Slika 3.31: Vpliv razmerja dolžine proti višini nosilca (L/h) na navpične pomike prostoležečega dvoslojnega Timoshenkovega kompozitnega nosilca.

Figure 3.31: The influence of L/h ratios on vertical deflections of a simply supported two-layer Timoshenko composite beam.

Naslednji računski primer prikazuje uporabo predlagane družine končnih elementov za določitev napetostnega in deformacijskega stanja zahtevnejših (statično nedoločenih) konstrukcij. Obravnavamo nesimetrični kontinuirni Timoshenkov nosilec preko dveh polj in togostjo stika $K = 0.243$ kN/cm^2. Geometrijski in materialni podatki ter podatki o obtežbi so podani na sliki 3.32.

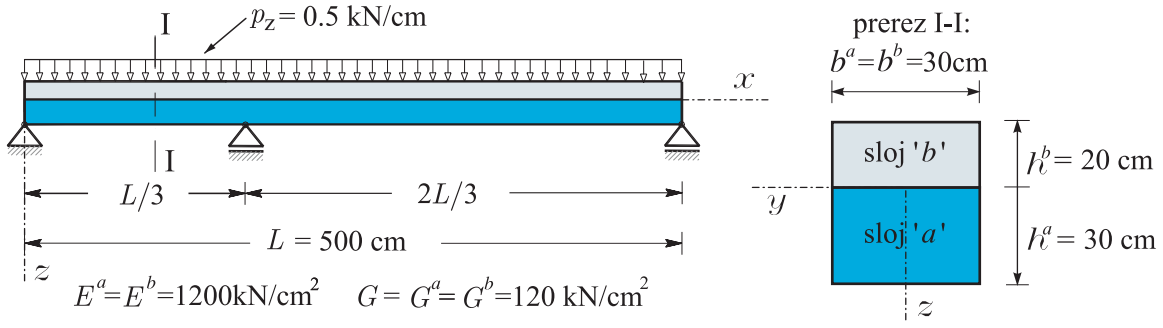

Slika 3.32: Geometrijski in materialni podatki ter podatki o obtežbi nesimetričnega dvoslojnega kontinuirnega Timoshenkovega kompozitnega nosilca preko dveh polj.

Figure 3.32: The descriptive geometric, material and loading data of a continuous two-layer Timoshenko composite beam over two spans.

Izvedli smo analizo vpliva strižne togosti posameznega sloja na statične in kinematične količine. Sliki 3.33 in 3.34 prikazujeta razporeditev zdrsov Δ in navpičnih pomikov w v odvisnosti od strižnega modula $G = G^a = G^b$. Nosilec smo modelirali z desetimi elementi E_4 in enakomerno razporejenimi kolokacijskimi točkami (E). Strižni modul ima pomemben vpliv na vrtikalne pomike in zdrsa. Vpliv na deformacijske količine, kot sta ε^a in κ^a, je nekoliko manjši. Vpliv strižne deformacije na mehansko obnašanje dvoslojnih Timoshenkovih nosilcev smo natančno analizirali v poglavju Dvoslojni nosilec z upoštevanjem strižne deformacije prereza.

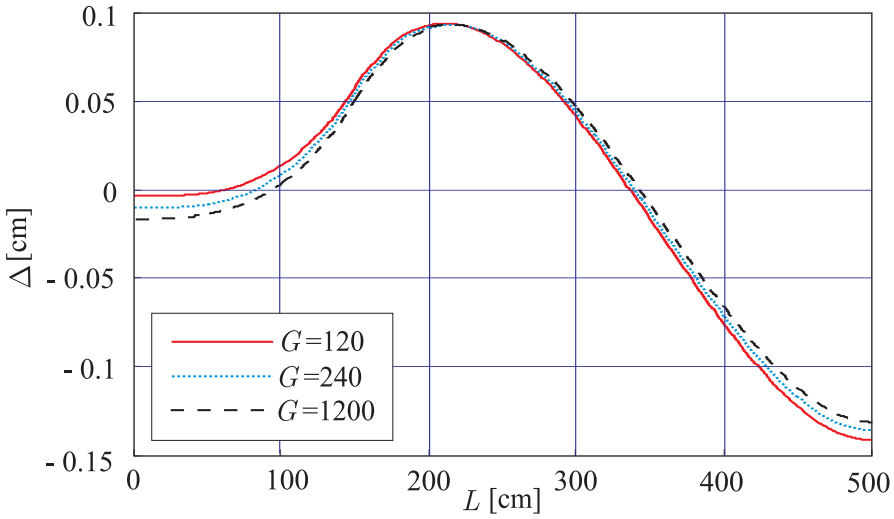

Slika 3.33: Porazdelitev zdrsa Δ v odvisnosti od strižnega modula $G = G^a = G^b$.
Figure 3.33: Distribution of Δ along the span as a function of different values of shear moduli, $G = G^a = G^b$.

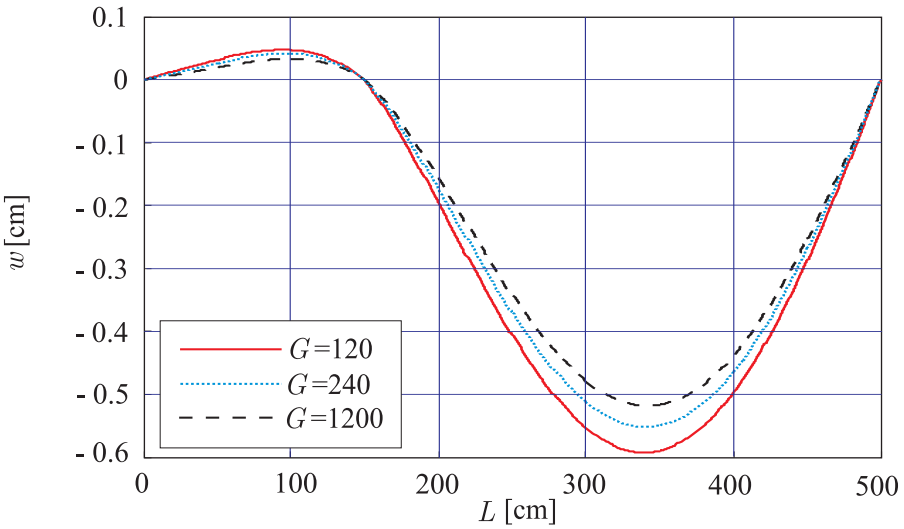

Slika 3.34: Porazdelitev navpičnih pomikov w v odvisnosti od strižnega modula $G = G^a = G^b$.
Figure 3.34: Distribution of w along the span as a function of different values of shear moduli, $G = G^a = G^b$.

3.3.5.2 Slojeviti nosilec z upoštevanjem oglenenja prereza

Z naslednjim računskim primerom prikažemo uporabnost predlaganega matematičnega modela za račun mehanskega odziva slojevitih kompozitnih nosilcev na hkratno delovanje zunanje statične obtežbe in požara. Obravnavamo lesen dvoslojni kompozitni nosilec, ki je na enem robu vpet na drugem pa vrtljivo podprt (glej sliko 3.35). Poleg tega je obremenjen s konzervativno enakomerno zvezno linijsko obtežbo p_Z in standarnim požarom ISO 834 (1999). Pri tem predpostavimo, da je temperaturno stanje nosilca in okolice vzdolž nosilca konstantno. Geometrijski in materialni podatki ter podatki o obtežbi so podani na sliki 3.35.

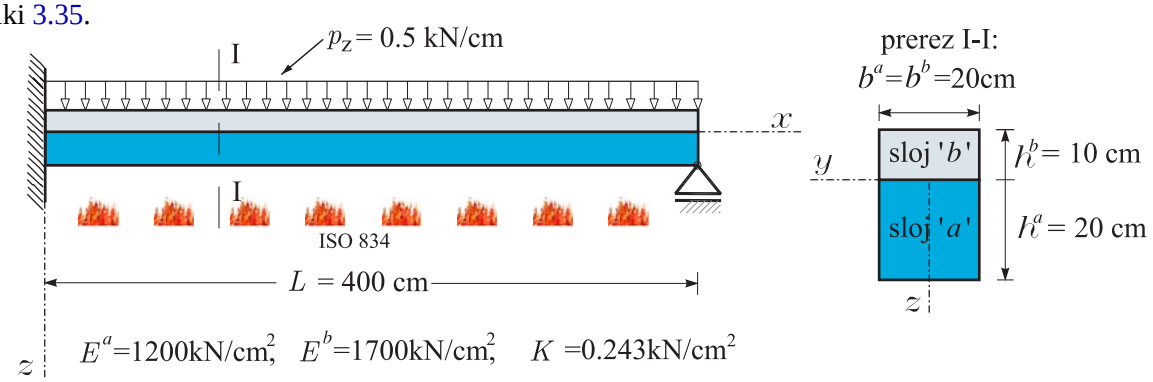

Slika 3.35: Geometrijski in materialni podatki ter podatki o obtežbi lesenega dvoslojnega kompozitnega nosilca.

Figure 3.35: The descriptive geometric, material and loading data of the two-layer wooden composite beam.

V analizi smo upoštevali temperaturno polje, ki smo ga določili v drugem poglavju, kjer smo obravnavali dvodimenzionalno oglenenje lesenega dvoslojnega kompozitega nosilca. Nosilec smo modelirali z desetimi končnimi elementi E_8, pri čemer smo kolokacijske točke izbrali ekvidistantno vzdolž kompozitnega nosilca. Celotno požarno analizo ($t = 60$ min) smo izvedli v časovnih korakih ($\Delta t = 1$ min).

Na sliki 3.36 je poleg statičnega pomika, ki je s časom konstanten ($w_S = 2.993$ cm), prikazan tudi časovni razvoj maksimalnega navpičnega pomika ($w_{\max}$) v odvisnosti od izbire uporabljenega modela, ki predvideva zmanjšanje mehanskih lastnosti lesa pri visokih temperaturah.

V računu smo uporabili različne faktorje zmanjšanja elastičnega modula, ki smo jih za različne avtorje podali v Mehanske lastnosti lesa pri visokih temperaturah. Navpični pomiki kompozitnega nosilca se s časom povečujejo. Opaziti je pričakovano veliko odstopanje dobljenih rezultatov, ki je posledica upoštevanja zelo različnih redukcijskih faktorjev zmanjšanja elastičnega modula. Maksimlni navpični pomiki se lahko pri $t = 30$ min razlikujejo tudi do 4-krat. Izračunani maksimalni pomiki kompozitnega nosilca so največji v primeru Evrokoda 5 (1999), medtem ko so v primeru Nyman-a najmanjši. Razlike med posameznimi modeli se s časom povečujejo.

V disertaciji predstavljeni matematični model lahko uporabimo za določitev požarne odpornosti kompozitnih nosilcev. Požarna odpornost oziroma porušitev konstrukcije je običajno definirana kot stanje: (i) ko so napetosti v prerezu višje od trdnosti materiala; (ii) ko je velikost navpičnih pomikov takšna, da je razmerje dolžine razpona proti maksimalnemu pomiku $\frac{L}{w_{\max}} \approx 30$, (Benichou, 2004). Odločimo se, da kot kriterij porušitve uporabimo kriterij dovoljenega maksimalnega pomika. V tem primeru je kritični oziroma maksimalni dovoljeni pomik $w_{\mathrm{cr}} \approx 13$ cm.

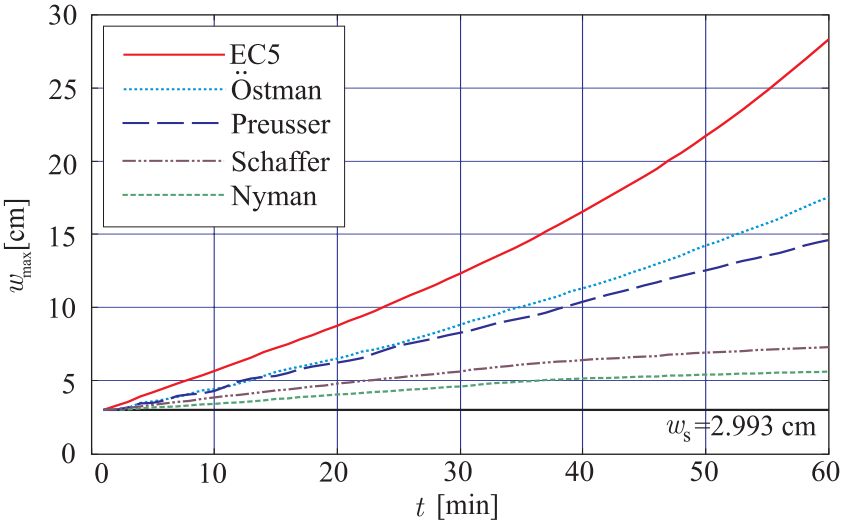

Slika 3.36: Vpliv oglenenja na časovni razvoj navpičnih pomikov dvoslojnega kompozitnega nosilca.

Figure 3.36: Vertical deflections versus time for the two-layer beam calculated by different material models.

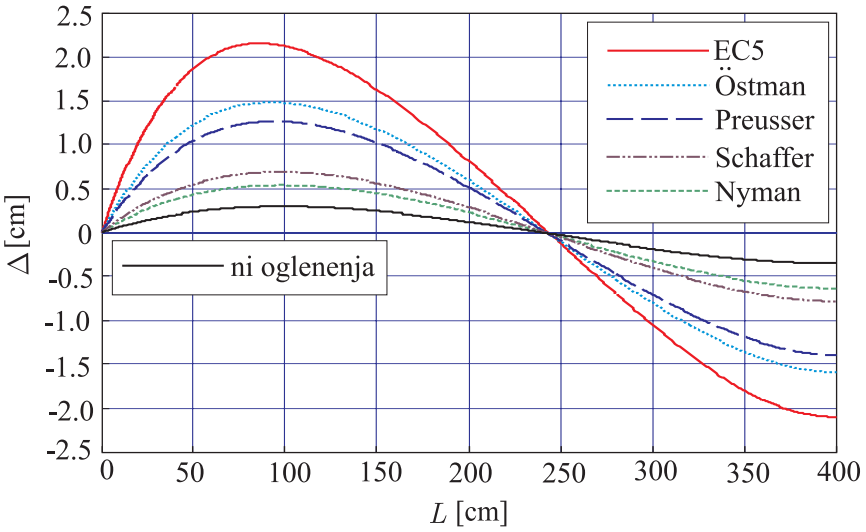

Slika 3.37: Vpliv oglenenja na porazdelitev zdrsov vzdolž dvoslojnega kompozitnega nosilca pri $t = 60$ min.

Figure 3.37: Distributions of the interlayer slips along the span of the two-layer beam calculated by different material models at $t = 60$ min.

Pri tako določenem pogoju požarne odpornosti pride do porušitve le v primerih Evrokoda 5 (1999), Östmana ter Preusserja. Čas porušitve v primeru Evrokoda 5 (1999) je $t \approx 30$ min, Östman $t \approx 47$ min in Preusserja $t \approx 56$ min, (slika 3.36).

S slikama 3.37 in 3.38 prikažemo vpliv oglenenja na porazdelitev zdrsa Δ oziroma navpičnega pomika w vzdolž razpona kompozitnega nosilca. Podobno kot se s časom povečujejo navpični pomiki, se v primeru različnih faktorjev zmanjšanja elastičnega modula, povečujejo tudi zdrsi med slojema a in b.

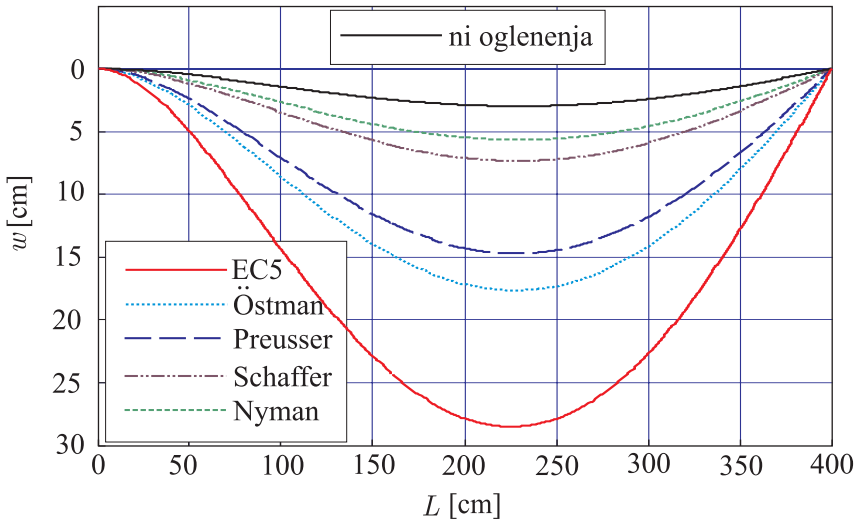

Slika 3.38: Vpliv oglenenja na porazdelitev navpičnih pomikov vzdolž dvoslojnega kompozitnega nosilca pri $t = 60$ min.

Figure 3.38: Distributions of the vertical deflections along the span of the two-layer beam calculated by different material models at $t = 60$ min.

Časovno spreminjanje porazdelitve Δ in w vzdolž razpona kompozitnega nosilca prikažemo v primeru Evrokoda 5 (1999) s slikama 3.39 in 3.40. Porazdelitve omenjenih količin so izračunane pri $t = 0, 10, 20, 30, 40, 50$ in 60 min.

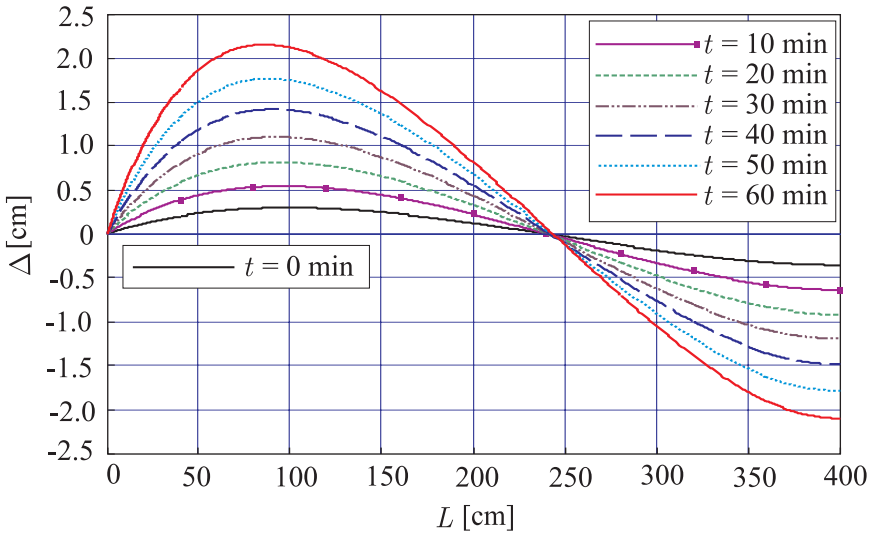

Slika 3.39: Porazdelitve zdrsov Δ vzdolž dvoslojnega kompozitnega nosilca v primeru Evrokoda 5 (1999) pri različnih časih.

Figure 3.39: Distributions of the interlayer slips Δ along the span of the two-layer beam calculated by Eurocode 5 (1999) at different times.

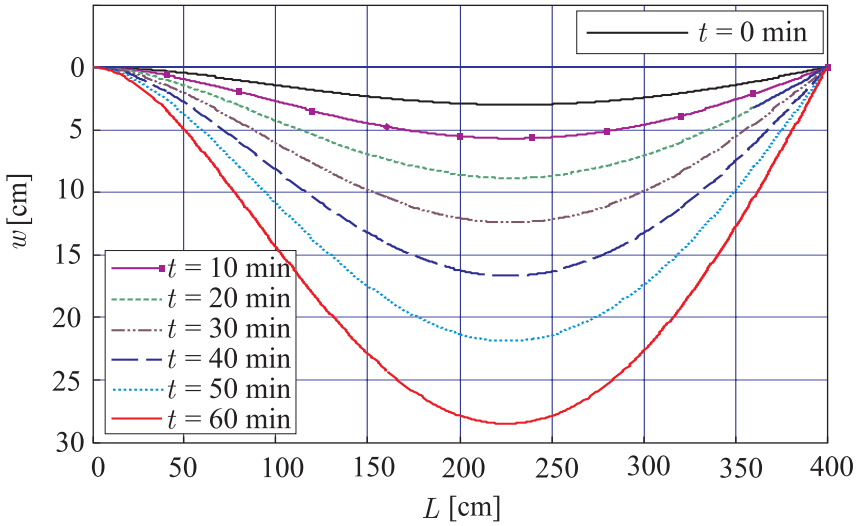

Slika 3.40: Navpični pomiki w vzdolž dvoslojnega kompozitnega nosilca v primeru Evrokoda 5 (1999) pri različnih časih.

Figure 3.40: Distributions of the vertical deflections w along the span of the two-layer beam calculated by Eurocode 5 (1999) at different times.

4 ZAKJUČKI

V disertaciji smo predstavili računski postopek za določitev napetostnega in deformacijskega stanja nelinearnih slojevitih kompozitnih nosilcev z upoštevanjem delne povezanosti slojev, strižne deformacije prečnega prereza in oglenenja pri sočasnem delovanju statične mehanske obtežbe in obtežbe požara. Izdelali smo računalniški program v programskem okolju *Matlab*. Nalogo smo vsebinsko razdelili na dva dela. V prvem delu smo analizirali temperaturno-vlažnostno stanje slojevitih lesenih kompozitnih nosilcev pri požaru z upoštevanjem oglenenja lesa. Pri tem smo za opis povezanega prehoda toplote in vlage skozi les uporabili nelinearni parcialni diferencialni enačbi Luikova (1966). Upoštevali smo temperaturno in vlažnostno odvisne materialne lastnosti lesa. Ker analitičnih rešitev v splošnem ne poznamo, smo enačbe začetnega robnega problema povezanega prehoda toplote in vlage v lesenih kompozitnih nosilcih, ki izpostavljeni požaru oglenijo, diskretizirali in rešili z uporabo numerične metode končnih razlik. Dobljene rezultate hitrosti enodimenzionalnega oglenenja homogenih nosilcev smo primerjali z rezultati empiričnih modelov enodimenzionalnega oglenenja homogenih nosilcev, ki smo jih našli v literaturi. Poleg tega smo rezultate enodimenzionalnega oglenenja primerjali tudi z eksperimentalnimi rezultati švedskega raziskovalca Fredlunda (1988, 1993). Predstavljeni matematični model oglenenja smo v nadaljevanju uporabili za parametrično študijo vpliva različnih parametrov na hitrost oglenenja. Na koncu smo prikazali tudi oglenenja dvodimenzionalnih homogenih in slojevitih prečnih prerezov. Rezultat analize je bila časovna razporeditev temperature, vlage in oglja po prečnem prerezu dvoslojnega kompozitnega nosilca. Omenjeno razporeditev smo potrebovali v drugem delu naloge, kjer smo analizirali mehanski odziv slojevitega kompozitnega nosilca na sočasno mehansko in požarno obtežbo. Na osnovi rezultatov in primerjave le teh smo prišli do naslednjih zaključkov:

- Primerjava numeričnih rezultatov enodimenzionalnega oglenenja homogenih lesenih nosilcev potrjuje dobro ujemanje rezultatov predstavljenega matematičnega modela oglenenja z numeričnimi rezultati Fredlunda (1993) ter empiričnimi modeli, ki jih predlagajo White in Nordheim (1992) ter Evrokod 5 (2004). Ujemanje z ostalimi modeli je slabše. Velika večina avtorjev namreč predvideva konstantno hitrost oglenenja, čeprav eksperimenti in rezultati natančnejših matematičnih modelov potrjujejo nasprotno.

- Primerjava pokaže, da se modeli oglenenja razlikujejo predvsem glede časa začetka oglenenja, kar je lahko posledica različne definicije začetka oglenenja. Večina modelov predlaga začetek oglenenja ob nastopu požarne obtežbe. To seveda ne predstavlja dejanskega stanja. Fredlund (1988, 1993) nastanek oglja definira kot stanje, kjer gostota lesa pade pod 300 kg/m^3, medtem ko v našem primeru oglje nastane, ko les doseže temperaturo ($300\,^\circ$C).

- Primerjava rezultatov v nalogi razvitega matematičnega modela oglenenja z eksperimetnalnimi rezultati Fredlunda (1988) pokaže dobro ujemanje. Kljub temu se zavedamo, da primerjava samo z enim eksperimentom ne more služiti za zanesljivo oceno učinkovitosti predstavljenega matematičnega modela oglenenja lesa. Za zanesljivo oceno učinkovitosti so tako potrebne dodatne primerjave z eksperimentalnimi rezultati.

- Izvedena parametrična analiza vpliva različnih parametrov na hitrost oglenenja lesa pokaže, da imata začetna vlažnost in specifična gostota lesa pomemben vpliv na hitrost oglenenja. Določitev vpliva ostalih parametrov na hitrost oglenenja bo predmet nadaljnjih raziskav. Na tem mestu opozorimo na velik raztros materialnih karakteristik lesa. Natančna določitev le teh je bistvena za natančen opis oglenenja lesenih nosilcev pri požaru.

- Relativno preprost matematični model oglenenja je uporaben za napoved temperaturno-vlažnostnega stanja lesenih nosilcev, ki so izpostavljeni visokim temperaturam požara.

V drugem delu smo najprej predstavili osnovne enačbe, ki opisujejo mehansko obnašanje kompozitnih nosilcev z upoštevanjem zdrsa med sloji in strižne deformacije prečnega prereza. Posebno pozornost smo namenili analitičnemu reševanju osnovnih enačb slojevitih Bernoullijevih in Timoshenkovih kompozitnih nosilcev. Predstavili smo algoritma za analitično reševanje. Razvita algoritma smo v nadaljevanju uporabili pri reševanju konkretnih primerov. V prvem primeru smo analitično rešitev razširili s prostoležečih troslojnih kompozitnih nosilcev na kontinuirne troslojne kompozitne nosilce. V drugem pa smo analitično rešitev Timoshenkovih kompozitnih nosilcev prikazali na primeru dvoslojnega prostoležečega kompozitnega nosilca. Na osnovi analitične rešitve Timoshenkovih kompozitnih nosilcev smo izvedli detajlno parametrično analizo vpliva strižne deformacije prečnega prereza na mehansko obnašanje omenjenih konstrukcij. V nadaljevanju smo z uporabo modificiranega principa virtualnega dela (Planinc, 1998) izpeljali družino deformacijskih končnih elementov za nelinearno analizo kompozitnih nosilcev z upoštevanjem zdrsa med sloji ter strižne deformacije prečnega prereza. Z analizo različnega števila končnih elementov, stopnje interpolacije in izbire kolokacijskih točk smo pokazali, da so tako razviti končni elementi točni, učinkoviti in odporni na kakršnokoli vrsto blokiranja. To je bil tudi razlog, da smo družino razvitih deformacijskih končnih elementov kasneje priredili za analizo mehanskega odziva slojevitih kompozitnih lesenih nosilcev pri sočasnem delovanju mehanske statične obtežbe in požara. Pri določitvi napetostnega in deformacijskega stanja v poljubnem materialnem vlaknu prečnega prereza, smo v analizi poleg mehanske deformacije upoštevali tudi prispevke temperaturne deformacije lesa. S časovno razporeditvijo temperature, vlage in oglja po prerezu, ki smo jo določili v prvem delu, smo z računskim primerom prikazali uporabnost predlaganega matematičnega modela za račun odziva slojevitih kompozitnih nosilcev na hkratno delovanje zunanje statične obtežbe in požara. Zaključimo lahko:

- Prikazana algoritma analitičnega reševanja kompozitnih nosilcev predstavljata razširitev analitičnega reševanja na bolj zahtevne kompozitne nosilce.

- Z analitično rešitvijo izvedena parametrična študija je v primeru kompozitnih nosilcev z upoštevanjem zdrsa med sloji pokazala, da ima strižna deformacija pomemben vpliv na mehansko obnašanje kompozitnih nosilcev. Vpliv strižne deformacije je izrazit pri kratkih ($L/h < 10$) lesenih ($E/G \approx 16 - 20$) kompozitnih nosilcih. Vpliv je večji z večanjem togosti povezave med sloji. Odvisen je tudi od vrste materiala, iz katerega je kompozitni nosilec. V primeru izotropnega materiala ($E/G \approx 2.68$) in nosilcih iz steklenih vlaken ($E/G \approx 8.67$) postane vpliv striga pomemben šele pri $L/h < 5$. Zanimivo je, da je vpliv strižne deformacije prečnega prereza na različne količine različen. Nekatere količine, kot so $w, \varphi^b, \kappa^b, \mathcal{N}^a$ se povečajo, medtem ko se druge, npr. $q_n, \varepsilon^a, \varphi^a$, zmanjšajo v primerjavi s količinami izračunanimi s klasičnim Euler-Bernoullijevim modelom kompozitnega nosilca. Parametrična študija pokaže, da je vpliv strižne deformacije na navpične pomike vedno najmanjši, kadar imata sloja približno enako višino, tj. kadar je razmerje $h^a/h^b \simeq 1$. Vpliv je manjši za manjše vrednosti K. V primeru podajne povezave, kjer je $K \leq 1\mathrm{kN/cm}^2$, je lahko vpliv tudi do 4-krat manjši kot v primeru relativno toge povezave, kjer je $K = 1000\mathrm{kN/cm}^2$. Primerjava prečnih sil $\mathcal{Q}^a$ in $\mathcal{Q}^b$ pokaže, da je vpliv strižne deformacije, podobno kot pri navpičnih pomikih, najmanjši v primeru, ko sta sloja približno enakih višin, takrat

je $h^a/h^b \simeq 1$. Izkaže se, da so lahko prečne sile v sloju, ki je zelo tanek v primerjavi z drugim slojem, v primeru podajnega stika ($K \leq 1\mathrm{kN/cm^2}$), tudi do 2.5-krat večje, kot so prečne sile v tem sloju, izračunane po klasični upogibni teoriji kompozitnih nosilcev z upoštevanjem zdrsa med sloji. V primeru zelo toge povezave ($K \geq 1000\mathrm{kN/cm^2}$) je vpliv strižne deformacije na prečne sile zanemarljiv. Izjema so nosilci, kjer je zgornji sloj b, zelo tanek v primerjavi z spodnjim slojem a. V tem primeru, so lahko prečne sile $\mathcal{Q}^a$, tudi do 2-krat manjše, kot so prečne sile $\mathcal{Q}^b$. Togost stika K ima zelo pomemben vpliv na velikost in razpored strižnih in normalnih napetosti po prerezu. V primeru zelo podajnih stikov so maksimalne strižne in normalne napetosti dosti večje od napetosti, ki jih dobimo z upoštevanjem klasičnega modela nosilcev s togo povezanimi sloji. Strižne napetosti σ_{xz} so v primeru zelo podajnih stikov tudi za 25% večje od napetosti homogenega nosilca s togo povezanimi sloji. Razlike so še večje v primeru normalnih napetostih σ_{xx}.

- Izpeljana družina deformacijskih končnih elementov za nelinearno analizo kompozitnih nosilcev z upoštevanjem delne povezanosti slojev in strižne deformacije prereza je točna, učinkovita in odporna na vse vrste blokiranja. Poleg tega je primerna tudi za analizo mehanskega odziva slojevitih kompozitnih nosilcev na hkratno delovanju zunanje statične obtežbe in požara.

- Analiza vpliva oglenenja na požarno odpornost slojevitih kompozitnih nosilcev je pokazala, da ima oglenenje zelo pomembno vlogo pri požarni odpornosti lesenih konstrukcij. Navpični pomiki kompozitnega nosilca se s časom povečujejo. Opaziti je pričakovano veliko odstopanje dobljenih rezultatov, ki je posledica upoštevanja zelo različnih redukcijskih faktorjev zmanjšanja elastičnega modula. Maksimalni navpični pomiki se lahko pri $t = 30$ min razlikujejo tudi do 4-krat. Izračunani maksimalni pomiki kompozitnega nosilca so največji v primeru Evrokoda 5 (1999), medtem ko so v primeru Nyman-a najmanjši. Razlike med posameznimi modeli se s časom povečujejo. Podobno odstopanje dobimo tudi pri izračunu požarne odpornosti. Glede na kriterij požarne odpornosti, ki smo si ga izbrali, je porušitev v konkretnem računskem primeru nastopila ob zelo različnih časih. V obdobju opazovanja požara ($t = 60$ min) je do porušitve prišlo le v primerih Evrokoda 5 (1999), Östmana ter Preusserja. Čas porušitve v primeru Evrokoda 5 (1999) je $t \approx 30$ min, Östmana $t \approx 47$ min in Preusserja $t \approx 56$ min.

VIRI

Adekola, A.O 1968. Partial interaction between elastically connected elements of a composite beam. International Journal of Solids and Structures 4, 11: 1125–1135.

ASTM E-119-76. Standard methods of fire tests of building construction and materials. Annual book of ASTM standars, Part 18, American Society for Testing and Materials, West Conshohocken, PA.

Ayoub, A., Filippou, F.C. 2000. Mixed formulation of nonlinear steel-concrete composite beam element. Journal of Structural Engineering 126, 3: 371–381.

Ayoub, A. 2001. A two-field mixed variational principle for partially connected composite beams. Finite Elements in Analysis and Design 37: 929–959.

Ayoub, A 2005. A force-based model for composite steel-concrete beams with partial interaction. Journal of Constructional Steel Research 61: 387–414.

Benichou, N. 2004. Structural response modelling of wood-joist floor assemblies exposed to fires. Interflam 2004 Conference, Edinburg, Scotland: 233–244.

Betti, R., Gjelsvik, A. 1994. Elastic composite beams. Computers and Structures 59, 3: 437–451.

Can, M. 1998. Simultaneous concective heat and mass transfer in impingement ink drying. International Communications in Heat and Mass Transfer 25, 6: 863–874.

Chang, W.J., Weng, C.I. 2000. An analytical solution to coupled heat and moisture diffusion transfer in porous materials. International Journal of Heat and Mass Transfer 43: 3621–3632.

Chui, Y.H., Barclay, D.W. 1998. Analysis of three-layer beams with non-identical layers and semi-rigid connections. Canadian Journal of Civil Enginnering 25: 271–276.

Cosenza, E., Pecce, M. 2001. Shear and normal stresses interaction in coupled structural systems. Journal of Structural Engineering ASCE 127, 1: 84–88.

Cowper, G.R. 1966. The shear coefficient in Timoshenko's beam theory. Journal of Applied Mechanics 33, 2: 335–340.

Čas, B., Saje, M., Planinc, I. 2004a. Nonlinear finite element analysis of composite planar frames with

inter-layer slip. Computers and Structures 82: 1901–1912.

Čas, B., Bratina, S., Saje, M., Planinc, I. 2004b. Non-linear analysis of composite steel-concrete beams with incomplete interaction. Steel and Composite Structures 4, 6: 489–507.

Čas, B. 2004. Nelinearna analiza kompozitnih nosilcev z upoštevanjem zdrsa med sloji. Doktorska disertacija. Ljubljana, Univerza v Ljubljani, Fakulteta za gradbeništvo in geodezijo, Oddelek za gradbeništvo, Konstrukcijska smer: 136 f.

Čas, B., Saje, M., Planinc, I. 2007. Buckling of layered wood columns. Advances in Engineering Software 38: 586-597.

Dall'Asta, A. 2001. Composite beams with weak shear connection. International Journal of Solids and Structures 38: 5605–5624.

Dall'Asta, A., Zona, A. 2002. Nonlinear analysis of composite beams by a displacement approach. Computers and Structures 80: 2217–2228.

Dall'Asta, A., Zona, A. 2004a. Three-field mixed formulation for the non-linear analysis of composite beams with deformable shear connection. Finite Elements in Analysis and Design 40: 425–448.

Dall'Asta, A., Zona, A. 2004b. Slip locking in finite elements for composite beams with deformable shear connection. Finite Elements in Analysis and Design 40: 1907–1930.

Dall'Asta, A., Zona, A. 2005. Finite element model for externally prestresses composite beams with deformable connection. Journal of Structural Engineering 131, 5: 706–714.

De-Vries, D. 1968. Simultaneous transfer of heat and moisture in porous media. Trans American Geophysics 39: 909–916.

Dezi, L., Tarantino, A.M. 1993a. Creep in composite conitnuous beams. I: Theoretical treatment. Journal of Structural Engineering 119, 7: 2095-2111.

Dezi, L., Tarantino, A.M. 1993b. Creep in composite conitnuous beams. II: Parametric study. Journal of Structural Engineering 119, 7: 2112-2133.

Dias, A.M.P.G 2005. Mechanical behaviour of timber-concrete joints. Ph.D Thesis, Delft, Delft University of Technology: 293 f.

Elghazouli, A.Y., Izzuddin, B.A., Richardsin, A.J. 2000. Numerical modelling of the structural fire behaviour of composite buildings. Fire Safety Journal 35: 279–297.

Eurocode 5, 2004. Design of timber structures, Part 1-1: Common rules and rules for buildings, ENV 1-1:2004.

Faella, C., Martinelli, E., Nigro, E. 2002. Steel and concrete composite beams with flexible shear connection: "exact"analytical expression of the stiffness matrix and applications. Computers and Structures 80: 1001–1009.

Faella, C., Martinelli, E., Nigro, E. 2003. Shear connection nonlinearity and deflections of steel-concrete composite beams: A simplified method. Journal of Structural Engineering 129, 1: 12–20.

Fernandez, J.R., Sofonea, M. 2002. Variational and numerical analysis of the Signorini's contact problem in viscoplasticity with damage. Journal of Applied Mathematics 2: 87–114.

Fragiacomo, M., Ceccotti, A. 2005. A finite element model for long-term analysis of timber-concrete composite beams. Structural Engineering and Machanics 20, 2: 173-189.

Fragiacomo, M., Ceccotti, A. 2006a. Long-term behavior of timber-concrete composite beams. I: Finite element modeling and validation. Journal of Structural Engineering 132, 1: 13-22.

Fragiacomo, M., Ceccotti, A. 2006b. Long-term behavior of timber-concrete composite beams. II: Numerical analysis and simplified evaluation. Journal of Structural Engineering 132, 1: 23-33.

Fredlund, B. 1988. A model for heat and mass transfer in timber structures during fire - a theoretical, numerical and experimental study. Doctoral dissertation. Lund, Lund University, Report LUTVDG/(TVBB-1003): 254 f.

Fredlund, B. 1993. Modelling of heat and mass transfer in wood structures during fire. Fire Safety Journal 20: 39–69.

Gams, M. 2003. Povezan prenos vlage in toplote v poroznem materialu. Diplomska naloga. Ljubljana, Univerza v Ljubljani, Fakulteta za gradbeništvo in geodezijo, Oddelek za gradbeništvo, Konstrukcijska smer: 78 f.

Gara, F., Ranzi, G., Leoni, G. 2006. Displacement-based formulations for composite beams with longitudinal slip and vertical uplift. International Journal for Numerical Methods in Engineering 65: 1197–1220.

Girhammar, U.A., Gopu, V.K.A. 1993. Composite beam-columns with interlayer slip–Exact analysis. Journal of Structural Engineering ASCE 119, 4: 1265–1282.

Girhammar, U.A., Pan, D. 1993. Dynamic analysis of composite members with interlayer slip. International Journal of Solids and Structures 30, 6: 797–823.

Goodman, J.R., Popov, E.P. 1968. Layered beam systems with interlayer slip. Journal of Structural Division, Proceeding of ASCE 94, 11: 2535–2547.

Goodman, J.R., Popov, E.P. 1969. Layered wood systems with interlayer slip. Wood Science 1, 3: 148–158.

Gorik, A.V. 2003. Theoretical and experimental deformation parameters of composite beams with account of deplanation of cross sections in bending. Mechanics of Composite Materials 39, 1: 57–64.

Hakkarainen, T. 2002. Post-flashover fires in light and heavy timber construction compartments. Journal of Fire Sciences 20: 133–175.

Harmathy, T.Z. 1969. Simultaneous moisture and heat transfer in porous systems with particular reference to drying. Industrial and Engineering Chemistry Fundamentals 8: 92–103.

Harmathy, T.Z. 1995. Properties of building materials. The SFPE Handbook of Fire Protection Engineering, Section1, Chapter 10, SFPE/NFPA, USA: 141–151.

Huang, Z., Burgess, I.W., Plank, R.J. 1999. The influence of shear connectors on the behaviour of composite steel-framed buildings in fire. Journal of Constructional Steel Research 51: 219–237.

Hussain, M.H., Dincer, I. 2003. Numerical simulation of two-dimensional heat and moisture transfer during drying of a rectangular object. Numerical Heat Transfer, Part A 43: 867–878.

Irudayaraj, J., Haghighi, K., Stroshine, R.L. 1990. Nonlinear finite element analysis of coupled heat and mass transfer problems with an application to timber drying. Drying Technology 8, 4: 731–749.

ISO 834 1999. Fire resistance test- Elements of building construction - Part 1. General Requirements. ISO 834-1. International Organization for Standardization, Geneva, Switzerland.

Janssens, M.L. 1994. Thermo-physical properties for wood pyrolysis models. Pacific Timber Engineering Conference, Gold Coast, Australia: 607–618.

Janssens, M.L., White, R.H. 1994. Short communications: Temperature profiles in wood members exposed to fire. Fire and Materials 18: 263–265.

Janssens, M.L. 2004. Modeling of the thermal degradation of structural wood members exposed to fire. Fire and Materials 28: 199–207.

Jasim, N.A. 1997. Computation of deflections for continuous composite beams with partial interaction. Proceedings of the Institutions of Civil Engineers, Structures and Buildings 122: 374–354.

Jasim, N.A., Ali, A.A.M. 1997. Deflections of composite beams with partial shear connection. The Structural Engineer 75, 4: 374–354.

Jasim, N.A. 1999. Deflections of partially composite beams with linear connector density. Journal of Constructional Steel Research 49: 241–254.

Jasim, N.A., Atalla, A. 1999. Deflections of partially composite continuous beams: A simple approach. Journal of Constructional Steel Research 49: 291–301.

Johnson, K.L. 1987. Contact mechanics. Cambridge University Press, U.K.: 456 f.

Kamiya, F. 1987. Buckling theory of sheated walls: linear analysis. Journal of Structural Engineering ASCE 113, 9: 2009–2022.

Kalker, J.J. 1990. Three-dimensional elastic bodies in rolling contact. Series: Solid Mechanics and its Application, Kluwer , Dordrecht, The Netherland: 344 f.

Kocaefe, D., Younsi, R., Chaudry, B., Kocaefe, Y. 2006. Modeling of heat and mass transfer during high temperature treatment of aspen. Wood Science and Technology 40: 371–391.

Křistek, V., Studnička, J. 1982. Analysis of composite girders with deformable connectors. Proceedings of the Institutions of Civil Engineers, Part 2 73: 699–712.

Kruppa, J., Zhao, B. 1995. Fire resistance of composite beams to Eurocode 4 Part 1.2. Journal of Constructional Steel Research 33: 51–69.

Kwak, H.G., Seo, Y.J. 2000. Long-term behaviour of composite girder bridges. Computers and Structures 74: 583-599.

Kwak, H.G., Seo, Y.J. 2002. Time-dependent behavior of composite beams with flexible connectors. Computer methods in applied mechanics and engineering 191: 3751–3772.

Lau, P.W.C, White, R., Van Zeeland, I. 1999. Modelling the charring behaviour of structural lumber. Fire and Materials 23: 209–216.

Lawson D.I., Webster, C.T, Ashton, L.A. 1952. Fire endurance of timber beams and floors. Journal of Structural Engineering 30, 2: 27–34.

Leceister R.H. 1983. Fire resistance of timber, Part 1 - Performance of timber structures in fire. Workshop on Timber Engineering, Melbourne, Australia, 2-20 May.

Leon, R.T., Viest, I.M. 1998. Theories of incomplete interaction in composite beams. Composite Construction in Steel and Concrete III ASCE: 858–870.

Lie, T.T. 1977. A method for assessing the fire resistance of laminated timber beams and coulmns. Canadian Journal of Civil Engineering 4: 161–169.

Lien, H.P., Wittmann, F.H. 1995. Coupled heat and mass transfer in concrete elements at elevated temperatures. Nuclear Engineering and Design 156: 109–119.

Liu, J.Y., Cheng, S. 1991. Solutions of Luikov equations of heat and mass transfer in capillary-porous bodies. International Journal of Heat and Mass Transfer 34, 7: 1767–1754.

Lobo, P.D., Mikhailov, M.D., Ozisik, M.N. 1987. On the complex eigenvalues of Luikov system of equations. Drying Technology 5, 2: 273–286.

Luikov, A.V. 1966b. Heat and mass transfer in capillary porous bodies. Pergamon Press, Oxford, England: 623 str.

Luikov, A.V., Mikhailov, Yu.A. 1966. Theory of energy and mass transfer. Pergamon Press, Oxford, United Kingdom: 392 str.

Luikov, A.V. 1975a. Systems of differential equations of heat and mass transfer in capillary-porous bodies (Review). International Journal of Heat and Mass Transfer 18: 1–14.

Luikov, A.V. 1980c. Heat and mass transfer. Mir Publishers, Moscow, Soviet Union: 623 str.

Manfredi, G., Pecce, M. 1998. A refined R.C. beam element including bond-slip relationship for the analysis of continuous beams. Computers and Structures 69: 53–62.

Marsden, J.E., Hughes, T.J.R. 1983. Mathematical Foundations of Elasticity. Dover Publications. New York.

Matsunaga, H. 2002. Interlaminar stress analysis of laminated composite beams according to global higher-order deformation theories. Composite Structures 34: 105–114.

McCutheon, W.J. 1986. Stiffness of framing members with partial composite action. Journal of the Structural Division ASCE 112, 7: 1623–1637.

Mikkola, E. 1990. Charring of wood. Technical Research Centre of Finland, Research Reports 689. Espoo, Finland, VTT, Fire Technology Laboratory: 35 str.

Newmark, N.M:, Siess, C.P., Viest, I.M. 1951. Tests and analysis of composite beams with incomplete interaction. Proceedings of the Society for Experimental Stress Analysis 1: 75–92.

Nguyen, N.T., Oehlers, D.J., Bradford, M.A. 2001. An analytical model for reinforced concrete beams with bolted side plates accounting for longitudinal and transverse partial ineraction. International Journal of Solids and Structures 38: 6985–6996.

Nie, J., Cai, C.S. 2003. Steel–concrete composite beams considering shear slip effects. Journal of Structural Engineering ASCE 129, 4: 495–506.

Nijdam, J.J., Langrish, T.A.G., Keey, R.B. 2000. A high-temperature drying model for softwood timber. Chemical Engineering Science 55: 3585–3598.

Oven, V.A., Burgess, I.W., Plank, R.J., Abdul Wali, A.A. 1997. An analytical model for the analysis of composite beams with partial interaction. Computers and Structures 62: 493–504.

Özisik, M.N. 1985. Heat transfer: A basic approach. McGraww-Hill Book Company, Singapore: 780 str.

Özisik, M.N. 1994. Finite difference methods in heat transfer. CRC Press, Boca Raton, Florida, USA: 412 str.

Pandey, R.N, Pandey, S.K., Mikhailov, M.D. 1999a. temperature and moisture distributions in a moist spherical capillary-porous body–a new approach. International Journal for Numerical Methods in Engineering 45: 125–146.

Pandey, R.N., Srivastava, S.K., Mikhailov, M.D. 1999b. Solutions of Luikov equations of heat and mass transfer in capillary porous bodies through matrix calculus: a new approach. International Journal of Heat and Mass Transfer 42: 2649–2660.

Piskunov, V.G., Grinevitskii, B.V. 2004. Variant of an analytical shear model for the stress-strain state of heterogeneous composite beams. Mechanics of Composite Materials 40, 5: 409–417.

Planinc, I. 1998. Račun kritičnih točk konstrukcij s kvadratično konvergentnimi metodami. Doktorska disertacija. Ljubljana, Univerza v Ljubljani, Fakulteta za gradbeništvo in geodezijo, Oddelek za gradbeništvo, Konstrukcijska smer: 83 f.

Plum, D.R., Horne, M.R. 1975. The analysis of continuous composite beams with partial inetraction. Proceedings of the Institutions of Civil Engineers, Part 2 59: 571–593.

Ranzi, G., Bradford, M.A., Uy, B. 2003. A general method of analysis of composite beams with partial interation. Steel and Composite Structures 3, 3: 169–184.

Rabinowicz, E. 1995. Friction and wear of materials. Second Edition, John Wiley & Sons, Interscience, New York: 336 f.

Ranzi, G., Bradford, M.A., Uy, B. 2004. A direct stiffness analysis of composite beam with partial interation. International Journal for Numerical Methods in Engineering 61: 657–672.

Ranzi, G., Bradford, M.A. 2006. Analytical solutions for the time-dependent behaviour of composite beams with partial interaction. International Journal of Solids and Structures 43, 13: 3770–3793.

Ranzi, G., Gara, F., Ansourian, P. 2006. General method for composite beams with longitudinal and transverse partial interaction. Computers and Structures 84, 31–32: 2373–2384.

Raous, M. 1999. Quasistatic Signorini problem with coulomb friction and coupling to adhesion. International Centre for Mechanical Sciences, Courses and Lectures - No. 384, Chapter 3: 101–178.

Rassam, H.Y., Goodman, J.R. 1970. Buckling behavior of layered wood coulmns. Wood Science 2, 4: 238–246.

Rassam, H.Y., Goodman, J.R. 1971. Design of layered wood columns with interlayer slip. Wood Science 3, 3: 149–155.

Reddy, J.N. 1986. Applied functional analysis and variational methods in engineering. McGraw-Hill Book Co., Singapore: 546 f.

Reissner, E. 1972. On one-dimensional finite-strain beam theory: The plane problem. Journal of Applied Mechanics and Physics (ZAMP) 23: 795–804.

Renaud, C., Feng, Z.Q. 2003. BEM and FEM analysis of Signorini contact problems with friction. Computational Mechanics 31: 390–399.

Ribeiro, J.W., Cotta, R.M. 1995. On the solution of non-linear drying problems in capillary porous media through integral transformation of Luikov equations. International Journal for Numerical Methods in Engineering 38: 1001–1020.

Roberts, T.M. 1985. Finite difference analysis of composite beams with partial interaction. Computers and Structures 21, 3: 469–473.

Salari, M.R., Spacone, E., Shing, P.B., Frangopol, D.M. 1998. Nonlinear analysis of composite beams with deformable shear connectors. Journal of Structural Engineering 124, 10: 1148–1158.

Salari, M.R., Spacone, E. 2001. Analysis of steel-concrete composite frames with bond-slip. Journal of Structural Engineering 127, 11: 1243–1250.

Schaffer E.L. 1965. An approach to the mathematical prediction of temmperature rise within a semi-infinite wood slab subjected to high-temperature conditions. Pyrodynamics 2: 117–132.

Schnabl, S., Planinc, I., Saje, M. in Turk, G. 2005. Točna analiza dvoslojnih nosilcev z upoštevanjem striga in zdrsa. = Exact solution of two-layered beams with shear and interlayer slip. V: Korelc, J. (ur.), Zupan, D. (ur.). Kuhljevi dnevi 2005. Podčetrtek, 22.–23. september 2005. Ljubljana: Slovensko društvo za mehaniko: str. 267–274.

Schnabl, S., Planinc, I. Saje, M. and Turk, G. 2006. A two-layer beam element with interlayer slip and shear: Paper 264. V: Topping, B.H.V. (ur.), Montero, G. (ur.), Montenegro, R. (ur.). Proceedings of the eight International conference on computational structures technology. Las Palmas de Gran Canaria, 12.–15. September 2006. Stirling: Civil-Comp: str. 615–616.

Schnabl, S., Saje, M., Turk, G. and Planinc, I. 2007. Analytical solution of two–layer beam taking into account interlayer slip and shear deformation. Journal of Structural Engineering ASCE 133, 6: 886–894.

Schnabl, S., Saje, M., Turk, G. and Planinc, I. 2007. Locking-free two-layer Timoshenko beam element with interlayer slip. Finite Elements in Analysis and Design 43: 705-714.

Schnabl, S., Planinc, I., Saje, M., Čas, B., Turk, G. 2006. An analytical model of layered continuous beams with partial interaction. Structural Engineering and Mechanics 22, 3: 263–278.

Schnabl, S., Turk, G. 2006. Numerical modelling of charring in timber beams exposed to fire : Paper 144. V: Topping, B.H.V. (ur.), Montero, G. (ur.), Montenegro, R. (ur.). Proceedings of the eight International conference on computational structures technology. Las Palmas de Gran Canaria, 12.–15. September 2006. Stirling: Civil-Comp: str. 319–320.

Schnabl, S., Turk, G. 2006. Coupled heat and moisture transfer in timber beams exposed to fire. V: WCTE 2006 : conference proceedings. Portland: s.n., 2006: str. 1–8.

Schnabl, S., Turk, G. 2006. Povezan prehod toplote in vlage v lesenih nosilcih pri požaru. = Coupled heat and moisture transfer in timber beams exposed to fire. V: Korelc, J. (ur.), Zupan, D. (ur.). Kuhljevi dnevi 2006. Lipica, 21.–22. september 2006. Ljubljana: Slovensko društvo za mehaniko: str. 239–246.

Seracino, R., Oehlers, D.J., Yeo, M.F. 2001. Partial-interaction flexural stresses in composite steel and concrete bridge beams. Engineering Structures 23: 1186–1193.

Simo, J.C. 1985. A finite strain beam formulation. The three-dimensional dynamic problem. Part I. Computer methods in applied mechanics and engineering 49: 55–70.

Soldatos, K.P., Watson, P. 1997. A general theory for accurate stress analysis of homogeneous and laminated composite beams. International Journal of Solids and Structures 34, 22: 2857–2885.

Suzuki, H., Chang T.P. 1979. Bending of laminated cantilever beams with interlayer slip. Journal of the Structural Division ASCE 105, 2: 269–281.

Takeda, H., Mehaffey, J.R. 1998. WALL2D: a model for predicting heat transfer through wood-stud walls exposed to fire. Fire and Materials 22: 133–140.

Takeda, H., 2003. A model to predict fire resistance of wood-stud walls. Fire and Materials 27: 19–39.

Theuns, E., Merci, B., Vierendeels, J., Vandevelde, P. 2005 Critical evaluation of an integral model for the pyrolysis of charring materials. Fire Safety Journal, 40: 121-140.

Thomas, H.R., Morgan, K., Lewis, R.W. 1980. A fully nonlinear analysis of heat and mass transfer problems in porous bodies. International Journal for Numerical Methods in Engineering 15: 1381–1393.

Thomas, G.C. 1997. Fire resistance of light timber timber framed walls and floors. Fire Engineering Research Report 97/7. University of CanterburyCanterbury, New Zeland: 318 f.

Thompson, E.G., Goodman, J.R., Vanderbilt, M.D. 1975. Finite element analysis of layered wood systems. Journal of Structural Division, Proceeding of ASCE 101, ST12: 2659–2672.

Timoshenko, S.P. 1921. On the correction for shear of the differential equation for transverse vibrations of prismatic bars. Philosophical Magazine, Series 6, 41: 744–746.

Turk, G. 1987. Programska oprema za račun nelinearnega in nestacionarnega prevajanja toplote z upoštevanjem raznih robnih pogojev in notranjega vira toplote zaradi hidratacije cementa. Diplomska naloga. Ljubljana, Univerza v Ljubljani, Fakulteta za arhitekturo gradbeništvo in geodezijo, Oddelek za gradbeništvo in geodezijo, Konstrukcijska smer.

Van der Linden, M.L.R. 1999. Timber-concrete composite floor systems. Ph.D Thesis, Delft, Delft University of Technology: 364 f.

Viest, I.M. 1960. Review of research on composite steel–concrete beams. Journal of the Structural Division, Proceeding of ASCE 86, 6: 1–21.

Vratanar, B., Saje, M. 1998. A consistent equilibrium in a cross-section of an elastic-plastic beam. International Journal of Solids and Structures ASCE 36, 7: 311–337.

Qin, M., Belarbi, R. 2005. Development of an analytical method for simultaneous heat and moisture transfer in building materials utilizing transfer function method. Journal of Materials in Civil Engineering 17, 5: 492–497.

Yang, L., Chen, X.,Zhou, X.,Fan, W. 2003. The pyrolysis and ignition of charring materials under an external heat flux. Combustion and Flame 133: 407-413.

Younsi, R., Kocaefe, D., Poncsak, S., Kocaefe, Y. 2006a. Thermal modelling of the high temperature treatment of wood based on Luikov's approach. International Journal of Energy Research 30: 699–711.

Younsi, R., Kocaefe, D., Poncsak, S., Kocaefe, Y. 2006b. A diffusion-based model for transient high temperature treatment of wood. Journal of Building Materials 30, 2: 113–135.

Younsi, R., Kocaefe, D., Poncsak, S., Kocaefe, Y. 2006c. Transient multiphase model for the high-temperature thermal treatment of wood. Fluid Mechanics and Transport Phenomena AIChE 52, 7: 2310–2657.

Younsi, R., Kocaefe, D., Kocaefe, Y. 2006. Three-dimensional simulation of heat and moisture transfer in wood. Applied Thermal Engineering 26: 1274–1285.

Wang, J.C. 1998. Deflection of steel-concrete composite beams with partial shear interaction. Journal of Structural Engineering ASCE 124, 10: 1159–1165.

Whitaker, S. 1977. Simultaneous heat, mass and momentum transfer in porous media: a theory of drying. Advances in Heat Transfer 22: 257–266.

White, R.H., Nordheim, E.V. 1992. Charring rate of wood for ASTM E 119 exposure. Fire Technology 28, 1: 5–30.

White, R.H., Tran, H.C. 2004. Charring rate of wood exposed to a constant heat flux. Wood and Fire Safety. Proceedings of the 3rd International Scientific Conference. The High Tatras, Slovak Republic, 18.–22. April: 175–183.

Wolfram, S. 2003. Mathematica, Addison-Wesley Publishing Company.

Wriggers, P. 1999. Finite elements for thermomechanical contact and adaptive finite element analysis of contact problems. International Centre for Mechanical Sciences, Courses and Lectures - No. 384, Chapter 4: 179–246.

Zienkiewich, O.C., Taylor, R.L. 1991. The finite element method. Volumen 2, McGraw-Hill, London: 403 f.

Zona, A. 2002. Finite element modelling of composite beams. Ph.D Thesis, Ancona, University of Ancona (Italy): 158 f.

Zona, A., Barbato, M., Conte, J.P. 2006. Finite element response sensitivity analysis of continuous steel-concrete composite girders. Steel and Composite Structures 6, 3: 183-202.

PRILOGE

Kot priloge so priloženi naslednji članki, ki so bili objavljeni oziroma so v tisku v revijah, ki so indeksirane v SCI:

A) Schnabl, S., Planinc, I., Saje, M., Čas, B., Turk, G. 2006. An analytical model of layered continuous beams with partial interaction. Structural Engineering and Mechanics 22, 3: 263–278.

B) Schnabl, S., Saje, M., Turk, G. and Planinc, I. 2007. Analytical solution of two–layer beam taking into account interlayer slip and shear deformation. Journal of Structural Engineering ASCE 133, 6: 886–894.

C) Schnabl, S., Saje, M., Turk, G. and Planinc, I. 2007. Locking-free two-layer Timoshenko beam element with interlayer slip. Finite Elements in Analysis and Design 43: 705–714.

D) Toratti, T., Schnabl, S., Turk, G. 2007. Reliability analysis of a glulam beam. Structural Safety. (v tisku)

Izmed prispevkov, ki so bili predstavljeni na različnih konferencah je priložen prispevek, ki je bil predstavljen na svetovni konferenci WCTE 2006:

E) Schnabl, S., Turk, G. 2006. Coupled heat and moisture transfer in timber beams exposed to fire. V: WCTE 2006 : conference proceedings. Portland: s.n., 2006: str. 1–8.

An analytical model of layered continuous beams with partial interaction

Simon Schnabl†, Igor Planinc‡, Miran Saje‡†, Bojan Čas‡‡ and Goran Turk‡‡†

University of Ljubljana, Faculty of Civil and Geodetic Engineering, Jamova 2, SI-1115 Ljubljana, Slovenia

(Received December 10, 2004, Accepted October 28, 2005)

Abstract. Starting with the geometrically non-linear formulation and the subsequent linearization, this paper presents a consistent formulation of the exact mechanical analysis of geometrically and materially linear three-layer continuous planar beams. Each layer of the beam is described by the geometrically linear beam theory. Constitutive laws of layer materials and relationships between interlayer slips and shear stresses at the interface are assumed to be linear elastic. The formulation is first applied in the analysis of a three-layer simply supported beam. The results are compared to those of Goodman and Popov (1968) and to those obtained from the formulation of the European code for timber structures, Eurocode 5 (1993). Comparisons show that the present and the Goodman and Popov (1968) results agree completely, while the Eurocode 5 (1993) results differ to a certain degree. Next, the analytical solution is used in formulating a general procedure for the analysis of layered continuous beams. The applications show the qualitative and quantitative effects of the layer and the interlayer slip stiffnesses on internal forces, stresses and deflections of composite continuous beams.

Key words: composite; layered beam; interlayer slip; mathematical model; analytical solution; elasticity.

1. Introduction

Due to their cost-effective construction and a good bearing capacity, layered composite systems are widely used in buildings and bridges. The behaviour of layered structures largely depends on the flexibility of a connection between the layers. Rigid connectors develop a full action between individual components, so that conventional principles of the solid beam analysis can be employed. Flexible connectors, on the other hand, permit the development of only partial interaction. As a result, an interlayer slip develops, with a sufficient magnitude to have a major effect on the deflection and stress distribution of the composite system.

When the force-slip relation of the connector is non-linear, which is usually the case, the response of the layered beam is also non-linear, even if component materials behave linearly. Consequently, the related non-linear mathematical model is described by the system of non-linear equations which

† Young Researcher
‡ Assistant Professor
‡† Professor, Corresponding author, E-mail: msaje@fgg.uni-lj.si
‡‡ Research Associate
‡‡† Associate Professor

can generally be solved only numerically. A variety of interesting formulations and numerical solution algorithms for the analysis of layered structures with continuous or discrete connectors has been proposed, e.g., Ayoub (2001), Ayoub and Filippou (2000), Čas *et al.* (2004a,b), Dall'Asta and Zona (2002), Fabbrocino *et al.* (2000), Faella *et al.* (2003), Fragiacomo *et al.* (2004), Gatessco (1999), Linden (1999), Oven *et al.* (1997), Thompson *et al.* (1975), Wheat and Calixto (1994), which consider, along with the non-linear tangential force-slip relation, also the non-linearity of material behaviour.

The building codes allow a structural engineer to perform a fully linear analysis for the determination of stress resultants. In a linear analysis, the governing equations of the mathematical model are linear and can be solved analytically. Many exact analytical solutions of simply supported, layered planar beams for combinations of simple loading cases and simple boundary conditions have been presented in professional literature, e.g., Adekola (1968), Cosenza and Pecce (2001), Fabbrocino *et al.* (2002), Girhammar and Gopu (1993), Girhammar and Pan (1993), Goodman and Popov (1968), Goodman and Popov (1969), Heinisuo (1988), Jasim (1997), Jasim and Mohamad (1997), Jasim (1999), Kristek and Studnicka (1982), Newmark *et al.* (1951), Nie *et al.* (2004), Ranzi and Bradford (2003), Silfwerbrand (1997), Smith and Teng (2001), Wang (1998). Some analytical solutions of two-layer continuous beams have also been presented (Jasim 1997, Plum and Horne 1975). Apart from the above presented numerical and analytical solutions a lot of experiments have been conducted on simply supported and continuous two-layer composite beams, e.g., Ansourian (1981), Newmark *et al.* (1951), Plum and Horne (1975), Wheat and Calixto (1994). On the other hand, there exist only few reports about experiments on simply supported three-layer composite beams (Goodman and Popov 1968, McCutheon 1986). To the author's best knowledge, there seems to be no exact solution reported on multilayered (three layers or more) simply supported and continuous beams having different material and geometric characteristics of layers. The present paper aims to fill the gap. Our formulation of the planar layered beam uses the following assumptions: (1) material is linear elastic; (2) displacements, strains and rotations are small; (3) shear deformations are disregarded (the 'Euler-Bernoulli beam'); (4) strains vary linearly over each layer (the 'Bernoulli hypothesis'); (5) the layers are continuously connected and the slip modulus of the connection is constant; (6) friction between the layers is not considered; (7) the bending strain is the same for all layers; (8) the number of layers is arbitrary; (9) the shapes of the cross-sections are symmetrical with respect to the deformation plane and preserve unchanged form and size during deformation.

For the purpose of clarity of presentation, our derivation is limited to the three-layer beam. The generalization to the multilayered beams is straightforward.

2. Basic non-linear equations of a three-layer beam and their linearization

Due to the exact geometrical introduction of interlayer slips between the layers, we started the derivation of our formulation with the non-linear kinematic and equilibrium equations first presented by Reissner (1972). After the linearization of Reissner's equations and taking into consideration the introduced assumptions, the simplified linear formulation of the three-layer beam with an interlayer slip is derived. Alternatively, the same linearized equilibrium equations can be obtained, if the linear kinematic equations are introduced in the principal of virtual displacements as constraining equations. However, in order to understand the actual kinematics, we belive it is important to start

the derivation from the exact formulation. The present formulation assumes that the effect of shear strains is negligible. Our further assumption is that an interlayer tangential slip can occur at the interface between the layers, but no delamination or transverse separation between them is possible.

The mechanical behaviour of the composite beam is governed by the system of kinematic, equilibrium, and constitutive equations, combined with natural and essential boundary conditions for each layer, and with the constraining conditions for the contact between the layers.

2.1 Kinematic, equilibrium and constitutive equations

2.1.1 Kinematic equations

We consider an initially straight, planar, layered beam element of undeformed length L. Without a loss of generality, we assume that the layered beam element is made up of three layers. Layers are marked by letters a, b and c (see Fig. 1). The beam element is placed in the (x, z)-plane of a spatial Cartesian coordinate system with coordinates (x, y, z) and unit base vectors $\mathbf{E}_x$, $\mathbf{E}_y$, $\mathbf{E}_z$. The undeformed reference axis of the layered beam element is common to all layers and is assumed to coincide with the geometric centroidal axis of the undeformed layered beam element. The layered beam element is subjected to conservative distributed loads p_x, p_z and m_y only along the span of layer c, and to generalized forces S_i^a, S_i^b and S_i^c (i =1, 2, ..., 6) at the ends of layers a, b and c.

The deformed configurations of layers a, b and c are defined by vector-valued functions

$$\begin{aligned}
\mathbf{R}^a(x, z) &= (x + u^a(x) + z\varphi^a(x))\mathbf{E}_x + (z + w^a(x))\mathbf{E}_z \\
\mathbf{R}^b(x^*, z) &= (x^* + u^b(x^*) + z\varphi^b(x^*))\mathbf{E}_x + (z + w^b(x^*))\mathbf{E}_z \\
\mathbf{R}^c(x^{**}, z) &= (x^{**} + u^c(x^{**}) + z\varphi^c(x^{**}))\mathbf{E}_x + (z + w^c(x^{**}))\mathbf{E}_z
\end{aligned} \tag{1}$$

In Eqs. (1) and in all further expressions, the notations $(\bullet)^a$, $(\bullet)^b$ and $(\bullet)^c$ mark that quanatities $(\bullet)$ are related to layer a, b or c. Functions u^a, w^a, φ^a denote the components of the displacement vector and the rotation angle of layer a at the reference axis with respect to the base vectors $\mathbf{E}_x$, $\mathbf{E}_z$ and $\mathbf{E}_y$, respectively. Variables u^b, w^b, φ^b, u^c, w^c, φ^c are related to layers b and c.

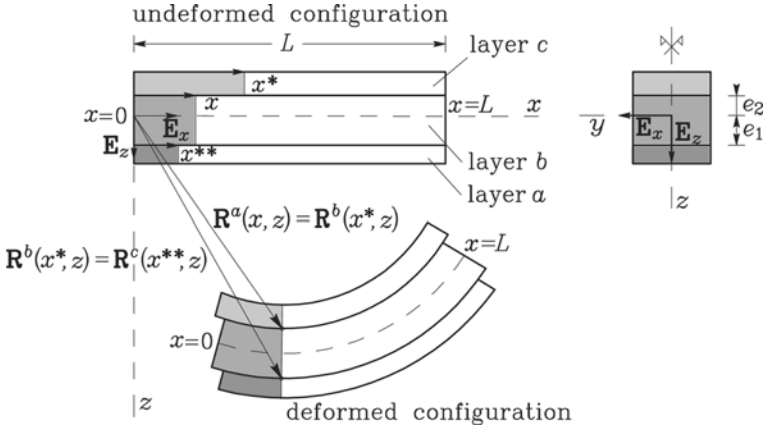

Fig. 1 Undeformed and deformed configuration of the three-layer beam

If the effect of shear strains is neglected, Reissner's equations read (Reissner 1972)

$$\begin{aligned} 1 + u' - (1 + \varepsilon)\cos\varphi &= 0 \\ w' + (1 + \varepsilon)\sin\varphi &= 0 \\ \varphi' - \kappa &= 0 \end{aligned} \tag{2}$$

In Eqs. (2) the prime ($'$) denotes the derivative with respect to x, whereas the functions ε, φ and κ mark the extensional strain (or the specific elongation), the rotation and the bending strain of the reference axis, respectively.

The linearized kinematic equations are obtained by the linearization of Eqs. (2) around the undeformed configuration for each layer. After the linearization has been completed, we obtain

$$\begin{aligned} &\delta u^{a\prime} - \delta\varepsilon^a = 0 \qquad \delta u^{b\prime} - \delta\varepsilon^b = 0 \qquad \delta u^{c\prime} - \delta\varepsilon^c = 0 \\ &\delta w^{a\prime} + \delta\varphi^a = 0 \qquad \delta w^{b\prime} + \delta\varphi^b = 0 \qquad \delta w^{c\prime} + \delta\varphi^c = 0 \\ &\delta\varphi^{a\prime} - \delta\kappa^a = 0 \qquad \delta\varphi^{b\prime} - \delta\kappa^b = 0 \qquad \delta\varphi^{c\prime} - \delta\kappa^c = 0 \end{aligned} \tag{3}$$

Here, $\delta u^{a\prime}, \delta\varepsilon^a, \ldots, \delta\kappa^c$ are the variations of the independent variables. As the independent variables $[u^{a\prime}, \varepsilon^a, \ldots, \kappa^c]$ are zero in the undeformed configuration, we can without any loss of clarity of the presentation change the notations and drop the variation sign 'δ'. Eqs. (3) will then assume the form

$$\begin{aligned} &u^{a\prime} - \varepsilon^a = 0 \qquad u^{b\prime} - \varepsilon^b = 0 \qquad u^{c\prime} - \varepsilon^c = 0 \\ &w^{a\prime} + \varphi^a = 0 \qquad w^{b\prime} + \varphi^b = 0 \qquad w^{c\prime} + \varphi^c = 0 \\ &\varphi^{a\prime} - \kappa^a = 0 \qquad \varphi^{b\prime} - \kappa^b = 0 \qquad \varphi^{c\prime} - \kappa^c = 0 \end{aligned} \tag{4}$$

u^a, u^b, u^c, w^a, w^b, w^c, ε^a, ε^b, ε^c, κ^a, κ^b, κ^c, φ^a, φ^b, φ^c now play the role of displacements, strains and rotations of the linearized theory. These variables are assumed to be small.

The geometric or total extensional strains, D^a, D^b and D^c, of an arbitrary fibre in layers a, b and c are functions of extensional strains ε^a, ε^b and ε^c and bending strains κ^a, κ^b and κ^c of the reference axes of the layers. According to Bernoulli's hypothesis, they are linear functions of z

$$\begin{aligned} D^a(x,z) &= \varepsilon^a(x) + z\,\kappa^a(x) \\ D^b(x,z) &= \varepsilon^b(x) + z\,\kappa^b(x) \\ D^c(x,z) &= \varepsilon^c(x) + z\,\kappa^c(x) \end{aligned} \tag{5}$$

The substitution of ε^a, ε^b, ε^c with u^a, u^b, u^c using Eqs. (4) gives

$$\begin{aligned} u^{a\prime}(x) - D^a(x,z) + z\,\kappa^a(x) &= 0 \\ u^{b\prime}(x) - D^b(x,z) + z\,\kappa^b(x) &= 0 \\ u^{c\prime}(x) - D^c(x,z) + z\,\kappa^c(x) &= 0 \end{aligned} \tag{6}$$

2.1.2 Equilibrium equations

When in equilibrium, the axial force $\mathcal{N}$, the shear force $\mathcal{Q}$, the bending moment $\mathcal{M}$, and the distributed loads p_x, p_z and m_y, must satisfy the equilibrium equations (Reissner 1972)

$$\begin{aligned} \mathcal{N}' + p_x &= 0 \\ \mathcal{Q}' + p_z &= 0 \\ \mathcal{M}' - (1+\varepsilon)\mathcal{Q} + m_y &= 0 \end{aligned} \tag{7}$$

Once the equilibrium equations have been written for all three layers and linearized, they read

$$\begin{aligned} &\mathcal{N}^{a\prime} - p_t^{ab} = 0 \qquad \mathcal{N}^{b\prime} + p_t^{ab} - p_t^{bc} = 0 \qquad \mathcal{N}^{c\prime} + p_x + p_t^{bc} = 0 \\ &\mathcal{Q}^{a\prime} + p_n^{ab} = 0 \qquad \mathcal{Q}^{b\prime} - p_n^{ab} + p_n^{bc} = 0 \qquad \mathcal{Q}^{c\prime} - p_n^{bc} + p_z = 0 \\ &\mathcal{M}^{a\prime} - \mathcal{Q}^a - p_t^{ab} e_1 = 0 \qquad \mathcal{M}^{b\prime} - \mathcal{Q}^b + p_t^{ab} e_1 + p_t^{bc} e_2 = 0 \qquad \mathcal{M}^{c\prime} - \mathcal{Q}^c - p_t^{bc} e_2 = 0 \end{aligned} \tag{8}$$

Here p_t^{ab}, p_t^{bc} and p_n^{ab}, p_n^{bc} represent the tangential and normal interlayer contact tractions. The distances from the reference axis to the contact planes between the layers are denoted by e_1 and e_2 (Fig. 1).

2.1.3 Constitutive equations

The third set of the basic equations is provided by the constitutive law. The constitutive law relates the stress resultants, i.e., the generalized forces $\mathcal{N}_C^a, \mathcal{N}_C^b, \mathcal{N}_C^c, \mathcal{M}_C^a, \mathcal{M}_C^b, \mathcal{M}_C^c$ to the equilibrium internal forces, $\mathcal{N}^a, \mathcal{N}^b, \mathcal{N}^c, \mathcal{M}^a, \mathcal{M}^b, \mathcal{M}^c$, which are the solutions of Eqs. (8). These relations assume the form

$$\begin{aligned} &\mathcal{N}^a - \mathcal{N}_C^a(\varepsilon^a, \kappa^a) = 0 \qquad \mathcal{M}^a - \mathcal{M}_C^a(\varepsilon^a, \kappa^a) = 0 \\ &\mathcal{N}^b - \mathcal{N}_C^b(\varepsilon^b, \kappa^b) = 0 \qquad \mathcal{M}^b - \mathcal{M}_C^b(\varepsilon^b, \kappa^b) = 0 \\ &\mathcal{N}^c - \mathcal{N}_C^c(\varepsilon^c, \kappa^c) = 0 \qquad \mathcal{M}^c - \mathcal{M}_C^c(\varepsilon^c, \kappa^c) = 0 \end{aligned} \tag{9}$$

We postulate that layer material is linear elastic. Therefore, Eqs. (9) are assumed to be given by the linear relations with respect to ε and κ:

$$\begin{aligned} &\mathcal{N}_C^a = C_{11}^a \varepsilon^a + C_{12}^a \kappa^a \qquad \mathcal{M}_C^a = C_{21}^a \varepsilon^a + C_{22}^a \kappa^a \\ &\mathcal{N}_C^b = C_{11}^b \varepsilon^b + C_{12}^b \kappa^b \qquad \mathcal{M}_C^b = C_{21}^b \varepsilon^b + C_{22}^b \kappa^b \\ &\mathcal{N}_C^c = C_{11}^c \varepsilon^c + C_{12}^c \kappa^c \qquad \mathcal{M}_C^c = C_{21}^c \varepsilon^c + C_{22}^c \kappa^c \end{aligned} \tag{10}$$

in which material and geometrical constants are marked by $C_{11}^a, C_{12}^a, \ldots, C_{22}^c$; e.g., $C_{22}^a = E_a J_a$, where E_a is elastic modulus of layer a, and J_a is the moment of inertia of layer a with respect to the geometric centroidal point of the whole cross-section.

2.2 Constraining equations

The constraining equations define the conditions that assemble an individual layer into a layered composite beam.

As already stated, the transverse separation or penetration between the layers is not allowed. This fact is expressed by the requirements

$$\begin{aligned} \mathbf{R}^a(x, z) &= \mathbf{R}^b(x^*, z) \\ \mathbf{R}^b(x^*, z) &= \mathbf{R}^c(x^{**}, z) \end{aligned} \tag{11}$$

where $x \in \mathcal{I}^a, x^* \in \mathcal{I}^b$ are undeformed coordinates of two distinct particles of layers a and b which are in the deformed state in contact, and thus their vector-valued functions $\mathbf{R}^a(x, z)$ and $\mathbf{R}^b(x^*, z)$ coincide. Similarly, $x^{**} \in \mathcal{I}^c$ is a material, undeformed coordinate of particle of layer c, which is in the deformed state in contact with particle of layer b, and therefore their vector-valued functions $\mathbf{R}^b(x^*, z)$ and $\mathbf{R}^c(x^{**}, z)$ in the deformed state coincide (see Fig. 1). The contact regions of layers a, b and c are marked by $\mathcal{I}^a$, $\mathcal{I}^b$, $\mathcal{I}^c$. Eqs. (11) are rewritten in a more convenient component form:

$$\begin{aligned} x + u^a(x) &= x^* + u^b(x^*) \\ x^* + u^b(x^*) &= x^{**} + u^c(x^{**}) \\ w^a(x) &= w^b(x^*) \\ w^b(x^*) &= w^c(x^{**}) \end{aligned} \tag{12}$$

The relative tangential displacement (slip) that occurs between the two particles which coincide in the undeformed configuration is denoted by Δ. By definition, it is the difference of the deformed arc-lengths of contact curves of layers a and b, and b and c. For a geometrically linear layered beam theory, the arc-length differences can easily be calculated and are simply given by

$$\Delta^{ab} = U^a - U^b \qquad \Delta^{bc} = U^b - U^c \tag{13}$$

U^a, U^b, U^c denote displacements of a particular material particle of the related layer at the interlayer contact.

In general, the flexibility of the contact highly depends on the characteristics of layer materials and on the way the contact is enforced. The constitutive law of the bond slip between the layers generally assumes the form

$$p_t^{ab} = \mathcal{F}^{ab}(\Delta^{ab}) \qquad p_t^{bc} = \mathcal{F}^{bc}(\Delta^{bc}) \tag{14}$$

where $\mathcal{F}^{ab}$ and $\mathcal{F}^{bc}$ can be arbitrary non-linear functions. In the present paper, however, we will assume the linear relationships between p_t and Δ, see Eqs. (30), as it is generally proposed by structural engineering standards (e.g., Eurocode 5(1993)). In this case the analytical solution of the problem can be derived. On the other hand, if the problem is solved numerically, a general non-linear relationship in Eqs. (14) can be assumed.

2.3 System of equations of a three-layer beam with an interlayer slip

Since deformations, displacements and rotations are assumed to be small quantities, the generalized equilibrium equations can further be simplified using the following two assumptions (see, e.g., Čas *et al*. 2004b): (i) $dx \cong dx^* \cong dx^{**}$; (ii) bending strains of the reference axis of individual layers are equal $\kappa^a(x) = \kappa^b(x^*) = \kappa^c(x^{**}) = \kappa(x)$. Consequently, $\varphi^a(x) = \varphi^b(x^*) = \varphi^c(x^{**}) = \varphi(x)$, $w^a(x) = w^b(x^*) = w^c(x^{**}) = w(x)$, $\mathcal{I}^a \cong \mathcal{I}^b \cong \mathcal{I}^c = [0, L]$. Thus, $(\bullet)^b(x^*) = (\bullet)^b(x)$, $(\bullet)^c(x^{**}) = (\bullet)^c(x)$ holds true for any quantity of layers b and c, e.g., $u^c(x^{**}) = u^c(x)$. Kinematic, equilibrium and constraining equations can now be considerably simplified. After considering the assumptions mentioned above, we can decompose the basic equations of the three-layer beam with an interlayer slip into two separate systems of differential and algebraic equations (see, e.g., Čas *et al*. 2004b):

$$u^{a\prime} - \varepsilon^a = 0 \tag{15}$$

$$u^{b\prime} - \varepsilon^b = 0 \tag{16}$$

$$u^{c\prime} - \varepsilon^c = 0 \tag{17}$$

$$w' + \varphi = 0 \tag{18}$$

$$\varphi' - \kappa = 0 \tag{19}$$

$$\mathcal{N}^{a\prime} - p_t^{ab} = 0 \tag{20}$$

$$\mathcal{N}^{b\prime} + p_t^{ab} - p_t^{bc} = 0 \tag{21}$$

$$\mathcal{N}^{c\prime} + p_t^{bc} + p_x = 0 \tag{22}$$

$$(\mathcal{Q}^a + \mathcal{Q}^b + \mathcal{Q}^c)' + p_z = 0 \rightarrow \mathcal{Q}' + p_z = 0 \tag{23}$$

$$(\mathcal{M}^a + \mathcal{M}^b + \mathcal{M}^c)' - (\mathcal{Q}^a + \mathcal{Q}^b + \mathcal{Q}^c) + m_y = 0 \rightarrow \mathcal{M}' - \mathcal{Q} + m_y = 0 \tag{24}$$

$$\mathcal{N}^a = \mathcal{N}_C^a = C_{11}^a \varepsilon^a + C_{12}^a \kappa \tag{25}$$

$$\mathcal{N}^b = \mathcal{N}_C^b = C_{11}^b \varepsilon^b + C_{12}^b \kappa \tag{26}$$

$$\mathcal{N}^c = \mathcal{N}_C^c = C_{11}^c \varepsilon^c + C_{12}^c \kappa \tag{27}$$

$$\mathcal{M} = \mathcal{M}_C^a + \mathcal{M}_C^b + \mathcal{M}_C^c \rightarrow \mathcal{M} = C_{21}^a \varepsilon^a + C_{21}^b \varepsilon^b + C_{21}^c \varepsilon^c + (C_{22}^a + C_{22}^b + C_{22}^c)\kappa \tag{28}$$

$$\begin{aligned} \Delta^{ab} &= u^a - u^b \\ \Delta^{bc} &= u^b - u^c \end{aligned} \tag{29}$$

$$\begin{aligned} p_t^{ab} &= \mathcal{F}^{ab}(\Delta^{ab}) \rightarrow p_t^{ab} = K^{ab}\Delta^{ab} \\ p_t^{bc} &= \mathcal{F}^{bc}(\Delta^{bc}) \rightarrow p_t^{bc} = K^{bc}\Delta^{bc} \end{aligned} \tag{30}$$

and

$$x + u^a = x^* + u^b \rightarrow x^* = x + \Delta^{ab} \tag{31}$$

$$x^* + u^b = x^{**} + u^c \rightarrow x^{**} = x^* + \Delta^{bc} \tag{32}$$

$$\mathcal{Q}^{a\prime} + p_n^{ab} = 0, \quad \mathcal{Q}^{b\prime} - p_n^{ab} + p_n^{bc} = 0 \tag{33}$$

$$\mathcal{M}^{a\prime} - \mathcal{Q}^a = 0, \quad \mathcal{M}^{b\prime} - \mathcal{Q}^b = 0 \tag{34}$$

$$\mathcal{M}^a = \mathcal{M}_C^a = C_{21}^a \varepsilon^a + C_{22}^a \kappa \quad \text{and} \quad \mathcal{M}^b = \mathcal{M}_C^b = C_{21}^b \varepsilon^b + C_{22}^b \kappa \tag{35}$$

$$\mathcal{Q} = \mathcal{Q}^a + \mathcal{Q}^b + \mathcal{Q}^c \tag{36}$$

$$\mathcal{M} = \mathcal{M}^a + \mathcal{M}^b + \mathcal{M}^c \tag{37}$$

Eqs. (15)-(30) consist of 18 equations for 18 unknown functions u^a, u^b, u^c, w, φ, ε^a, ε^b, ε^c, κ, $\mathcal{N}^a$, $\mathcal{N}^b$, $\mathcal{N}^c$, $\mathcal{Q}$, $\mathcal{M}$, Δ^{ab}, Δ^{bc}, p_t^{ab}, p_t^{bc}, whereas Eqs. (31)-(37) constitute a system of ten equations for ten unknown functions $x^*, x^{**}, p_n^{ab}, p_n^{bc}$, $\mathcal{Q}^a$, $\mathcal{Q}^b$, $\mathcal{Q}^c$, $\mathcal{M}^a$, $\mathcal{M}^b$, $\mathcal{M}^c$. In Eqs. (30), K^{ab} and K^{bc} denote the slip moduli of connections.

3. Solution algorithm

If the slips between the layers are known functions of x, the solution of the system of Eqs. (15)-(37) can easily be obtained with the following sequence of tasks.

In the first step, we integrate Eqs. (23) and (24) and obtain the expressions for the total equilibrium shear force and the total equilibrium bending moment of the three-layer beam element:

$$\begin{aligned} \mathcal{Q}(x) &= \mathcal{Q}(0) - \int_0^x p_z(\xi)d\xi \\ \mathcal{M}(x) &= \mathcal{M}(0) + \int_0^x (\mathcal{Q}(\xi) - m_y(\xi))d\xi \end{aligned} \tag{38}$$

In the second step, we twice differentiate Eqs. (29) with respect to x and insert Eqs. (15)-(16). The following differential equations for the interlayer slips emerge

$$\begin{aligned} \Delta^{ab\prime\prime} &= \varepsilon^{a\prime} - \varepsilon^{b\prime} \\ \Delta^{bc\prime\prime} &= \varepsilon^{b\prime} - \varepsilon^{c\prime} \end{aligned} \tag{39}$$

The derivatives $\varepsilon^{a\prime}$, $\varepsilon^{b\prime}$ and $\varepsilon^{c\prime}$ are obtained by the differentiation of Eqs. (25)-(28) with respect to

x. Solving the differentiated Eqs. (25)–(28) for $\varepsilon^{a\prime}$, $\varepsilon^{b\prime}$, $\varepsilon^{c\prime}$ and κ' yields

$$\begin{Bmatrix} \varepsilon^{a\prime} \\ \varepsilon^{b\prime} \\ \varepsilon^{c\prime} \\ \kappa' \end{Bmatrix} = \mathbf{C}^{-1} \begin{Bmatrix} \mathcal{N}^{a\prime} \\ \mathcal{N}^{b\prime} \\ \mathcal{N}^{c\prime} \\ \mathcal{M}' \end{Bmatrix} \tag{40}$$

$\mathbf{C}$ is the matrix of constitutive constants (see Eqs. (10)), and $\mathbf{C}^{-1}$ is its inverse:

$$\mathbf{C}^{-1} = \begin{bmatrix} C_{11}^a & 0 & 0 & C_{12}^a \\ 0 & C_{11}^b & 0 & C_{12}^b \\ 0 & 0 & C_{11}^c & C_{12}^c \\ C_{21}^a & C_{21}^b & C_{21}^c & C_{22}^a + C_{22}^b + C_{22}^c \end{bmatrix}^{-1} = \begin{bmatrix} D_{11} & 0 & 0 & D_{14} \\ 0 & D_{22} & 0 & D_{24} \\ 0 & 0 & D_{33} & D_{34} \\ D_{41} & D_{42} & D_{43} & D_{44} \end{bmatrix} \tag{41}$$

When Eqs. (20)-(24), (30) and (40) are inserted into Eqs. (39), we obtain a system of two second-order linear differential equations with constant coefficients for the slips between layers *a, b* and *c*

$$\begin{aligned} \Delta^{ab\prime\prime} - A^{ab}\Delta^{ab} + B^{ab}\Delta^{bc} &= f^{ab} \\ \Delta^{bc\prime\prime} + A^{bc}\Delta^{ab} - B^{bc}\Delta^{bc} &= f^{bc} \end{aligned} \tag{42}$$

with A^{ab}, B^{ab}, A^{bc}, B^{bc} and f^{ab}, f^{bc} being constants

$$\begin{aligned} A^{ab} &= K^{ab}(D_{11} + D_{22}) \qquad B^{ab} = K^{bc}D_{22} \\ A^{bc} &= K^{ab}D_{22} \qquad B^{bc} = K^{bc}(D_{22} - D_{33}) \end{aligned} \tag{43}$$

$$\begin{aligned} f^{ab} &= (D_{14} - D_{24})(\mathcal{Q} - m_y) \\ f^{bc} &= D_{22}p_x + (D_{34} - D_{24})(\mathcal{Q} - m_y) \end{aligned} \tag{44}$$

Boundary conditions associated with Eqs. (42) are the values of the interlayer slips at the edges $x = 0$ and $x = L$ of the beam element. An exact solution of Eqs. (42) was obtained by MATHEMATICA (2003). After the slips have been obtained, the remaining equations of the system (15)-(30) can simply be solved. We first determine the boundary rotations and displacements from the system of linear equations

$$\mathbf{K}_T\mathbf{u} = \mathbf{g} \tag{45}$$

for the composite structure. In Eq. (45), $\mathbf{K}_T$ denotes the tangent stiffness matrix, $\mathbf{u}$ is the vector of end-point displacements, and $\mathbf{g}$ is the load vector. Once $\mathbf{u}$ has been known, the values of the end forces can easily be computed. This step completes the solution of the system (15)-(30) for unknown functions u^a, u^b, u^c, w, φ, ε^a, ε^b, ε^c, κ, $\mathcal{N}^a$, $\mathcal{N}^b$, $\mathcal{N}^c$, $\mathcal{Q}$, $\mathcal{M}$, Δ^{ab}, Δ^{bc}, p_t^{ab}, p_t^{bc}. Finally, the unknown functions x^*, x^{**}, p_n^{ab}, p_n^{bc}, $\mathcal{Q}^a$, $\mathcal{Q}^b$, $\mathcal{Q}^c$, $\mathcal{M}^a$, $\mathcal{M}^b$, $\mathcal{M}^c$ are obtained from Eqs. (31)-(37).

The interlayer tractions in the normal direction of the contact are obtained from equations

$$\begin{aligned} p_n^{ab} &= -\mathcal{M}_C^{a\prime\prime} - p_t^{ab\prime} e_1 \\ p_n^{bc} &= -\mathcal{M}_C^{b\prime\prime} - p_t^{ab\prime} e_1 - p_t^{bc\prime} e_2 + p_n^{ab} \end{aligned} \tag{46}$$

which are derived if we insert Eqs. (33) into Eqs. (34).

4. Numerical examples

Numerical examples will demonstrate the ability of the present exact analytical model for the stress-strain analysis of the three-layer simply supported and continuous beams with partial interaction between the layers the geometric and material characteristics of which may vary over the cross-section. They will describe accurately the behaviour of layered beams at small elastic strains and will also provide for the referential, or bench-mark solutions suitable for assessing the accuracy of new finite element formulations. We consider two cases: (i) a simply supported three-layer beam; and (ii) a continuous three-layer beam over two spans.

4.1 A simply supported three-layer beam

The geometrically and materially linear models of two-layer beams are often encountered in literature (see, e.g., Adekola 1968, Cosenza and Peece 2001, Čas *et al.* 2004b, Girhammar and Gopu 1993, Girhammar and Pan 1993, Goodman and Popov 1968, 1969, Jasim 1997, 1999, Jasim and Mohamad 1997, Kristek and Studnicka 1982, Newmark *et al.* 1951, Plum and Horne 1975, Ranzi and Bradford 2003, Rassam and Goodman 1971, Smith and Teng 2001).

In contrast, the analytical solution for the three-layer simply supported composite beam appears only to be derived by Goodman and Popov (1968). Moreover, some experiments have been conducted on these types of beams. They analysed a simply supported three-layer beam subjected to force P at the mid-span of the timber beam, with layers of equal thickness and made up of the same wood material. Here, we analyse this simply supported three-layer beam subjected both to point load and uniformly distributed load. The descriptive geometric, material and loading data are given in Fig. 2.

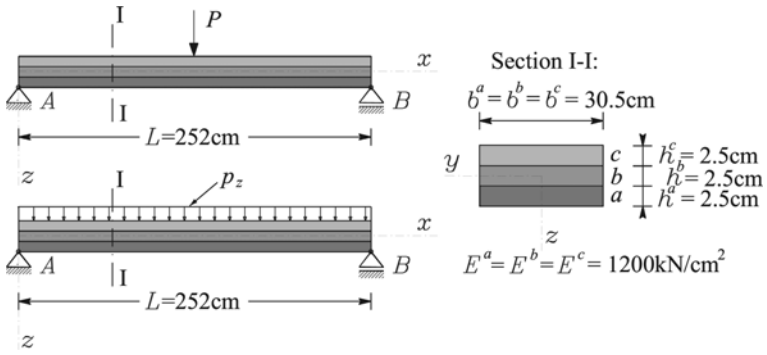

Fig. 2 Simply supported three-layer beam

The contributions of the connection flexibility to the vertical deflections at the mid-span have been calculated for various values of the slip moduli of connections and are shown in Tables 1 and 2 for the comparison reasons in the numerical form rather than graphically. The tables also present the comparisons with the results in Goodman and Popov (1968), and with the results given by Eurocode 5 formulae (1993). The results are presented for the range of the slip modulus from 0.01 to 100 kN/cm^2. Observe that the results of Goodman and Popov (1968) and of the present formulation are in perfect agreement both for the point and the distributed load. Since, the validation of Goodman and Popov mathematical model shows excellent agreement with all their

Table 1 Simply supported three-layer beam subjected to the point load. The contribution of the flexible connection to the vertical deflections in cm as a function of slip modulus, $K = K^{ab} = K^{bc}$. Deflection of a solid beam is 0.246 cm.

P = 1 kN				
K [kN/cm^2]	Goodman (1968)	Present	EC 5 (1993)	EC 5 (1993) relative error [%]
0.01	1.953	1.953	1.953	–0.01
0.1	1.852	1.852	1.852	–0.08
0.5	1.506	1.506	1.499	0.39
1	1.222	1.222	1.212	0.76
2	0.899	0.899	0.877	1.45
3	0.701	0.701	0.686	2.06
4	0.579	0.579	0.564	2.62
5	0.494	0.494	0.479	3.12
10	0.287	0.287	0.273	5.13
100	0.035	0.035	0.031	13.56

Table 2 Simply supported three-layer beam subjected to the uniform load. The contribution of the flexible connection to the vertical deflections in cm as a function of slip modulus, $K = K^{ab} = K^{bc}$. Deflection of a solid beam is 0.386 cm.

p_z = 1 kN/m				
K [kN/cm^2]	Goodman (1968)	Present	EC 5 (1993)	EC 5 (1993) relative error [%]
0.01	3.069	3.069	3.069	0.00
0.1	2.907	2.907	2.908	0.02
0.5	2.355	2.355	2.357	0.10
1	1.902	1.902	1.906	0.20
2	1.373	1.373	1.378	0.37
3	1.073	1.073	1.079	0.52
4	0.881	0.881	0.887	0.66
5	0.747	0.747	0.753	0.78
10	0.423	0.423	0.429	1.24
100	0.048	0.048	0.049	2.52

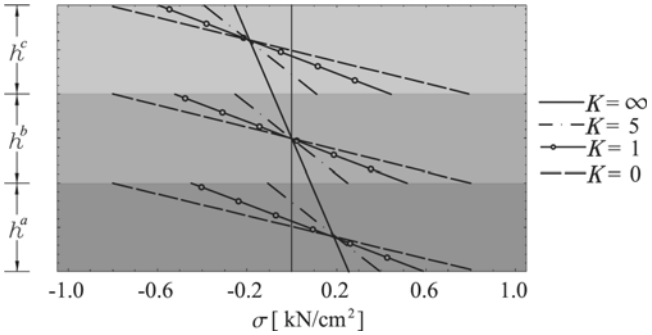

Fig. 3 Simply supported three-layer beam subjected to point load. The distribution of the normal stresses over the cross-section.

experimental results, we can conclude that the present formulation is in good correlation with the experiments performed on three-layer beams subjected to serviceability loads.

When the beam is subjected to the point load, the analytical values for the contributions to the vertical deflections at small values of interlayer slip modulus ($K < 1$ kN/m^2) are almost equal to those in Eurocode 5 (1993), although Eurocode 5 limits its application to the distributed load. For higher values of slip moduli, they are somewhat smaller. Thus, we see that Eurocode 5 (1993) gives rather accurate deflections (although somewhat smaller) even in the case of a point load.

When the beam is subjected to the uniformly distributed load, the Eurocode 5 (1993) results practically agree with the analytical results for any K.

The values in Table 2 indicate that the contributions to the deflections due to the nonstiff interaction between the layers may be as big as about 8-times the deflections in rigidly connected layered beam, which is equal to 0.386 cm.

One of the basic assumptions of the Goodman and Popov (1968) model is that the thicknesses of layers are equal, which leads to the assumption that the bending moments and the axial forces are equal in each layer. This assumption holds, provided that the layers have identical material and geometric characteristics. However, it may cause large errors in results, if this criterion is not fulfilled, as can be seen in the example below.

The distributions and the values of the normal stresses in the layers are very much affected by the degree of the contact rigidity. The effect is depicted in Fig. 3 for stiffnesses $K = 0$, 1, 5 and ∞. The stress distributions over the mid-point section of the beam subjected to the point load are shown. We can see that the peak values of the stress in each layer increase with the decreasing stiffness of the contact, the values with regard to the absolutely stiff contact being substantially larger. Note that for the flexible contact, the stresses in each layer vary from tension on the bottom side of the layer to compression on its top (the 'zig zag' variation).

4.2 A continuous three-layer timber beam over two spans

We study a continuous three-layer beam the layers of which are made up of timber of strength classes defined in Eurocode 5 (1993). In addition, slip moduli between the layers are different: $K^{ab} = 3$ kN/cm^2 and $K^{bc} = 0.01$ kN/cm^2. The continuous beam is subjected to the uniformly distributed load $p_z = 0.01$ kN/cm. The geometric, material and loading data are given in Fig. 4.

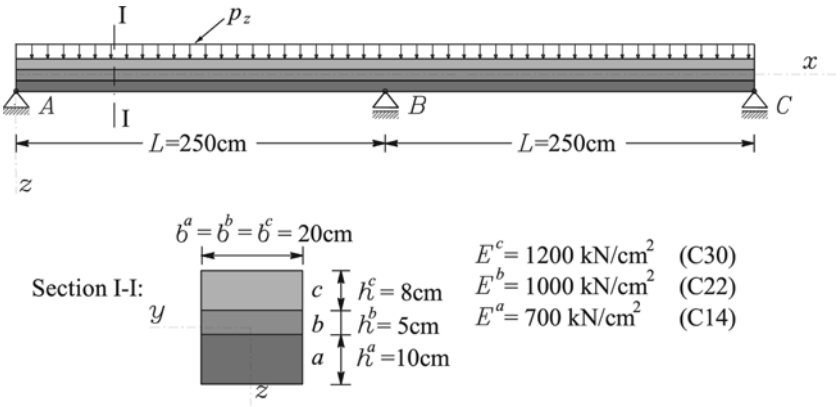

Fig. 4 Continuous three-layer beam over two spans

Table 3 Continuous beam over two spans (Fig. 4). Displacements and rotations at nodal points

u_b^A	u_c^A	φ^A	u_a^B	$u_b^B = u_c^B$	φ^B	u_a^C	u_b^C	u_c^C	φ^C
–0.064	–0.151	–0.011	–0.065	–0.065	0	–0.131	–0.067	0.021	0.012

Table 4 Continuous beam over two spans (Fig. 4). Internal forces at nodes A and B

Node A	Node B				
$\mathcal{Q}_{e1}(0)$	$\mathcal{N}_{e2}^a(0)$	$\mathcal{N}_{e2}^b(0)$	$\mathcal{N}_{e2}^c(0)$	$\mathcal{Q}_{e2}(0)$	$\mathcal{M}_{e2}(0)$
9.53 kN	–5.38 kN	5.39 kN	–0.01 kN	15.47 kN	–743.04 kNcm

The values of the nodal displacements and rotations are presented in Table 3. The displacements are given in centimeters and the rotations in radians.

The axial and shear forces and the bending moment in layers a, b, c at nodal points are shown in Table 4. Only the non-zero values are shown.

Fig. 5 shows the variations of Δ^{ab}, Δ^{bc}, $\mathcal{N}$, $\mathcal{Q}$, $\mathcal{M}$ along the axis of each layer. It can be seen that the interlayer slips reach their maxima at the end supports. Graphs of slips Δ^{ab} and Δ^{bc} nearly agree. The lower (a) and the upper layer (c) are subjected to a considerable axial force in contrast to the intermediate layer (b), the axial force of which is negligible. The resultant axial force of the composite beam is, obviously, equal to zero ($\mathcal{N} = \mathcal{N}^a + \mathcal{N}^b + \mathcal{N}^c = 0$). Note that when $\mathcal{N}^a$ is tensile, $\mathcal{N}^c$ is compressive, and vice versa. In contrast to axial forces in layers, the signs of the shear forces and bending moments are equal an all ayers. Their values are only roughly proportional to the bending rigidity of the layer. The largest portion of the shear force and the bending moment is taken over by the lower layer a, while the contribution of layer b to the shear and bending capacity of the beam is rather small.

The influence of the different interlayer slip moduli on the values of various static and kinematic quantities is also examined. Fig. 6 shows the graphs of Δ^{ab}, w, p_n^{bc} and $\mathcal{M}^c$ as a function of the interlayer slip moduli $K = K^{ab} = K^{bc}$. From Fig. 6 it is obvious that the interlayer slip modulus has an important influence on static and kinematic quantities. The slip Δ^{ab} between the layers a and b

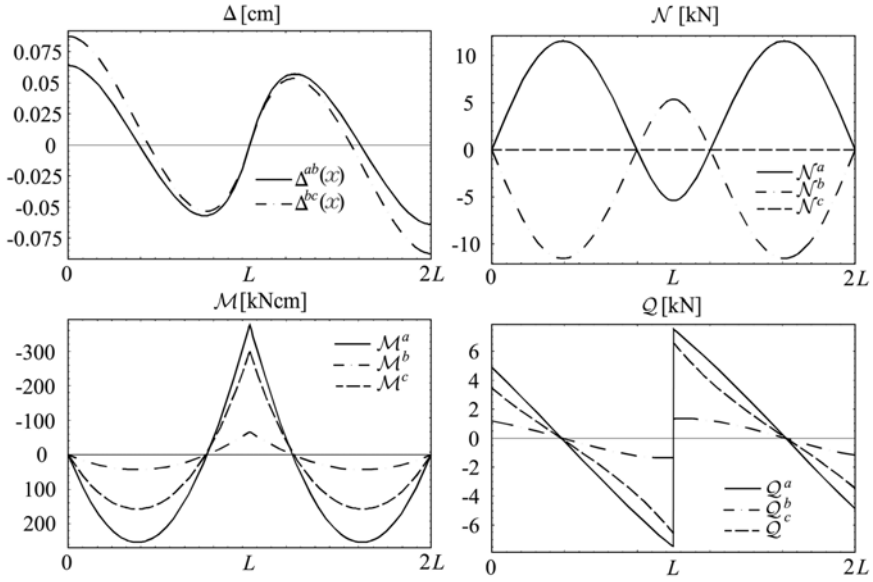

Fig. 5 Distribution of Δ^{ab}, Δ^{bc} and $\mathcal{N}$, $\mathcal{Q}$, $\mathcal{M}$ in layers along the span. Continuous three-layer beam over two spans (Fig. 4).

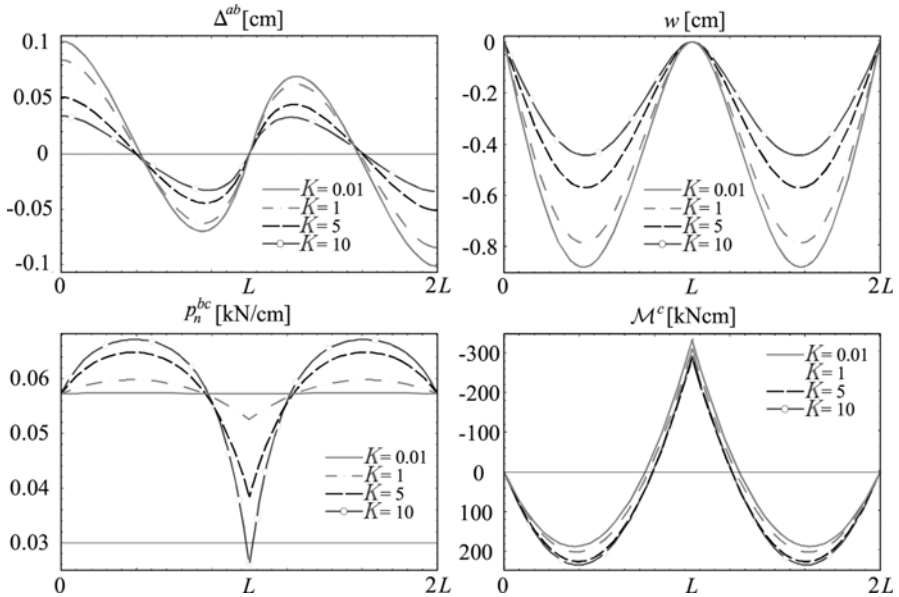

Fig. 6 Distribution of Δ^{ab}, w, p_n^{bc}, and $\mathcal{M}^c$ along the span as a function of different values of the interlayer slip moduli, $K = K^{ab} = K^{bc}$

and the vertical deflection w are much smaller for higher slip moduli K. Static quantities, such as interlayer stresses p_n^{bc} between layers b and c, and bending moment $\mathcal{M}^c$ in layer c are, in contrast, higher for higher slip moduli.

5. Conclusions

We proposed a mathematical model and found its analytical solution for the analysis of geometrically and materially linear layered, simply supported and continuous beams with an arbitrary number of layers and with variable material and geometric characteristics of the layers. The model is compared to the analytical model of Goodman and Popov (1968) for a simply supported three-layer beam, who assumed that the layers are identical. The model was applied to a two-span continuous composite timber beam. The advantage of the present exact analytical model is that, unlike in Goodman and Popov (1968), the thickness as well as material of the individual layers are arbitrary. The method is also suitable for obtaining referential or bench-mark solutions applicable in assessing the accuracy and convergence of newly developed finite element formulations.

Acknowledgements

The work of S. Schnabl was financially supported by the Ministry of Education, Science and Sport of the Republic of Slovenia under contract 3311-02-831625. Their support is gratefully acknowledged.

References

Adekola, U.O. (1968), "Partial interaction between elastically connected elements of a composite beam", *Int. J. Solids Struct.,* **4**, 1125-1135.

Ayoub, A. and Filippou, F.C. (2000), "Mixed formulation of nonlinear steel-concrete composite beam element", *J. Struct. Eng.*, ASCE, **126**(3), 371-381.

Ayoub, A. (2001), "A two-field mixed variational principle for partially connected composite beams", *Finite Elements in Analysis and Design*, **37**, 929-959.

Čas, B. (2004a), "Non-linear analysis of composite beams with interlayer slip", PhD Thesis (in Slovenian), University of Ljubljana, Faculty of Civil and Geodetic Engineering.

Čas, B., Saje, M. and Planinc, I. (2004b), "Non-linear finite element analysis of composite planar frames with an interlayer slip", *Comput. Struct.*, **82**, 1901-1912.

Cosenza, E. and Pecce, M. (2001), "Shear and normal stresses interaction in coupled structural systems", *J. Struct. Eng.*, ASCE, **127**(1), 84-88.

Dall'Asta, A. and Zona, A. (2002), "Nonlinear analysis of composite beams by displacement approach", *Comput. Struct.*, **80**, 2217-2228.

Eurocode 5 (1993), "Design of timber structures, Part 1-1: General rules and rules for buildings", ENV 1995-1-1.

Fabbrocino, G., Manfredi, G. and Cosenza, E. (2000), "Analysis of continuous composite beams in cluding partial interaction and bond", *J. Struct. Eng.*, ASCE, **126**(11), 1288-1294.

Fabbrocino, G., Manfredi, G. and Cosenza, E. (2002), "Modelling of continuous steel-concrete composite beams: Computational aspects", *Comput. Struct.*, **80**, 2241-2251.

Faella, C., Martinelli, E. and Nigro, E. (2002), "Steel and concrete composite beams with flexible shear connection: 'exact' analytical expression of the stiffness matrix and applications", *Comput. Struct.*, **80**, 1001-1009.

Faella, C., Martinelli, E. and Nigro, E. (2003), "Shear connection nonlinearity and deflections of steel-concrete composite beams with: A simplified method", *J. Struct. Eng.*, ASCE, **129**(1), 12-20.

Fragiacomo, M., Amadio, C. and Macorini, L. (2004), "Finite-element model for collapse and long-term analysis

of steel-concrete composite beams", *J. Struct. Eng.*, ASCE, **130**(3), 489-497.
Gatessco, N. (1999), "Analytical modeling of nonlinear behavior of composite beams with deformable connection", *J. Const. Steel Res.*, **52**, 195-218.
Girhammar, U.A. and Gopu, V.K.A. (1993), "Composite beam-columns with interlayer slip-exact analysis", *J. Struct. Eng.*, ASCE, **199**(4), 1265-1282.
Girhammar, U.A. and Pan, D. (1993), "Dynamic analysis of composite member with interlayer slip", *Int. J. Solids Struct.*, **30**(6), 797-823.
Goodman, J.R. and Popov, E.P. (1968), "Layered beam systems with interlayer slip", *J. Struct. Div.*, ASCE, **94**(11), 2535-2547.
Goodman, J.R. and Popov, E.P. (1969), "Layered wood systems with interlayer slip", *Wood Science*, **1**(3), 148-158.
Heinisuo, M. (1988), "An exact finite element technique for layered beams", *Comput. Struct.*, **30**(3), 615-622.
Jasim, N.A. (1997), "Computation of deflections for continuous composite beams with partial interaction", *Proc. of The Institution of Civil Engineers, Structures and Buildings*, **122**, 347-354.
Jasim, N.A. and Mohamad, A.A. (1997), "Deflections of composite beams with partial shear connection", *The Struct. Eng.,* **75**(4), 58-61.
Jasim, N.A. (1999), "Deflections of partially composite beams with linear connector density", *J. Const. Steel Res.*, **49**, 241-254.
Kristek, V. and Studnicka, J. (1982), "Analysis of composite girders with deformable connectors", *Proc. of The Institution of Civil Engineers*, Part 2, **73**, 699-712.
Linden, M.V. (1999), "Timber-concrete composite beams", *HERON*, **44**(3), 215-239.
McCutheon, W.J. (1986), "Stiffness of framing members with partial composite action", *J. Struct. Eng.*, ASCE, **112**(7), 1623-1637.
Newmark, N.M., Siess, C.P. and Viest, I.M. (1951), "Test and analysis of composite beams with incomplete interaction", *Proc. of the Society for Experimental Stress Analysis*, **1**, 75-92.
Nie, J., Fan, J. and Cai, C.S. (2004), "Stiffness and deflection of steel-concrete composite beams under negative bending", *J. Struct. Eng.*, ASCE, **130**(11), 1842-1851.
Oven, V.A., Burgess, I.W., Plank, R.J. and Abdul Wali, A.A. (1997), "An analytical model for the analysis of composite beams with partial interaction", *Comput. Struct.*, **62**(3), 493-504.
Plum, D.R. and Horne, M.R. (1975), "The analysis of continuous composite beams with partial interaction", *Proc. of The Institution of Civil Engineers, Structures and Buildings*, Part 2, **59**, 625-643.
Ranzi, G., Bradford, M.A. and Uy, B. (2003), "A general method of analysis of composite beams with partial interaction", *Steel and Composite Structures*, **3**(3), 169-184.
Rassam, H.Y. and Goodman, J.R. (1971), "Design of layered wood columns with interlayer slip", *Wood Science*, **3**(3), 149-155.
Reissner, E. (1972), "On one-dimensional nite-strain beam theory: The plane problem", *J. of Appl. Mech. and Physics* (ZAMP), **23**, 795-804.
Silfwerbrand, J. (1997), "Stresses and strains in composite concrete beams subjected to differential shrinkage", *ACI Struct. J.*, **94**(4), 347-353.
Smith, S.T. and Teng, J.G. (2001), "Interfacial stresses in plated beams", *Eng. Struct.*, **23**, 857-871.
Thompson, E.G., Goodman, J.R. and Vanderbilt, M.D. (1975), "Finite element analysis of layered wood systems", *J. Struct. Div.*, ASCE, **101**(ST12), 2659-2672.
Wang, Y.C. (1998), "Deflection of steel-concrete composite beams with partial shear interaction", *J. Struct. Eng.*, ASCE, **124**(10), 1159-1165.
Wheat, D.L. and Calixto, J.M. (1994), "Nonlinear analysis of two-layered wood members with inter-layer slip", *J. Struct. Eng.*, ASCE, **120**(6), 1909-1929.
Wolfram, S. (2003), *Mathematica*, Addison-Wesley Publishing Company.

Analytical Solution of Two-Layer Beam Taking into account Interlayer Slip and Shear Deformation

Simon Schnabl[1]; Miran Saje[2]; Goran Turk[3]; and Igor Planinc[4]

Abstract: A mathematical model is proposed and its analytical solution derived for the analysis of the geometrically and materially linear two-layer beams with different material and geometric characteristics of an individual layer. The model takes into account the effect of the transverse shear deformation on displacements in each layer. The analytical study is carried out to evaluate the influence of the transverse shear deformation on the static and kinematic quantities. We study a simply supported two-layer planar beam subjected to the uniformly distributed load. Parametric studies have been performed to investigate the influence of shear by varying material and geometric parameters, such as interlayer slip modulus (K), flexural-to-shear moduli ratios (E/G) and span-to-depth ratios (L/h). The comparison of the results for vertical deflections shows that shear deformations are more important for high slip modulus, for "short" beams with small L/h ratios, and beams with high E/G ratios. In these cases, the effect of the shear deformations becomes significant and has to be addressed in design. It also becomes apparent that models, which consider the partial interaction between the layers, should be employed if beams have very flexible connections.

DOI: 10.1061/(ASCE)0733-9445(2007)133:6(886)

CE Database subject headings: Beams; Shear deformation; Elasticity; Composite structures; Slip.

Introduction

Due to their economy of construction and high bearing capacity, layered systems are widely used to optimize the performance of components in structural engineering. Classic cases are steel–concrete composite beams in buildings and bridges, wood–concrete floor systems, coupled shear walls, concrete beams externally reinforced with laminates, sandwich beams, and many more. The behavior of these structures largely depends on the type of the connection between the layers. Mechanical shear connectors are usually employed to provide a desired composite action. With the use of the rigid shear connectors, a full shear connection and, consequently, a full composite action between the individual components can be achieved. The result is that conventional principles of the solid beam analysis can be employed. Unfortunately, the rigid shear connectors can hardly be realized in practice. Therefore, most of shear connections result in only a partial composite action. As a result, an interlayer slip often develops; if it has a sufficient magnitude, it significantly effects the deformation and the stress distribution of the composite system.

The first appreciation of a composite construction probably originated from observations of highway bridges in service. After the experimental studies had indicated the absence of full composite interaction between the layers in composite beams, new theories were presented accounting for the slip between the layers. These early theories of incomplete or partial interaction between the layers of a composite beam were developed independently during the 1940s in Switzerland, Sweden, and the United States (Leon and Viest 1998). These theories were based on the assumptions of linear elastic material models and the Euler–Bernoulli hypothesis of plane sections. Perhaps the first but certainly the most quoted partial action theory was developed by Newmark et al. (1951). The subsequent theories differ in one or more aspects regarding the additional assumptions and resulted in similar second-order differential equations. Until now, a number of elastic theories with fewer simplifying assumptions and of greater sophistication have been developed. Several exact analytical solutions of simply supported, layered planar beams for different combinations of simple loading cases and simple boundary conditions have been presented in professional literature, e.g., (Girhammar and Gopu 1993; Goodman and Popov 1968; Goodman and Popov 1969; Jasim 1997; Jasim and Ali 1997; Ranzi et al. 2003). With the development of computational tools and computers over the last few decades, these elastic theories have been refined to incorporate numerous aspects of nonlinear geometric and material behavior, as well as time-dependent effects, fatigue, and load reversals, e.g., (Ayoub 2001; Čas et al. 2004a,b; Čas 2004; Fabbrocino et al. 2002; Faella et al. 2002; Gattesco 1999; Smith and Teng 2001).

One of the basic assumptions of all the above-mentioned exact analytical models with partial interaction theory of composite

[1]Graduate Student, Faculty of Civil and Geodetic Engineering, Univ. of Ljubljana, Jamova 2, 1000 Ljubljana, Slovenia. Email: sschnabl@fgg.uni-lj.si

[2]Professor, Faculty of Civil and Geodetic Engineering, Univ. of Ljubljana, Jamova 2, 1000 Ljubljana, Slovenia. Email: msaje@fgg.uni-lj.si

[3]Associate Professor, Faculty of Civil and Geodetic Engineering, Univ. of Ljubljana, Jamova 2, 1000 Ljubljana, Slovenia. Email: gturk@fgg.uni-lj.si

[4]Associate Professor, Faculty of Civil and Geodetic Engineering, Univ. of Ljubljana, Jamova 2, 1000 Ljubljana, Slovenia. Email: iplaninc@fgg.uni-lj.si

Note. Associate Editor: Enrico Spacone. Discussion open until November 1, 2007. Separate discussions must be submitted for individual papers. To extend the closing date by one month, a written request must be filed with the ASCE Managing Editor. The manuscript for this paper was submitted for review and possible publication on May 11, 2006; approved on November 27, 2006. This paper is part of the ***Journal of Structural Engineering***, Vol. 133, No. 6, June 1, 2007. ©ASCE, ISSN 0733-9445/2007/6-886–894/$25.00.

beams was the Euler–Bernoulli hypothesis of plane sections of each individual layer. It is well known that the classical Euler–Bernoulli theory of beam bending, also known as the elementary theory of bending, disregards the effects of the shear deformation. The theory is based on the assumption that the cross section remains perpendicular to the deformed centroidal axis of the beam during bending. This assumption implies a zero shear strain and an infinite shear stiffness. In reality, no material exists that possesses such a property. Since the Euler–Bernoulli theory neglects the transverse shear deformation, its suitability for composite beams can be questioned. This is particularly true in circumstances where shear effects can be significant, as in thick and short composite beams, where flexural-to-shear rigidity ratio parameters are large and the span-to-depth ratio is small. Timoshenko (1921) was the pioneering investigator to include refined effects, such as the shear deformation, in the beam theory. In the literature, this theory is now widely referred to as the Timoshenko beam theory. The effect of shear deformation in Timoshenko's theory is accounted for by an additional rotation angle of transverse cross sections. Consequently, the distribution of the transverse shear deformation is assumed to be constant through the beam thickness. In the beginning of the 1970s, Reissner (1972) has introduced a similar shear distortion in his one-dimensional finite-strain beam model.

To improve the accuracy of the transverse stress prediction, nonclassical higher-order shear-deformable iterative models have been proposed (Gorik 2003; Matsunaga 2002; Piskunov and Grinevitskii 2004; Soldatos and Watson 1997). According to these propositions, a zero-iteration model corresponds to the classical Euler–Bernoulli theory, while the above-mentioned nonclassical Timoshenko theory corresponds to the first-iteration model. Higher-order iteration models introduce further deformation modes, such as cross-sectional bulging and warping, which are important in the modeling of thin-walled composites structures, employed in the aerospace industry. It is not the goal of this paper to model the higher-order deformations. Only the first-iteration model will be considered and the Reissner one-dimensional finite-strain beam model used in the present analytical model. To the best of the authors' knowledge, no report seems to exist on the exact analytical solution of the Timoshenko composite beams with the partial interaction between the layers. In this paper, we aim to fill this gap, and present an exact analytical model of the composite beam, which takes into account the effect of the shear deformation. Then we make the parametric studies on the influence of shear deformation effects on the mechanical behavior of composite beams with the partial interaction between the layers. This way we show when the effect of the shear deformation in the individual layer can be neglected.

Analytical Model

Assumptions

Our formulation of the planar Timoshenko two-layer composite beam model uses the following assumptions: (1) material is linear elastic; (2) displacements, strains, and rotations are small; (3) shear deformations are taken into account (the "Timoshenko beam"); (4) strains vary linearly over each layer (the "Bernoulli hypothesis"); (5) the layers are continuously connected and the slip modulus of the connection is constant; (6) friction between the layers is not considered; and (7) the shapes of the cross sections are symmetrical with respect to the plane of deformation and remain unchanged in the form and size during deformation. Our further assumption (8) is that an interlayer tangential slip can occur at the interface between the layers, but no delamination or the transverse separation between them is possible.

Governing System of Equations

We consider an initially straight, planar, two-layer composite beam element of undeformed length L. Layers are marked by letters a and b (see Fig. 1). The beam element is placed in the (x,z) plane of a spatial Cartesian coordinate system with coordinates (x,y,z) and unit base vectors $\mathbf{E}_x,\mathbf{E}_y,\mathbf{E}_z$. The undeformed reference axis of the layered beam element is common to both layers and lies in their contact plane. The layered beam element is subjected to the action of the conservative distributed load $\boldsymbol{p}=p_x\mathbf{E}_x+p_z\mathbf{E}_z$ and the distributed moment $\boldsymbol{m}=m_y\mathbf{E}_y$ along the span, and to external point forces and moments S_i^a and S_i^b $(i=1,2,\ldots,6)$ at its ends, respectively; see, e.g., (Čas et al. 2004).

The deformed configurations of both layers are defined by vector-valued functions

$$\mathbf{R}^a(x,z)=(x+u^a(x)+z\varphi^a(x))\mathbf{E}_x+(z+w^a(x))\mathbf{E}_z$$
$$\mathbf{R}^b(x^*,z)=(x^*+u^b(x^*)+z\varphi^b(x^*))\mathbf{E}_x+(z+w^b(x^*))\mathbf{E}_z \tag{1}$$

where x^* represents a material, undeformed coordinate of that point of layer b which, in the deformed state, gets in contact with the point of layer a with coordinate x (see Fig. 1). In Eq. (1) and in all further expressions, the notations $(\cdot)^a$ and $(\cdot)^b$ refer to layers a and b. Functions u^a,w^a,φ^a denote the components of the displacement vector and the rotation angle of layer a at the reference axis with respect to the base vectors $\mathbf{E}_x$, $\mathbf{E}_z$, and $\mathbf{E}_y$, respectively. Variables u^b,w^b,φ^b are related to layer b.

The system of governing equations of the two-layer composite beam consists of kinematic, equilibrium, and constitutive equations with accompanying boundary conditions for each of the two layers, and the constraining equations that assemble each layer into a two-layer composite beam. Since deformations, displacements, and rotations are assumed to be small quantities, the generalized equilibrium equations can be simplified using the following two assumptions [see, e.g., (Čas et al. 2004b)]: (i) $dx\approx dx^*$; (ii) vertical deflections of the reference axis of individual layers are equal $w^a(x)=w^b(x^*)=w(x)$ and $\mathcal{I}^a\approx\mathcal{I}^b=[0,L]$. Thus, $(\cdot)^b(x^*)=(\cdot)^b(x)$ holds true for any quantity of layer b, e.g., $u^b(x^*)=u^b(x)$. Kinematic, equilibrium, and constraining equations can now be considerably simplified. After considering the assumptions mentioned above, we can decompose the basic equations of the two-layer beam with an interlayer slip into two separate systems of differential and algebraic equations

$$u^{a\prime}-\varepsilon^a=0,\quad u^{b\prime}-\varepsilon^b=0$$
$$w^{a\prime}+\varphi^a-\gamma^a=0,\quad w^{b\prime}+\varphi^b-\gamma^b=0 \tag{2}$$
$$\varphi^{a\prime}-\kappa^a=0,\quad \varphi^{b\prime}-\kappa^b=0$$

$$w^a-w^b=0 \tag{3}$$

$$\mathcal{N}^{a\prime}-p_t=0,\quad \mathcal{N}^{b\prime}+p_t+p_x=0$$
$$\mathcal{Q}^{a\prime}+p_n=0,\quad \mathcal{Q}^{b\prime}-p_n+p_z=0 \tag{4}$$
$$\mathcal{M}^{a\prime}-\mathcal{Q}^a=0,\quad \mathcal{M}^{b\prime}-\mathcal{Q}^b+m_y=0$$

$$\mathcal{N}^a - \mathcal{N}^a_C = 0, \quad \mathcal{N}^b - \mathcal{N}^b_C = 0$$

$$\mathcal{Q}^a - \mathcal{Q}^a_C = 0, \quad \mathcal{Q}^b - \mathcal{Q}^b_C = 0 \tag{5}$$

$$\mathcal{M}^a - \mathcal{M}^a_C = 0, \quad \mathcal{M}^b - \mathcal{M}^b_C = 0$$

$$\Delta = u^a - u^b \tag{6}$$

$$p_t = \mathcal{F}(\Delta) = K\Delta \tag{7}$$

and

$$x + u^a = x^* + u^b \rightarrow x^* = x + \Delta$$
$$\mathcal{N} = \mathcal{N}^a + \mathcal{N}^b \tag{8}$$

$$\mathcal{Q} = \mathcal{Q}^a + \mathcal{Q}^b \tag{9}$$

$$\mathcal{M} = \mathcal{M}^a + \mathcal{M}^b \tag{10}$$

In Eqs. (2)–(7), ε^a and ε^b=extensional strains of the reference axes of layers a and b; κ^a, and κ^b=pseudocurvatures; while γ^a and γ^b=transverse shear strains of the corresponding cross sections of layers a and b, respectively. $\mathcal{N}^a, \mathcal{N}^b, \mathcal{Q}^a, \mathcal{Q}^b$, and $\mathcal{M}^a, \mathcal{M}^b$ represent equilibrium axial forces, equilibrium shear forces, and equilibrium bending moments of both layers. p_t and p_n denote the tangential and the normal interlayer contact tractions in the contact plane between the layers. $\mathcal{N}^a_C, \mathcal{N}^b_C$, $\mathcal{Q}^a_C, \mathcal{Q}^b_C$, and $\mathcal{M}^a_C, \mathcal{M}^b_C$=constitutive axial forces, constitutive shear forces, and constitutive bending moments of layers a and b, respectively. In the case of linear elastic material, the constitutive forces are assumed to be given by the linear relations with respect to ε^a, ε^b, κ^a, κ^b, γ^a, and γ^b and, therefore, take the following notation:

$$\mathcal{N}^a_C = E^a A^a \varepsilon^a + E^a S^a \kappa^a = C^a_{11}\varepsilon^a + C^a_{12}\kappa^a$$

$$\mathcal{Q}^a_C = k_y G^a A^a \gamma^a = C^a_{33}\gamma^a$$

$$\mathcal{M}^a_C = E^a S^a \varepsilon^a + E^a J^a \kappa^a = C^a_{21}\varepsilon^a + C^a_{22}\kappa^a$$
$$\mathcal{N}^b_C = E^b A^b \varepsilon^b + E^b S^b \kappa^b = C^b_{11}\varepsilon^b + C^b_{12}\kappa^b \tag{11}$$

$$\mathcal{Q}^b_C = k_y G^b A^b \gamma^b = C^b_{33}\gamma^b$$

$$\mathcal{M}^b_C = E^b S^b \varepsilon^b + E^b J^b \kappa^b = C^b_{21}\varepsilon^b + C^b_{22}\kappa^b$$

where E^a, E^b=elastic and G^a, G^b=shear moduli of layers a and b; A^a, A^b denote the areas of the cross-sections of layers a and b; S^a, S^b=static moments; and J^a, J^b=moments of inertia of layers a and b with respect to the interlayer contact line. k_y=shear coefficient of the cross section of the layer. In the case of a rectangular cross section and isotropic material, the shear coefficient is 5/6 (Cowper 1966).

The system of Eqs. (2)–(7) consists of 21 equations for 21 unknown functions u^a, u^b, w^a, w^b, φ^a, φ^b, ε^a, ε^b, κ^a, κ^b, γ^a, γ^b, $\mathcal{N}^a$, $\mathcal{N}^b$, $\mathcal{Q}^a$, $\mathcal{Q}^b$, $\mathcal{M}^a$, $\mathcal{M}^b$, Δ, p_t, and p_n, whereas Eqs. (8)–(10) constitute a system of three equations for three unknown functions x^*, $\mathcal{Q}$, $\mathcal{M}$. In Eq. (7), K denotes the slip modulus at the interlayer surface.

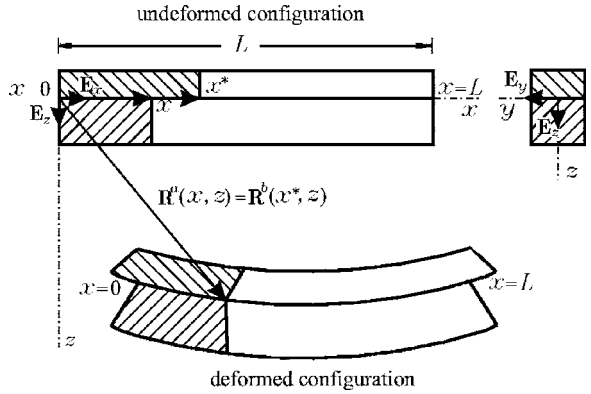

Fig. 1. Undeformed and deformed configuration of the two-layer beam

Solution Algorithm

If the slip Δ and normal traction p_n between the layers is a known function of x, the solution of the system of Eqs. (2)–(7) can easily be obtained with the following sequence of steps.

In the first step, we differentiate Eqs. (3) and (6) twice with respect to x and insert Eq. (2). The following differential equations for the interlayer slip and the pseudocurvatures are derived:

$$\Delta'' = \varepsilon^{a\prime} - \varepsilon^{b\prime} \tag{12}$$

$$\kappa^b = \kappa^a + \gamma^{b\prime} - \gamma^{a\prime} \tag{13}$$

The derivatives $\varepsilon^{a\prime}$, $\varepsilon^{b\prime}$, $\gamma^{a\prime}$, and $\gamma^{b\prime}$ are obtained from Eq. (5), if differentiated with respect to x. Solving the differentiated Eq. (5) for $\varepsilon^{a\prime}$, $\varepsilon^{b\prime}$, $\gamma^{a\prime}$, $\gamma^{b\prime}$, $\kappa^{a\prime}$, and $\kappa^{b\prime}$ gives

$$\begin{Bmatrix} \varepsilon^{a\prime} \\ \gamma^{a\prime} \\ \kappa^{a\prime} \\ \varepsilon^{b\prime} \\ \gamma^{b\prime} \\ \kappa^{b\prime} \end{Bmatrix} = \mathbf{C}^{-1} \begin{Bmatrix} \mathcal{N}^{a\prime} \\ \mathcal{Q}^{a\prime} \\ \mathcal{M}^{a\prime} \\ \mathcal{N}^{b\prime} \\ \mathcal{Q}^{b\prime} \\ \mathcal{M}^{b\prime} \end{Bmatrix} \tag{14}$$

$\mathbf{C}$=matrix of constitutive constants [see Eq. (11)], and $\mathbf{C}^{-1}$=its inverse

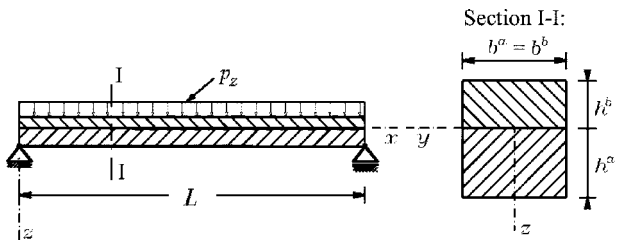

Fig. 2. Simply supported two-layer beam

$$\mathbf{C}^{-1} = \begin{bmatrix} C_{11}^a & 0 & C_{12}^a & 0 & 0 & 0 \\ 0 & C_{33}^a & 0 & 0 & 0 & 0 \\ C_{21}^a & 0 & C_{22}^a & 0 & 0 & 0 \\ 0 & 0 & 0 & C_{11}^b & 0 & C_{12}^b \\ 0 & 0 & 0 & 0 & C_{33}^b & 0 \\ 0 & 0 & 0 & C_{21}^b & 0 & C_{22}^b \end{bmatrix}^{-1}$$

$$= \begin{bmatrix} D_{11}^a & 0 & D_{12}^a & 0 & 0 & 0 \\ 0 & D_{33}^a & 0 & 0 & 0 & 0 \\ D_{21}^a & 0 & D_{22}^a & 0 & 0 & 0 \\ 0 & 0 & 0 & D_{11}^b & 0 & D_{12}^b \\ 0 & 0 & 0 & 0 & D_{33}^b & 0 \\ 0 & 0 & 0 & D_{21}^b & 0 & D_{22}^b \end{bmatrix} \tag{15}$$

Furthermore, we differentiate Eq. (13) twice with respect to x. By insertion of Eq. (4) into Eq. (14), the second and third derivatives of strains are obtained by differentiation of Eq. (14) twice and three times with respect to x. Introducing $\varepsilon^{a\prime}$, $\varepsilon^{b\prime}$, $\kappa^{a\prime\prime}$, $\kappa^{b\prime\prime}$, $\gamma^{a\prime\prime\prime}$, and $\gamma^{b\prime\prime\prime}$ in Eq. (12) and differentiated Eq. (13), results in a coupled system of two higher-order linear differential equations with constant coefficients for the slip and the normal interlayer traction between layers a and b

$$\Delta''' + K_1\Delta' + K_2 p_n = D_{12}^b p_z$$
$$K_5 p_n'' + K_4 p_n + K_3\Delta' = -D_{22}^b p_z \tag{16}$$

with K_1, K_2, K_3, K_4, and K_5 being constants

$$K_1 = -K(D_{11}^a + D_{11}^b), \quad K_2 = D_{12}^a + D_{12}^b, \quad K_3 = K(D_{21}^a + D_{21}^b)$$
$$K_4 = -(D_{22}^a + D_{22}^b), \quad K_5 = D_{33}^a + D_{33}^b \tag{17}$$

Boundary conditions associated with Eq. (16) are the values of the interlayer slip and its first two derivatives, and the values of the normal interlayer traction and its first derivative at the edge $x=0$ of the beam element. An exact solution of Eq. (16) was easily obtained by MATHEMATICA (Wolfram 2003). Due to its length and complexity, the closed-form expressions are not shown throughout the paper. When the slip and the normal interlayer traction have been obtained, the remaining equations of the system (2)–(7) can simply be solved. We first determine the boundary rotations and displacements from the system of linear equations

$$\mathbf{K}_T\mathbf{u} = \mathbf{g} \tag{18}$$

for the composite structure. In Eq. (18), $\mathbf{K}_T$ denotes the tangent stiffness matrix, $\mathbf{u}$=vector of end-point displacements, and $\mathbf{g}$=load vector. Once $\mathbf{u}$ is known, the values of the end forces can easily be computed. By integrating Eqs. (2) and (4) and considering Eqs. (3), (6), and (7), the solution for unknown functions u^a, u^b, w^a, w^b, φ^a, φ^b, ε^a, ε^b, κ^a, κ^b, γ^a, γ^b, $\mathcal{N}^a$, $\mathcal{N}^b$, $\mathcal{Q}^a$, $\mathcal{Q}^b$, $\mathcal{M}^a$, $\mathcal{M}^b$, Δ, p_t, and p_n can easily be obtained. Finally, the unknown functions x^*, $\mathcal{Q}$, and $\mathcal{M}$ are obtained from Eqs. (8)–(10).

Parametric Studies

This section presents parametric studies performed on a simply supported two-layer planar beam subjected to a uniformly distributed load (see Fig. 2) with the aim to investigate the influence of the shear deformation in an individual layer and a variety of other material and geometric parameters, such as flexural-to-shear and span-to-depth ratios, interlayer slip modulus, etc., on the mechanical behavior of the Timoshenko composite beams.

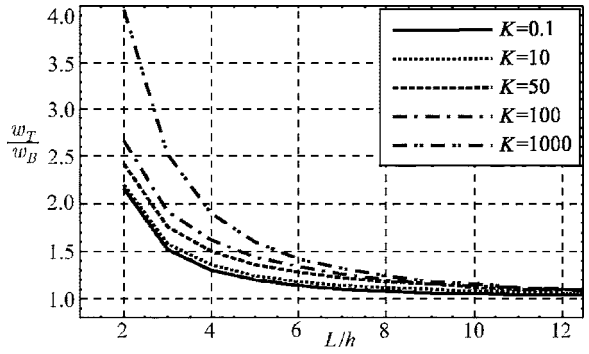

Fig. 3. Influence of slip modulus and L/h ratios on vertical deflections for $E/G=16$

The main interest was focused on the assessment of the contribution effect of the transverse shear deformation to the deformation and stresses in composite beams with partial interaction between the layers. To this end, the vertical deflections were calculated for different values of parameters (K,E/G,L/h) and compared to those obtained by the analytical model of Euler–Bernoulli composite beams with partial interaction between the individual components. Results are given in Figs. 3 and 4, and Table 1.

In Fig. 3, the vertical deflections (w_T) of the Timoshenko composite beam with the partial interlayer interaction are compared to the vertical deflections (w_B) obtained by the Euler–Bernoulli composite beam model with the same partial interlayer interaction (here also called the classical composite beam model), for different L/h ratios and various interlayer slip moduli K. It can be observed in Fig. 3 that decreasing the L/h ratios and increasing interlayer slip modulus K, increases the influence of the transverse shear deformation on vertical deflections. This influence is considerable in the case of timber composite beams ($E/G=16$) even for relatively slender beams ($L/h=10$), as can be seen from Fig. 4 and Table 1. The effect is even more pronounced for timber composite beams with $L/h=5$, where the shear deformations increase the vertical deflections for the values in the range from 19.2 to 59.5%.

The effect of shear deformation on the vertical deflections at the midspan of a composite beam has been investigated for vari-

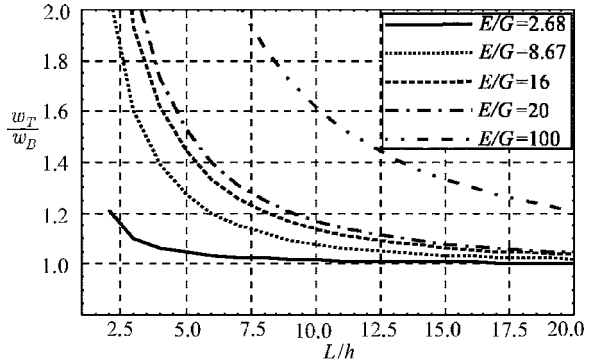

Fig. 4. Influence of E/G and L/h ratios on vertical deflections for $K=100$

Table 1. Influence of K, E/G, and L/h on Vertical Deflections (ω_T/ω_B)

K [kN/cm^2]	E/G=2.68			E/G=8.67			E/G=16		
	I	II	III	I	II	III	I	II	III
0.001	1.090	1.032	1.008	1.287	1.104	1.026	1.524	1.192	1.048
0.01	1.090	1.032	1.008	1.287	1.104	1.026	1.524	1.192	1.048
0.1	1.090	1.032	1.008	1.288	1.105	1.027	1.524	1.192	1.049
1	1.091	1.033	1.008	1.293	1.110	1.032	1.529	1.197	1.054
10	1.092	1.034	1.010	1.341	1.152	1.056	1.581	1.244	1.087
50	1.098	1.040	1.014	1.494	1.237	1.075	1.767	1.370	1.128
100	1.105	1.046	1.017	1.603	1.274	1.080	1.931	1.445	1.139
1000	1.182	1.083	1.024	1.875	1.329	1.084	2.534	1.595	1.154

Note: I: L/h=3; II: L/h=5; and III: L/h=10.

ous E/G and L/h ratios and different interlayer slip moduli K. Here, we present (see Table 1) only the results for beams with E/G=2.68 (the ratio, typical for isotropic materials such as steel, aluminum, and copper) and beams with E/G=8.67 (transversely isotropic glass-fiber-reinforced unidirectional composite beams) and for anisotropic wood beams with E/G=16÷20. The results for a beam with E/G=100, which is not a realistic value for material, have been added in Fig. 4 as well.

A comparative analysis of the analytical results for the vertical deflections at the midspan of a simply supported composite beam with the partial interlayer interaction shows that the influence of shear effects is significant for composite beams where $E/G \geq 16$, particularly in the case of rather stiff connections with very high interlayer slip moduli K, where the influence of shear effects on the increase of deflections can be as high as 15.4% for L/h=10, and more than 250% for short beams with L/h=3.

The contribution of the shear effects to the vertical deflections ranges, in the case of steel, aluminum, and copper composite beams with E/G=2.86, from 0.3 to 8.3% for $5 \leq L/h \leq 15$. Therefore, for such composite beams, the shear effects are insignificant, except for short beams with $L/h \leq 3$ and high Ks.

In the case of glass-fiber-reinforced composite beams with E/G=8.67, the influence for beams with $L/h \geq 10$ is still beyond 8.4% and, thus less significant, while the influence on beams with $L/h \leq 5$ becomes important (it ranges from 10.4 to 32.9%).

It is illustrative to study the influence of the shear deformation in an individual layer on the static and kinematic quantities rather than w, such as Δ, p_n, ε^a, $\mathcal{N}^a$, etc.

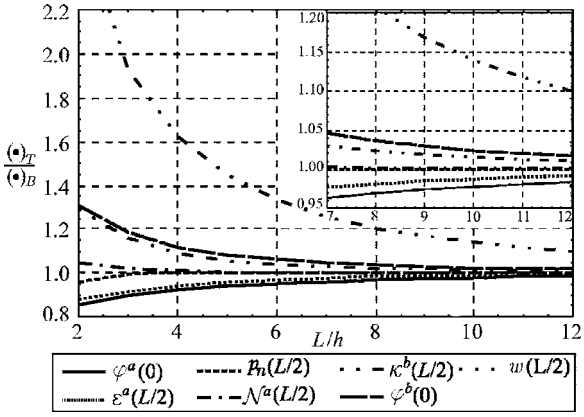

Fig. 5. Static and kinematic quantities as a function of L/h for E/G=16 and K=100 kN/cm^2

These quantities have been calculated for timber composite beams with E/G=16 and for various values of parameters L/h and K. The results are presented in Fig. 5 and in Table 2, where the notations $(\cdot)_T$ and $(\cdot)_B$ mark that the quantities have been calculated by different beam models. Thus, $(\cdot)_B$ represents quantities calculated by the Euler–Bernoulli composite beam model with the partial interlayer interaction, and $(\cdot)_T$ represents quantities obtained by the Timoshenko composite beam model.

The examination of analytical results in Table 2 and in Fig. 5 reveals that the shear deformation has an important influence not only on the vertical deflections, but also on the other mechanical quantities of composite beams with the partial interlayer interaction.

An interesting detail at this point is that the influence of the shear deformation has different effects on different quantities. Some quantities, like w, φ^b, κ^b, and $\mathcal{N}^a$ increase due to the shear deformation, while the others, like p_n, ε^a, and φ^a decrease when compared to the quantities calculated by the classical beam model. For example, an increasing influence of shear effects on $\varphi^b(0)$ for interlayer slip modulus K=0.1 kN/cm^2 and L/h=3 is found to be 25.0%, while for L/h=15 it is only 1.2%. On the other hand, a decreasing influence of shear effects on $\varepsilon^a(L/2)$ is found (−10.3%) for K=100 kN/cm^2 and L/h=3, and it is −2.2% for L/h=10. It is clear from the results depicted in Fig. 6 that, in addition to the increase in the L/h, the increase of K leads to a significant enlargement of tangential interlayer tractions with respect to normal interlayer tractions in the contact plane between the layers. For example, in the case of relatively slender two-layer composite beams ($L/h \geq 10$) with $K \geq 10$ kN/cm^2, the tangential

Table 2. Static and Kinematic Quantities as Functions of K and L/h for E/G=16

$(\cdot)_T/(\cdot)_B$	K=0.1 kN/cm^2			K=100 kN/cm^2		
	I	II	III	I	II	III
$w(L/2)$	1.524	1.192	1.049	1.931	1.445	1.139
$\Delta(0)$	1.046	1.020	1.006	1.026	1.012	1.005
$\varphi^a(0)$	0.939	0.973	0.992	0.919	0.960	0.988
$\varphi^b(0)$	1.250	1.092	1.026	1.185	1.083	1.030
$\kappa^a(L/2)$	0.944	0.977	0.994	0.927	0.969	0.992
$\kappa^b(L/2)$	1.188	1.077	1.020	1.156	1.059	1.015
$\mathcal{N}^a(L/2)$	1.044	1.019	1.005	1.022	1.007	1.001
$\varepsilon^a(L/2)$	0.944	0.977	0.994	0.897	0.942	0.978
$p_n(L/2)$	0.968	0.994	1.000	1.993	1.004	1.001

Note: I: L/h=3; II: L/h=5; and III: L/h=10.

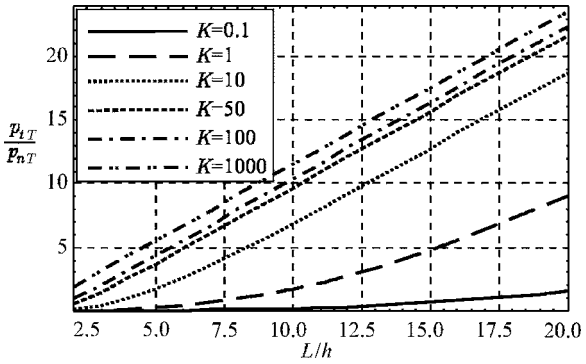

Fig. 6. Tangential and normal tractions as a function of L/h for $E/G=16$ and different Ks

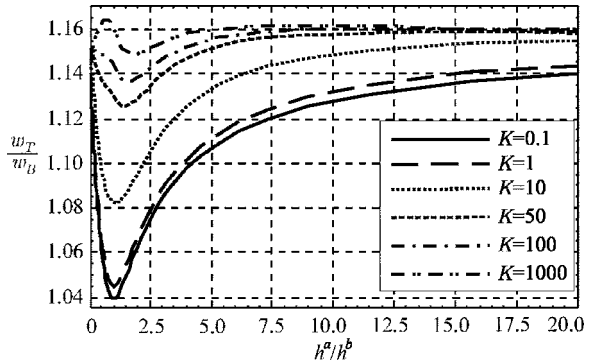

Fig. 8. Vertical deflections as a function of h^a/h^b for $L/h=10$ and $E/G=16$ and different Ks

interlayer tractions may be as high as about 20 times the normal interlayer tractions. Although it has been shown that the influence of shear effects on the interlayer tractions is negligible, it is apparent from the graphs in Fig. 7, that the shear deformation has an important impact on the ratio of the interlayer tractions, especially for the two-layer beams with $L/h \leqslant 10$, where the influence of shear effects is more than 29.0%.

A parametric study has also been conducted to assess the effects of different parameters, such as h^a/h^b and K on the vertical deflections and shear forces. For this purpose, the vertical deflections at the midspan and the shear forces at the edge $x=0$ of the two-layer composite beam have been calculated for various h^a/h^b and K. In the case of relatively slender timber beams with $L/h=10$ and $E/G=16$, the parametric study reveals, that minimum shear effects occur when layers have approximately equal depths. In Fig. 8, it is shown that the corresponding discrepancies are higher for smaller values of K and can be, in the case of a rather flexible connection ($K \leqslant 1$ kN/cm^2), as much as about four times smaller than in the case of stiff interaction between the layers.

Figs. 9 and 10 show that the contribution to the shear forces due to shear effects can be considerable, especially when the depth of one layer is very small compared to the depth of the other one and for small values of K.

It is observed that for a very thin bottom layer a ($h^a/h^b \leqslant 0.1$) and the nonstiff interlayer contact ($K=0.1$ kN/cm^2), the shear force $\mathcal{Q}^a$ can be due to shear effects about 2.8 times bigger than the one obtained by the Euler–Bernoulli model. By contrast, for high values of K, the shear force $\mathcal{Q}^a$ may be about twice as small as in the case of the Euler–Bernoulli beam. It is also apparent from Fig. 10, that the value of the shear force $\mathcal{Q}^b$ in Timoshenko's theory is in the nonstiff connection about 2.5 times bigger if the top layer is very thin compared to the bottom one. Thus, it has been shown, that the shear deformations have considerable influence on static shear forces of individual layers of the two-layer composite beam and hence should not be neglected in the analysis of such structures.

In addition, the vertical deflections have been calculated for timber composite beams with $E/G=16$ and $L/h=10$ by different beam models: (1) using empirical formulas given in the European code for timber structures Eurocode 5 (Eurocode 5 1993); (2) with the classical Euler–Bernoulli beam model with and without considering the interlayer slip; (3) with the Timoshenko beam model for beams without the interlayer slip; and finally (4) with the present analytical Timoshenko composite beam model with the consideration of the partial interaction between the layers.

In Table 3, the results of different beam models and for a wide range of slip modulus from 0.001 to 1000 kN/cm^2 are presented and compared. Observe that the influence of the interlayer slip modulus on the vertical deflections is negligible for the range of the slip modulus from 0.001 to 0.1 kN/cm^2, and that the influence of solely slip modulus on the deflections due to the interlayer slip (w_B/w_B^*) decreases with the increase of the slip modulus. On the other hand, the combined influence of the shear deformation and slip (w_T/w_B) on the deflections increases with the increase of the slip modulus between the layers. Thus, for high values of K, deflections obtained by both Euler–Bernoulli and Timoshenko models with the consideration of the partial interaction differ from deflections obtained by the complete inter-

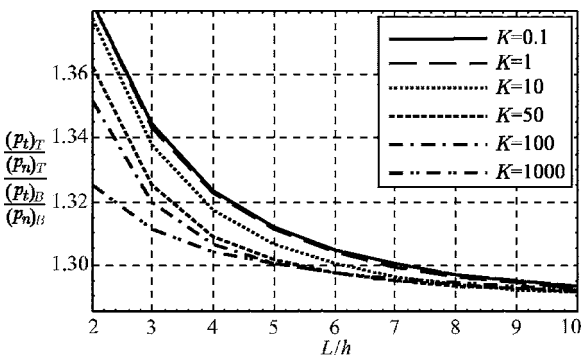

Fig. 7. Ratio of tangential and normal tractions as a function of L/h for $E/G=16$ and different Ks

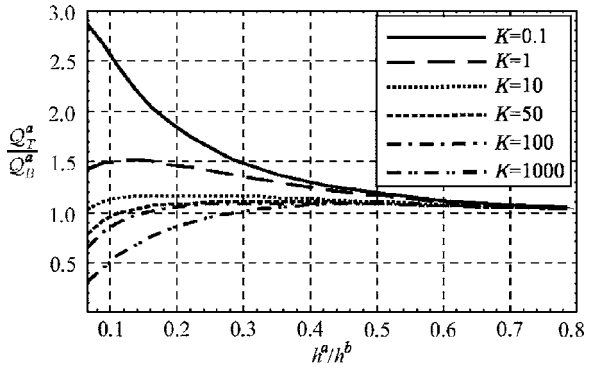

Fig. 9. Shear force $\mathcal{Q}^a$ as a function of h^a/h^b for $L/h=10$, $E/G=16$, and different Ks

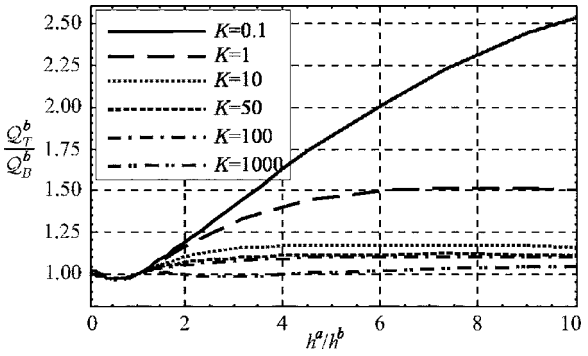

Fig. 10. Shear force Q^b as a function of h^a/h^b for $L/h=10$, $E/G=16$, and different Ks

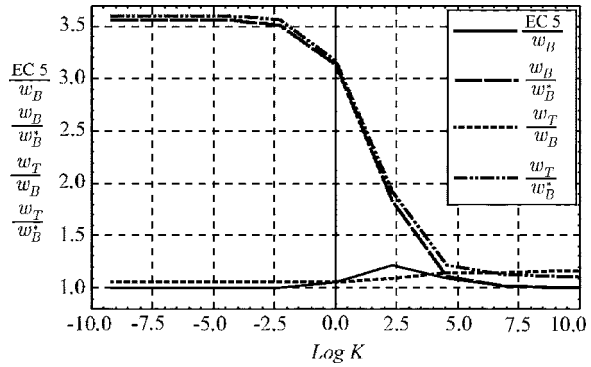

Fig. 11. Comparisons of vertical deflections calculated by different beam models, for different Ks with $L/h=10$ and $E/G=16$

action models by less than 1.2%. Note that the deflections, obtained by the formula given in Eurocode (Eurocode 5 1993) for composite beams with interlayer slip between the layers, agree with the present results for the Euler–Bernoulli beam for $0.001<K<10$ kN/m^2 and $100<K<1000$ kN/m^2, but not for $10<K<100$ kN/m^2, where the maximum difference is 22.5%. The comparison with the Timoshenko beam is more promising.

Fig. 11 shows comparisons of vertical deflections obtained by different beam models. It can be seen from the results in Table 3 and Fig. 11 that the models with the partial interaction are essential for the accurate prediction of vertical deflections, especially for more flexible connections between the layers, i.e., for the range of slip moduli from 0.001 to 1 kN/cm^2, since the comparisons of w_B/w_B^* and w_T/w_T^* show that the deflections may be as high as about 3.5 times of the deflections of a rigidly connected layered beam. Furthermore, based on the comparisons between the analytical results for vertical deflections shown in Table 3 and Fig. 11, it is clear that the proposed model needs to be employed even for the range of the slip modulus $K>50$ kN/cm^2. The comparison of vertical deflections w_T/w_B shows that the effect of the shear deformation on the increase of vertical deflections can be about 15.4%.

Next, let us inspect the stress distributions over the depth of the two-layer composite beam. The longitudinal normal stresses σ_{xx} have been evaluated at the midspan section, and the tangential stresses σ_{xz} at the edge section of the beam shown in Fig. 2. From Fig. 12, it can be seen that the distributions and the values of the normal and the tangential stresses in the layers are very much affected by the stiffness of the contact. The effect is depicted for various stiffnesses and the "zig-zag" linear variation of normal stresses and the quadratic distribution of tangential stresses is obtained. Note that for small Ks the maximum tangential stresses considerably exceed the stresses obtained from the classical solid beam model. It is apparent that the classical beam theory underestimates both the normal and the tangential stresses in layered beams. In the case of the nonstiff connection between the layers, the tangential stresses σ_{xz} may increase up to 25% compared to the stresses in the "solid beam."

Conclusions

A mathematical model is proposed and its analytical solution is found for the analysis of the geometrically and materially linear layered beams with different material and geometric characteristics of each layer. The proposed analytical model takes into account the transverse shear deformation of each layer of a multilayer beam. The analytical study is carried out for evaluating the influence of the transverse shear deformation on the static and kinematic quantities. Particular emphasis is given to the vertical deflections at the midspan of a simply supported two-layer planar beam subjected to the uniformly distributed load. For this purpose, several parametric studies have been performed to investigate the influence of shear effects and various material and geometric parameters, such as flexural-to-shear rigidity ratios and span-to-depth ratios, on the mechanical behavior of the layered Timoshenko beams.

Based on the results of this analytical study and the parametric evaluations undertaken, the following conclusions can be drawn:

1. The present mathematical model is general and relatively easy to comprehend.

Table 3. Vertical Deflections Calculated by Different Beam Models for Different Ks with $L/h=10$ and $E/G=16$

K [kN/cm^2]	EC 5 [cm]	w_B^* [cm]	w_B [cm]	w_T^* [cm]	w_T [cm]	$\frac{\text{EC5}}{w_B}$	$\frac{w_T}{w_B}$	$\frac{w_B}{w_B^*}$	$\frac{w_T}{w_T^*}$	$\frac{w_T}{w_B^*}$
0.001	3.875	1.085	3.875	1.252	4.062	1.000	1.048	3.571	3.243	3.743
0.01	3.872	1.085	3.869	1.252	4.057	1.000	1.048	3.566	3.239	3.738
0.1	3.845	1.085	3.818	1.252	4.005	1.007	1.049	3.518	3.197	3.691
1	3.602	1.085	3.391	1.252	3.573	1.062	1.054	3.125	2.853	3.293
10	2.427	1.085	1.982	1.252	2.154	1.225	1.087	1.826	1.720	1.985
50	1.526	1.085	1.325	1.252	1.494	1.153	1.128	1.221	1.193	1.377
100	1.326	1.085	1.230	1.252	1.379	1.096	1.139	1.115	1.101	1.270
1000	1.111	1.085	1.098	1.252	1.267	1.012	1.154	1.012	1.012	1.168

Note: *=without interlayer slip.

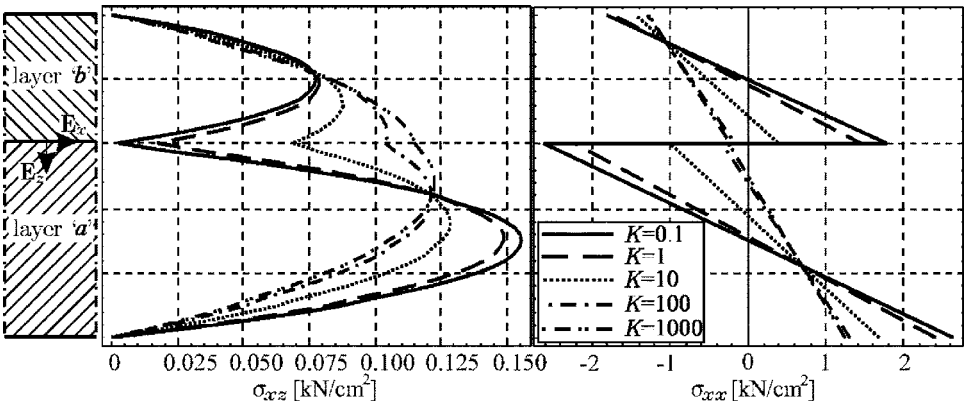

Fig. 12. The distribution of normal and tangential stresses over the cross section for different Ks

2. The influence of the shear deformation on vertical deflections is increasing with decreasing L/h ratios and increasing K. In the case of a timber composite beam ($E/G=16$), the contribution of shear deformations to vertical deflections can be about 15% for ratios $L/h=10$. The effect is even more pronounced for beams with $L/h=5$, where the effect of shear deformation on vertical deflections ranges between 19 and 60%.
3. The influence of shear effects is significant for composite beams with $E/G \geq 16$, particularly in the case of very high interlayer slip moduli, where the influence is about 15% for $L/h=10$, and about 250% for short beams with $L/h=3$.
4. In the case of steel, aluminum, and copper composite beams with $E/G=2.86$, the extra contribution to the vertical deflections due to shear effects ranges from 0.3 to 8% for $5 \leq L/h \leq 15$. Therefore, for such composite beams, shear effects are insignificant, except possibly for short beams with $L/h \leq 3$ and higher values of K.
5. In the case of glass-fiber reinforced unidirectional composite beams with $E/G=8.67$, the influence of shear effects on vertical deflections increases with an increase in K and a decrease in L/h. Thus, the influence for beams with $L/h \geq 10$ is still beyond 8% and, hence, insignificant, in contrast to beams with $L/h=5$, where the increase of the deflection ranges from 10 to 33%, and particularly for very short and rigidly connected composite beams, where the influence of shear effects can reach values up to 85%.
6. In the case of relatively slender two-layer composite beams ($L/h \geq 10$) with $K \geq 10$ kN/cm^2, the tangential interlayer tractions are about 20 times bigger than the related normal interlayer tractions. The shear deformation has an important impact on the actual ratio of the interlayer tractions. For the two-layer beams with $L/h \leq 10$, the influence of shear effects is more than 29%.
7. In the case of one very thin layer and a rather flexible connection ($K=0.1$ kN/cm^2), the corresponding shear force in the thin layer can be considerably bigger than in the classical theory. This is, $\mathcal{Q}_T$ is about 2.8 times larger for nonstiff and about twice smaller than $\mathcal{Q}_B$ obtained by the classical Euler–Bernoulli beam model. Similarly, the shear force $\mathcal{Q}_T$ of a very thin top layer is 2.5 times larger than that of the classical theory. Thus, we have shown, that the shear has a considerable impact on the values of the shear forces in the layers, and therefore should not be neglected.
8. The influence of shear deformation on vertical deflections is negligible, if $0.001 \leq K \leq 0.1$ kN/cm^2, $E/G=16$, and $L/h=10$.
9. The results of the deflection formula given in Eurocode 5 (Eurocode 5 1993) agree completely with the present results if $0.001 \leq K \leq 0.1$ kN/cm^2, while discrepancies may occur for other values of K.
10. The comparison of the results w_B/w_B^* and w_T/w_T^* shows that larger shear deformations develop for large slip moduli K, for short beams with small L/h ratios and for materials with high E/G ratios. In all these cases, the role of shear deformations is significant and they have to be addressed in design. It also becomes clear that the beam models should consider the partial interaction between the layers if K takes small values.
11. The zig-zag linear variation of the normal stresses and the piecewise quadratic distribution of the tangential stresses over the composite cross section has been obtained. For $K \leq 0.1$ kN/cm^2, the maximum tangential stresses σ_{xz} may exceed the values obtained from the classical solid beam model for about 25%. It is apparent then that the classical solid beam model provides nonconservative estimates for the tangential and normal stresses in layered beams.

Acknowledgments

The work of S. Schnabl was financially supported by the Ministry of Education, Science and Sport of the Republic of Slovenia under Contract No. 3311-02-831625. The support is gratefully acknowledged.

References

Ayoub, A. (2001). "A two-field mixed variational principle for partially connected composite beams." *Finite Elem. Anal. Design*, 37, 929–959.

Čas, B. (2004). *Nonlinear analysis of composite beams with inter-layer slip*, Ph.D. thesis, Univ. of Ljubljana, Faculty of Civil and Geodetic Engineering, Ljubljana, Slovenia (in Slovene).

Čas, B., Bratina, S., Saje, M., and Planinc I. (2004a). "Nonlinear analysis of composite steel-concrete beams with incomplete interaction." *Steel Compos. Struct.*, 4(6), 489–507.

Čas, B., Saje, M., and Planinc, I. (2004b). "Nonlinear finite element analysis of composite planar frames with inter-layer slip." *Comput.*

Struct., 82, 1901–1912.
Cowper, G. R. (1966). "The shear coefficient in Timoshenko's beam theory." *J. Appl. Mech.*, 33(2), 335–340.
Eurocode 5. (1993). "Design of timber structures. Part 1–1: General rules and rules for buildings." *ENV 1995-1–1*.
Fabbrocino, G., Manfredi, G., and Cosenza, E. (2002). "Modeling of continuous steel–concrete composite beams: Computational aspects." *Comput. Struct.*, 80, 2241–2251.
Faella, C., Martinelli, E., and Nigro, E. (2002). "Steel and concrete composite beams with flexible shear connection: 'Exact' analytical expression of the stiffness matrix and applications." *Comput. Struct.*, 80, 1001–1009.
Gattesco, N. (1999). "Analytical modeling of nonlinear behavior of composite beams with deformable connection." *J. Constr. Steel Res.*, 52, 195–218.
Girhammar, U. A., and Gopu, V. K. A. (1993). "Composite beam-columns with inter-layer slip—Exact analysis." *J. Struct. Eng.*, 119(4), 1265–1282.
Goodman, J. R., and Popov, E. P. (1968). "Layered beam systems with interlayer slip." *J. Struct. Div.*, 94(11), 2535–2547.
Goodman, J. R., and Popov, E. P. (1969). "Layered wood systems with interlayer slip." *Wood Sci.*, 1(3), 148–158.
Gorik, A. V. (2003). "Theoretical and experimental deformation parameters of composite beams with account of deplanation of cross sections in bending." *Mech. Compos. Mater.*, 39(1), 57–64.
Jasim, N. A. (1997). "Computation of deflections for continuous composite beams with partial interaction." *Proc., Inst. Civil Engineers, Structures and Buildings*, 122, 347–354.
Jasim, N. A., and Ali, A. A. M. (1997). "Deflections of composite beams with partial shear connection." *Struct. Eng.*, 75(4), 58–61.
Leon, R. T., and Viest, I. M. (1998). "Theories of incomplete interaction in composite beams." *Composite construction in steel and concrete III*, ASCE, Reston, Va., 858–870.
Matsunaga, H. (2002). "Interlaminar stress analysis of laminated composite beams according to global higher-order deformation theories." *Compos. Struct.*, 34, 105–114.
Newmark, N. M., Siest, C. P., and Viest, C. P. (1951). "Test and analysis of composite beams with incomplete interaction." *Proc., Society for Experimental Stress Analysis*, 1, 75–92.
Piskunov, V. G., and Grinevitskii, B. V. (2004). "Variant of an analytical shear model for the stress-strain state of heterogeneous composite beams." *Mech. Compos. Mater.*, 40(5), 409–417.
Ranzi, G., Bradford, M. A., and Uy, B. (2003). "A general method of analysis of composite beams with partial interaction." *Steel Compos. Struct.*, 3(3), 169–184.
Reissner, E. (1972). "On one-dimensional finite-strain beam theory: The plane problem." *Z. Angew. Math. Phys.*, 23, 795–804.
Smith, S. T., and Teng, J. G. (2001). "Interfacial stresses in plated beams." *Eng. Struct.*, 23, 857–871.
Soldatos, K. P., and Watson, P. (1997). "A general theory for accurate stress analysis of homogeneous and laminated composite beams." *Int. J. Solids Struct.*, 34(22), 2857–2885.
Timoshenko, S. P. (1921). "On the correction for shear of the differential equation for transverse vibrations of prismatic bars." *Philos. Mag.*, 41(245), 744–746.
Wolfram, S. (2003). *Mathematica*, Addison-Wesley, Reading, Mass.

Available online at www.sciencedirect.com
ScienceDirect
Finite Elements in Analysis and Design 43 (2007) 705–714
FINITE ELEMENTS IN ANALYSIS AND DESIGN
www.elsevier.com/locate/finel

Locking-free two-layer Timoshenko beam element with interlayer slip

S. Schnabl, M. Saje, G. Turk*, I. Planinc

University of Ljubljana, Faculty of Civil and Geodetic Engineering, Jamova 2, SI-1115 Ljubljana, Slovenia

Received 6 October 2006; received in revised form 12 January 2007; accepted 13 March 2007
Available online 19 April 2007

Abstract

A new locking-free strain-based finite element formulation for the numerical treatment of linear static analysis of two-layer planar composite beams with interlayer slip is proposed. In this formulation, the modified principle of virtual work is introduced as a basis for the finite element discretization. The linear kinematic equations are included into the principle by the procedure, similar to that of Lagrangian multipliers. A strain field vector remains the only unknown function to be interpolated in the finite element implementation of the principle. In contrast with some of the displacement-based and mixed finite element formulations of the composite beams with interlayer slip, the present formulation is completely locking-free. Hence, there are no shear and slip locking, poor convergence and stress oscillations in these finite elements. The generalization of the composite beam theory with the consideration of the Timoshenko beam theory for the individual component of a composite beam represents a substantial contribution in the field of analysis of non-slender composite beams with an interlayer slip. An extension of the present formulation to the non-linear material problems is straightforward. As only a few finite elements are needed to describe a composite beam with great precision, the new finite element formulations is perfectly suited for practical calculations.

Keywords: Composite beam; Interlayer slip; Timoshenko beam theory; Locking; Finite element method

1. Introduction

Multi-layered structures have been playing an increasingly important role in different areas of engineering practice, perhaps most notably in civil, automotive, aerospace and aeronautic technology. Classical cases of such structures in civil engineering are steel–concrete composite beams in buildings and bridges, wood–concrete floor systems, coupled shear walls, concrete beams externally reinforced with laminates, sandwich beams, and many more. It is well known that the behaviour of these structures largely depends on different materials of individual components and by the type of their connection. There exist many ways how to obtain the connection between the components. Usually, mechanical shear connectors are employed to provide a desired composite action. With the use of rigid shear connectors, a full shear connection and full composite action between the individual components can be achieved. Consequently, conventional principles of the solid beam analysis can be employed. Unfortunately, the full shear connection can hardly be materialized in practice and thus only an incomplete or partial interaction between the layers can be obtained and an interlayer slip often develops. In some cases it significantly effects the mechanical behaviour of composite systems.

Hence, the inclusion of the interlayer-slip effect into multi-layered beam theory is essential for optimal design and accurate representation of the actual mechanical behaviour of multi-layered structures with partial interaction between the components. Many efforts and large number of research studies have been devoted to obtain the solution of the aforementioned problem. Early studies on beams with partial interaction between the layers were based on the assumptions of linear elastic material models and the Euler–Bernoulli hypothesis of plane sections. Perhaps the first but certainly the most quoted partial action theory was developed by Newmark et al. [1]. Up to now, a number of elastic theories have been developed and presented in professional literature [2–9]. The main disadvantage of all these elastic theories and their closed form analytical solutions is that they could be obtained only for problems with simple geometry, loading and boundary conditions. Therefore, in recent years numerous investigators have refined these theories

* Corresponding author. Tel.: +386 1 47 68 614; fax: +386 1 47 68 629.
E-mail address: gturk@fgg.uni-lj.si (G. Turk).

0168-874X/$ - see front matter © 2007 Elsevier B.V. All rights reserved.
doi:10.1016/j.finel.2007.03.002

to incorporate several aspects of non-linear geometric and material behaviour [10–14] as well as torsion [15], time dependent effects [8], uplift [16] and dynamics [17]. Such complex problems are usually solved using numerical methods such as finite difference methods and finite element methods. Among all those numerical methods, the majority of researchers have employed the displacement-based [16,18], force-based [19] and mixed [18–22] finite element method. It is well known that finite element models which use low-order interpolation and a few finite elements experience so-called slip locking for high values of stiffness of the shear connection [18,21]. This locking is due to the inconsistent approximation of different fields governing the beam model. It is possible to reduce or completely eliminate locking by lowering the degree of interpolation functions for the slip or by introducing elements with larger numbers of degrees of freedom [18,21].

Besides, one of the basic assumptions of all aforementioned models with partial interaction between the layers was the most commonly used Euler–Bernoulli beam theory for each individual layer, respectively. The main shortcoming of the classical Euler–Bernoulli beam theory is that no transverse shear deformation is allowed for. This implies an infinite shear stiffness of individual layer. Since, in reality, no material exists that possesses such a property, the suitability of the Euler–Bernoulli beam theory for composite beams with an interlayer slip can be questioned, especially for thick and short composite beams. In these cases, the application of the Timoshenko beam theory is indispensable for accurate prediction of the mechanical behaviour of aforementioned structures. A large number of homogeneous beam elements based on Timoshenko beam theory have appeared in the literature. To eliminate shear and membrane locking, several approaches have been proposed. Among them, the reduced or selective integration technique is the most common. An extensive list of references on locking in Timoshenko beams is not among the goals of this work. On the other hand, there seems to exist only one report on the exact solution of Timoshenko composite beam with an interlayer slip [23], and no reports on the finite element formulation of Timoshenko composite beams with the partial interaction between the layers. In the present paper, we aim to fill this gap.

The objective of this paper is two-fold. Firstly, we present a new locking-free strain-based finite element formulation for the linear static analysis of two-layer planar beams with interlayer slip. In this formulation, the principle of virtual work has been employed as a basis for the finite element discretization. Thus, we have proposed a modified form of the principle of virtual work by including the linear kinematic equations as constraining equations by a procedure, similar to that of Lagrangian multipliers. In this way we eliminate the displacement field vector from the principle of virtual work. As a result, the strain field vector remains the only unknown function to be approximated in the finite element implementation. This means, that only the extensional strains and pseudocurvatures of reference axis of individual layers and transverse shear strains of layer cross-sections need to be interpolated. Furthermore, the present approach uses the concept of the consistent equilibrium of constitutive and equilibrium-based stress-resultants [24] and the Galerkin type of the finite element formulation is employed [25]. In contrast with many of the aforementioned displacement-based, force-based and mixed finite element formulations of composite beams with interlayer slip, the present formulation is completely locking-free. Consequently, the ambiguous selection of consistent polynomial approximations for physically different field variables can thus be fully avoided.

The second objective of the present paper is the incorporation of the transverse shear deformation into the two-layer composite beam theory with an interlayer slip. The Timoshenko beam theory for each of the individual layer has been adopted. Since, the distribution of the transverse shear strain in the Timoshenko beam theory is assumed to be constant across the cross-section, the shear correction factor is necessary to use [26] for the appropriate representation of shear stresses through the cross-section. The proposed generalization of the composite beam theory with the Timoshenko beam theory is therefore an improvement in the field of analysis of non-slender (thick and short) composite beams with an interlayer slip. Finally, the common outcome of the present formulation is a family of more accurate and efficient beam finite elements for the linear static analysis of two-layer planar Timoshenko beams with an interlayer slip. Any kind of locking (shear, slip, curvature), poor convergence and stress oscillations are absent in these finite elements.

2. Formulation of basic equations of a two-layer Timoshenko beam

The following formulation of a two-layer planar Timoshenko composite beam with an interlayer slip is based on Reissner's [27] finite-strain beam theory, in which Bernoulli's hypothesis of plane cross-sections for each individual layer is assumed. Plane cross-sections remain planar during deformation but not necessarily perpendicular to the deformed centroidal axis of the beam. Under this assumption, the effect of a constant transverse shear strain of the individual layer can be approximately taken into account by decoupling the rotation of the cross-section from the slope of the deformed line of centroid. Accordingly, the Timoshenko [28] beam theory for each layer is applied. In addition, we assumed that displacements, strains and rotations are small and that the shapes of the cross-sections are symmetrical with respect to the plane of deformation and remain unchanged in the form and size during deformation. Layers are assumed to be continuously connected and interlayer stiffness of the connection is taken as constant. Besides, tangential slip can occur at the interface between the layers but no delamination or transverse separation between them is possible. In what follows, we briefly describe the basic equations of the two-layer Timoshenko beam.

2.1. Kinematic, constitutive and constraining equations

We consider an initially straight, planar, two-layer Timoshenko beam element of undeformed length L, see Fig. 1. Layers are marked by letters a and b, respectively. The two-layer beam element is analysed in the (x, z)-plane of a spatial Cartesian coordinate system with coordinates (x, y, z) and unit base

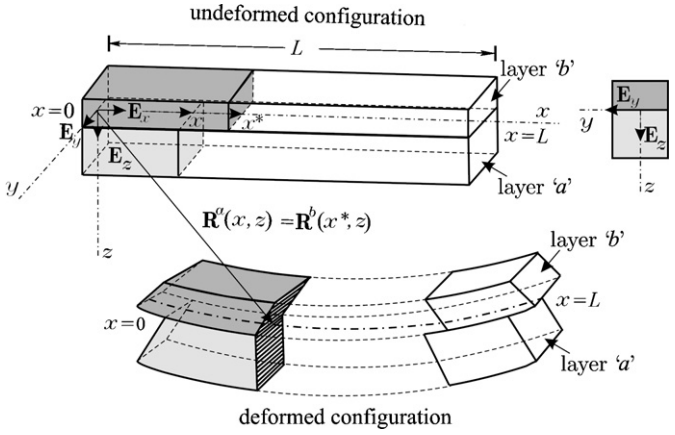

Fig. 1. Undeformed and deformed configuration of the two-layer beam.

vectors $\mathbf{E}_x, \mathbf{E}_y, \mathbf{E}_z$. The reference axis of the two-layer beam element is common to both layers. It coincides with the axis x and it lies in the contact plane between the layers. The geometric shape of the cross-section of each layer is assumed to be arbitrary but symmetric with respect to (x, z) plane and constant along its longitudinal axis x. Only for the sake of clearness the cross-sections plotted in Fig. 1 are rectangular. The two-layer beam element is subjected to the action of the conservative distributed load $\boldsymbol{p} = p_x\mathbf{E}_x + p_z\mathbf{E}_z$ along the span on the upper face of layer b. Besides, it is also subjected to generalized point forces S_i^a and S_i^b $(i = 1, 2, \ldots, 6)$ at the ends of layers a and b.

The position vectors of material particles of the deformed configurations of layers a and b in the plane of deformation $(y = 0)$ are defined by vector-valued functions

$$\mathbf{R}^a(x, z) = (x + u^a(x) + z\varphi^a(x))\mathbf{E}_x + (z + w^a(x))\mathbf{E}_z, \tag{1}$$

$$\mathbf{R}^b(x^*, z) = (x^* + u^b(x^*) + z\varphi^b(x^*))\mathbf{E}_x + (z + w^b(x^*))\mathbf{E}_z. \tag{2}$$

In Eqs. (1) and (2), and in all further expressions, the notations $(\bullet)^a$ and $(\bullet)^b$ denote whether quantities correspond to layer a or b. Thus, functions $u^a(x)$, $w^a(x)$, $\varphi^a(x)$ denote the longitudinal displacement along the direction of the reference axis, the transverse displacement, and the rotation of the cross-section of layer a with respect to the base vectors $\mathbf{E}_x$, $\mathbf{E}_z$ and $\mathbf{E}_y$, respectively. Variables $u^b(x^*)$, $w^b(x^*)$, $\varphi^b(x^*)$ are related to layer b. The components of the generalized displacement vectors $\boldsymbol{u}^a = \{u^a(x), w^a(x), \varphi^a(x)\}$ and $\boldsymbol{u}^b = \{u^b(x^*), w^b(x^*), \varphi^b(x^*)\}$ are related to the components of the generalized strain vectors $\boldsymbol{\varepsilon}^a = \{\varepsilon^a(x), \gamma^a(x), \kappa^a(x)\}$ and $\boldsymbol{\varepsilon}^b = \{\varepsilon^b(x^*), \gamma^b(x^*), \kappa^b(x^*)\}$ by the linearized Reissner's kinematic equations [9,12]:

$$u^{a\prime}(x) - \varepsilon^a(x) = 0, \quad u^{b\prime}(x^*) - \varepsilon^b(x^*) = 0, \tag{3}$$

$$\begin{aligned} &w^{a\prime}(x) + \varphi^a(x) - \gamma^a(x) = 0, \\ &w^{b\prime}(x^*) + \varphi^b(x^*) - \gamma^b(x^*) = 0, \end{aligned} \tag{4}$$

$$\varphi^{a\prime}(x) - \kappa^a(x) = 0, \quad \varphi^{b\prime}(x^*) - \kappa^b(x^*) = 0. \tag{5}$$

In Eqs. (3)–(5) the prime $(')$ denotes the first derivative with respect to either x or x^*, whereas functions ε, γ, κ mark the extensional strain, the transverse shear strain and the pseudocurvature of the individual layer, respectively. Conjugate to these strains we have stress resultants $\boldsymbol{\sigma}^a = \{\mathcal{N}^a(x), \mathcal{Q}^a(x), \mathcal{M}^a(x)\}$ and $\boldsymbol{\sigma}^b = \{\mathcal{N}^b(x^*), \mathcal{Q}^b(x^*), \mathcal{M}^b(x^*)\}$ for the equilibrium axial forces $\mathcal{N}^a(x), \mathcal{N}^b(x^*)$, the transverse shear forces $\mathcal{Q}^a(x)$, $\mathcal{Q}^b(x^*)$ and the bending moments $\mathcal{M}^a(x)$, $\mathcal{M}^b(x^*)$ of the individual layer. In order to relate the equilibrium axial and shear forces, and the equilibrium moments to material models of layers, we introduce a set of constitutive equations which assures the balance of the equilibrium and constitutive cross-sectional resultants. For linear elastic material, the constitutive functions $\mathcal{N}_{\mathrm{C}}^a(x), \mathcal{N}_{\mathrm{C}}^b(x^*), \mathcal{Q}_{\mathrm{C}}^a(x), \mathcal{Q}_{\mathrm{C}}^b(x^*), \mathcal{M}_{\mathrm{C}}^a(x), \mathcal{M}_{\mathrm{C}}^b(x^*)$ can be given in terms of the components of the generalized strain vectors $\boldsymbol{\varepsilon}^a$ and $\boldsymbol{\varepsilon}^b$. Thus, the constitutive equations of layers are defined by equations

$$\mathcal{N}^a(x) = \mathcal{N}_{\mathrm{C}}^a(x, \varepsilon^a(x), \kappa^a(x)) = E^a A^a \varepsilon^a(x) + E^a S^a \kappa^a(x), \tag{6}$$

$$\begin{aligned} \mathcal{N}^b(x^*) &= \mathcal{N}_{\mathrm{C}}^b(x^*, \varepsilon^b(x^*), \kappa^b(x^*)) \\ &= E^b A^b \varepsilon^b(x^*) + E^b S^b \kappa^b(x^*), \end{aligned} \tag{7}$$

$$\mathcal{Q}^a(x) = \mathcal{Q}_{\mathrm{C}}^a(x, \gamma^a(x)) = G^a A_{\mathrm{S}}^a \gamma^a(x), \tag{8}$$

$$\mathcal{Q}^b(x^*) = \mathcal{Q}_{\mathrm{C}}^b(x^*, \gamma^b(x^*)) = G^b A_{\mathrm{S}}^b \gamma^b(x^*), \tag{9}$$

$$\begin{aligned} \mathcal{M}^a(x) &= \mathcal{M}_{\mathrm{C}}^a(x, \varepsilon^a(x), \kappa^a(x)) \\ &= E^a S^a \varepsilon^a(x) + E^a J^a \kappa^a(x), \end{aligned} \tag{10}$$

$$\begin{aligned} \mathcal{M}^b(x^*) &= \mathcal{M}_{\mathrm{C}}^b(x^*, \varepsilon^b(x^*), \kappa^b(x^*)) \\ &= E^b S^b \varepsilon^b(x^*) + E^b J^b \kappa^b(x^*), \end{aligned} \tag{11}$$

in which A^a, A^b are the areas of cross-sections, E^a, E^b are the elastic modulus, S^a, S^b are the static moments of area and J^a, J^b are the cross-sectional moments of inertia of layers a and b with respect to the reference axis of the whole cross-section of the two-layer beam element. In addition, the A_{S}^a and A_{S}^b represent the areas of the shear cross-sections [26].

Once the layers are connected together, the upper layer is constrained to follow the deformation of lower layer, and vice versa. As already stated, the layers can slip along each other, but their transverse separation or penetration is not allowed. This fact is expressed by the kinematic-constraint requirement

$$\mathbf{R}^a(x, z) = \mathbf{R}^b(x^*, z), \tag{12}$$

where $x \in \mathcal{I}^a, x^* \in \mathcal{I}^b$ are undeformed coordinates of two distinct particles of layers a and b which are in the deformed state in contact, and thus their vector-valued functions $\mathbf{R}^a(x, z)$ and $\mathbf{R}^b(x^*, z)$ coincide (see Fig. 1). Eq. (12) can be rewritten in a more convenient component form:

$$x + u^a(x) = x^* + u^b(x^*), \tag{13}$$

$$w^a(x) = w^b(x^*). \tag{14}$$

The relative displacements (slip) that occurs between the two particles which coincide in the undeformed configuration is denoted by Δ, and is in the case of geometrically linear beam theory simply given by

$$\Delta(x) = u^a(x) - u^b(x) = u^a(0) - u^b(0) + \int_0^x (\varepsilon^a(x) - \varepsilon^b(x))\,\mathrm{d}\xi. \tag{15}$$

In the present paper, the linear constitutive law of the bond slip between the layers is assumed.

$$p_t = K\Delta, \tag{16}$$

where K represents the interlayer-slip modulus. For a detailed explanation of the constraining equations, a reader is directed to Refs. [9,11–13,23].

Assuming strains, displacements, rotations and slips to be small quantities, Eqs. (3)–(5) can be simplified using the following two assumptions (see, e.g. [12]): (i) $\mathrm{d}x \approx \mathrm{d}x^*$; (ii) vertical deflections of the reference axis of individual layers are equal $w^a(x) = w^b(x^*) = w(x)$ and $\mathcal{I}^a \approx \mathcal{I}^b = [0, L]$. Thus, all quantities of layer b are equal at x and x^*, e.g. $u^b(x^*) = u^b(x)$. Due to the last two assumptions, the arguments in the following equations can be omitted. This implies that a simplified version of Eqs. (3)–(5) reads:

$$u^{a\prime} - \varepsilon^a = 0, \quad u^{b\prime} - \varepsilon^b = 0, \tag{17}$$

$$w' + \varphi^a - \gamma^a = 0, \quad w' + \varphi^b - \gamma^b = 0, \tag{18}$$

$$\varphi^{a\prime} - \kappa^a = 0, \quad \varphi^{b\prime} - \kappa^b = 0. \tag{19}$$

Since the constraining equations define the conditions that assemble an individual layer into a layered composite beam, Eqs. (17)–(19) are not independent of each other. The application of Eqs. (18)–(19) to the first and second derivative of Eq. (14) with respect to x, gives modified Eqs. (18)–(19) by which the rotations and pseudocurvatures of layers are constrained to each other. According to the above simplification, the modified kinematic equations of the two-layer Timoshenko beam read

$$u^{a\prime} - \varepsilon^a = 0, \tag{20}$$

$$u^{b\prime} - \varepsilon^b = 0, \tag{21}$$

$$w^{a\prime} + \varphi^a - \gamma^a = 0, \tag{22}$$

$$\varphi^{a\prime} - \kappa^a = 0, \tag{23}$$

$$\varphi^b - \varphi^a + \gamma^a - \gamma^b = 0, \tag{24}$$

$$\kappa^b - \kappa^a + \gamma^{a\prime} - \gamma^{b\prime} = 0. \tag{25}$$

2.2. The modified principle of virtual work and its finite element formulation

The principle of virtual work states that the difference of virtual works of internal and external forces is zero

$$\begin{aligned}\delta W = \delta W^a + \delta W^b &= \int_0^L (\mathcal{N}^a\delta\varepsilon^a + \mathcal{Q}^a\delta\gamma^a + \mathcal{M}^a\delta\kappa^a)\,\mathrm{d}x \\ &+ \int_0^L (\mathcal{N}^b\delta\varepsilon^b + \mathcal{Q}^b\delta\gamma^b + \mathcal{M}^b\delta\kappa^b)\,\mathrm{d}x \\ &+ \int_0^L (p_t\delta u^a - p_n\delta w)\,\mathrm{d}x \\ &- \int_0^L ((p_t + p_x)\delta u^b + (p_n - p_z)\delta w)\,\mathrm{d}x \\ &- S_1^a\delta u^a(0) - S_2^a\delta w(0) - S_3^a\delta\varphi^a(0) - S_4^a\delta u^a(L) \\ &- S_5^a\delta w(L) - S_6^a\delta\varphi^a(L) - S_1^b\delta u^b(0) - S_2^b\delta w(0) \\ &- S_3^b\delta\varphi^b(0) - S_4^b\delta u^b(L) - S_5^b\delta w(L) - S_6^b\delta\varphi^b(L) \\ &= 0.\end{aligned} \tag{26}$$

Here, δu^a, δu^b, δw are virtual displacements, $\delta\varepsilon^a$, $\delta\varepsilon^b$, $\delta\gamma^a$, $\delta\gamma^b$, $\delta\kappa^a$, $\delta\kappa^b$ are virtual strains of the reference axis of the composite beam; $\delta u^a(0)$, $\delta u^a(L)$, $\delta w(0)$, etc., denote the virtual boundary displacements, whereas p_n represents the normal interlayer contact traction. The principle given in Eq. (26) has been derived on the basis of the assumption that the kinematic and strain variables as well as their variations are constraint by the kinematic and constitutive Eqs. (20)–(25) and (6)–(11). Hence, only six among the 11 functions u^a, u^b, w, φ^a, φ^b, ε^a, ε^b, γ^a, γ^b, κ^a and κ^b are mutually independent. These constraints are released if the Hu–Washizu functional is introduced with Eqs. (20)–(25) as being a set of constraining equations of the functional. Eqs. (20)–(25) are scalarly multiplied by arbitrary, independent, and at least once differentiable Lagrangian multipliers Λ_i. The scalar products of the multipliers and the constraining equations are integrated along the length L and varied with respect to displacements, strains and Lagrangian multipliers. The terms that contain first derivatives of displacements and strains are partially integrated. After adding the obtained expressions to Eq. (26), the strain-based principle of virtual work called a modified principle of virtual work is derived [12,25]

$$\begin{aligned}\delta W_{\mathrm{mod}} = &\int_0^L ((\mathcal{N}_{\mathrm{C}}^a - \Lambda_1)\delta\varepsilon^a + (\mathcal{N}_{\mathrm{C}}^b - \Lambda_2)\delta\varepsilon^b \\ &+ (\mathcal{Q}_{\mathrm{C}}^a - \Lambda_3 + \mathcal{M}_{\mathrm{C}}^{b\prime})\delta\gamma^a \\ &+ (\mathcal{Q}_{\mathrm{C}}^b - \mathcal{M}_{\mathrm{C}}^{b\prime})\delta\gamma^b + (\mathcal{M}_{\mathrm{C}}^a + \mathcal{M}_{\mathrm{C}}^b - \Lambda_4)\delta\kappa^a)\,\mathrm{d}x \\ &+ \left(u^a(L) - u^a(0) - \int_0^L \varepsilon^a\,\mathrm{d}x\right)\delta\Lambda_1(0) \\ &+ \left(u^b(L) - u^b(0) - \int_0^L \varepsilon^b\,\mathrm{d}x\right)\delta\Lambda_2(0) \\ &+ \left(w(L) - w(0) - \int_0^L (\gamma^a - \varphi^a)\,\mathrm{d}x\right)\delta\Lambda_3(0)\end{aligned}$$

$$+\left(\varphi^a(L)-\varphi^a(0)-\int_0^L \kappa^a\,\mathrm{d}x\right)\delta\Lambda_4(0)$$
$$-(S_1^a+\Lambda_1(0))\delta u^a(0)-(S_1^b+\Lambda_2(0))\delta u^b(0)$$
$$-(S_2^a+S_2^b+\Lambda_3(0))\delta w(0)$$
$$-(S_3^a+S_3^b+\Lambda_4(0))\delta\varphi^a(0)-(S_4^a-\Lambda_1(L))\delta u^a(L)$$
$$-(S_4^b-\Lambda_2(L))\delta u^b(L)-(S_5^a+S_5^b-\Lambda_3(L))\delta w(L)$$
$$-(S_6^a+S_6^b-\Lambda_4(L))\delta\varphi^a(L)=0. \tag{27}$$

This strain-based formulation offers a number of advantages, such as a consistent cross-sectional equilibrium and a derivation of locking-free strain-based finite elements. Functional (27) stated above represents the starting point of the strain-based Galerkin-type of the finite element discretization. The only unknown functions defining principle (27) are the strain variables—the axial strains ε^a, ε^b, the transverse shear strains γ^a, γ^b and the pseudocurvature κ^a. Notice, that the displacements, rotations, forces and moments are included only through their boundary values. Thus, functions ε^a, ε^b, γ^a, γ^b, κ^a and 12 parameters $\Lambda_1(0)$, $\Lambda_2(0)$, $\Lambda_3(0)$, $\Lambda_4(0)$, $u^a(0)$, $u^a(L)$, $u^b(0)$, $u^b(L)$, $w(0)$, $w(L)$, $\varphi^a(0)$, $\varphi^a(L)$ where Λ_1, Λ_2, Λ_3, Λ_4 represent the Euler–Lagrange multipliers (in this case, the forces and moments in global coordinate system), fully describe functional (27). In the finite element implementation of the principle, we need to interpolate five strain functions $\varepsilon^a(x)$, $\varepsilon^b(x)$, $\gamma^a(x)$, $\gamma^b(x)$, $\kappa^a(x)$ and their variations. In this way, the reference axis of the two-layer Timoshenko beam is divided into finite elements. Within each element, the strain functions and their variations are interpolated. For the interpolation of the strain functions, the Lagrangian polynomials P_n $(n=1,2,\ldots,N_I)$ of degree N_I-1 are employed. Additionally, it is assumed that the variations of strain functions are approximated by the Dirac δ-function. The definition of Dirac-delta function, collocation method and the fundamental lemma of the calculus of variation used to derive the discrete system of Euler–Lagrange equations can be found in [29]. The selection of the collocation points x_i $(i=1,2,\ldots,N_K)$ is crucial in obtaining a well conditioned system of equations and a convergent solution. Thus, the interpolation of the unknowns takes the form

$$\varepsilon^a(x)\doteq\sum_{n=1}^{N_I}P_n(x)\,\varepsilon_n^a,\quad \delta\varepsilon^a(x)\doteq\delta(x-x_i), \tag{28}$$

$$\varepsilon^b(x)\doteq\sum_{n=1}^{N_I}P_n(x)\,\varepsilon_n^b,\quad \delta\varepsilon^b(x)\doteq\delta(x-x_i), \tag{29}$$

$$\gamma^a(x)\doteq\sum_{n=1}^{N_I}P_n(x)\,\gamma_n^a,\quad \delta\gamma^a(x)\doteq\delta(x-x_i), \tag{30}$$

$$\gamma^b(x)\doteq\sum_{n=1}^{N_I}P_n(x)\gamma_n^b,\quad \delta\gamma^b(x)\doteq\delta(x-x_i), \tag{31}$$

$$\kappa^a(x)\doteq\sum_{n=1}^{N_I}P_n(x)\,\kappa_n^a,\quad \delta\kappa^a(x)\doteq\delta(x-x_i). \tag{32}$$

Discrete values ε_n^a, ε_n^b, γ_n^a, γ_n^b, κ_n^a represent the nodal values of the interpolated functions. Thus, for the construction of the finite-element model of the two-layer Timoshenko beam with an interlayer slip the Petrov–Galerkin collocation method is used. For the sake of the simplicity, we assume that the interpolation and collocation points within the element coincide: $N=N_I=N_K$. Assuming further that equilibrium equations

$$\begin{aligned}&\mathcal{N}^{a\prime}-p_t=0,\quad \mathcal{N}^{b\prime}+p_t+p_x=0,\\ &\mathcal{Q}^{a\prime}+p_n=0,\quad \mathcal{Q}^{b\prime}+p_z-p_n=0,\\ &\mathcal{M}^{a\prime}+Q^a=0,\quad \mathcal{M}^{b\prime}-Q^b=0\end{aligned} \tag{33}$$

are identically satisfied, the boundary forces $\Lambda_1(L)$, $\Lambda_2(L)$, $\Lambda_3(L)$, and the boundary moment $\Lambda_4(L)$ in Eq. (27) can easily be expressed only by $\Lambda_1(0)$, $\Lambda_2(0)$, $\Lambda_3(0)$, $\Lambda_4(0)$ and p_z, p_x, p_x and p_z. Insertion of Eqs. (28)–(32) into the variational principle (27) and using the fundamental lemma of the calculus of variation yield the discrete system of Euler–Lagrange equations of the principle:

$$f_i=(\mathcal{N}_{\mathrm{C}}^a-\Lambda_1)|_{x=x_i}=0,\quad i=1,\ldots,N, \tag{34}$$

$$f_{N+j}=(\mathcal{N}_{\mathrm{C}}^b-\Lambda_2)|_{x=x_j}=0,\quad j=1,\ldots,N, \tag{35}$$

$$f_{2N+k}=(\mathcal{Q}_{\mathrm{C}}^a-\Lambda_3+\mathcal{M}_{\mathrm{C}}^{b\prime})|_{x=x_k}=0,\quad k=1,\ldots,N, \tag{36}$$

$$f_{3N+l}=(\mathcal{Q}_{\mathrm{C}}^b-\mathcal{M}_{\mathrm{C}}^{b\prime})|_{x=x_l}=0,\quad l=1,\ldots,N, \tag{37}$$

$$f_{4N+m}=(\mathcal{M}_{\mathrm{C}}^a+\mathcal{M}_{\mathrm{C}}^b-\Lambda_4)|_{x=x_m}=0,\quad m=1,\ldots,N, \tag{38}$$

$$f_{5N+1}=u^a(L)-u^a(0)-\int_0^L\varepsilon^a\,\mathrm{d}x=0, \tag{39}$$

$$f_{5N+2}=u^b(L)-u^b(0)-\int_0^L\varepsilon^b\,\mathrm{d}x=0, \tag{40}$$

$$f_{5N+3}=w(L)-w(0)-\int_0^L(\gamma^a-\varphi^a)\,\mathrm{d}x=0, \tag{41}$$

$$f_{5N+4}=\varphi^a(L)-\varphi^a(0)-\int_0^L\kappa^a\,\mathrm{d}x=0, \tag{42}$$

$$f_{5N+5}=S_1^a+\Lambda_1(0)=0, \tag{43}$$

$$f_{5N+6}=S_1^b+\Lambda_2(0)=0, \tag{44}$$

$$f_{5N+7}=S_2^a+S_2^b+\Lambda_3(0)=0, \tag{45}$$

$$f_{5N+8}=S_3^a+S_3^b+\Lambda_4(0)=0, \tag{46}$$

$$f_{5N+9}=S_4^a-\Lambda_1(0)-\int_0^L p_t\,\mathrm{d}x=0, \tag{47}$$

$$f_{5N+10} = S_4^b - \Lambda_2(0) + \int_0^L (p_x + p_t)\,\mathrm{d}x = 0, \tag{48}$$

$$f_{5N+11} = S_5^a + S_5^b - \Lambda_3(0) + \int_0^L p_z\,\mathrm{d}x = 0, \tag{49}$$

$$f_{5N+12} = S_6^a + S_6^b - \Lambda_4(0) - \int_0^L \Lambda_3\,\mathrm{d}x = 0. \tag{50}$$

For a given load factor, λ, Eqs. (34)–(50) constitute a system of $5N + 12$ linear algebraic equations for $5N + 12$ unknowns. There are $5N + 4$ internal degrees of freedom ε_n^a, ε_n^b, γ_n^a, γ_n^b, κ_n^a, $\Lambda_1(0)$, $\Lambda_2(0)$, $\Lambda_3(0)$, $\Lambda_4(0)$, and eight external degrees of freedom, i.e., nodal displacement and rotations $u^a(0)$, $u^a(L)$, $u^b(0)$, $u^b(L)$, $w(0)$, $w(L)$, $\varphi^a(0)$, $\varphi^a(L)$ of the finite element. The internal degrees of freedom are eliminated from the structural assemblage by the static condensation at the element level. The condensed global tangent stiffness matrix and the condensed residual force vector of the structure are then assembled in a classical way. For the solution of the equations a standard method for solutions of linear system can be employed. Notice, that for non-singular solution of Eqs. (34)–(50) at least one longitudinal boundary displacement, belonging either to layer a or b, must be prescribed.

3. Numerical examples

The following examples demonstrate high accuracy and excellent performance of the proposed family of locking-free two-layer Timoshenko beam finite elements. The purposes of the discussion presented herein are the following: (i) to check the convergence properties and locking (slip and shear) behaviour of presented finite elements and (ii) to briefly investigate the influence of shear rigidity on the mechanical behaviour of continuous two-layer Timoshenko composite beam with interlayer slip.

For this purpose, we consider two simple, but indicative examples: (1) a simply supported two-layer Timoshenko composite beam with length L and (2) a continuous two-layer Timoshenko composite beam over two spans. In both cases the beams are subjected to conservative distributed load of intensity p_z. The elastic properties E^a, E^b, G^a and G^a, cross-sectional areas A^a, A^b and all other material and geometric parameters are shown in Figs. 2 and 6. A shear-correction factor k_S for a rectangular cross-section is taken to be $\frac{5}{6}$ [26].

In order to validate and confirm the accuracy and the convergence performance of the elements developed in the earlier section, the numerical results such as mid-point vertical deflections and interlayer slips at the edge of the beam are evaluated for different types of elements and compared to the corresponding reference solution, which is taken to be the solution by 1000 finite elements with degree of interpolation polynomials, here termed by E_0. This way we analyse the influence of the degree of interpolation functions (Lagrange interpolation polynomials), the number of elements and the location of collocation points $\{x_1, \ldots, x_n\}$ on the numerical results of the Timoshenko two-layer beam. As discussed in Section 2, the set of collocation points can generally be prescribed arbitrarily. Thus, the results for mid-point vertical deflection $w^a(L/2)$, interlayer slip at the left edge of the beam $\Delta(0)$, and L^2-norm of a balance function of equilibrium and constitutive bending moments $\|\mathcal{M}_C - \mathcal{M}\|_2$, as a function of number of elements, the collocation points and the order of interpolation polynomials are displayed in Tables 1–4 for collocation points distributed equidistantly including boundary nodes (E), by Lobatto (L), Gaussian (G), and Chebyshev (C) quadrature points. Since the type and the degree of numerical integration are always chosen such that numerical integration is exact, their influence on the results is not investigated.

As mentioned above, a variety of finite elements and element meshes have been applied. The simply supported two-layer Timoshenko beam has been modeled by 1, 2, 4, 8, 10, 20, 50, 100 and 1000 elements with 0, 1st, 2nd, ..., 5th degree interpolation polynomials, here termed as $E_0, E_1, E_2, \ldots, E_5$. By employing only one element E_0 and E_1, the relative error of the computed mid-point vertical deflection and interlayer slip is significant; by increasing the number of elements E_0 and E_1, the error decreases but, the convergence to the reference solution is relatively slow. On the other hand, the error is much smaller and the convergence is much faster, if, the degree of interpolation polynomials is increased. As observed from Tables 1–4, 2 elements E_4, 4 elements E_3, 8 or 10 elements E_2, 1000 elements E_0, or only one element E_5 give the mid-point vertical deflection and interlayer slip which are accurate to 6 digits. Note that good agreement between the various collocation schemes is observed. Different choices of the location of the collocation points give nearly identical results for elements E_2–E_5, but not for elements E_1. In this case, the Gaussian (G) collocation scheme indicates to be the most appropriate. It can also be observed from Tables 1–4 that the norm $\|\mathcal{M}_C - \mathcal{M}\|_2$ decreases uniformly by increasing the number of elements and

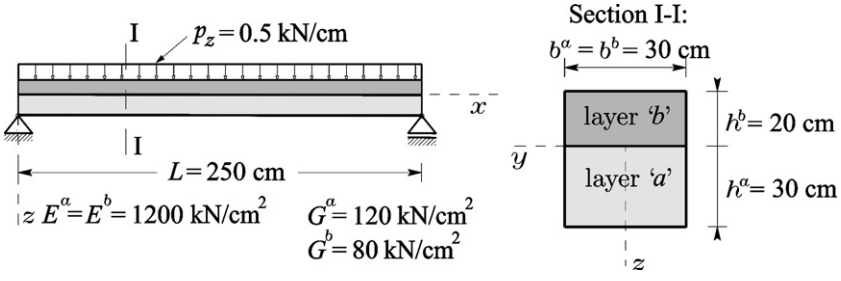

Fig. 2. The descriptive geometric, material and loading data of the simply supported two-layer Timoshenko beam.

Table 1
The comparison of numerical results for one element with the reference solution

n_e	d.o.i.	type	$w^a(L/2)$	$\Delta(0)$	$\|\mathcal{M}_C - \mathcal{M}\|_2$
1	0	E/L/G/C	0.290 643	0.116 257	1.78210×10^4
1	1	E/L	0.033 613	0.002 988	2.83842×10^4
		G	0.225 855	0.079 659	1.18826×10^4
		C	0.178 063	0.060 640	1.34222×10^4
1	2	E/L	0.270 938	0.077 249	1.93548×10^{-10}
		G	0.270 972	0.077 287	4.32163×10^{-10}
		C	0.270 959	0.077 273	3.18158×10^{-10}
1	3	E	0.270 988	0.077 271	3.56716×10^{-10}
		L	0.271 028	0.077 289	2.29257×10^{-10}
		G	0.270 996	0.077 288	3.25371×10^{-10}
		C	0.271 005	0.077 286	3.31368×10^{-10}
1	4	E	0.270 993	0.077 293	1.87862×10^{-10}
		L	0.270 993	0.077 293	2.89523×10^{-10}
		G	0.270 993	0.077 293	2.34103×10^{-10}
		C	0.270 993	0.077 540	3.30434×10^{-10}
1	5	E	0.271 026	0.077 293	1.42962×10^{-10}
		L	0.271 026	0.077 293	2.29257×10^{-10}
		G	0.271 026	0.077 293	1.23514×10^{-10}
		C	0.271 026	0.077 293	2.82211×10^{-10}
Reference solution			0.271 026	0.077 293	0

n_e—number of elements, d.o.i.—degree of interpolation, E—equidistant, L—Lobatto, G—Gaussian, C–Chebyshev.

Table 2
The comparison of numerical results with the reference solution

n_e	d.o.i.	type	$w^a(L/2)$	$\Delta(0)$	$\|\mathcal{M}_C - \mathcal{M}\|_2$
2	0	E/L/G/C	0.246 928	0.086 513	1.72959×10^4
2	1	E/L	0.215 860	0.060 491	1.00353×10^4
		G	0.263 520	0.079 511	4.20113×10^3
		C	0.251 622	0.074 765	4.74548×10^3
2	2	E/L	0.271 029	0.077 288	2.87028×10^{-10}
		G	0.271 014	0.077 290	2.31795×10^{-10}
		C	0.271 020	0.077 290	4.21815×10^{-10}
2	3	E	0.271 031	0.077 290	4.54423×10^{-10}
		L	0.271 033	0.077 291	3.35126×10^{-10}
		G	0.271 034	0.077 291	3.24815×10^{-10}
		C	0.271 033	0.077 291	2.86409×10^{-10}
2	4	E	0.271 026	0.077 293	3.96382×10^{-10}
		L	0.271 026	0.077 293	5.54296×10^{-10}
		G	0.271 026	0.077 293	4.08983×10^{-10}
		C	0.271 026	0.077 293	6.22722×10^{-10}
4	0	E/L/G/C	0.264 388	0.079 038	1.2927×10^4
4	1	E/L	0.251 631	0.074 756	3.54803×10^3
		G	0.263 518	0.079 501	1.48532×10^3
		C	0.260 547	0.078 315	1.67778×10^3
Reference solution			0.271 026	0.077 293	0

n_e—number of elements, d.o.i.—degree of interpolation, E—equidistant, L—Lobatto, G—Gaussian, C—Chebyshev.

the order of interpolation functions. We may then conclude that the present finite element solution is convergent to the reference one.

Table 3
The comparison of numerical results with the reference solution

n_e	d.o.i.	type	$w^a(L/2)$	$\Delta(0)$	$\|\mathcal{M}_C - \mathcal{M}\|_2$
4	2	E/L	0.271 023	0.077 291	5.11367×10^{-10}
		G	0.271 021	0.077 291	7.05474×10^{-10}
		C	0.271 022	0.077 291	6.60154×10^{-10}
4	3	E	0.271 026	0.077 293	1.03876×10^{-10}
		L	0.271 026	0.077 293	3.65277×10^{-10}
		G	0.271 026	0.077 293	4.67220×10^{-10}
		C	0.271 026	0.077 293	4.07509×10^{-10}
8	0	E/L/G/C	0.268 728	0.077 167	9.26026×10^3
8	1	E/L	0.260 549	0.078 315	1.25442×10^3
		G	0.263 519	0.079 501	5.25141×10^2
		C	0.262 776	0.079 204	5.93185×10^2
8	2	E/L	0.271 026	0.077 293	6.92304×10^{-10}
		G	0.271 026	0.077 293	7.45907×10^{-10}
		C	0.271 026	0.077 293	1.01180×10^{-10}
10	0	E/L/G/C	0.269 248	0.0769 432	8.29534×10^3
10	1	E/L	0.261 619	0.078 742	8.9758×10^2
		G	0.263 519	0.079 501	3.7576×10^2
		C	0.263 044	0.079 312	4.2445×10^2
10	2	E/L	0.271 026	0.077 293	4.14354×10^{-10}
		G	0.271 026	0.077 293	6.45604×10^{-10}
		C	0.271 026	0.077 293	1.01005×10^{-10}
Reference solution			0.271 026	0.077 293	0

n_e—number of elements, d.o.i.—degree of interpolation, E—equidistant, L—Lobatto, G—Gaussian, C—Chebyshev.

Table 4
The comparison of numerical results for constant interpolation with the reference solution

n_e	d.o.i.	type	$w^a(L/2)$	$\Delta(0)$	$\|\mathcal{M}_C - \mathcal{M}\|_2$
20	0	E/L/G/C	0.269 942	0.077 187	5.87765×10^2
50	0	E/L/G/C	0.270 457	0.077 278	3.71945×10^{-2}
100	0	E/L/G/C	0.271 013	0.077 286	2.31448×10^{-7}
1000	0	E/L/G/C	0.271 026	0.077 293	1.31255×10^{-10}
Reference solution			0.271 026	0.077 293	0

n_e—number of elements, d.o.i.—degree of interpolation, E—equidistant, L—Lobatto, G—Gaussian, C—Chebyshev.

Another advantage of the present finite elements is that they are completely locking-free. It is well known that the inherent disadvantage of some finite element models is the so-called locking. In the case of Timoshenko composite beam finite elements with an interlayer slip, the typical locking problems are shear and slip locking. The latter strongly depends on the connection stiffness [18,21]. This is a problem of particular interest especially in the case of high connection stiffnesses, where the slip oscillations may occur [18,21]. In order to show that the present finite elements are slip locking-free, the distribution of interlayer slip along the span of a simply supported beam is shown for low (Fig. 3) and high (Fig. 4) connection stiffness. It can be observed, that in both cases, the finite elements posses neither slip locking nor slip oscillations.

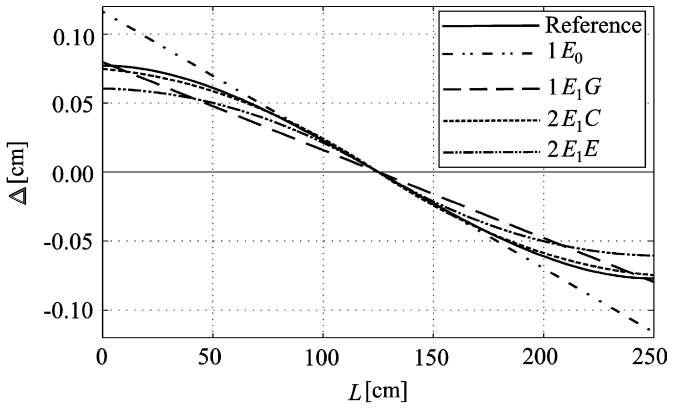

Fig. 3. The distribution of interlayer slip over the span of a simply supported beam for $K = 0.243\,\mathrm{kN/cm^2}$.

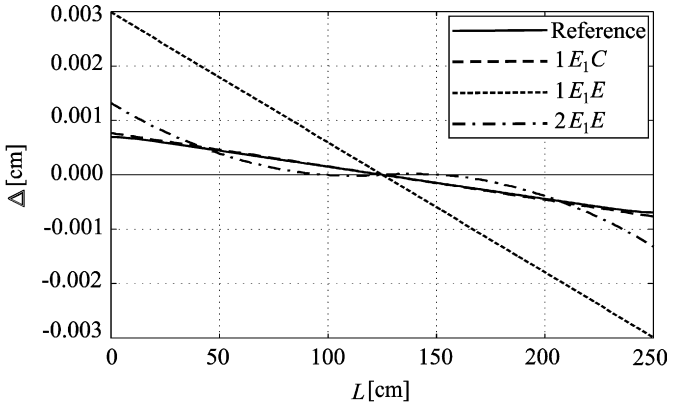

Fig. 4. The distribution of interlayer slip over the span of a simply supported beam for $K = 2430\,\mathrm{kN/cm^2}$.

Only the results for one and two elements with low order interpolation polynomials are shown (e.g. $1E_1/G$ means one element E_1 with the collocation points chosen to be distributed accordingly to the Gaussian integration scheme). For other cases not shown in Figs. 3 and 4 the results practically coincide with the reference distribution of interlayer slip, which would not have been the case, if slip locking would be present.

In order to demonstrate that the present finite elements are also free of shear locking, the vertical deflections (w_T) of the two-layer Timoshenko composite beam with the partial interlayer interaction are compared to the vertical deflections (w_B) obtained by the Euler–Bernoulli composite beam model with the same partial interlayer interaction, for different L/h ratios and different number of finite elements with different degrees of interpolation polynomials and different collocation point schemes. It can be observed from Fig. 5, that in the limiting case where the beam becomes very slender, the results of the Timoshenko two-layer beam converge to the Euler–Bernoulli solution of the two-layer beam with an interlayer slip which is not the case for finite elements which exhibit shear locking. Thus, we may conclude, that the present finite elements of the two-layer Timoshenko composite beam are shear-locking-free.

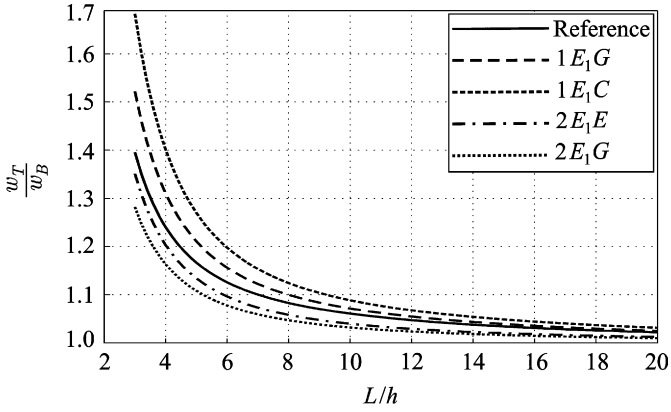

Fig. 5. The influence of L/h ratios on vertical deflections of a simply supported two-layer Timoshenko composite beam.

The next example will demonstrate the application of the present locking-free strain-based finite element method to stress–strain analysis of more complex structures. We consider a continuous asymmetric Timoshenko composite beam over two spans with the interlayer-slip modulus $K = 0.243\,\mathrm{kN/m^2}$. The descriptive geometric, material and loading data are described in Fig. 6.

A parametric study has been conducted to briefly asses the influence of shear moduli of the layers on the values of various static and kinematic quantities. Figs. 7 and 8 show only the graphs of interlayer slip Δ and vertical deflection w as a function of shear modulus $G = G^a = G^b$. The beam has been modelled by 10 elements E_4 with the equidistantly distributed collocation points (E). It is obvious from Figs. 7 and 8, that the shear modulus G has an important influence on static and kinematic quantities. Observe that slip Δ over the left span is smaller, while slip over the right span is, in contrast, higher for higher shear moduli. On the other hand, the vertical deflection w over the left span is higher, while vertical deflection over the right span is smaller for higher shear moduli. For a detailed analysis of the influence of shear moduli on the mechanical behaviour of two-layer Timoshenko beams with interlayer slip the reader is referred to [23].

4. Conclusions

A new locking-free strain-based finite element formulation for the numerical treatment of linear static analysis of two-layer planar composite beams with interlayer slip has been proposed. In this formulation, the modified principle of virtual work has been employed as a basis for the finite element discretization. The linear kinematic equations have been included into the principle by the procedure similar to that of Lagrangian multipliers. A strain field vector remains the only unknown function to be approximated in the finite element implementation of the principle. As a result, in contrast with many of the displacement-based and mixed finite element formulations of the composite beams with an interlayer slip, the present formulation is completely locking-free. The generalization of the composite beam theory with the inclusion of the Timoshenko beam theory for

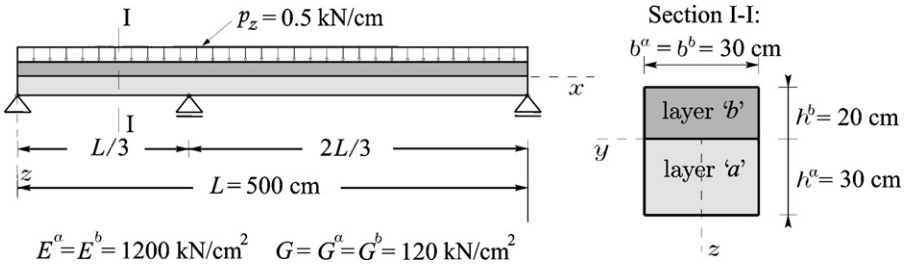

Fig. 6. The descriptive geometric, material and loading data of a continuous two-layer Timoshenko composite beam over two spans.

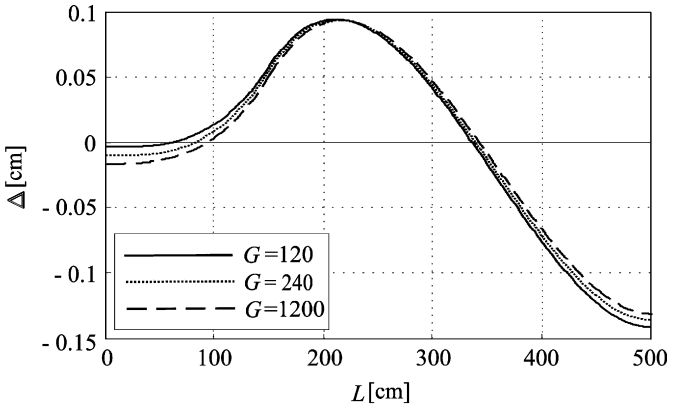

Fig. 7. Distribution of Δ along the span as a function of different values of shear moduli, $G = G^a = G^b$.

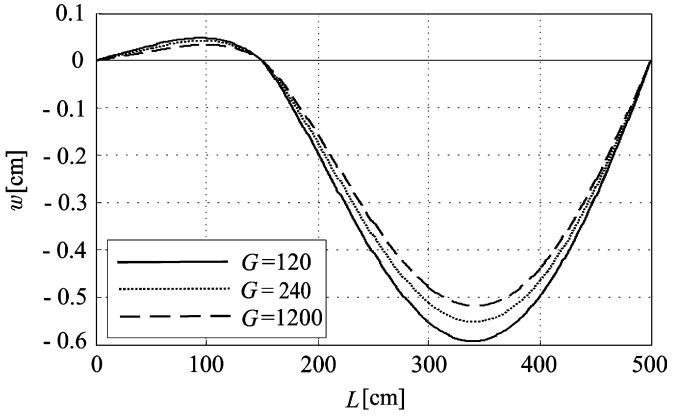

Fig. 8. Distribution of w along the span as a function of different values of shear moduli, $G = G^a = G^b$.

the individual layer of composite beam represents a substantial contribution in the field of analysis of non-slender composite beams with an interlayer slip. The main outcome of the present formulation is a family of efficient beam finite elements for the linear static analysis of two-layer planar Timoshenko beams with an interlayer slip. An extension of the present formulation to non-linear material problems is straightforward. There are no locking (shear and slip), poor convergence or stress oscillations in these finite elements. As only a few finite elements are needed to describe a composite beam of a frame with great precision, the new finite element formulations is perfectly suited for practical calculations.

Acknowledgements

The work of S. Schnabl was financially supported by the Ministry of Education, Science and Sport of the Republic of Slovenia under Contract 3311-02-831625. The support is gratefully acknowledged.

References

[1] N.M. Newmark, C.P. Siest, C.P. Viest, Test and analysis of composite beams with incomplete interaction, Proc. Soc. Exp. Stress Anal. 9 (1) (1951) 75–92.
[2] J.R. Goodman, E.P. Popov, Layered beam systems with inter-layer slip, J. Struct. Div. ASCE 94 (11) (1968) 2535–2547.
[3] J.R. Goodman, E.P. Popov, Layered wood systems with inter-layer slip, Wood Sci. 1 (3) (1969) 148–158.
[4] U.A. Girhammar, V.K.A. Gopu, Composite beam-columns with interlayer slip-exact analysis, J. Struct. Eng. ASCE 199 (4) (1993) 1265–1282.
[5] N.A. Jasim, Computation of deflections for continuous composite beams with partial interaction, Proc. Inst. Civil Eng. Struct. Build. 122 (1997) 347–354.
[6] N.A. Jasim, A.A.M. Ali, Deflections of composite beams with partial shear connection, Struct. Eng. 75 (1997) 58–61.
[7] G. Ranzi, M.A. Bradford, B. Uy, A general method of analysis of composite beams with partial interaction, Steel Compos. Struct. 3 (3) (2003) 169–184.
[8] G. Ranzi, M.A. Bradford, Analytical solution for the time-dependent behaviour of composite beams with partial interaction, Int. J. Solids Struct. 43 (2006) 3770–3793.
[9] S. Schnabl, I. Planinc, M. Saje, B. Čas, G. Turk, An analytical model of layered continuous beams with partial interaction, Struct. Eng. Mech. 22 (3) (2006) 263–278.
[10] A. Ayoub, A two-field mixed variational principle for partially connected composite beams, Finite Elem. Anal. Des. 37 (2001) 929–959.
[11] B. Čas, M. Saje, I. Planinc, Nonlinear finite element analysis of composite planar frames with inter-layer slip, Comput. Struct. 82 (2004) 1901–1912.
[12] B. Čas, S. Bratina, M. Saje, I. Planinc, Non-linear analysis of composite steel-concrete beams with incomplete interaction, Steel Compos. Struct. 4 (6) (2004) 489–507.
[13] B. Čas, Non-linear analysis of composite beams with inter-layer slip, Ph.D. Thesis, Faculty of Civil and Geodetic Engineering, University of Ljubljana, Slovenia, 2004 (in Slovene).
[14] G. Fabbrocino, G. Manfredi, E. Cosenza, Modelling of continuous steel-concrete composite beams: computational aspects, Comput. Struct. 80 (2002) 2241–2251.
[15] A. Dall'Asta, Composite beams with weak shear connection, Int. J. Solids Struct. 38 (2001) 5605–5624.
[16] G. Ranzi, P. Ansourian, F. Gara, G. Leoni, L. Dezi, Displacement-based formulations for composite beams with longitudinal slip and vertical uplift, Research Report No. R837, The University of Sydney, January, 2005.

[17] U.A. Girhammar, D. Pan, Dynamic analysis of composite members with interlayer slip, Int. J. Solids Struct. 33 (6) (1993) 797–823.
[18] A. Dall'Asta, A. Zona, Three-field mixed formulation for the non-linear analysis of composite beams with deformable shear connection, Finite Elem. Anal. Des. 40 (2004) 425–448.
[19] M.R. Salari, E. Spacone, Analysis of steel-concrete composite frames with bond-slip, J. Struct. Eng. ASCE 127 (11) (2001) 1241–1250.
[20] A. Dall'Asta, A. Zona, Non-linear analysis of composite beams by a displacement approach, Comput. Struct. 80 (2002) 2217–2228.
[21] A. Dall'Asta, A. Zona, Slip locking in finite elements for composite beams with deformable shear connection, Finite Elem. Anal. Des. 40 (2004) 1907–1930.
[22] A. Ayoub, F. Filippou, Mixed formulation of nonlinear steel-concrete composite beam element, J. Struct. Eng. ASCE 126 (3) (2000) 371–381.
[23] S. Schnabl, M. Saje, G. Turk, I. Planinc, Analytical solution of two-layer beam taking into account interlayer slip and shear deformation, J. Struct. Eng. ASCE. 133 (6) (2007).
[24] B. Vratanar, M. Saje, A consistent equilibrium in a cross-section of an elastic–plastic beam, Int. J. Solids Struct. 36 (1999) 311–337.
[25] I. Planinc, M. Saje, B. Čas, On the local stability condition in the planar beam finite element, J. Struct. Eng. Mech. 12 (5) (2001) 507–526.
[26] G.R. Cowper, The shear coefficient in Timoshenko's beam theory, J. Appl. Mech. 33 (2) (1966) 335–340.
[27] E. Reissner, On one-dimensional finite-strain beam theory: the plane problem, J. Appl. Mech. Phys. (ZAMP) 23 (1972) 795–804.
[28] S.P. Timoshenko, On the correction for shear of the differential equation for transverse vibrations of prismatic bars, Philos. Mag. Ser. 6 41 (245) (1921) 744–746.
[29] J.N. Reddy, Applied Functional Analysis and Variational Methods in Engineering, McGraw-Hill Book Company, Singapore, 1986.

Available online at www.sciencedirect.com
ScienceDirect
Structural Safety 29 (2007) 279–293
STRUCTURAL SAFETY
www.elsevier.com/locate/strusafe

Reliability analysis of a glulam beam

Tomi Toratti [a,*], Simon Schnabl [b], Goran Turk [b]

[a] VTT Technical Research centre of Finland, P.O. Box 1000, FI-02044 VTT, Finland
[b] University of Ljubljana, Faculty of Civil and Geodetic Engineering, Jamova 2, 1000 Ljubljana, Slovenia

Available online 11 September 2006

Abstract

The present case study is an example of the use of reliability analysis to asses the failure probability of a tapered glulam beam. This beam is part of a true structure built for a super market in the town of Kokemäki in Finland. The reliability analysis is carried out using the snow load statistics available from the site and on material strength information available from previous experiments. The Eurocode 5 and the Finnish building code are used as the deterministic methods to which the probabilistic method is compared to. The calculations show that the effect of the strength variation is not significant, when the coefficient of variation of the strength is around 15% as usually assumed for glulam. The probability of failure resulting from a deterministic design based on Eurocode 5 is low compared to the target values and lower sections are possible if applying a probabilistic design method. In fire design, if a 60 min resistance is required, this is not the case according to Eurocode 5 design procedures, a higher section would be required. However, a probabilistic based fire analysis results in bounds for the yearly probability of failure which are comparable to the target value and to the values obtained from the normal probabilistic based design.

Keywords: Reliability; Eurocode; Design; Glulam; Fire

1. Introduction

The structure of the Kokemäki K-Market is analysed in this case study. This is a timber beam-column structure of glued laminated wood (glulam). Glulam columns support 17 m long beams which compose the roof structure (see Fig. 1).

The reliability analysis will be carried out on the main glulam beam, which is tapered from the bottom edge. The analysis will first be done in a normal design situation, during which also the sensitivity of the beam strength variation will be assessed. The reliability in a fire situation will also be carried out. Lateral torsional buckling of the beam was taken into account according to Eurocode 5 [4]. The calculated probabilities are for a one year reference period, unless otherwise stated.

* Corresponding author.
E-mail addresses: tomi.toratti@vtt.fi (T. Toratti), sschnabl@fgg.uni-lj.si (S. Schnabl), gturk@fgg.uni-lj.si (G. Turk).

0167-4730/$ - see front matter © 2006 Elsevier Ltd. All rights reserved.
doi:10.1016/j.strusafe.2006.07.011

Fig. 1. Kokemäki K-Market and the geometry of the tapered glulam beam analysed in this case study.

2. Statistical distributions of the variables

For the present analysis, two main sources for input data are used. Namely, the probabilistic model code [6,10], which is a Nordic study on the calibration of partial safety factors for various building materials. Table 1 summarises the input recommended in [10]. Extensive reliability studies have also been carried out by Thelandersson et al. [12] and Ranta-Maunus [8,9]. In Ranta-Maunus [9], the emphasis was on the precise description of the strength lower tail distribution for wooden products and on the calibration of partial safety factors for wooden structures. In Thelandersson et al. [12], the emphasis was on the long-term load analysis and related calibration of the strength modification factors.

Some further background is given in the following to the distributions concerning the glulam material strength and snow loads.

Table 1
Statistical distributions and coefficients of variation recommended in [10]

Type of parameter		Parameter	Coefficient of variation			Distribution type
			Concrete	Steel	Glulam	
Actions	Permanent	Self-weight	0.06	0.02	0.06	Normal
		Other	0.10	0.10	0.10	Normal
	Variable	Environmental	0.40	0.40	0.40	Gumbel
		Imposed	0.20	0.20	0.20	Gumbel
Strength		Concrete	0.10			Log-normal
		Reinforcement	0.04			Log-normal
		Structural Steel		0.05		Log-normal
		Glulam			0.15	Log-normal
Geometry		Effective depth	0.02			Normal
		Beam depth	0.02	0.01	0.01	Normal
		Beam width	0.02	0.01	0.01	Normal
		Plate thickness		0.04		Normal
Model uncertainties		R-model	0.05	0.05	0.05	Normal

2.1. Glulam strength distribution

There exists few test data which could be used to describe the glulam strength distribution. Much more is available for other wooden materials like structural timber, LVL or plywood. To obtain the lower tail strength distribution with enough accuracy, a high number of tests are required. The largest test sample available to the authors is summarised in Table 2. This data was obtained in a joint Nordic project on the reliability of timber. The tests were carried out in NTI Norway.

In these test samples, the target characteristic values were achieved. The tail fitting of the strength distribution resulted in a coefficient of variation of 13% and 19% when using the log-normal distribution. It was concluded in the above reference, that until further evidence, a log-normal distribution with a coefficient of variation of 15% may be recommended. More test results on glulam are however needed.

2.2. The snow load distribution

In Ref. [2] Perälä and Reuna, the snow load values for different locations in Finland are given for the period of 33 years. The example analysis here is done to a building in the city of Kokemäki and a measurement sight with closest location is chosen. Fig. 2 shows the Gumbel plot of the yearly maximum snow loads (water equivalents). ISO CW 4355 [1] recommends using the extreme value distribution (Gumbel) for the annual maximum snow loads. The characteristic ground snow load $V_{0.98}$ extrapolated from the figure is 220 mm (water equivalent). The characteristic ground snow loads in Eurocode 5 for the area give values of 2–2.5 kN/m^2, which is in agreement with the measurements. The measured value is used in the proceeding analysis.

2.3. Statistical distributions of the variables used in this study

In the present study, the distributions used for the loads and strengths are:

- permanent load: normal ($V_G = 0.05$),
- snow load: Gumbel ($V_Q = 0.40$),

Table 2
Available glulam test data [9]

	Target $f_{0.05}$ (N/mm^2)	$f_{0.05}$ in test (N/mm^2)	Explanation of test	Sample size	Tail fitted (%)	Fitting distribution	COV (%)
Glulam	30	33.5	Edgewise bending	126	10	Normal	11
						Log-normal	13
Glulam	37	39.9	Edgewise bending	109	10	Normal	14
						Log-normal	19

Table 3
Snow loads from location 35312 [2] modelled as normal distributions

Month	Snow load water equivalent (mm)		Snow load on the beam (kN/m)	
	Mean	Standard deviation	Mean	Standard deviation
January	41.6	24.9	2.06	1.23
February	67.5	30.3	3.34	1.50
March	79.9	35.9	3.95	1.78
April	41.0	36.9	2.03	1.82
May	0	–	0	–
June	0	–	0	–
July	0	–	0	–
August	0	–	0	–
September	0	–	0	–
October	0	–	0	–
November	0	–	0	–
December	18.7	14.8	0.93	0.73

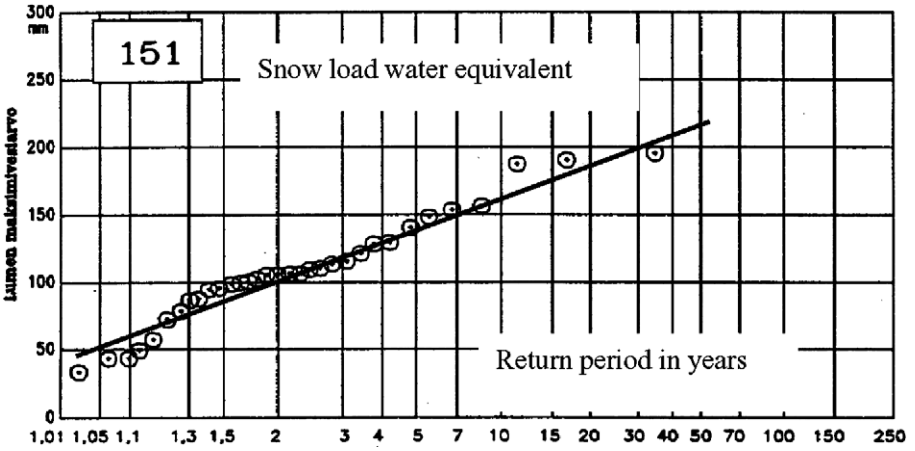

Fig. 2. The measured ground snow load close to Kokemäki [2].

- glulam strength (bending and shear): log-normal ($V_F = 0.15$),
- dimensions (height and width): normal ($V_{h \text{ or } b} = 0.01$),
- model uncertainty: normal ($V_m = 0.05$ or 0.10).

3. Load and strength parameters

The dead load, G, is normally distributed. The glulam beam self-weight is assumed to be 0.88 kN/m acting on the beam as a line-load and the roof self-weight 0.44 kN/m^2 acting on the whole roof area. Since the beams are 6.3 m apart the width of the roof loading lumped to each beam is 6.3 m. It is assumed also that the coefficient of variation is $V_G = 5\%$. This is a slightly lower value than presented in Table 1 for glulam self-weight, but it is a value of the whole roof which is composed of different materials. This value has been widely used in previous reliability studies for self-weight of structures. Therefore, the values used in analysis are

$$m_G = 6.3 \cdot 0.44 + 0.88 = 3.65 \text{ kN/m} \quad \sigma_G = m_G V_G = 0.18 \text{ kN/m}.$$

The snow load, Q, is distributed by Gumbel distribution. The 98th percentile of the distributed load is $q' = 1.73$ kN/m^2 (characteristic ground snow load is 2.15 kN/m^2).

The ground to roof snow load conversion factor has been assigned a constant value of 0.8 in most calculations of this example. A sensitivity study is however performed in one example where a stochastic normally distributed value with a COV of 10% and of 20% is considered for this factor.

Thus the 98th percentile of the snow load Q is $q = Q_{0.98} = 6.3 \cdot 1.73 = 10.9$ kN/m. The coefficient of variation is assumed to be $V_Q = 0.40$. The parameters u and α of Gumbel distribution are determined from the following equations:

$$V_Q = \frac{\sigma_Q}{m_Q} = \frac{\pi}{\sqrt{6}\alpha}\frac{1}{u + \frac{\gamma}{\alpha}} = 0.40,$$
$$F_Q(Q_{0.98}) = F_Q(10.9) = 0.98 = \exp(-\exp(-\alpha(Q_{0.98} - u))) = \exp(-\exp(-\alpha(10.9 - u))),$$

where $\gamma = 0.577216$ is the Euler constant. These equations can easily be solved

$$\alpha = \frac{1.28255 + 3.32472 V_q}{Q_{0.98} V_q} = 0.5992,$$
$$u = \frac{Q_{0.98}(1.11201 - 0.500462 V_Q)}{1.11201 + 2.88263 V_Q} = 4.3879.$$

The bending strength is lognormally distributed. The glulam material is of structural quality L40, thus it is assumed that the characteristic value is $f_k = F_{0.05} = 39\ \mathrm{N/mm^2}$ (short term strength). The coefficient of variation V_F is assumed as 0.15, except in the first analysis, where the parameter is varied from 0.05 to 0.40. The parameters of the lognormal distributions $\tilde{m}_F$ and $\sigma_{\ln F}$ are evaluated from the following equations:

$$\sigma_{\ln F}^2 = \ln(V_F^2 + 1),$$
$$F_F(F_{0.05}) = F_F(39) = F_U\left(\frac{\ln F_{0.05} - \ln \tilde{m}_F}{\sigma_{\ln F}}\right),$$

where $F_U(\cdot)$ denotes cumulative distribution function of the standardised normal distribution. Thus, the relation between the parameters and characteristic value and coefficient of variation is given as follows:

$$\sigma_{\ln F} = \sqrt{\ln(V_F^2 + 1)},$$
$$\tilde{m}_F = F_{0.05}\exp(-\sigma_{\ln F} F_U^{-1}(0.05)),$$

where $F_U^{-1}(.)$ is the inverse of the cumulative distribution function of the standardised normal distribution. Sometimes it is more convenient to describe the random variable by its moments instead of the distribution parameters. In the case of lognormal distribution the relations between the parameters and moments are

$$m_F = \tilde{m}_F \exp\left(\frac{\sigma_{\ln F}^2}{2}\right),$$
$$\sigma_F^2 = m_F^2(\exp(\sigma_{\ln F}^2) - 1).$$

The strength is reduced by the modification factor k_{mod}, which takes into account the effect of the duration of the load and the moisture content in the structure on strength parameters. The cross-section dimensions are assumed normally distributed, with a coefficient of variation of 1%.

4. Mechanical analysis

Since the beam is simply supported, the evaluation of internal forces is elementary. The structural analysis was carried out on bending at the critical cross-section, bending at the apex section and shear. The initial analysis showed that the critical cross-section is situated where the bending stresses are the highest. The beam height at this point is 1060 mm. Bending at the apex zone is not critical. Also the shear capacity resulted in much lower probabilities of failure. Therefore in the following, only the critical cross-section in bending is analysed. The strength reducing factor for torsional buckling is not required for normal design, but it becomes necessary for the fire design where more slender sections are analysed. Thus the strength reducing parameter k_{crit} is omitted from the design Eqs. (1)–(4) for the normal design situation. In the fire design situation, this parameter is included.

The stresses in the critical cross-section are calculated in two different ways:

(a) according to the Finnish building code on the design of timber structures B10 [7] and
(b) according to Eurocode 5 [4].

The difference between the calculation methods of the glulam beam between these codes is the following:

(a) According to B10, the normal stress σ_{xx} should not exceed the bending strength F taking into consideration a height effect in the critical cross-section

$$\sigma_{xx} \leqslant C_F F, \quad C_F = \left(\frac{300}{h}\right)^{\frac{1}{9}}, \tag{1}$$

where h is 1060 mm. Thus, the value of C_F is 0.87. The design equation according to B10 is then

$$\frac{F}{\gamma_m} k_{\mathrm{mod}} C_F > \left(\frac{N_{xp}(1.2G + 1.6Q)}{bh} + \frac{6M_{yp}(1.2G + 1.6Q)}{bh^2} \right), \tag{2}$$

where $\gamma_m = 1.3$ is the material partial safety factor, $k_{\mathrm{mod}} = 1.0$ is the strength modification factor for load duration and moisture conditions, $C_F = 0.87$ is the height effect factor and the dead and snow loads have been multiplied by the respective load safety factors.

(b) According to Eurocode 5, the normal stress σ_{xx} should not exceed the bending strength F at the outermost fibre of the tapered edge

$$\sigma_{xx} \leqslant k_{m,\alpha} F, \quad k_{m,\alpha} = \frac{1}{\sqrt{1 + \left(\frac{f_{m,k}}{1.5 f_{v,k}} \tan\alpha \right)^2 + \left(\frac{f_{m,k}}{f_{c,90,k}} \tan^2\alpha \right)^2}}. \tag{3}$$

The angle between the beam main axis and the fibre direction deviate in the compressive side of the beam. In this case, the strength is reduced by the factor $k_{m,\alpha}$, which takes into account the influence of the taper in the compression side. $f_{m,k}$, $f_{v,k}$, $f_{c,90,k}$, and α are the characteristic values of the bending strength, the shear strength, the compression strength perpendicular to the grain, and the angle of taper, respectively. The following values were taken (short-term characteristic strengths): $f_{m,k} = 39.0\ \mathrm{N/mm^2}$, $f_{v,k} = 3.5\ \mathrm{N/mm^2}$, $f_{c,90,k} = 6\ \mathrm{N/mm^2}$, and $\alpha = 2.5°$, these values result in $k_{m,\alpha} = 0.95$. The design equation according to Eurocode 5 is then

$$\frac{F}{\gamma_m} k_{\mathrm{mod}} k_{m,\alpha} > \left(\frac{N_{xp}(1.2G + 1.5Q)}{bh} + \frac{6M_{yp}(1.2G + 1.5Q)}{bh^2} \right) \tag{4}$$

where $\gamma_m = 1.3$ is the material partial safety factor, $k_{\mathrm{mod}} = 1.0$ is the strength modification factor for load duration and moisture conditions, $k_{m,\alpha} = 0.95$ is the reduction factor described above and the dead and snow loads have been multiplied by the respective load safety factors.

5. Reliability analysis for normal design

5.1. Reliability analysis using Gumbel distribution for yearly snow load

The reliability analysis was performed by the computer program Comrel [11]. Initially, different reliability methods were tried. Since the problem is relatively simple, different methods (FORM, SORM, crude Monte Carlo, adaptive sampling, etc.) gave almost identical results. In adaptive sampling 20 000 repetitions of the calculation were performed, whereas the number of simulations in crude Monte Carlo was 5 000 000. There were clearly advantages with the other methods compared to crude Monte Carlo simulations: the solutions were more stable and the calculation was faster. In the following, the adaptive sampling procedure is used in the reliability analysis.

The limit state equation for the maximum bending stress case is

$$g = F k_{\mathrm{mod}} \begin{matrix} k_{m,\alpha} \\ \text{or} \\ C_F \end{matrix} - \left(\frac{N_{xp}(G + Q)}{bh} + \frac{6M_{yp}(G + Q)}{bh^2} \right) k_{\mathrm{model}} \tag{5}$$

with variables

- G: permanent load (normal, $V_G = 0.05$),
- Q: snow load (Gumbel, $C_Q = 0.40$),
- F: glulam strength (log-normal, $V_f = 0.15$),
- b and h: section dimensions, height and width (normal, $V_{b\mathrm{or}h} = 0.01$),
- k_{model}: model uncertainty (normal, mean = 1.0, $V_m = 0.05$ or 0.10) and constants.

$k_{\mathrm{mod}} = 1/1.3$ (B10) or 0.8 (Eurocode 5), $C_F = 0.87$ (B10) or $k_{m,\alpha} = 0.95$ (Eurocode 5), $N_{xp} = 0.346$ (kN per unit load kN/m) and $M_{yp} = 29.144$ (kNm per unit load kN/m) (N_{xp} and M_{yp} are obtained by the mechanical analysis).

The probability of failure for the two different design codes as a function of the coefficient of variation of strength is shown in Fig. 3. The relationship is not monotonic; instead it has a maximum between 0.125 and 0.15. The failure probability increases for larger or smaller coefficients of variation. From Fig. 3 we may notice that the probability of failure increases over 10-fold as the coefficient of variation increases from 0.15 to 0.40.

The probability of failure P_f is close to a minimum at a strength variation of about 15%, a value usually assumed for glulam, and it is not very sensitive to the strength variation in this range. Considering the failure probability, there seems to be no reason for attempting to decrease the strength variation, unless the material strength characteristic value is affected. This low sensitivity of the strength variation is also an advantage considering the accuracy of a reliability analysis of a glulam structure, since the variation of strength is not precisely known.

The sensitivity analysis also shows that there is some effect on increasing the model uncertainty parameter COV to 10% and a very similar effect on treating the ground to roof snow load conversion factor as a normally distributed random parameter with a COV of 10%. These effects are however small. The effect is high for the case of COV of 20% on the ground to roof snow load factor, comparable to the difference in the β-value that results when using the two standards.

The calculation shows that for a glulam having a strength COV of 15%, according to B10 the β-value is 4.49 corresponding to a failure probability of $P_f = 3.56 \times 10^{-6}$ and according to EC5 the β-value is 4.89 corresponding to a failure probability of $P_f = 0.51 \times 10^{-6}$. In all the following calculations the glulam strength coefficient of variation is 15%, the model uncertainty coefficient of variation is 5% and the ground to roof snow load factor is treated as a constant deterministic parameter.

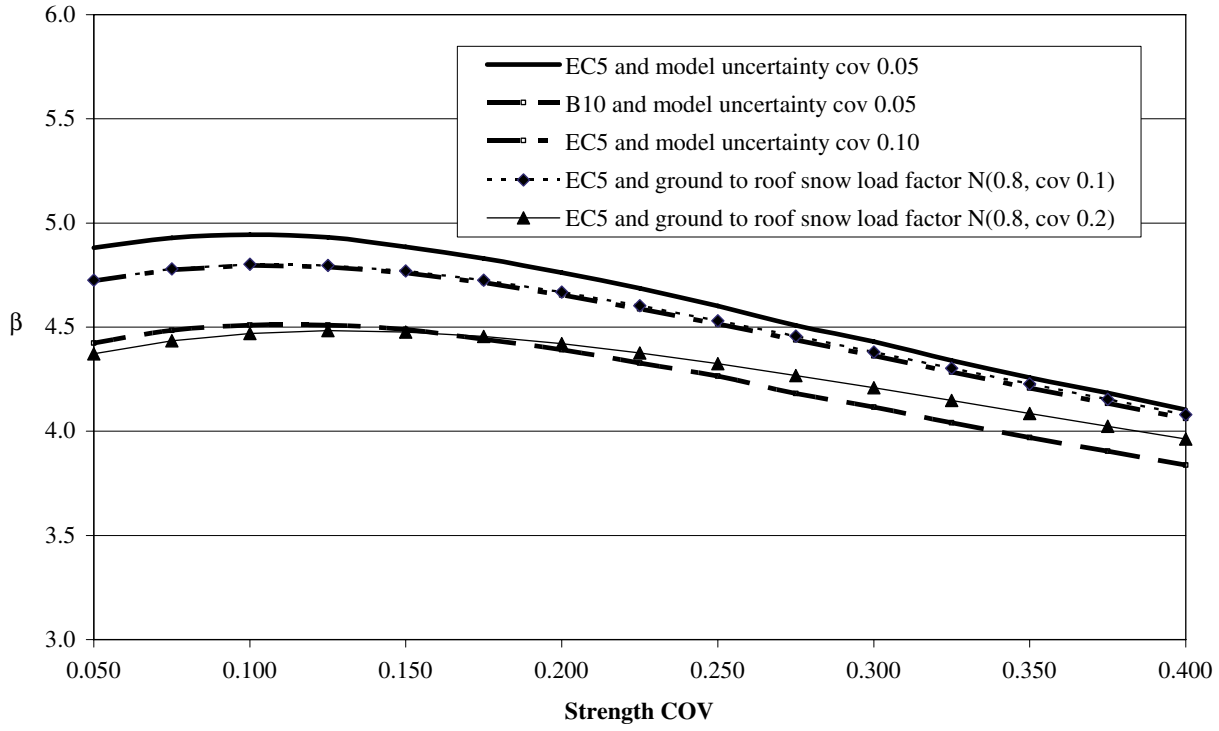

Fig. 3. Reliability index β as a function of strength coefficient of variation V_F. The comparison between EC5 and B10, the influence of model uncertainty COV (0.05 and 0.10), and the influence of random ground to roof snow load factor (COV 0.10 and 0.20).

5.2. Reliability of the beam at different months of a year

In the following, the monthly measured snow load water equivalents were used in the analysis. This was done in order to see the variation of the reliability during a year and to compare the yearly maximum value with the code format calculated in the preceding chapter. The monthly snow loads were evaluated for a given day of every month using data of 33 years during the period between 1960 and 1993. These monthly snow load values were analysed and found to be normally distributed (personal communication [13]). The ground snow loads were transformed to roof loads using the conversion factor of 0.8.

The maximum probability of failure occurs during March in this case and the value is $P_f = 1.16 \times 10^{-6}$ according to EC5 and $P_f = 4.80 \times 10^{-6}$ according to B10 (Fig. 4). The simple bounds for yearly probability of failure are determined by

$$\max(P_{f,\text{january}}, P_{f,\text{february}}, \ldots, P_{f,\text{december}}) \leqslant P_{f,\text{year}} \leqslant 1 - (1 - P_{f,\text{january}})(1 - P_{f,\text{february}}) \cdots (1 - P_{f,\text{december}}). \quad (6)$$

As may be observed from Table 4, there is noticeable effect of the distribution model used for the snow load on the probability of failure. The differences are not high when the β-values are compared. The monthly normal distribution method gave a double failure probability, in the case of B10, and triple, in the case of EC5.

5.3. Comparison to target reliability values

The calculated reliabilities may be compared to the target values given in Table 5 for reliability class 2 (moderate consequences of failure). The probabilistic model code gives a value of 4.2, and prEN 1990 [3] gives

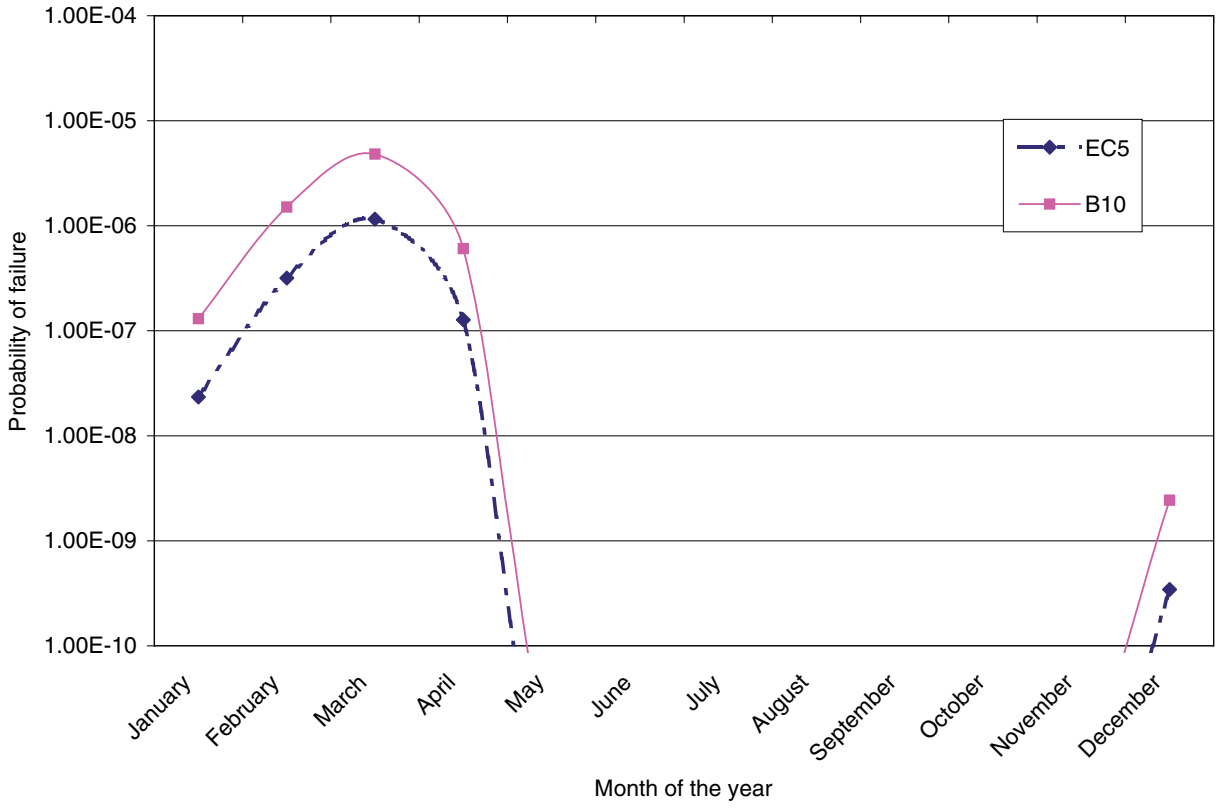

Fig. 4. Probability of failure during one year (bending failure mode at maximum bending stress location).

Table 4
Probability of failure during a year, the comparison between the values obtained using the yearly Gumbel distribution and the monthly normal distributions for the snow load

Code used	β-value and $P_{f,\text{year}}$ from Fig. 3, based on yearly maximum Gumbel distributed snow load	Bounds for β-value and $P_{f,\text{year}}$ from Eq. (4), based on normally distributed monthly snow loads	
EC5	4.885 (5.18×10^{-7})	4.654 (1.63×10^{-6})	4.724 (1.16×10^{-6})
B10	4.489 (3.58×10^{-6})	4.344 (7.05×10^{-6})	4.426 (4.80×10^{-6})

Table 5
Recommended target β-values in ultimate limit state for a one year period according to the probabilistic model code [6] and prEN 1990 [3]

Relative cost of safety measure		Class 1		Class 2		Class 3	
		Minor consequences of failure		Moderate consequences of failure		Large consequences of failure	
		β	P_f	β	P_f	β	P_f
Probab. model code	Large (A)	3.1	$\approx9.7\times10^{-4}$	3.3	$\approx4.8\times10^{-4}$	3.7	$\approx1.1\times10^{-4}$
	Normal (B)	3.7	$\approx1.1\times10^{-4}$	**4.2**	$\approx1.3\times10^{-5}$	4.4	$\approx5.4\times10^{-6}$
	Small (C)	4.2	$\approx1.3\times10^{-5}$	4.4	$\approx5.4\times10^{-6}$	4.7	$\approx1.3\times10^{-6}$
prEN 1990		4.2	$\approx1.3\times10^{-5}$	**4.7**	$\approx1.3\times10^{-6}$	5.2	$\approx10^{-7}$

Table 6
Ratios of the failure probability between deterministic and stochastic (COV = 0.2) charring rates at different fire duration times

	15 min	30 min	45 min	60 min
Deterministic	1	1	1	1
Stochastic, independent	1.2	2.0	3.5	0.9
Stochastic, dependent	1.4	4.3	6.8	0.8

Yearly max. snow load Gumbel distributed.

a β-value of 4.7. The calculated reliabilities are higher than the target levels given in the probabilistic model code [6].

Dimensioning this beam using the deterministic design code method results in a β-value of 4.5 using the B10 code and in a β-value of 4.9 using the EC5 code design procedures (for yearly snow load the maximum Gumbel distribution is used). These values are rather close to the target values. However, it would be possible to reduce the section height especially in the case of EC5, if the target reliabilities defined above are applied instead (Fig. 5).

6. Reliability analysis of the beam under a fire situation

In the following, several reliability analyses are carried out for the same beam under a fire condition. The analyses are done based on the methods given in prEN 1995-1-2 [5] on loading conditions under fire and on the charring rate of the wood section. Based on the previous example, only the most critical section is analysed for bending stresses, since this will be the determining section also in a fire condition. It is here assumed that the secondary structure spaced to 2.4 m on the top of the beam will be functional during the fire duration and this will support the top edge of the beam from buckling at these points.

6.1. Failure probability in fire condition based on different month of the year

In the first analysis, the charring rate is regarded as deterministic with the fixed value given in the design codes. Both design codes EC5 and B10 are compared in this analysis. The limit state equation for the maximum bending stress in a fire condition case is

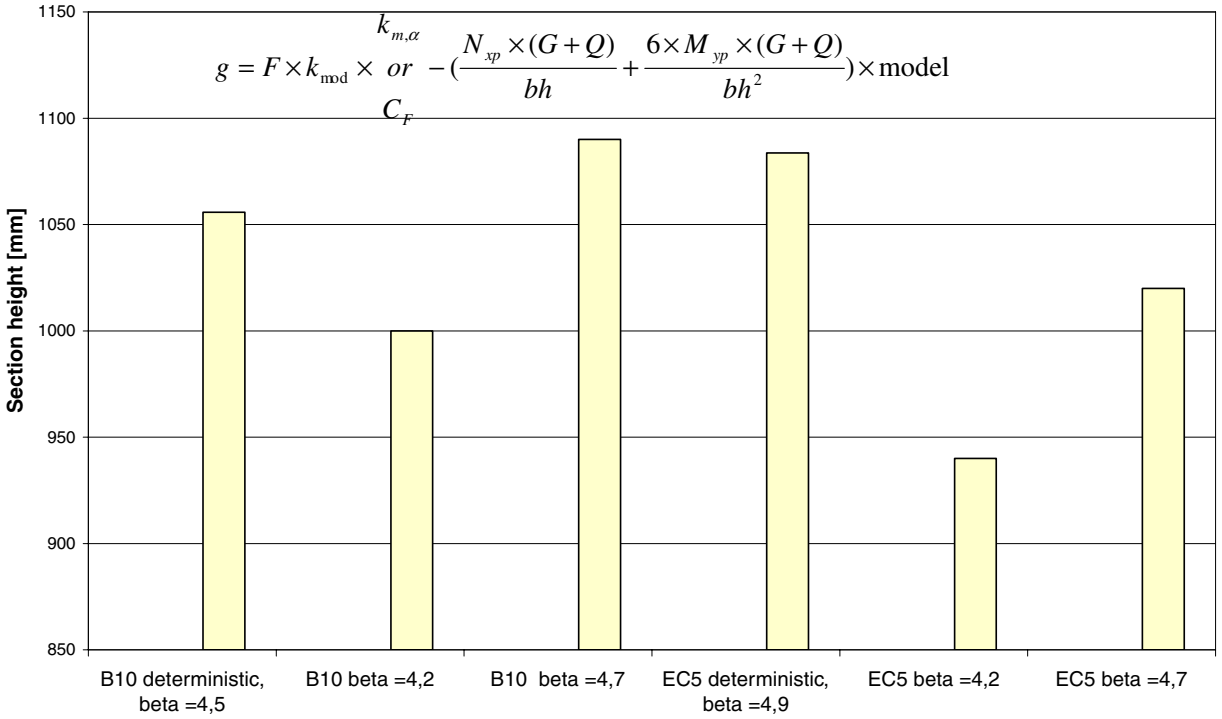

Fig. 5. Required beam section heights based on design codes B10 (Finnish timber design code) (Eq. (2)) and EC5 (Eurocode 5) (Eq. (4)). The β-values resulting from a deterministic dimensioning, based on these design codes, are also given. If target β-values of Table 6 are applied, the required heights are shown.

$$g = Fk_{\mathrm{crit}}k_{\mathrm{mod},fi} \begin{matrix} k_{m,\alpha} \\ \text{or} \\ C_F \end{matrix} - \left(\frac{N_{xp}(G+Q)}{b_{\mathrm{red}}h_{\mathrm{red}}} + \frac{6M_{yp}(G+Q)}{b_{\mathrm{red}}h_{\mathrm{red}}^2}\right)k_{\mathrm{model}} \tag{7}$$

with variables

- G: permanent load (normal, $V_G = 0.05$),
- Q: snow load (as given in Table 3 for the different months),
- F: glulam strength (log-normal, $V_f = 0.15$),
- k_{crit} is the strength reduction factor for torsional buckling of the beam (as given in EC5), considering it is supported at 2.4 m spacing from the top edge. This had no effect in normal design, but in fire design with reduced cross-sections this becomes highly significant,
- b_{red} and h_{red}: reduced section dimensions for height and width depending on fire exposure (normal, $V_{b\mathrm{or}h} = 0.01$) using a charring rate,
  EC5: $d_{ef} = \beta_n t + K_o d_o$ (with $\beta_n = 0.7$ mm/min, $K_o = 1$ and $d_o = 7$ mm),
  B10: $d_{ef} = \beta_n t$ (with $\beta_n = 0.7$ mm/min),
- k_{model}: Model uncertainty (normal, mean = 1.0, $V_m = 0.05$),

and constants

EC5: $k_{\mathrm{mod},fi} = 1.0$, $k_{m,\alpha} = 0.95$ or
B10: $C_F = 1$ (B10),
$N_{xp} = 0.346$ (kN per unit load (kN/m)),
$M_{yp} = 29.144$ (kNm per unit load (kN/m)) (N_{xp} and M_{yp} result from the mechanical analysis).

The winter months have the highest probability of failure due to snow loads and March is most critical in this sense. The fire design according to EC5 is more conservative than according to B10.

6.2. Failure probability considering a stochastic charring rate

It has been observed from previous charring experiments that charring rates are variable between test pieces. Variabilities in the order of COV = 20% have been observed for glulam, but higher and lower variabilities have also been observed [13]. The limit state equation for the maximum bending stress in a fire condition in this case is

$$g = Fk_{\mathrm{crit}}k_{\mathrm{mod},fi}\begin{matrix}k_{m,\alpha}\\ \text{or}\\ C_F\end{matrix} - \left(\frac{N_{xp}(G+Q)}{\left(b-d'_{ef}-d''_{ef}\right)\left(h-d'''_{ef}\right)}+\frac{6M_{yp}(G+Q)}{\left(b-d'_{ef}-d''_{ef}\right)\left(h-d'''_{ef}\right)^2}\right)k_{\mathrm{model}}. \tag{8}$$

The variables are the same as in Eq. (7), except here the charring rate is a normally distributed variable. The charring depths for the three different sides, d'_{ef}, d''_{ef} and d'''_{ef} are normally distributed with a coefficient of variation of 0.1, 0.2 or 0.3 and with a mean value as given in the EC5 design code. These are also compared to a deterministic charring depth corresponding to the EC5 code value. The 3 different charring depths of the different sides of the beam, may or may not be independent, therefore two separate calculations were done, one assuming these are independent and the other dependent.

Comparing the results obtained with the deterministic charring rate to the stochastic rate with a variability of COV = 0.2, the following may be observed. The effect of the charring rate being a stochastic variable is significant only after a fire duration of about 15–30 minutes, for shorter fire duration the failure probabilities are small and the differences negligible. At a fire duration approaching 60 min, the effect of stochastic charring

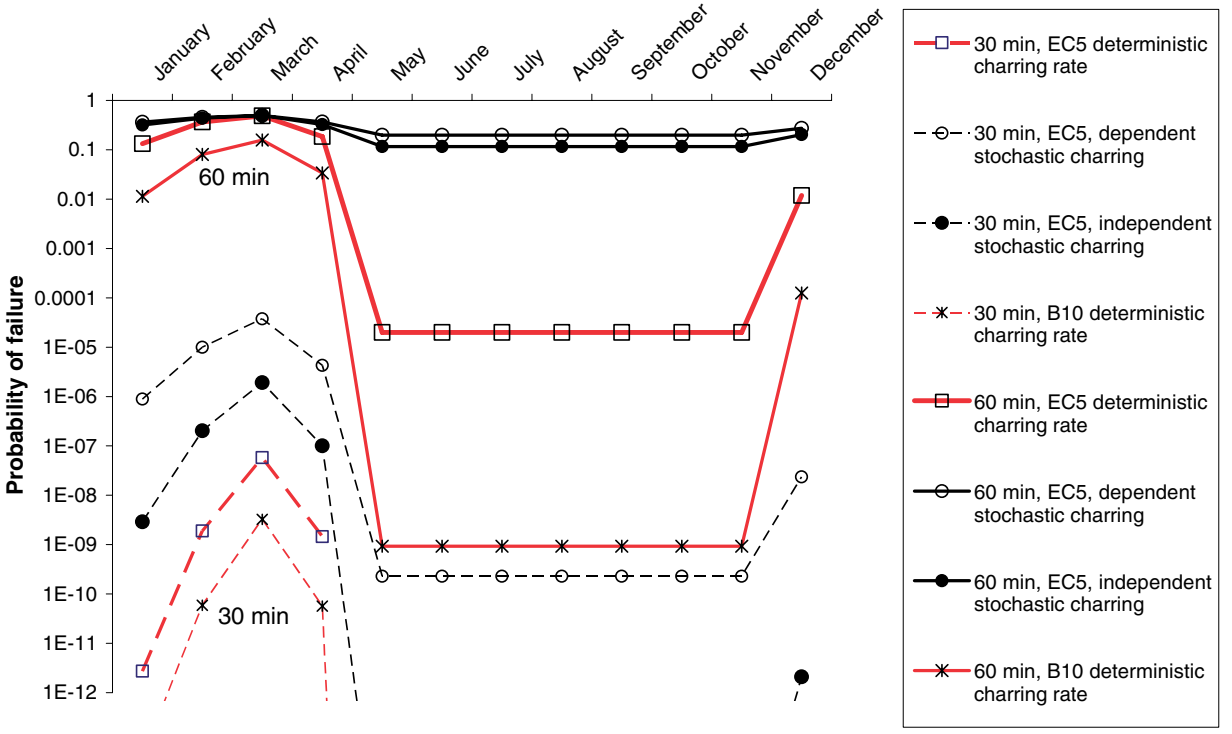

Fig. 6. Results of the reliability analysis during a fire situation at different months of a year. This figure also includes results using stochastic charring (COV = 0.2), which are calculated based on the following section.

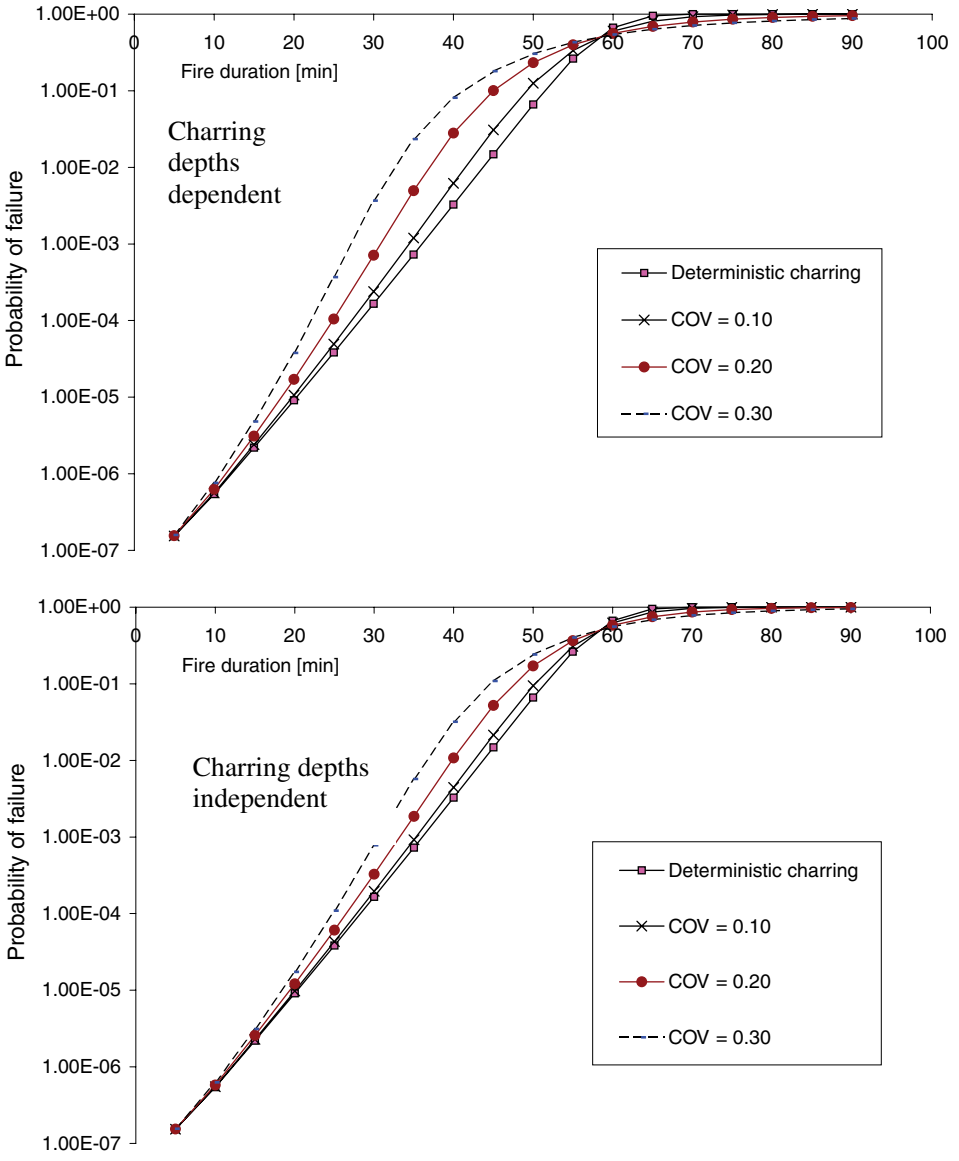

Fig. 7. Effect of charring variability on the probability of failure.

decreases again. This is true for high loads (Fig. 7), for low loads (Fig. 6 summer period) there is a high difference also at a 60 min fire duration time. Also whether the charring rates between the sides are dependent or independent is of significance. This is a characteristic not well known, that is, whether the variability is more pronounced between different glulam beams (dependent or fully correlated) or within a glulam beam (independent or non-correlated).

6.3. Failure probability of the beam during a 60 min fire

In the following calculations the following assumptions are taken: (1) the charring rate is taken deterministic as given in the codes, (2) the upper supporting structure is assumed to function during the fire in prevention of lateral buckling at the 2.4 m spacing points, (3) the snow load is modelled as

Table 7
Bounds for the yearly probability of failure due to fire

$P_{f,\text{fire,year}}$	EC5 method						B10 method	
	Deterministic charring		Stochastic dependent charring		Stochastic independent charring		Deterministic charring	
Fire duration 30 min	8.55×10^{-13}	9.04×10^{-13}	5.52×10^{-10}	7.77×10^{-10}	2.82×10^{-11}	3.27×10^{-11}	4.81×10^{-14}	5.00×10^{-14}
Fire duration 60 min	7.17×10^{-6}	1.74×10^{-5}	7.30×10^{-6}	4.91×10^{-5}	7.27×10^{-6}	3.82×10^{-5}	2.33×10^{-6}	4.18×10^{-6}

monthly normal distribution, (4) failure is defined as structural failure, that is bending stresses exceeding the capacity.

Based on the probabilistic model code [6], the annual target probability of failure level is recommended as $P_{f,\text{year}} = 1.3\times10^{-5}$. Based on the probabilistic model code [6] the following probabilities for a dangerous fire scenario are given: $P_i(\text{ignition}) = 10^{-6}/\text{year}/\text{m}^2$ or $0.083\times10^{-6}/\text{month}/\text{m}^2$ (value for shops/offices, area: 1768 m^2), $P_f(\text{flashover}|\text{ignition}) = 0.1$ (in the case of a public fire brigade).

Based on the above information, the bounds for yearly probability of failure of the structure can be calculated as

$$\begin{aligned}&\max(P_iP_fP_{f,\text{fire,january}}, P_iP_fP_{f,\text{fire,february}}, \ldots, P_iP_fP_{f,\text{fire,december}}) \leqslant P_{f,\text{fire,year}}\\ &\quad\leqslant 1-((1-P_iP_fP_{f,\text{fire,january}})(1-P_iP_fP_{f,\text{fire,february}})\cdots(1-P_iP_fP_{f,\text{fire,december}})).\end{aligned} \tag{9}$$

The following results are obtained using the two different code methods:

The yearly probability values above are comparable to the target level of the probabilistic model code (see Table 7).

Considering the limit state equation for fire, the k_{crit} term, which reduces the strength due to lateral torsional buckling, becomes critical. This reduces the beam capacity at a fast rate as the charring progresses and the cross-section becomes more slender. The fire design according to EC5 is conservative (compared to B10). Stochastic charring rates have an influence on the failure probabilities.

7. Summary

In this case study, an example reliability analysis is carried out for a glued laminated beam. The analysis is done under normal loading conditions, considering the measured snow load during the period of 30 years and under a fire condition. The following conclusions can be drawn from the present analysis:

The coefficient of variation of the glued laminated timber is not very precisely known, its value is around 15% based on the available test results. Values of this order have also been used in earlier studies. Based on a sensitivity analysis, it seems that the reliability is not very sensitive for this parameter and thus for practical reasons it does not matter if this is not precisely known.

The probability of failure resulting from a deterministic design based on Eurocode 5 is low compared to the target values and smaller beam cross-sections are possible if applying a probabilistic design method with the assigned target reliability.

If a 60 min fire resistance is required, the deterministic fire design based on Eurocode 5 requires higher cross-sections than normal design and it is determining. The fire design according to Eurocode 5 is more conservative than of the Finnish building codes due to differences in the charring rates and the modelling of lateral torsional buckling.

A probabilistic based fire analysis however results in bounds for the yearly probabilities of failure which indicate that the estimated reliability is in accordance with the target value and the values obtained from the normal probabilistic based design. In this case the probability of ignition and flashover occurring are taken as given in the probabilistic model code [6]. Applying stochastic charring rates has an increasing influence on the probability of failure for a fire duration of approximately 30 min or more. In the case of shorter fire duration the influence is relatively small.

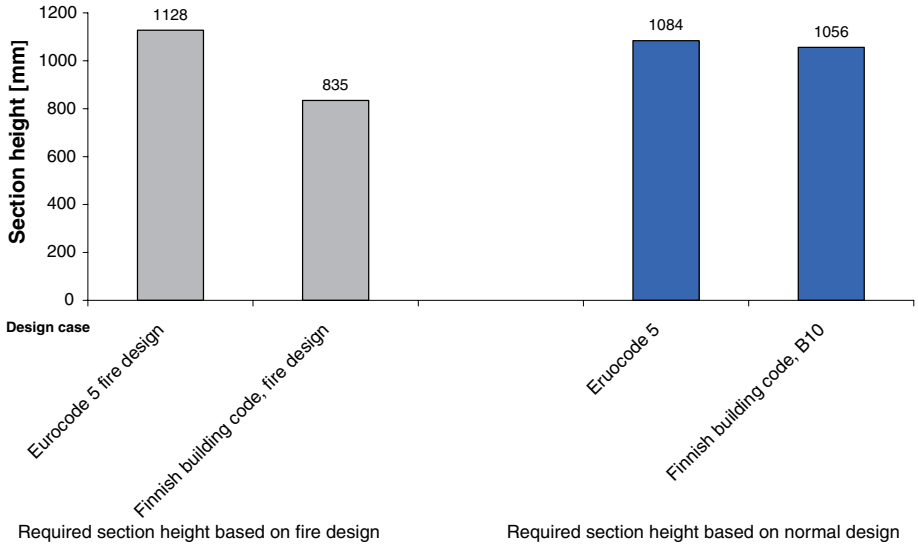

Fig. 8. Required beams section heights based on deterministic code design.

It should be emphasized that this example calculation involves a number of parameters and wood characteristics with distribution properties which are not fully known. The results should be considered as first estimates and the conclusions as indicative.

Acknowledgement

This work was partially supported by bilateral Finish–Slovenian project (BI-FI/04-05-006). The support is gratefully acknowledged.

Appendix

The required section height of the studied beam at the critical cross-section based on Eurocode 5 and the Finnish building code B10 is as shown below. The beam was actually designed according to the Finnish building code and the actual height is 1060 mm. The building does not actually have a 60 min resistance requirement, but if this was the case, it would be fulfilled by the Finnish code but not by the Eurocode (see Fig. 8).

References

[1] ISO CW 4355, Basis for design of structures – determination of snow loads on roofs; 1991.
[2] Perälä J, Reuna R. (Regional and temporal variability of snow loads in Finland [in finnish]) Lumen vesiarvon alueellinen ja ajallinen vaihtelu Suomessa. Vesi ja ympäristöhallitus. Julkaisuja-sarja A 56. Helsinki 1990.
[3] PrEN 1990 Eurocode – Basis of structural design – final draft July 2001. Document CEN/TC 250/SC 5:N 159.
[4] prEN 1995-1-1, Eurocode 5, Design of timber structures, Part 1-1, General rules, General rules and rules for buildings, Final draft, 2002-10-09.
[5] prEN 1995-1-2, Eurocode 5, Design of timber structures, Part 1-2, General – Struct fire design, Final draft, 2003-08-12.
[6] Probabilistic Model Code. Joint Committee of Structural Safety, JCSS; 2001. Available from: http://www.jcss.ethz.ch.
[7] Puurakenteiden suunnitteluohjeet B10 (Finnish timber structures design codes [in finnish]) RIL 120-2001. Helsinki 2001.
[8] Ranta-Maunus A, Fonselius M, Kurkela J, Toratti T. Reliability analysis of timber structures. In: Espoo 2001. Technical Research Centre of Finland. Research notes 2109. 102p + app. 3p.
[9] Ranta-Maunus A, Summary report of NI project on reliability of timber structures. October 2001. Joint Nordic wood project meeting and Cost E24 workshop. Copenhagen.
[10] SAKO 1999. Basis of design of structures – proposals for modification of partial safety factors in Eurocodes. Joint committee of NKB and INSTA-B. NKB Committee and work reports, 1999:01 E.
[11] Strurel, A structural reliability analysis program system, COMREL & SYSREL Users Manual, RCP GmbH, 1999.

[12] Thelandersson S, Larsen HJ, Östlund L, Isaksson T, Svensson S, Säkerhetsnivåer för trä och träproducter i konstruktioner. Lund Universität. Rapport TVBK-3039. 37p. + app.
[13] Personal communication with Jukka Hietaniemi VTT, Finland.

Coupled heat and moisture transfer in timber beams exposed to fire

Simon Schnabl
young researcher
University of Ljubljana, Faculty of Civil and Geodetic Engineering
SI-1115 Ljubljana, Jamova 2, Slovenia

Goran Turk
associate professor
University of Ljubljana, Faculty of Civil and Geodetic Engineering
SI-1115 Ljubljana, Jamova 2, Slovenia

Abstract

This paper describes a mathematical model developed to solve a coupled heat and moisture transfer and charring behavior of timber beam when exposed to fire. The model consists of two coupled non-linear partial differential equations for heat and moisture transfer with the corresponding boundary conditions. The model also predicts the char formation in the wood beam as a function of its temperature, moisture content, density, etc. Since the analytical solution is seldom obtainable, the problem is solved numerically by finite difference method.

The results are tested on the one dimensional case in standard fire conditions, for which comparison is made with the results of one-dimensional charring rate models for wood presented in the literature and experimental results published by Fredlund (1993) A comparison of different charring models shows that the charring rates obtained by the proposed mathematical model are proven to be in excellent agreement with the results obtained experimentally by Fredlund (1993). The model shows also to be in good agreement with the Eurocode 5 (2004) model and model proposed by White and Nordheim (1992), while compared to other charring models differs considerably.

The same model is used to analyze a two-dimensional behavior of wood beam exposed to fire from three sides. Faster charring at the corners and typical rounding effect are observed.

Since the comparison showed a good agreement with the proposed mathematical model and models presented in the literature, we can conclude that a relatively simple mathematical model is generally appropriate for the accurate prediction of the thermomechanical behaviour of timber beams exposed to fire.

References

[1] Fredlund B. 1993. Modelling of heat and mass transfer in wood structures during fire. *Fire Safety Journal* Vol. 20, pp. 39–69.

[2] EN 1995-1-2:2004. Eurocode 5: Design of timber structures Part 1-2: General-Structural fire design.

[3] White R. H. and Nordheim E. V. 1992. Charring rate of wood for ASTM E 119 exposure. *Fire Technology* Vol. 28, No. 1, pp. 5–30.

Coupled heat and moisture transfer in timber beams exposed to fire

Simon Schnabl
young researcher
University of Ljubljana, Faculty of Civil and Geodetic Engineering
SI-1115 Ljubljana, Jamova 2, Slovenia

Goran Turk
associate professor
University of Ljubljana, Faculty of Civil and Geodetic Engineering
SI-1115 Ljubljana, Jamova 2, Slovenia

Summary

This paper describes the modelling of timber beams behaviour when one or more faces are exposed to fire. A computer program for the prediction of two dimensional temperature and water content distribution in timber beams exposed to fire has been developed. The model consists of differential equations for coupled heat and moisture transfer with the corresponding boundary conditions. Furthermore, the model also predicts the char formation in the wood beam as a function of its temperature, moisture, density, etc. Owing to non-linear system of governing equations, solution is obtained by numerical procedures such as finite difference method. Results obtained by numerical model are be compared to the analytical solutions and experimental results published in the literature.

1. Introduction

Ever since prehistoric times wood has been recognized as a very popular construction material. Nowadays it has commonly been used in various fields of engineering. Due to its remarkable properties it has been used by many architects and designers of modern buildings. The capability to predict the behavior of wood, particularly when exposed to fire, has become increasingly important in the field of fire safety engineering.

The purpose of this paper is to study and understand a charring behavior of wood and compare those results to the one-dimensional charring rate models for wood presented in the literature and to the experimental results published by Fredlund (1993).

When numerically analysing mechanical behavior of load bearing timber beams in natural fires, the contributions of shrinkage-swelling, temperature, viscous creep and mechano-sorptive strains are of major importance. The development of all aforementioned strains is strongly affected by the actual temperature and moisture content distribution in the beams. Therefore, the determination of the spatial and temporal distribution of temperature and moisture content over the element according to ambient conditions is the first key phase of the analysis. When wood as a charring material is exposed to fire, it undergoes thermal degradation, i.e. pyrolysis. The pyrolysis of wood is a complex interplay of chemistry, heat, and mass transfer. It changes the wood to char and gases (such as carbon dioxide and hydrocarbons) and consequently changes the density and other material

characteristics. The process of thermal degradation starts when the temperature of wood reaches a certain threshold value which depends on the kind of wood, but is generally around $300\,^{\circ}\mathrm{C}$.

Because of the importance and complexity of the pyrolysis of wood, there is a substantial volume of work on the pyrolysis and charring of wood as a porous media, but the extensive literature review is not the aim of this work. Experimental observations of charring behavior prove the mutual effect of the temperature and moisture content gradients in wood, but it is rarely taken into consideration in the computational analysis of charring in fire situations. In this paper the transient heat and moisture transfer over a timber beam exposed to standard fire conditions is considered. The governing equations of simultaneous heat and moisture transfer in porous media like wood were provided by Luikov (1966).

Assuming a homogeneity of the temperature and moisture content field along the beam, the 2-D Luikov equations are solved for the cross-section of the timber beam. Due to rectangular cross-section the finite difference method using an equidistant mesh of finite difference points is chosen for the solution. For the spatial integration the symmetric formulae based on quadratic shape functions are introduced, whereas for the time-integration linear shape functions are employed.

2. Model theory and governing equations

Heat and mass transfer is governed by the two second order non-linear partial differential equations (Luikov, 1966). The first equation describes heat conduction governed predominantly by temperature gradient but affected also by the effect of phase-change and heat on sorption and desorption, which depend by the speed of moisture changes. The second equation describes moisture diffusion governed predominantly by moisture potential but is also considerably affected by temperature gradients. Furthermore, anisotropy and temperature and moisture content dependent material properties are assumed. The equations can be written as:

$$\rho\, C_p \frac{\partial T}{\partial t} - \rho\, C_m\, (\varepsilon\, h_{LV} + \gamma) \frac{\partial w}{\partial t} = \frac{\partial}{\partial x}\Big(k_x \frac{\partial T}{\partial x}\Big) + \frac{\partial}{\partial y}\Big(k_y \frac{\partial T}{\partial y}\Big), \tag{1}$$

$$\rho\, C_m \frac{\partial w}{\partial t} = \frac{\partial}{\partial x}\Big(D_{Mx}\Big(\frac{\partial w}{\partial x} + \delta_x \frac{\partial T}{\partial x}\Big)\Big) + \frac{\partial}{\partial y}\Big(D_{My}\Big(\frac{\partial w}{\partial y} + \delta_y \frac{\partial T}{\partial y}\Big)\Big). \tag{2}$$

In Eqs. (1–2) k_x, k_y represent thermal conductivity (W/mK) in two space directions x and y of a rectangular cross-section of the beam. Similarly, D_{Mx} and D_{My} represent conductivity coefficient of moisture content ($\mathrm{kg/m\,s\,^{\circ}M}$), ρ represents density ($\mathrm{kg/m^3}$), c_p heat capacity ($\mathrm{J/kgK}$), T temperature ($^{\circ}\mathrm{C}$), c_m moisture capacity ($\mathrm{kg/kg\,^{\circ}M}$), ε ratio of vapor diffusion coefficient to coefficient of total moisture diffusion, h_{LV} heat of phase change (J/kg), γ heat of sorption or desorption (J/kg), w moisture potential ($^{\circ}\mathrm{M}$), t is time (s) and δ_x, δ_y thermogradient coefficient ($^{\circ}\mathrm{M/K}$) in two independent orthogonal directions.

Moisture potential w is related to moisture content V by linear relation

$$V \;=\; c_m\; w. \tag{3}$$

The special solution of the system of governing differential equations (1–2) has to satisfy the initial and boundary conditions. The initial conditions prescribe the temperature and moisture potential of

the cross-section of the beam at the initial time $t = 0$

$$T(x, y, 0) = T_0(x, y), \tag{4}$$

and

$$w(x, y, 0) = w_0(x, y). \tag{5}$$

The boundary conditions prescribe the heat and moisture flow on the exposed boundaries of cross-section. It is assumed that the flow magnitudes depend on the differences between temperature and moisture potentials on the boundary and in the surrounding air. In the heat boundary condition the effect of evaporation on the heat flow is added while in the moisture boundary condition the effect of temperature gradient is taken into account. Thus, the boundary conditions at the exposed surface of the exterior siding are given by balancing heat conduction and moisture transfer at the surface with the radiative and convective heat and convective moisture input. The boundary conditions can be written as

$$-k_x \frac{\partial T}{\partial x}\, e_{nx} - k_y \frac{\partial T}{\partial y}\, e_{ny} = h_c\,(T - T_A) + \varepsilon_R \sigma (T^4 - T_A^4) + (1 - \varepsilon)\, h_{LV}\, h_m\,(w - w_A), \tag{6}$$

and

$$D_{Mx}\, \frac{\partial w}{\partial x}\, e_{nx} + D_{My}\, \frac{\partial w}{\partial y}\, e_{ny} + D_{Mx}\, \delta_x\, \frac{\partial T}{\partial x}\, e_{nx} + D_{My}\, \delta_y\, \frac{\partial T}{\partial y}\, e_{ny} = -h_m\,(w - w_A), \tag{7}$$

where e_{nx} and e_{ny} are components of the normal to the boundary surface, h_c and h_m are convective heat transfer coefficient ($\mathrm{W/m^2\,K}$) and convective moisture transfer coefficient ($\mathrm{kg/s\,m^2\,{}^\circ M}$), respectively. T_A is the temperature and w_A is the moisture potential of the ambient. The second term in the right-hand side of Eq. (7) represents the radiative heat input where ε_R is the effective surface emissivity of the exterior siding and σ is the Stephan-Boltzmann constant for radiation, ($\sigma = 5.671 \cdot 10^{-8}\ W/\mathrm{m^2} K^4$).

The ambiental moisture potential is obtained through sorption isotherms. The effects of stress state and history of sorption are neglected. The above system of the equations Eqs. (1–7) are solved using finite difference method and a computer program written in $Matlab$ enviroment.

3. Numerical examples

3.1 One-dimensional charring

The effect of charring of wood in timber construction has been a subject of intensive research for many years. Charring of wood during fire has been extensively studied and considerable efforts have been given to the development of theoretical models for wood charring that are intended to take into account more complex geometries and variation of heat exposure. Unfortunately, no completely satisfactorily charring model has yet been developed. On the other hand, an extensive char rate data is available for simple one-dimensional wood slabs. Data is also available for two-dimensional timbers, but most of this data is limited to larger cross-sections. Hence, a one-dimensional case of a wood slab made of spruce, with a thickness d, exposed to the standard fire (standard fire curve ISO 834, 1999) is considered in order to compare the charring rate of the wood slab with the

one-dimensional empirical models presented in the literature. Generally, charring behavior of wood can either be described by the mass loss rate (g/s) or by the rate of advance of the formed char front from the original surface (mm/s). The latter definition has been more widely used because it enables the determination of an effective residual cross-section area commonly employed in timber design calculations. The rate of charring is a complex process which depends upon the interaction between the pyrolysis of wood and the generation of heat, both of which are a function of a number of factors such as the species, density moisture content, permeability and thermophysical properties. Since the material properties at elevated temperatures are difficult to obtain, constant material properties of wood and char are used. The data for this case is as follows

$$\begin{aligned} &T_0 = 20°\mathrm{C},\ \ w_0 = 13°\mathrm{M},\ \ w_A = 4°\mathrm{M}, \rho = 370\ \mathrm{kg/m^3},\ \ k_{\mathrm{wood}} = 0.12\ \ k_{\mathrm{char}} = 0.15\ \mathrm{W/(m\,K)},\\ &D_M = 2.2 \times 10^{-8}\ \mathrm{kg/(m\,s\,°M)},\ \ h_{LV} = 2500\ \mathrm{kJ/kg},\ \ h_c = 22.5\ \mathrm{W/(m^2\,K)},\ \ \varepsilon = 0,3,\\ &c_{p\,\mathrm{wood}} = 1530\mathrm{J/(kg\,K)},\ \ c_{p\,\mathrm{char}} = 1050\ \mathrm{J/(kg\,K)},\ \ c_m = 0.01\ \mathrm{kg/(kg\,°M)},\ \ \delta = 2.0\ °\mathrm{M/K},\\ &h_m = 2.5 \times 10^{-6}, \mathrm{d} = 0.3\ \mathrm{m},\ \ \gamma = 0. \end{aligned} \tag{8}$$

The comparison of different charring models is presented in Fig. 1.

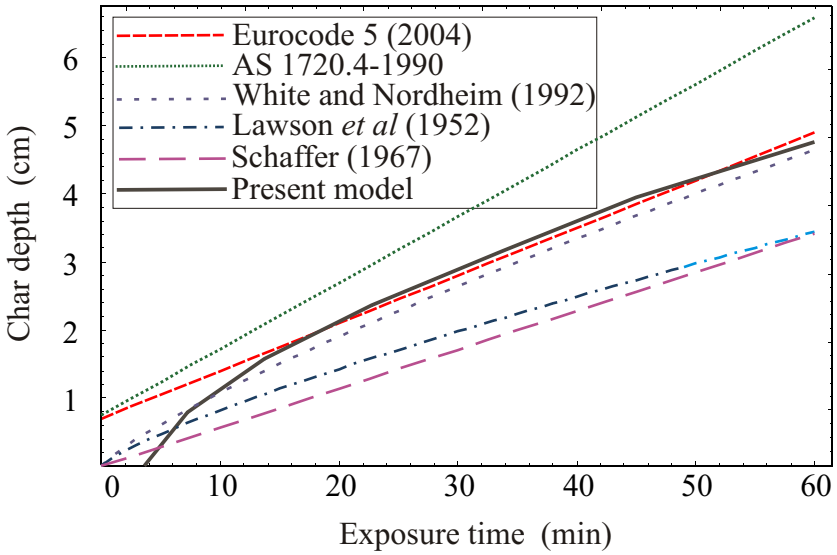

Figure 1: Comparison of different charring models to present one

Most of the aforementioned models (Eurocode 5, 2004, AS 1720.4, 1990, Schaffer, 1967) suggest constant charring rates. The use of these charring rates is convenient but does not accurately reflect the actual charring behavior of wood. To account for the char non-linearity, White (1988) developed a non-linear, one-dimensional char rate model based on the results of forty one-dimensional wood slab charring tests. Later on, White and Nordheim (1992) developed a non-linear empirical model for charring rate of eight different wood species. The comparison to the present model in the case of spruce is shown in Fig. 1. The non-linear charring rate model was also developed by Lawson et al. (1952) who studied the charring rates of spruce timber beams of different thickness at 12% moisture content when exposed to standard ASTME E 119 (2000) heating regime. The comparison in Fig. 1 shows, that the models proposed in AS 1720.4-1990 and by Schaffer (1967) differ considerably. The Lawson's and Schaffer's models differ slightly at the beginning, but are virtually equal at 60

minutes. Similarly, the model proposed by Eurocode 5 (2004), White's and Nordheim's model and the model proposed in this paper differ considerably in the first 15 minutes, but later show similar results. All models described above are relatively simple to use. However, all empirical models are limited to one-dimensional cases. Also in all empirical models it is assumed that the charring of wood starts instantaneously after exposure to fire. In reality, this is not the case. In our model, the charring starts when the temperature of wood reaches the temperature of pyrolysis, which is around $300\,^{\circ}\mathrm{C}$. This happens nearly 4 minutes after the fire starts.

To validate our numerical model for a coupled heat and moisture transfer of wooden beams exposed to fire we compare our numerical results to the experimental results obtained by Fredlund (1988), see Figure 2.

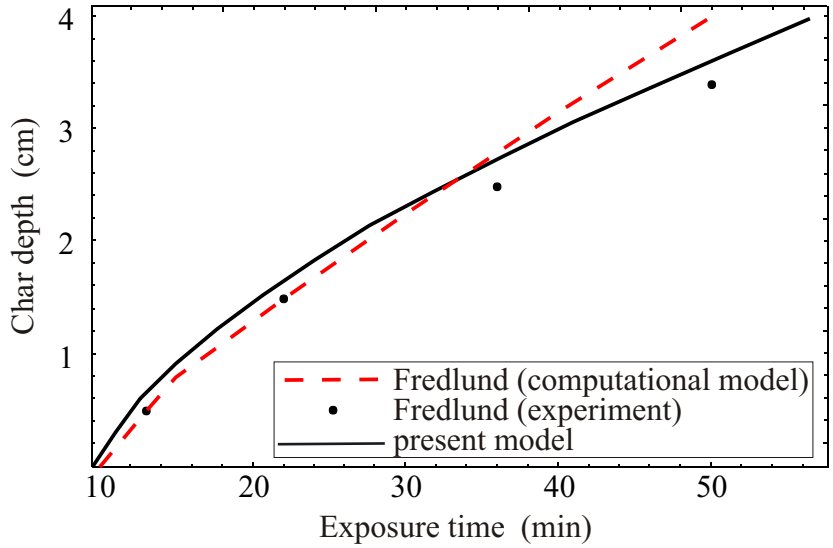

Figure 2: Comparison of experimental and numerical results for penetration of the char layer as a function of time for spruce with initial moisture content of 14.5%

The comparison between the calculations and the experiment is based on measured and calculated temperature-dependent thermo-mechanical properties of wood and char given by Fredlund (1988). The example given below deals with a specimen of spruce of initial moisture content of 14.5%. The results are also compared to the numerical model proposed by Fredlund (1988). Figure 2 shows a comparison of the penetration/formation of the char layer as a function of fire exposure time. In the Fredlund's calculations, the char front has been defined as the point at which density has dropped to 300 kg/m^3, while in our model the formation of the char is defined as the point at which temperature reaches $300\,^{\circ}\mathrm{C}$. As it can be seen from the Figure 2, there is a very good agreement between measured and calculated results of the penetration depth of the char. This allows us to conclude that the proposed mathematical model is generally appropriate for the prediction of charring behavior of wooden beams exposed to fire.

3.2 A two-dimensional charring

In this case the formation of a char layer in a wooden beam exposed on three sides to standard fire conditions defined in ISO 834 (1999) is considered. The upper edge is thermally isolated. The original beam cross-section is rectangular with dimensions 10×15 cm. The beam cross-section is discretized by the finite difference mesh of 30×45 points. Material properties are assumed to be the same as they are in the first one dimensional case. The results of the simulation at times 1.2, 10, 20 and 30 minutes after exposure to fire are set out in Figures 3–4.

Since the corners are subjected to heat and moisture transfer from two directions, charring is faster at these corners. Consequently, the formation of a char starts always at these corners. As a result, a rounding effect occurs and shortly after the ignition the remaining load bearing cross-section is no longer rectangular.

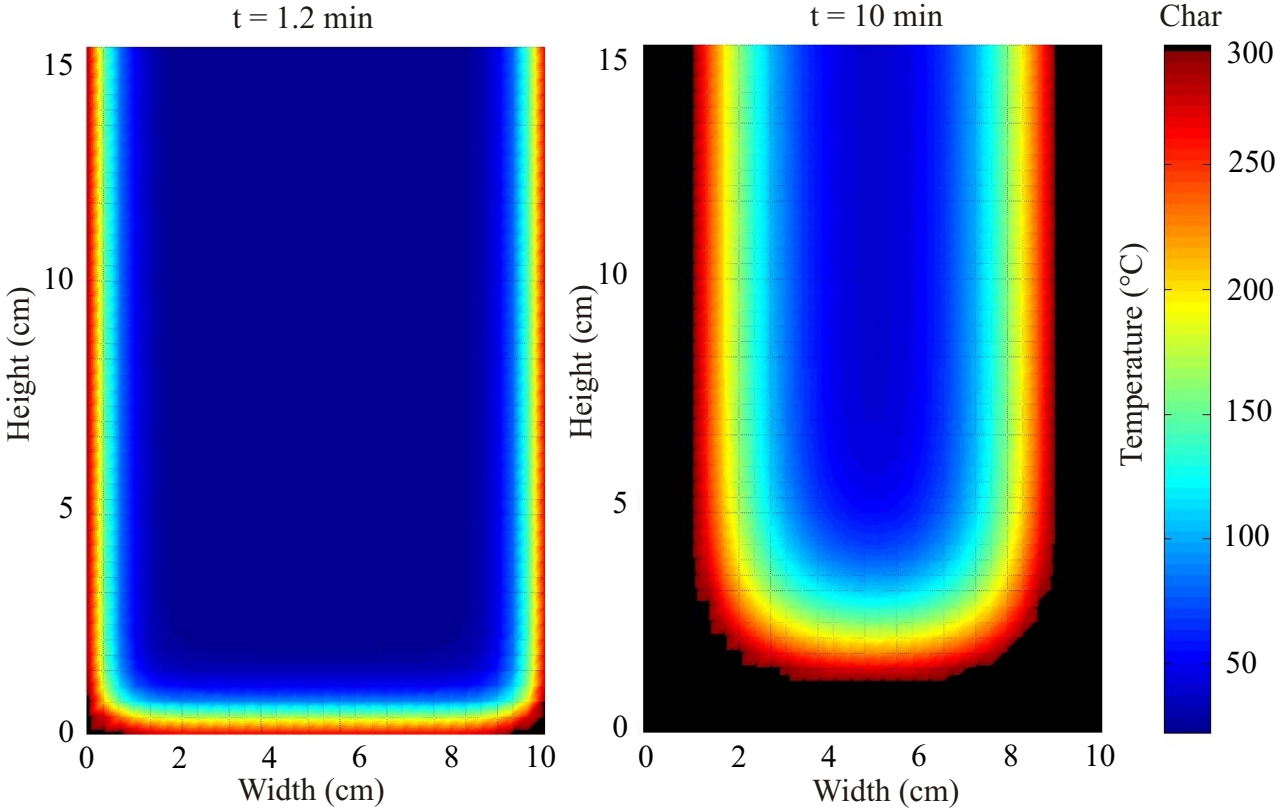

Figure 3: Temperature distribution in cross-section of spruce beam with initial moisture content of 13% *and the transformation of wood into a char at* 1.2 *and* 10 *minutes*

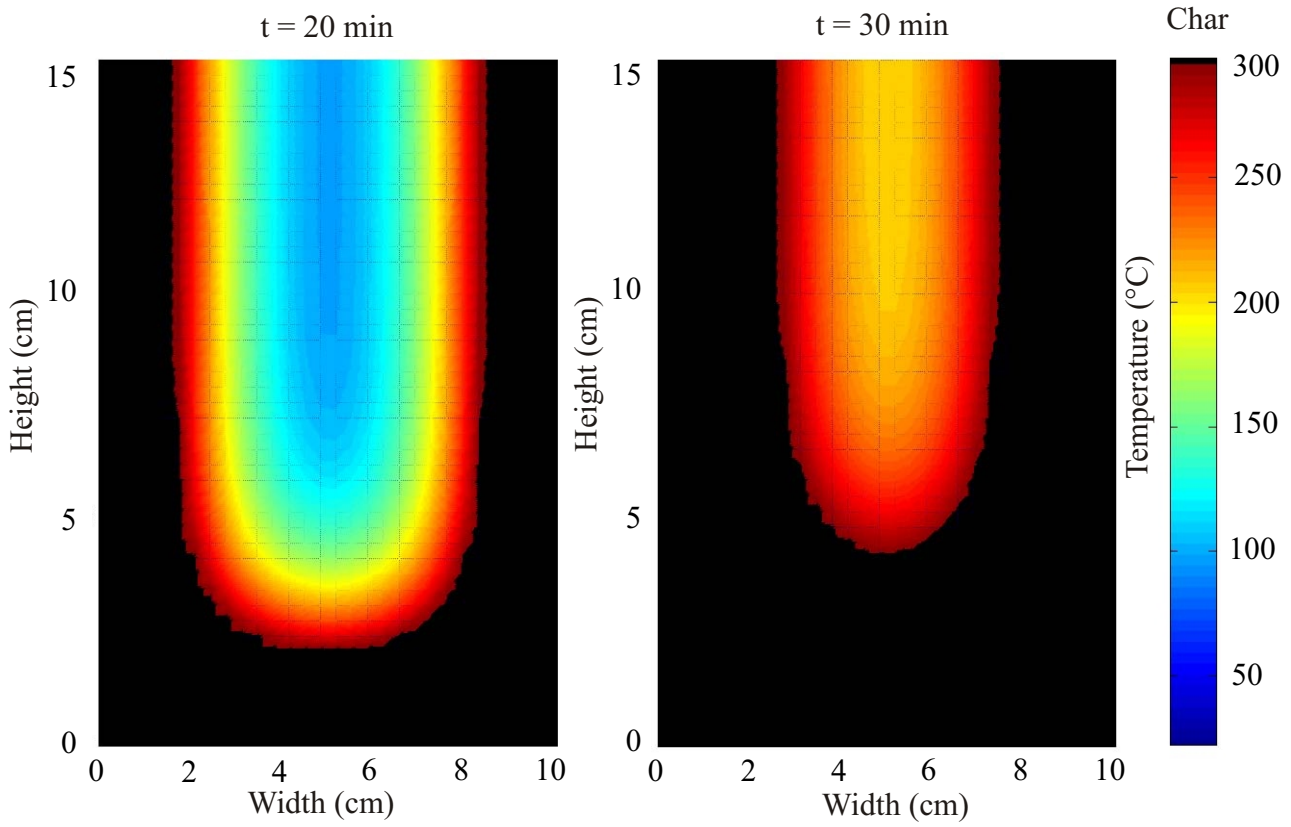

Figure 4: Temperature distribution in cross-section of spruce beam with initial moisture content of 13% *and the transformation of wood into a char at* 20 *and* 30 *minutes*

4. Conclusions

A mathematical model was developed to solve a coupled heat and moisture transfer and charring behavior of timber beam when exposed to fire. Since the analytical solution is seldom obtainable, the problem was solved numerically by finite difference method. The results were tested on the one dimensional case for which comparison was made with the results obtained numerically and experimentally. A comparison of different charring models showed that the charring rates obtained by the proposed mathematical model were proven to be in excellent agreement with the results obtained experimentally by Fredlund (1988). The model showed also to be in good agreement with the Eurocode 5 (2004) model and model proposed by White and Nordheim (1992), while compared to other charring models differ considerably. The same model was used to analyze a two-dimensional behavior of wood beam exposed to fire from three sides. Faster charring at the corners and typical rounding effect were observed. Thus, we can conclude that a relatively simple mathematical model is generally appropriate for the accurate prediction of the thermomechanical behavior of timber beams exposed to fire.

Acknowledgment

The work of S. Schnabl was financially supported by the Ministry of Education, Science and Sport of the Republic of Slovenia under contract 3311-02-831625. The support is gratefully acknowledged.

5. References

[1] Luikov A. V. 1966. Heat and Mass Transfer in Capillary-porous Bodies. *Pergamon Press*, Oxford.

[2] Fredlund B. 1988. A model for heat and mass transfer in timber structures during fire. A theoretical, numerical and experimental study. *Report LUTVDG/(TVBB–1033)*. Department of fire safety engineering, Lund institute of science and Technology, Sweden.

[3] Fredlund B. 1993. Modelling of heat and mass transfer in wood structures during fire. *Fire Safety Journal* Vol. 20, pp. 39–69.

[4] ISO 834. 1999. Fire-resistance test – Elements of building construction-Part 1. General requirements. ISO 834-1, *International organization for standardization*. Geneva, Switzerland.

[5] EN 1995-1-2:2004. Eurocode 5: Design of timber structures Part 1-2: General-Structural fire design.

[6] AS 1720.4. 1990. Timber structures – Fire resistance of structural timber members.

[7] Schaffer E.L. 1967. Charring rate of selected woods-transverse to grain. *Research paper FPL-69*. USDA Forest Product Laboratory, Madison, Wisconsin, USA

[8] White R. H. 1988. Charring rates of different wood species. *PhD Dissertation*. University of Wisconsin, Madison, WI, USA.

[9] White R. H. and Nordheim E. V. 1992. Charring rate of wood for ASTM E 119 exposure. *Fire Technology* Vol. 28, No. 1, pp. 5–30.

[10] Lawson D. I. Webster C. T. and Ashton L. A. 1952. Fire endurance of timber beams and floors. *Journal of Structural Engineering* Vol. 30, No. 2, pp. 27–34.

[11] ASTM. 2000. Standard test methods for fire tests of building construction and materials. *Standard designation E 119-00*. West Conshohocken, PA:ASTM.